

**GEOTECHNICAL CHARACTERIZATION
AND SLOPE STABILITY ANALYSES
OF THE TOWN BUSH VALLEY,
PIETERMARITZBURG
SOUTH AFRICA**

By

Keval Singh

2018

Supervisors:

Dr. E.D.C Hingston

Dr. M.B. Demlie

Submitted in fulfilment of the requirements for the degree of Master of Science

In the Discipline of Geological Sciences

At the School of Agricultural, Earth and Environmental Science

University of KwaZulu-Natal

Durban

South Africa

PREFACE

The experimental work described in this thesis was carried out in the School of Geological Sciences, University of KwaZulu-Natal, Westville, from January 2015 to November 2018, under the supervision of Dr. Hingston and Dr. Demlie.

These studies represent original work by the author and have not otherwise been submitted in any form for any degree or diploma to any tertiary institution. Where use has been made of the work of others it is duly acknowledged in the text.

As the candidate's supervisor I have approved this thesis for submission and examination.

Name:.....

Signature:..... **Date:**

As the candidate's co-supervisor I have approved this thesis for submission and examination.

Name:.....

Signature:..... **Date:**

DISCLAIMER

I, Keval Singh declare that:

1. The content presented in this dissertation is my own unaided work, except where suitable referenced and acknowledged as coming from other sources.
2. This thesis has not been submitted for any degree or examination at any other university.
3. This thesis does not contain other persons' data, graphs or other information, unless specifically acknowledged as being sourced from other persons.
4. This thesis does not contain any other persons writing, unless where specifically acknowledged as being sourced from other researchers. Where other written sources have been quoted then:
 - a. Their words have been re-written but the general information attributed to them has been referenced.
 - b. Where their exact words have been used, then their writing has been placed inside quotation marks, and referenced.
5. This thesis does not contain text, graphics or tables copied from the Internet, unless specifically acknowledged and the source being detailed in the thesis and in the References Section.

Signature:..... **Date:**

ABSTRACT

The construction of settlements over zones of instability is increasing the impact of disasters across the world both in developed and developing nations. Many areas in the greater Pietermaritzburg region in South Africa, such as the Town Bush Valley, are prone to slope instability due to the terrain morphology and high intensity rainfall. This study has investigated the geotechnical conditions at the Town Bush Valley, in Pietermaritzburg. A geotechnical characterization of the Town Bush Valley has been undertaken in order to understand the geotechnical conditions prevailing on site. Furthermore, two critical slopes were selected for slope stability analyses to investigate the conditions under which failure would occur. The method of analyses chosen was the Morgenstern and Price method using the Rocscience, SLIDE software. The analyses involved a deterministic approach and a probabilistic approach. In the deterministic approach, all the input variables were considered as constant values. In the case of the probabilistic approach, the effective shear strength parameters were chosen as the random variables in order to account for their uncertainty. Prior to the analyses, sensitivity analysis was conducted in order to see the effect of the effective shear strength parameters, c' and ϕ' , on the factor of safety. Various scenarios, including groundwater conditions and surcharge load, were considered during the analyses. Results from the site characterization show that the site is characterized by heterogeneous talus material, which is underlain at depth by shales of the Pietermaritzburg Formation and sandstones of the Vryheid Formation. Particle size analysis, Atterberg Limits Determination and consolidated-drained triaxial tests were undertaken on the talus material.

The slope stability analyses show that the probabilistic approach presents a better insight into the assessment of the slope than a deterministic approach in accounting for the uncertainty in the geotechnical parameters. The random behaviour of the geotechnical parameters was quantified through various probabilistic functions. The various functions derived during probabilistic slope stability analyses, allowed for an assessment of the reliability of the data sets.

Keywords/Phrases: Deterministic slope stability analysis; Phreatic surface; Probabilistic slope stability analysis; Random variables; Town Bush Valley

ACKNOWLEDGEMENTS

I would like to acknowledge the supportive role my parents Kishore and Carol Singh, have played over the years. I would like to thank Sasha Gengen for motivating me.

A thesis requires guidance from experienced professionals in this respect I would like to thank my supervisors, Dr. Hingston and Dr. Demlie for their professional advice and input.

I would like to thank Mr Neil Barr, Mr Balin Govender, Mr Richard Kelland and Ms Jan Norris for their assistance throughout my studies.

CONTENTS

TITLE	i
PREFACE	iii
DISCLAIMER	ii
ABSTRACT	iv
ACKNOWLEDGEMENTS	v
CONTENTS	vi
List of Figures	ix
List of Tables	xii
List of Equations	xiii
CHAPTER 1: INTRODUCTION	1
1.1 General Background	1
1.2 Problem Statement.....	2
1.3 Research Hypothesis.....	2
1.4 Aim and Objectives	2
1.5 Dissertation Structure	3
CHAPTER 2: DESCRIPTION OF THE STUDY AREA	5
2.1 General description of the study area	5
2.1.1 Location.....	5
2.1.2 Topography	6
2.1.3 Terrain evaluation.....	7
2.1.4 Climate and drainage.....	9
2.1.5 Vegetation	12
2.2 Regional Geological Setting	12
2.3 Local geology of the Town Bush Valley	12
2.3.1 Eccca Group.....	16
2.3.2 Karoo dolerite intrusives	16
2.3.3 Colluvial hillslope deposits	17
2.4 Hydrogeology	19
2.4.1 Aquifer Types.....	19
2.4.2 Hillslope hydrological processes and groundwater flow.....	20
CHAPTER 3: LITERATURE REVIEW	23
3.1 Slope Stability Analysis.....	23
3.1.1 Methods of slope stability analyses.....	23
3.1.2 Deterministic approach in slope stability analysis	25
3.1.3 Probabilistic approach in slope stability analysis	26
3.1.3.1 Mean, standard deviation and coefficient of variation	27

3.1.3.2 Probability of failure	27
3.1.3.3 Probability distribution functions	28
3.1.3.4 Reliability index	29
3.1.3.5 Random variables	29
3.1.3.6 Probabilistic approximation methods	30
3.2 Representation of pore water pressures	32
3.3 Conditions for Analyses	32
3.3.1 Drainage conditions.....	33
3.3.1.1 Undrained Conditions.....	33
3.3.1.2 Drained Conditions.....	33
3.4 Mechanical properties of Talus Material	34
3.4.1 Granular material.....	34
3.4.2 Silts	35
3.4.3 Clays	35
3.5 Review of the Engineering Geological Conditions at the Town Hill Escarpment	37
3.5.1 Geomorphological Description of the Town Bush Valley	38
3.5.2 Natural discontinuities in Town Bush Valley.....	40
3.5.3 Equilibrium Destabilising Forces	40
3.5.4 Instability in roadworks.....	41
3.5.5 Northdale investigation	42
3.5.6 Rickivy landslide.....	43
3.5.6.1 Influence of pore water pressures	44
3.5.7 Athlone slope failure	44
3.6 Review of subsurface drilling, augering and trial pitting in Town Bush Valley	45
3.6.1 Previous soil laboratory test results in the Town Bush Valley.....	46
CHAPTER 4: METHODOLOGY	48
4.1 Scientific framework	48
4.2 Soil sampling.....	50
4.2.1 Undisturbed sampling and <i>in-situ</i> density determination	50
4.3 Laboratory testing.....	51
4.3.1 Particle size analysis.....	52
4.3.1.1 Grading analysis	52
4.3.1.2 Hydrometer analysis.....	52
4.3.2 Atterberg Limits Determination	53
4.3.2.1 Liquid limit.....	53
4.3.2.2 Plastic limit.....	53
4.3.2.3 Linear shrinkage	54

4.3.3 Triaxial test.....	54
4.3.3.1 Saturation.....	55
4.3.3.2 Consolidation.....	55
4.3.3.3 Compression.....	55
4.4 Slope stability analyses.....	56
4.4.1 Selection of the method of analyses	57
4.4.2 Selection of the cross-sections for analyses	56
4.4.3 Representation of values	58
4.4.4 Representation of pore water pressures	60
4.4.5 Probabilistic slope stability analyses	60
4.4.5.1 Sensitivity analysis	60
4.4.5.2 Selection of scenarios and scientific procedures used during analyses	61
CHAPTER 5: RESULTS AND DISCUSSION	64
5.1 Introduction	64
5.2 Geotechnical characterization of the Town Bush Valley	64
5.2.1 Engineering geology descriptions of the material from boreholes, auger hole records and trial pitting	64
5.3 Results from laboratory testing	71
5.3.1 Grain Size Analysis and Atterberg Limits Determination.....	71
5.3.2 Triaxial test.....	74
5.4 Slope stability analyses of selected slopes in the Town Bush Valley	77
5.4.1 Sensitivity Analysis.....	78
5.4.2 Deterministic and probabilistic slope stability analyses for the LNP slope	79
5.4.2.1 LNP - analysis 1	79
5.4.2.2 LNP – analysis 2.....	82
5.4.3 Deterministic and probabilistic slope stability analyses for the MP slope	85
5.4.3.1 MP – analysis 1	85
5.4.3.2 MP – analysis 2	87
CHAPTER 6: CONCLUSIONS AND RECOMMENDATIONS.....	91
6.1 Conclusions	91
6.2 Recommendations for further research.....	93
REFERENCES	94
APPENDICES.....	105

List of Figures

Figure 2.1: Location map of the Town Bush Valley.....	5
Figure 2.2: Town Bush Valley site plan.....	6
Figure 2.3: Digital elevation model of the Town Bush Valley, indicating slopes $> 18^\circ$	7
Figure 2.4: Geotechnical map of Pietermaritzburg highlighting areas of geotechnical limitations to development based on the 1: 50 000 Geotechnical Series 2930CB Pietermaritzburg	8
Figure 2.5: Mean monthly rainfall, maximum and minimum temperatures at Pietermaritzburg (source: SA explorer, 2015)	9
Figure 2.6: Average monthly rainfall, maximum and minimum temperature range from 2005 to 2010 (SAWS, 2015).	9
Figure 2.7: The Town Bush Stream with boulder dolerite in the alluvial channel derived from talus material.	10
Figure 2.8: Drainage map indicating surface water flow directions	11
Figure 2.9: Generalized geological map of the Pietermaritzburg region based on the 1:50 000 Geological Series 2930CB Pietermaritzburg.....	14
Figure 2.10: Local geological map of the study area.	15
Figure 2.11: A dolerite sill observed from the Town Bush Valley looking towards World’s View....	17
Figure 2.12: Boulders intersected in the talus horizon during trial pitting in the Montrose Park Development	18
Figure 2.13: Town Bush Valley hillslope schematic presentation of groundwater flow	21
Figure 2.14: Contour map showing the depth to the groundwater table below natural ground level in Town Bush Valley.....	22
Figure 2.15: Vector map showing the localised groundwater flow regime in Town Bush Valley	22
Figure 3.1: Probability distribution function (<i>pdf</i>) for the factor of safety (adapted from Gover, 2014)	28
Figure 3.2: Probability distribution function types (adapted from Montgomery & Runger, 2011)	28
Figure 3.3: Steps involved in a Monte Carlo Simulation (Hutchinson & Bandalos, 1997)	31
Figure 3.4: Comparative aerial photographs of the Town Bush Valley outlined in red spanning 67 years spanning 67 years (adapted from Maurenbrecher and Booth, 1975).	39
Figure 3.5: Fissures intersected in the Cascades Development.....	40
Figure 3.6: Cutting failure near Hilton in 1967 (adapted from Maurenbrecher and Booth, 1975).	42
Figure 3.7: Sinkhole development in the N3 Highway in 2015	42
Figure 3.8: Rickivy embankment failure in 1970 (adapted from Maurenbrecher and Booth, 1975). ...	43
Figure 3.9: Cross-section of the Rickivy embankment (adapted from Maurenbrecher and Booth, 1975).	43
Figure 3.10: Cross-section of the Athlone slope failure (adapted from Maurenbrecher and Booth, 1975).	44

Figure 3.11: A shear plane on the Athlone Slope (adapted from Maurenbrecher and Booth, 1975)...	45
Figure 3.12: Location of the boreholes, auger holes and trial pits: Town Bush Valley site plan	46
Figure 3.13: Average particle size distribution curve for the Town Bush Valley talus material.	47
Figure 4.1: General flow chart indicating the scientific steps followed during the study	49
Figure 4.2: Soil sample positions in the Town Bush Valley	50
Figure 4.3: <i>In-situ</i> density retrieval from an undisturbed block at trial pit MPD3	50
Figure 4.4: Waxed soil block at trial pit MPD3	51
Figure 4.5: Changes in the soil state when water is added	53
Figure 4.6: Typical triaxial system setup in a laboratory	54
Figure 4.7: Flowchart illustrating the phases used during the probabilistic approach of slope stability analysis	56
Figure 4.8: Lines of cross-section covering the WVD, MPD, UNPD, LNPD and Cascades Development	57
Figure 4.9: Cross-section F-F' of the LNPD used for the slope stability analyses	58
Figure 4.10: Cross-section G-G' of the MPD used for the slope stability analyses	58
Figure 5.1: Location of lines of cross-section	65
Figure 5.2: Geological cross-section A-A' of the WVD	65
Figure 5.3: Geological cross-section B-B' of the WVD	66
Figure 5.4: Geological cross-section C-C' of the UNPD	66
Figure 5.5: Geological cross-section D-D' of the Cascades Development	66
Figure 5.6: Geological cross-section E-E' of the LNPD	66
Figure 5.7: Geological cross-section F-F' of the LNPD	67
Figure 5.8: Geological cross-section G-G' of the MPD	67
Figure 5.9: Geological cross-section H-H' of the MPD	67
Figure 5.10: Matrix supported talus profile intersected in trial pit LNPD1	70
Figure 5.11: Residual sandstone rock fragment preserved in the talus matrix (trial pit LNPD2).	70
Figure 5.12: Excavator used during trial pitting (Photo 1), talus material intersected in trial pit MPD2 (Photo 2)	71
Figure 5.13: Particle size distribution curves for the talus material: Cross-section of the Rickivy embankment adapted from Maurenbrecher and Booth, (1975)	72
Figure 5.14: Sample LNPD3 - Deviator stress (kPa) vs Axial strain (%) (left) and Pore water pressure (kPa) vs Axial strain (%) (right)	74
Figure 5.15: Sample MPD3 - Deviator stress (kPa) vs Axial strain (%) (left) and Pore water pressure (kPa) vs Axial strain (%) (right)	75
Figure 5.16: Barreling failure of specimens (Photo 1 - sample LNPD3; Photo 2 - LNPD specimen sets; Photo 3 - sample MPD3)	75
Figure 5.17: Mohr circles used to define the effective cohesion and effective angle of friction for sample LNPD3	76

Figure 5.18: Mohr circles used to define the effective cohesion and effective angle of friction for sample MPD3	76
Figure 5.19: Sensitivity analysis for the effective cohesion and effective angle of friction.....	78
Figure 5.20: LNPD analysis 1 scenario 1, at the measured groundwater table	80
Figure 5.21: LNPD analysis 1 probabilistic analysis, at the maximum increase in the groundwater table using the minimum range of effective shear strength parameters	80
Figure 5.22: LNPD analysis 1 scenario 4, histogram of the relative frequencies for the FOS, at the maximum increase in the groundwater level.....	81
Figure 5.23: LNPD analysis 2 probabilistic analysis, at the measured groundwater level using the mean effective shear strength parameters	83
Figure 5.24: LNPD analysis 2, histogram plot of the relative frequencies for the FOS, at the measured groundwater table.....	83
Figure 5.25: MPD scenario 1 analysis 1, at the measured groundwater table.....	85
Figure 5.26: MPD analysis 1 scenario 5, at the maximum groundwater table	86
Figure 5.27: MPD analysis 2 probabilistic analysis, at the measured groundwater table using the mean effective shear strength parameters	88
Figure 5.28: MPD analysis 2 probabilistic analysis, at the maximum increase in the groundwater table using the mean effective shear strength parameters	88
Figure 5.29: MPD analysis 2, histogram plot of the relative frequencies for the FOS, at the maximum increase in the groundwater table.....	89

List of Tables

Table 2.1: Stratigraphic sequences preserved in the study area	13
Table 2.2: General hydrogeological properties of water bearing units	20
Table 3.1: Summary of slope stability analyses methods and conditions under which they apply	25
Table 3.2: Summary of various probabilistic approximation methods	30
Table 3.3: Summary of various pore water pressure representation methods	32
Table 3.4: Typical friction angles for granular soils (Look, 2007)	34
Table 3.5: Typical friction angles for granular soils (Carter & Bentley, 1991)	34
Table 3.6: Typical friction angles for granular soils (Budhu, 2000; Murthy, 2003; Das, 2006;)	35
Table 3.7: Correlation of relative density with the angle of internal friction for clean sands (Duncan & Wright, 2005)	35
Table 3.8: Values for effective angle of friction for normally consolidated clays (Duncan & Wright, 2005)	36
Table 3.9: Typical values for compacted clays (Duncan & Wright, 2005)	36
Table 3.10: Typical values for effective friction angles for normally consolidated clays (Carter & Bentley, 1991)	36
Table 3.11: Factors influencing clay strength	37
Table 3.12: Destabilizing equilibrium conditions (Budhu, 2000; Duncan & Wright, 2005)	41
Table 3.13: Previous shear strength test results obtained in the Town Bush Valley	47
Table 4.1: Statistical distribution of the random variables	59
Table 4.2: Effective shear strength parameters of the residual horizons	60
Table 4.3: Baseline analyses and scenarios considered during slope stability analyses	61
Table 5.1: Generalized engineering geological descriptions	68
Table 5.2: Engineering geological descriptions, Cascades Development	69
Table 5.3: Engineering geological descriptions, LNPD	70
Table 5.4: Engineering geological descriptions, MPD	71
Table 5.5: Summary of index properties for the talus material	73
Table 5.6: Triaxial test results of various samples for the talus material	76
Table 5.7: Summarized analyses and scenarios considered for the LNPD and MPD slopes	78
Table 5.8: LNPD analysis 1, deterministic slope stability results	79
Table 5.9: LNPD analysis 1 scenario 4, FOS functions at the maximum increase in the phreatic surface	80
Table 5.10: LNPD analysis 2, summarized probabilistic slope stability analyses results	82
Table 5.11: LNPD analysis 2, FOS functions at the measured phreatic surface	83
Table 5.12: MPD analysis 1 deterministic slope stability results	85
Table 5.13: MPD analysis 2, summarized probabilistic slope stability analyses results	87
Table 5.14: MPD scenario 2 probabilistic parameters at a 1.49 m increase in the groundwater table	89

List of Equations

Equation 3.1: Factor of safety	23
Equation 3.2: Factor of safety expressed in terms of total stress analysis	24
Equation 3.3: Factor of safety expressed in terms of an effective stress analysis	24
Equation 3.4: Mean	27
Equation 3.5: Standard deviation	27
Equation 3.6: Coefficient of variation	27
Equation 3.7: Probability of failure	28
Equation 3.8: Probability of success	27
Equation 3.9: Normal reliability index	29
Equation 3.10: Lognormal reliability index	29
Equation 3.11: Piezometric surface vertical depth	32
Equation 3.12: Piezometric surface	32
Equation 3.13: Phreatic surface	32

CHAPTER 1

INTRODUCTION

1.1 General Background

The South African government faces an on-going challenge of providing basic housing and infrastructure for the citizens of its country. In the current economic climate, the government is challenged with the urgent need in upgrading impoverished areas through the provision of adequate infrastructure and services and at the same time, integrating these underdeveloped areas into growing urbanizing cities. The local government acknowledges this approach in several carefully planned and designed strategies, which has been implemented throughout the country. Traditionally, private housing estates have appealed to middle to high-income citizens. The escalating level of crime has however, initiated major changes in the urban landscape. Gated communities, in the form of private developments are transforming the face of emerging cities in South Africa.

The growth of private developments in the form of large luxury residential estates, golf estates, office parks, townhouse complexes and secured apartments, is an increasing trend in well-developed towns of South Africa. In general, the growth of gated communities has significantly increased over the past five years (Landman, 2002). The Midlands area in KwaZulu-Natal, South Africa has observed an exponential increase in such developments in the past decade with the development of Gowrie Estate, The Gates, Oakhill Park, Garlington Estate and Victoria Country Club Estate.

This has sparked the interest of investors in real estate investment potential in luxury private developments. As such, this has driven real estate fund managers to drastically rethink about the optimum utilization of land for gated communities. Richards *et al.* (2006) highlighted the importance of taking into account the geotechnical factors which influence the design and planning of future developments. The financial cost implication is an important factor where a financial input is required to change either the condition or reduce its impact on the proposed development or land use change. The construction of settlements over zones of instability is increasing the impact of natural disasters both in developed and developing nations across the world (Rosenfeld, 1994). Understanding the geotechnical conditions that render these zones hazardous is a challenging aspect of engineering geology.

The Town Bush Valley is one such area occupied by numerous commercial and residential developments. The Town Bush Valley is situated outside the town of Pietermaritzburg in the KwaZulu-Natal Midlands. Over the past half century, this area has been one of continuous debate and interest in the geotechnical field. The slopes of the Town Bush Valley area, which are characterized by colluvial and talus soils, have been widely regarded as unsuitable and in some cases hazardous ground to found on.

The stability of the slopes of the Town Hill Escarpment has been met by mixed reactions by practicing professionals such as Structural Engineers, Geotechnical Engineers and Engineering Geologists throughout KwaZulu-Natal. Hadlow (1993), Hadlow (2004), Kujawa (2005), Price (2006). The Council for Geoscience (2008) classified the study area as having active mass movement and unstable slopes on a regional scale. Limited site specific research has been undertaken on the geological, hydrogeological and geotechnical properties of the talus material and its influence on the slopes of the Town Bush Valley. Schreiner (2005a) recognized that the addition of loads exerted on the slopes may result in instability as these slopes are prone to long term downslope creep.

This study aims to evaluate the geotechnical properties and stability of critical slopes of the Town Bush Valley. The study further aims to determine the influence of seasonal groundwater changes and surcharge loads, on the stability of selected slopes using a probabilistic approach.

1.2 Problem Statement

The talus deposits of the Town Bush Valley are subject to downslope creep. The inherent heterogeneous nature of the soil, groundwater conditions and incised features created by palaeo-drainage incisions along with the geological arrangement of lithologies in the study site is conducive to mass wasting processes. Destabilizing forces in the form of anthropogenic activities and seasonal groundwater table fluctuations can easily upset the natural equilibrium processes operating on the Town Bush Valley.

1.3 Research Hypothesis

Steeply inclined slopes underlain by talus material in the Town Bush Valley exist in a delicate state of natural equilibrium. Increase in the groundwater level brought about by seasonal changes and the application of surcharge loads in the form of structural developments will result in slope instability. The use of a probabilistic approach to slope stability analyses accounts for the variability in material properties and affords a degree of reliability in the results obtained.

1.4 Aim and Objectives

The overall aim of this research is to investigate the prevailing geotechnical conditions at the Town Bush Valley and assess the stability of selected slopes on site.

The specific objectives of the investigation are:

- To establish the geological environment and conditions that gave rise to the deep talus deposits in the Town Bush Valley.
- To conduct a review on previous case studies on causative factors that have resulted in slope failures in the talus material of the Town Hill Escarpment.
- To undertake a geotechnical characterization of the area and determine the geotechnical parameters of the talus material.

- To construct cross-sections of critical sections of the Town Bush Valley based on available data sets, supplemented by data verification points.
- To conduct slope stability analyses on critical cross-sections using a deterministic and probabilistic approach, using the Rocscience Inc. SLIDE (2016) software.
- To evaluate and assess the reliability of the results obtained during probabilistic slope stability analyses.

1.5 Dissertation Structure

This dissertation is organized in six chapters. Each chapter presents specific but interlinked aspects of the study. The contents of the six chapters are briefly summarized as follows:

CHAPTER 1: *Introduction*

The introductory chapter presents a detailed overview of the general background setting of the study site. The chapter presented the basis on which the study was undertaken. In addition, the chapter discusses the research rationale, the problem statement, aim, objectives and structure used in the study.

CHAPTER 2: *Description of the Study Area*

This chapter presents the geographical setting of the study area its topography, terrain morphology, climatic and drainage conditions. Particular attention is given to the terrain morphology in which a digital elevation model is presented. The geological conditions of the study site are discussed from an overview to a site-specific level. The hydrogeological conditions are discussed, which includes the presentation of a conceptual model.

CHAPTER 3: *Literature Review*

A literature review was conducted on the concept of slope stability with attention being given to a probabilistic approach. The chapter further details the basic mathematical principles and approximation methods that are used in a probabilistic approach. The conditions for slope stability analyses and various material properties are presented. Selected slope stability case studies conducted in the Town Bush Valley are presented along with laboratory datasets obtained from historical tests.

CHAPTER 4: *Methodology*

The scientific framework and methods used to undertake the study is described in this chapter. It presents the methodology used during data collection, collation and verification. The chapter discusses the distribution of data points used to investigate and evaluate the ground conditions. The basic methods and standards used during soil sampling and laboratory testing are presented. Furthermore, the approach taken during limit equilibrium modelling and the parameters required for slope stability analyses, are presented.

CHAPTER 5: *Results and Discussion*

This chapter presents the results of the geotechnical characterization of the study area. These include a detailed discussion on the geological, hydrogeological and geotechnical conditions prevailing in the study area. Furthermore, the results of the laboratory tests are presented. The discussion is weighted around slope stability analyses, which are undertaken under various scenarios. The chapter culminates in an assessment of the probability of failure of selected slopes, with emphasis on critical conditions that may cause failure.

CHAPTER 6: *Conclusion and Recommendations*

The conclusion amalgamated the purpose of doing the research with the main findings of the study. The chapter presents important points concluded in each section of the study. Furthermore, it presents areas of further research.

CHAPTER 2

DESCRIPTION OF THE STUDY AREA

2.1 General description of the study area

2.1.1 Location

The Town Bush Valley is situated in the suburb of Montrose, approximately 6.50 km north-west of central Pietermaritzburg, KwaZulu-Natal province, South Africa (Figure 2.1).

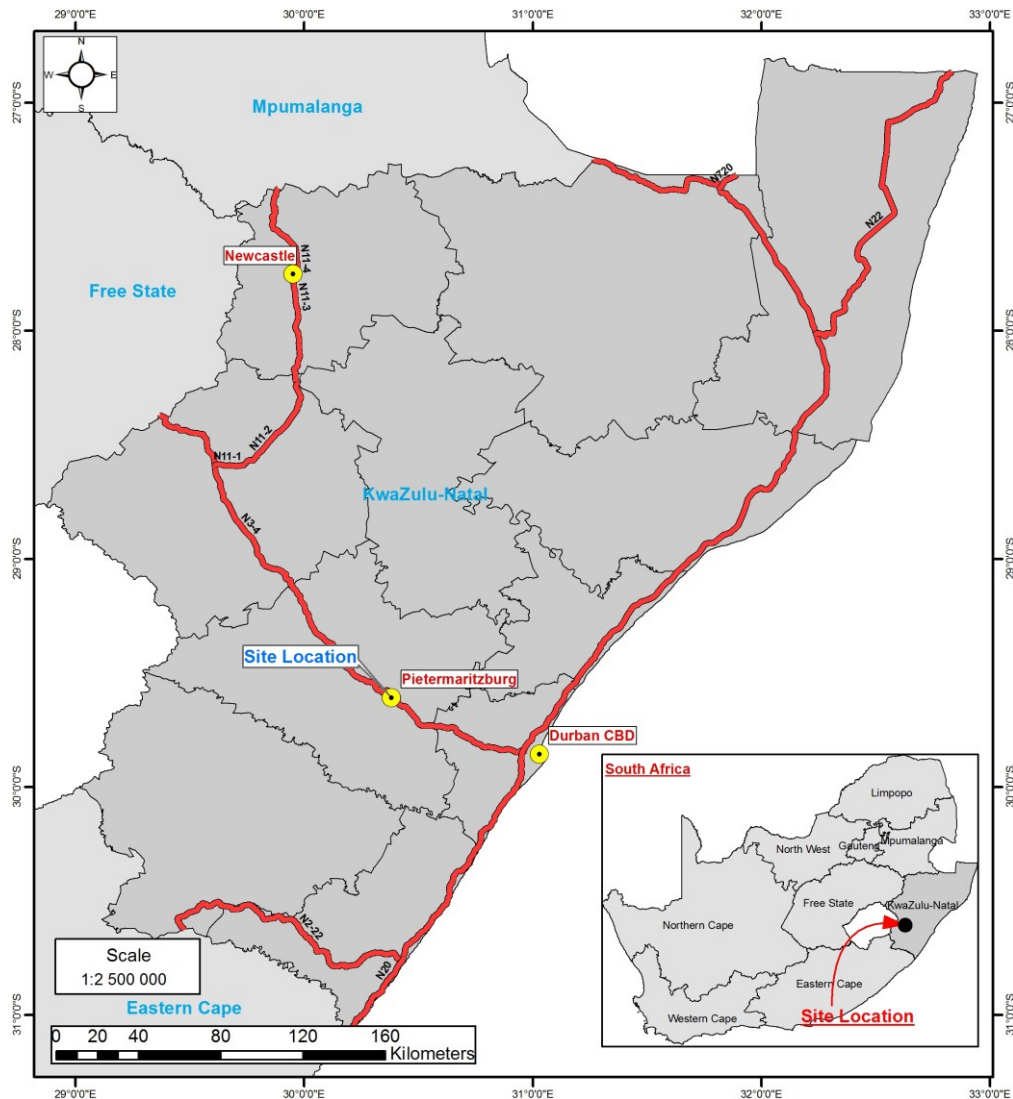


Figure 2.1: Location map of the Town Bush Valley.

The study area was formally known as the Queen Elizabeth Park which formed part of the Natal Parks Board property until 2004. For confidentiality issues and for the purpose of this dissertation, the study area has been divided into five developments as illustrated in Figure 2.2. These five subdivisions have been proposed by the developer with the internal border sub-divisions between developments. The northern portion comprises the main residential area which has been denoted the Cascades Development. The eastern portion situated close to the suburb of Montrose, comprises mainly office

blocks and has been denoted the Montrose Park Development (MPD). The smaller southern portion of the study area, which buffers the N3 National highway and lies near World’s View, has been denoted the World’s View Development (WVD). The developments located in the western portion of the study area adjacent to the Queen Elizabeth National Park have been split into the Upper National Park Development (UNPD) and the Lower National Park Development (LNPD). In addition, the peripheral land falling outside the study area adjacent to UNPD and LNPD, remains property of the Natal Parks Board. The five mentioned village developments ultimately culminate to form what is colloquially known as the Town Bush Valley which covers an approximate area of 1.90 km².

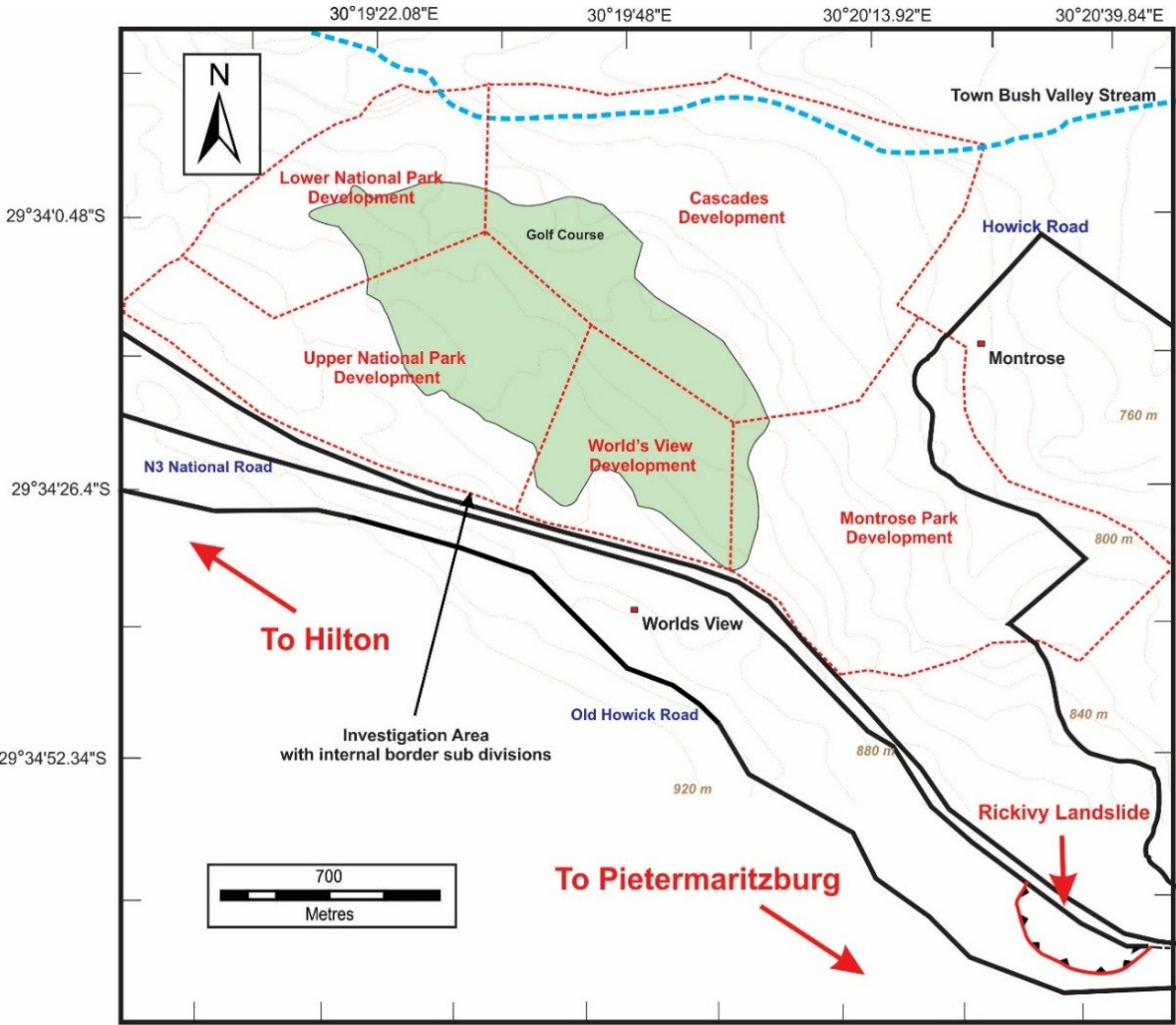


Figure 2.2: Town Bush Valley site plan.

2.1.2 Topography

The Town Bush Valley occupies the middle to lower, north-east facing slope of the Town Hill Escarpment. The morphology ranges from convex to concave. The elevation ranges from 790 to 950 m above mean sea level (mamsl). The hummocky landform generally dips towards the north-east, with natural slopes in the escarpment ranging from nearly flat to 18°. A digital elevation model (DEM) was developed for the Town Bush Valley study area and is shown in Figure 2.3 (spatial resolution: 2 m, vertical accuracy: 5 m). A DEM augmented by geotechnical information is an important tool used in

reconnaissance-level regional geological hazard analysis (Haneberg, 2004). The DEM presents a visual interpretation of the various landforms and slope geomorphologies in the Town Hill Escarpment and indicates the general decrease in elevation from the south-west to the north-east. An analysis of localized topographic variances suggests the strong prevalence of hummocky topography which is inferred to be micro-relief structures in the form of depressions and slumps, which mantle the slopes of the Town Bush Valley.

The DEM (Figure 2.3) is presented at an oblique angle in order to highlight the inclined slopes of the Town Bush Valley. Elevated areas in which slopes exceed 18° tend to form curvi-linear patterns on the high slopes near World's View on the south-western slopes. A concentrated matted pattern of slopes exceeding 18° is present in Chase Valley on the northern slopes, which attains similar elevations to World's View. The pattern gives an indication as to the hillslope processes operating in the Town Bush Valley as well as the way talus accumulates and deflects in the study area. Areas of deep talus accumulation on steep slopes, are potentially prone to slope stability issues.

Steeply inclined slopes, some of which exceed 18° and follow contour lines, are present in the study area in the Montrose Park Development (MPD), World's View Development (WVD), Lower National Park Development (LNPD) and Upper National Park Development (UNPD).

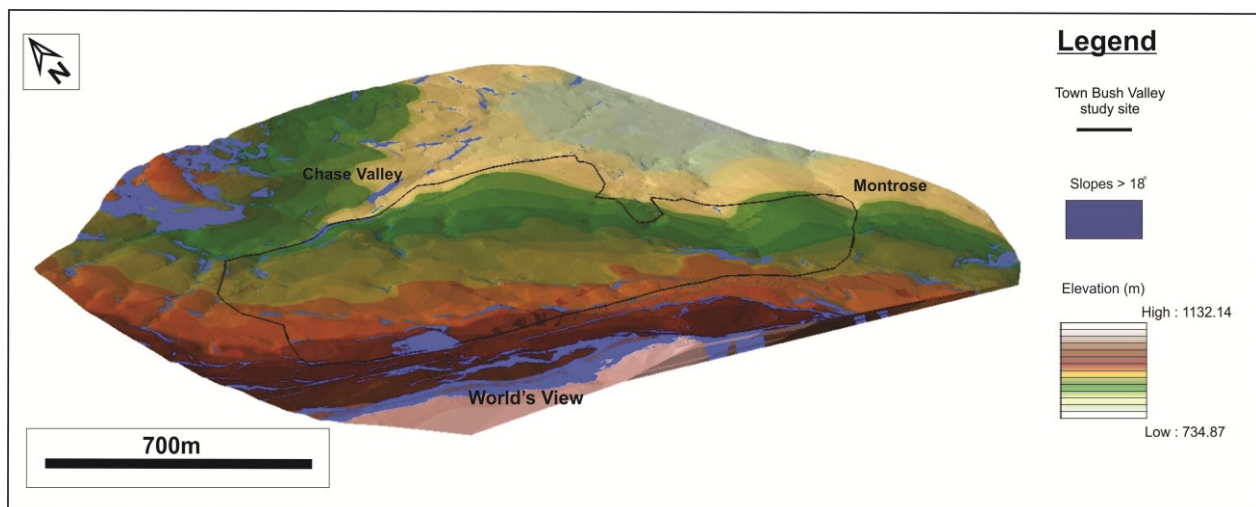


Figure 2.3: Digital elevation model of the Town Bush Valley, indicating slopes $> 18^\circ$.

2.1.3 Terrain evaluation

The topography and morphology of the Town Bush Valley has been shaped by colluvial and fluvial processes over a period of geological time. Richards *et al.* (2006) pointed out that the hummocky topography around the World's View to Otto's Bluff Escarpments and the Mpumzuza area in Pietermaritzburg is underlain by ancient landslide debris, which is potentially erodible and unstable. In addition, there are many instability features associated with these colluvial hillslope deposits. Richards *et al.* (2006) further added that micro-relief processes in the form of mass wasting occurs in the form of creep movements, debris slides and slumps. These processes are a direct result of changing equilibrium conditions caused by the incision of gullies, climatic change and anthropogenic activities.

Natural slope obstacles within individual slopes such as gullies, streams, sandstone platforms and dolerite ridges, would deflect downslope mass movement (Price, 2006). This will result in some areas being more receptive to debris accumulation than others and therefore zones with deeper talus accumulation (Price, 2006). Colluvial and alluvial deposits generally overly the bedrock of the lower slopes and valley bottoms of the Town Hill Escarpment and extends along the former floodplains of the Msunduzi River and its tributaries (Maud, 1981).

The main geotechnical problem in the study area is slope instability as shown in Figure 2.4. The Council for Geoscience (2008) classified the study area as having active mass movement and unstable slopes. In areas where slope gradients exceed 18°, there are not only limitations to development but a likelihood of slope instability (Richards *et al.*, 2006). The geotechnical map also indicates areas of mass movement where the potential for slope instability exists as these slope gradients exceed 18°.

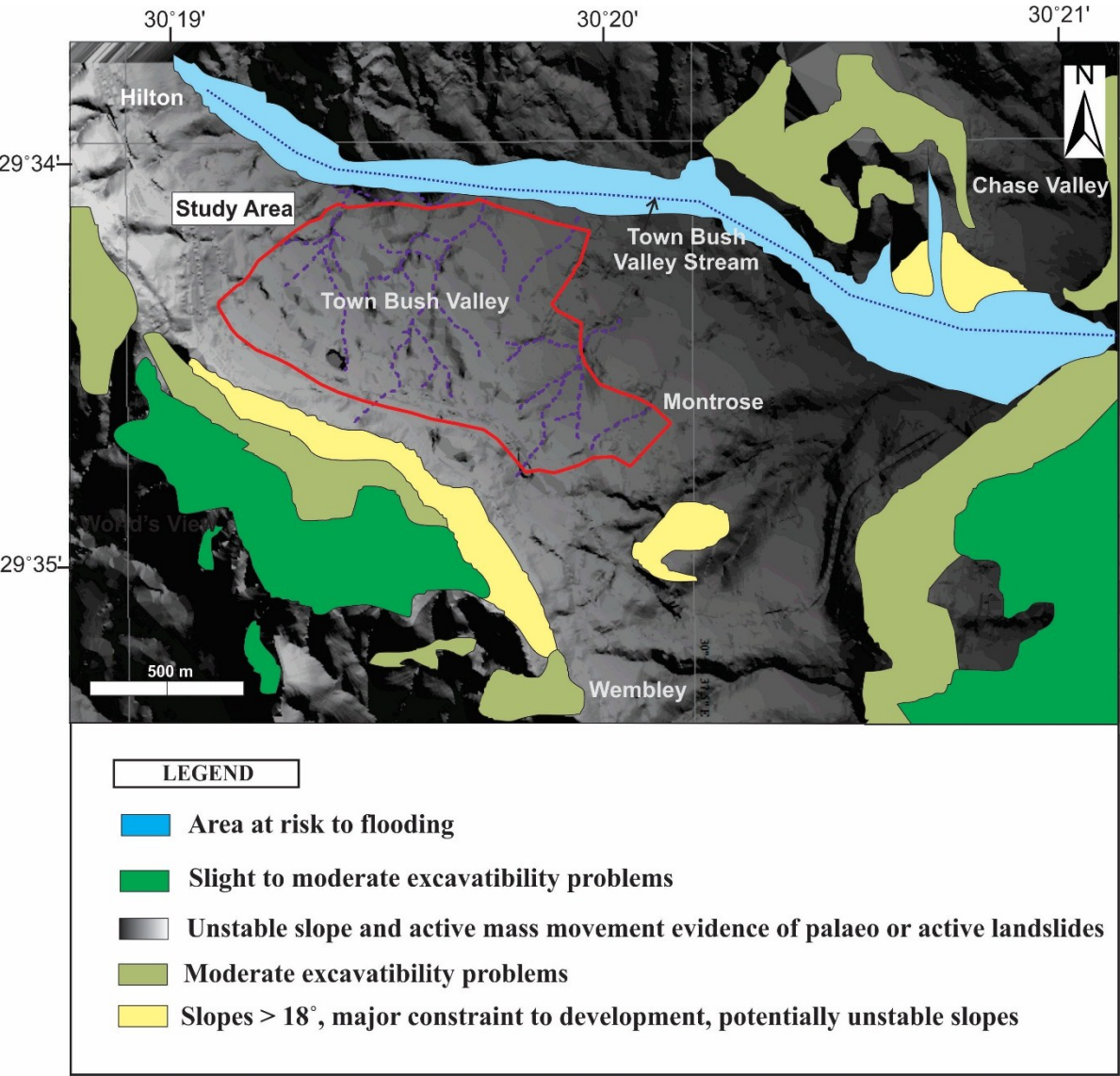


Figure 2.4: Geotechnical map of Pietermaritzburg highlighting areas of geotechnical limitations to development based on the 1: 50 000 Geotechnical Series 2930CB Pietermaritzburg.

2.1.4 Climate and drainage

The region is characterized by a subtropical climate with warm summers and moderately dry winters. The area receives about 695 mm of rainfall annually, with most rainfall occurring mainly during mid-summer. The study area falls within the Quaternary Catchment U20J and is located in rainfall zone U2D and evaporation zone 30B (Department of Water and Sanitation, 2015). Pietermaritzburg receives the lowest rainfall in June (6 mm) and the highest in January (112 mm). The average midday temperature for Pietermaritzburg ranges from 20.5°C in June to 27°C in February. Figure 2.5 summarizes the climatic conditions of the city of Pietermaritzburg.

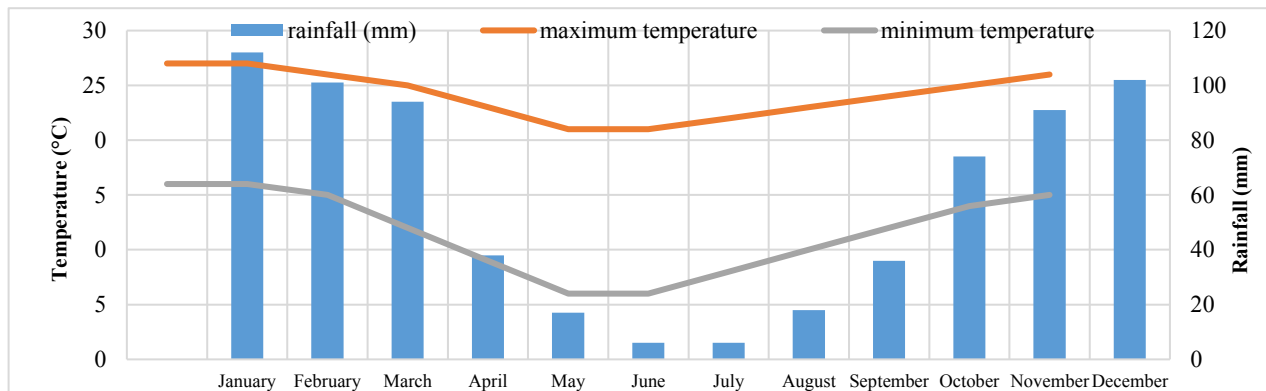


Figure 2.5: Mean monthly rainfall, maximum and minimum temperatures at Pietermaritzburg (source: SA explorer, 2015).

KwaZulu-Natal receives more rainfall than most parts of southern Africa, the majority of which falls in the summer months (Maurenbrecher & Booth, 1975). Figure 2.6 presents the average minimum and maximum temperatures over a ten-year period (2005-2010) recorded at the Cedara weather station (02394820) located in Cedara, Pietermaritzburg approximately 5 km from the study site. Figure 2.6 further presents a summary of the average rainfall conditions recorded at the Cedara weather station for the period of 2005 to 2010. Climatic data was acquired from the South African Weather Services (SAWS) the data spans from 2005 to 2010.

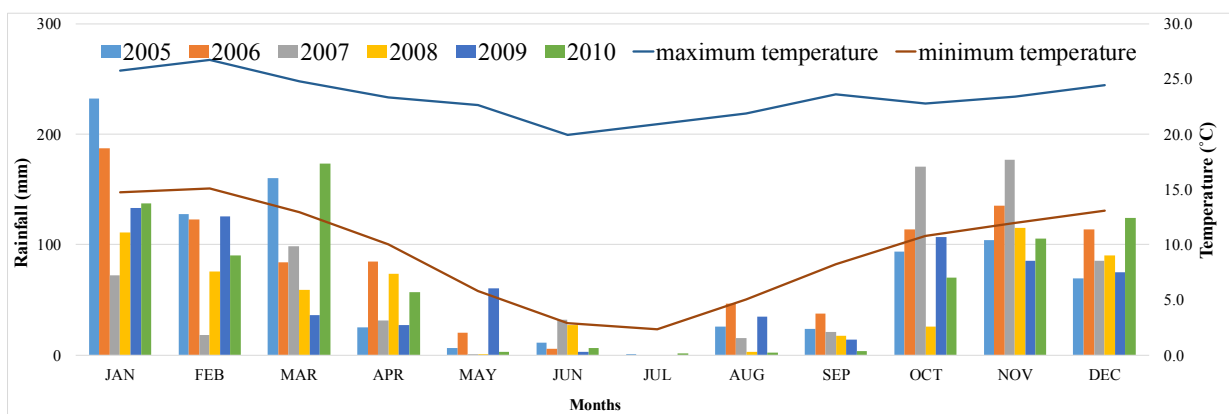


Figure 2.6: Average monthly rainfall, maximum and minimum temperature range from 2005 to 2010 (SAWS, 2015).

From the temperature data, the maximum temperatures generally peak over the months of December to February, where temperatures range between 23°C to 27°C during the summer months. The minimum temperatures are generally recorded over the winter months of June and July, where temperatures range between 1°C and 4°C.

A review of historic data obtained from the Cedara weather station indicate significant rainfall events in which the rainfall exceeded 100 mm were recorded in the years of 1958, 1971 and 1987. The former mentioned years noted significant flooding conditions, particularly during the year of 1987 when KwaZulu-Natal experienced its highest recorded rainfall to date.

The rainfall data indicates that the Town Bush Valley receives its highest rainfall during the warm, summer months of November to February. Over the ten-year period, January 2005 recorded the highest rainfall of 232 mm. This is followed by March 2010, which recorded 174 mm of rainfall. The year of 2006 received on average the highest annual rainfall (79 mm) over the ten-year period. Although a mild annual decrease in the rainfall pattern was observed over the ten-year period, sporadic and heavy monthly rainfalls offset the recorded average values. These sudden heavy rainfall events are few and isolated but are prevalent during the present years of 2010 to 2016.

KwaZulu-Natal is one of the few areas on the subcontinent where the annual rainfall exceeds the potential loss by evapotranspiration (Weinert, 1980). The Town Hill Escarpment is frequently covered in mist and consequently as a result the study site is subject to high humidity and frequent drizzle.

The Town Bush Stream is aligned perpendicular to the Town Bush Valley and has been identified as the central drainage feature which flows in a north-easterly direction and is shown in Figure 2.7.



Figure 2.7: The Town Bush Stream with boulder dolerite in the alluvial channel derived from talus material.

A network of second and third order drainage features link up to the Town Bush Stream. This concept is illustrated in Figure 2.8, which represents a drainage map done by the author for the Town Bush Valley.

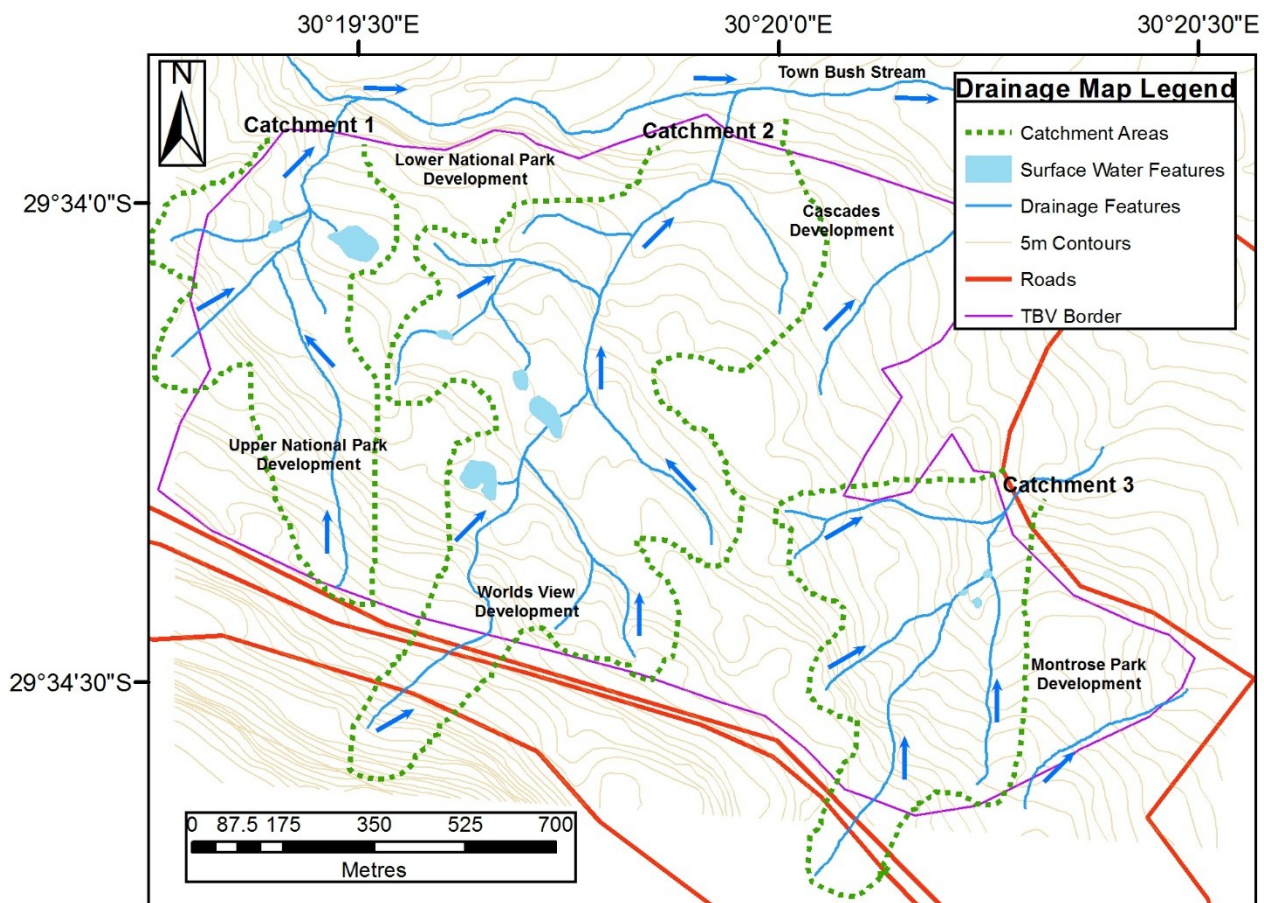


Figure 2.8: Drainage map indicating surface water flow directions.

Catchment areas denoted as Catchment 1 to Catchment 3 in Figure 2.8, define several second and third order drainage features which extend up the southern slopes of the Town Bush Valley. Two prominent drainage features drain the LNPD and UNPD, while the WVD is drained by a single drainage line.

Aerial photographic interpretation of the 1:10 000 scale orthophoto map of Pietermaritzburg acquired in 2015 indicates a drainage line, which commences in the WVD and dissects the Cascades Development, ultimately linking up to the Town Bush Stream. These drainage features can be traced up the Town Hill Escarpment and are defined by incised drainage channels.

A review of the 1936 (1:25 000 scale), 1967 (1:25 000 scale) and 2006 (1:50 000 scale) topographic maps acquired in 2015 suggests that these features perpendicularly cross contours with their flow directions governed by the hummocky topography, which is further expanded on in Chapter 3. The valley slopes of the MPD are drained by three streams. The main drainage feature, which cross-cuts the N3 highway above the MPD, is orientated in a north-east direction.

These documented drainage features have had a profound effect in shaping the landscape of the Town Bush Valley. These drainage features are sometimes discontinuous in nature and are concentrated along localized depressions of boulder-rich talus variants as documented by Allen (1981) and Singh (2016). These discontinuous features emphasize the erratic and unpredictable nature of the subsurface drainage system, which can cause subsoil erosion. This can lead to the formation of “softer” and weaker zones in the talus material, which can initiate slope instability

2.1.5 Vegetation

The vegetation on site consists of a mixture of low to high lying grass and dense pockets of woodland which intersperse the study area. Dense vegetation tends to buffer drainage features. Prior to development of the study site, the Town Bush Valley was occupied by wattle and gumtree plantations.

2.2 Regional Geological Setting

The regional geology of central KwaZulu-Natal, South Africa, is dominated essentially by the Karoo Supergroup which spans in age from 300 Ma to 178 Ma (Hunter *et al.*, 2006). Magmatic arcs were the provenance areas of turbiditic and deltaic Ecca Group and Beaufort Group sediments (Johnson, 1991). The Ecca Group is renowned for its coal-bearing facies, formed in shallow-marine, deltaic and fluvial environments (Hunter *et al.*, 2006). The Ecca Group is of Late Palaeozoic age and in the north-eastern region comprises the Pietermaritzburg Formation, the Vryheid Formation and the Volksrust Formation. At about 180 Ma, large extensive basaltic volcanism terminated the Karoo sedimentation. This coincided with the fragmentation of Gondwana, which also marked the intrusion of numerous dolerite dykes and sills. These geological successions are capped by Cenozoic deposits.

2.3 Local geology of the Town Bush Valley

The Town Bush Valley is underlain by micaceous sandy, lenticular bedded siltstone and sandstone of the Vryheid Formation. The various lithofacies of the Vryheid Formation are observed in an upward coarsening cycle which is deltaic in origin.

Typical coarsening upward successions of deltaic deposits essentially consist of muddy siltstone resulting from shelf suspension overlain by alternations of immature sandstones, dark siltstone and mudstone (Johnson *et al.*, 2006). Fining upward fluvial cycles with sheet-like geometry are often truncated by reactivation surfaces and scours either meandering or braided rivers (Le Blanc Smith, 1980).

In the study area, this is underlain by massive to laminated carbonaceous siltstone and shale of the Pietermaritzburg Formation. The Pietermaritzburg Formation forms the basal unit of the Karoo Supergroup and overlies the Dwyka Group. The Pietermaritzburg Formation consists of monotonous greyish-brown, slightly sandy shales, becoming progressively more clayey and mica rich towards the top (Maurenbrecher & Booth, 1975).

In addition, heavily bioturbated and penecontemporaneously deformed sandy and silty beds are noted at the top of the formation (Johnson *et al.*, 2006). In the Pietermaritzburg area, the Pietermaritzburg Formation and Vryheid Formation are about 330 m and 250 m in thickness respectively (Maurenbrecher & Booth, 1975).

These sequences have been intruded by fine-grained dolerite sills of varying thicknesses. The entire sequence is capped by massive, unsorted slumps and talus deposits of 6.00 m to 20.00 m in thickness. Deposits from mass wasting processes are widespread throughout South Africa and are derived from areas of topographic relief. Most are relatively thin deposits and comprise talus, colluvial gravel or pedisediment (Partridge *et al.*, 2006). In central and northern KwaZulu-Natal, thick unconsolidated colluvial deposits bury bedrock pediments on the lower hillslopes (Partridge *et al.*, 2006). These colluvial sediments are thought to accumulate during the sheetwash transport of sediment derived from the erosion of soils and talus on the upper slopes during the Late Pleistocene and Holocene (Botha & Partridge, 2000). The variation in profile characteristics of the palaeosols points to changing drainage conditions. Climatic change in the region led to periods of instability on hillslopes during which soils were eroded, dongas incised and colluvium accumulated on the lower slopes (Partridge *et al.*, 2006).

Table 2.1 presents the stratigraphic sequences preserved in the study area. Figure 2.9 shows a geological map illustrating the major geological successions present in the Pietermaritzburg area.

Table 2.1: Stratigraphic sequences preserved in the study area.

Era	Period	Lithology		Typical description	Mode of deposition	Thickness	
Cenozoic	Quaternary	Colluvial/ Talus deposit		Fine sandy, silty, clay mixed with residual Ecca Group bedrock fragments and dolerite & sandstone boulders	Colluvial	15-24 m	
Mesozoic	Jurassic		Dolerite sill	Medium-coarse grained crystals	Igneous Intrusion	3-8 m	
Palaeozoic	Permian	Karoo Supergroup	Ecca Group	Vryheid Formation	Sandstone, siltstone, shale	Fluvial	250 m
				Pietermaritzburg Formation	Mudstone, shale, siltstone	Fluvial	330 m

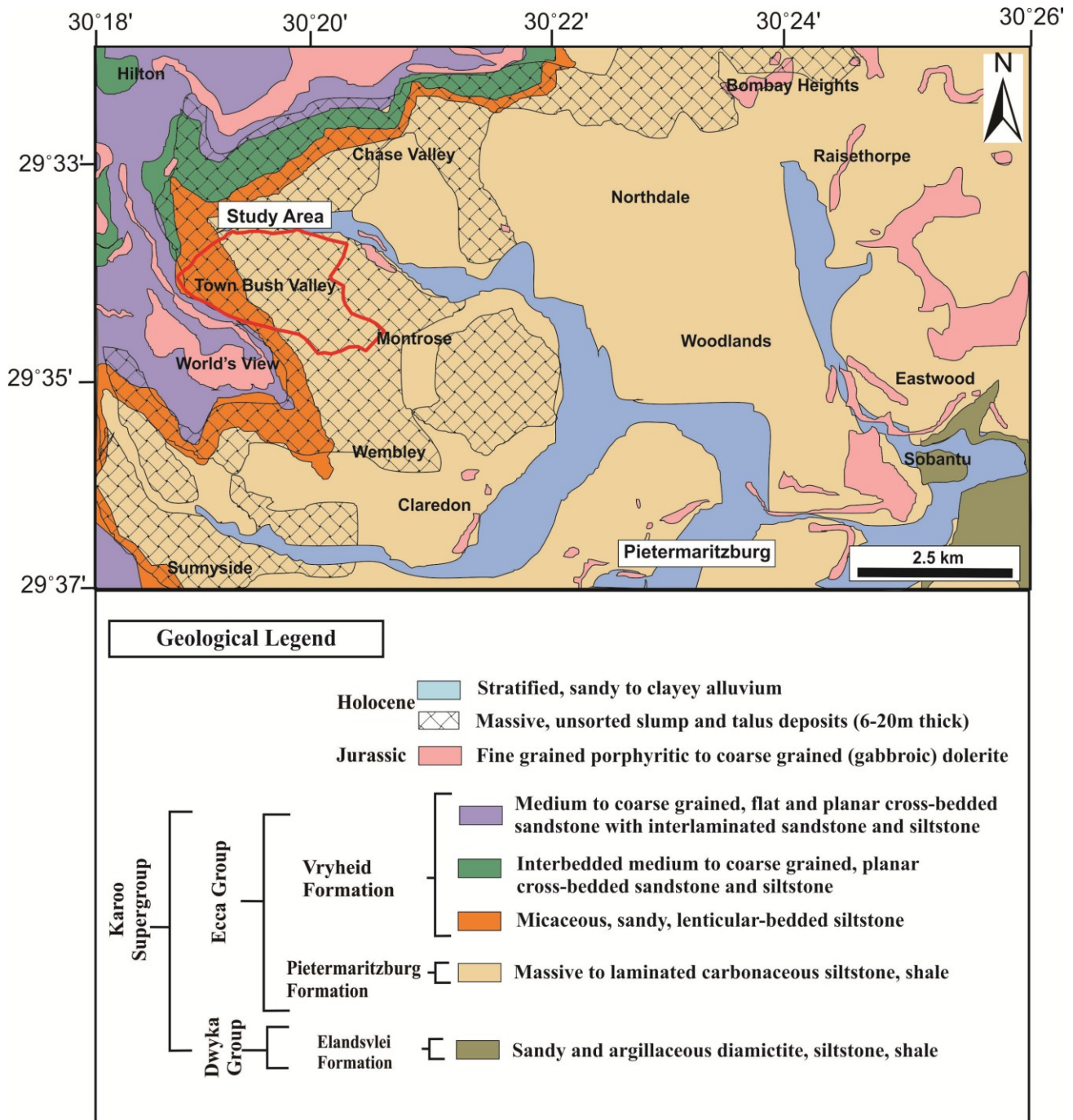


Figure 2.9: Generalized geological map of the Pietermaritzburg region based on the 1:50 000 Geological Series 2930CB Pietermaritzburg.

A site geological map has been produced and is presented in Figure 2.10. The map has been compiled based on sub-surface investigation results (borehole drilling, augering & trial pitting) and geological field mapping. The primary geological units, namely the Pietermaritzburg Formation, Vryheid Formation, dolerite intrusives and talus material are discussed in the following subsections in context with Figure 2.10.

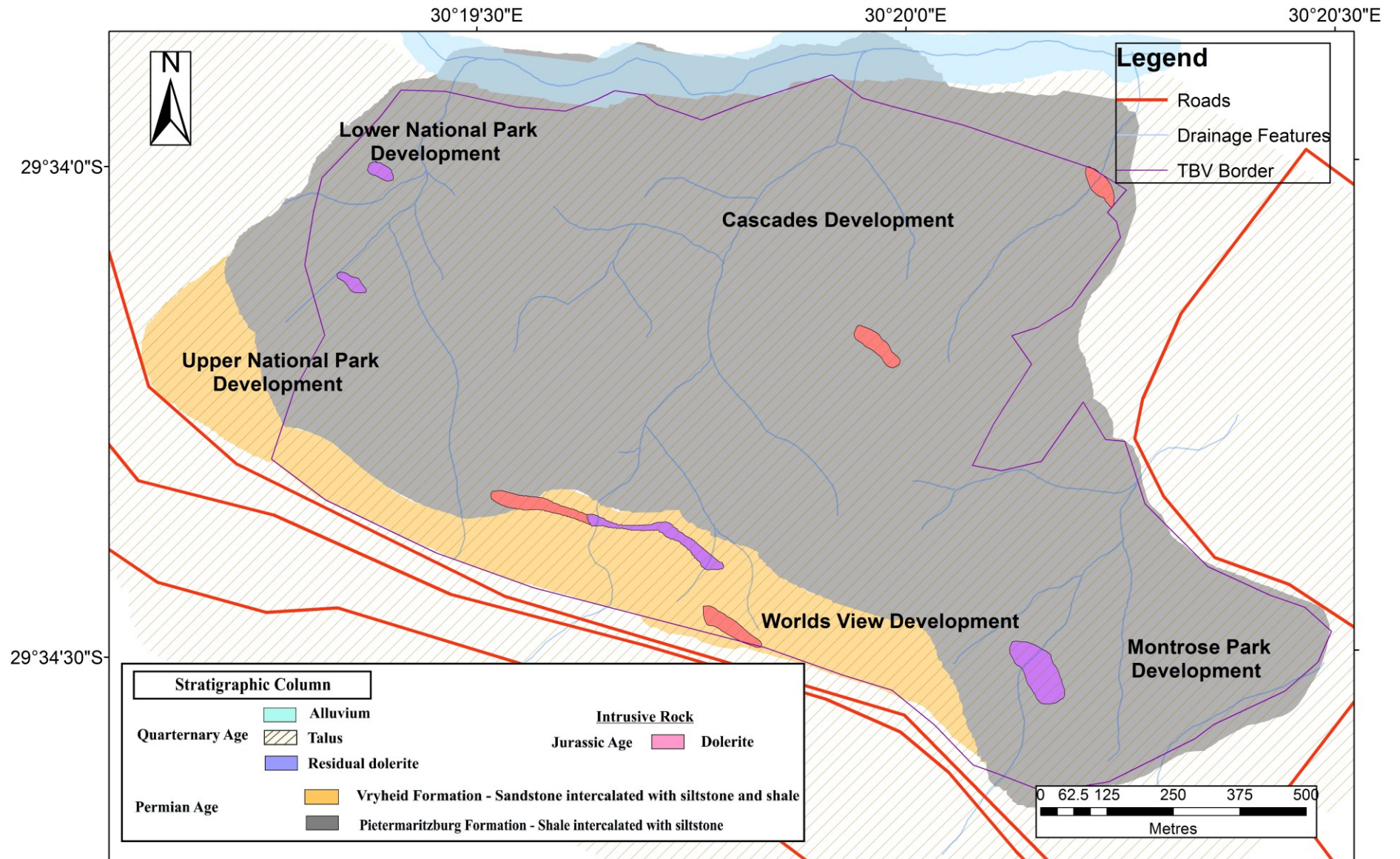


Figure 2.10: Local geological map of the study area.

2.3.1 Ecca Group

The Town Bush Valley is underlain by the Ecca Group which is represented on the mid to lower slopes by the Pietermaritzburg Formation, which in turn is capped by the Vryheid Formation on the high slopes.

The bedrock geology, which predominates the northern, western and eastern portions of the study area, consists of the Pietermaritzburg Formation. According to Price (2006), the Pietermaritzburg Formation mostly dips gently towards the north-west. Drilling investigations undertaken in the study area indicates that the Pietermaritzburg Formation is represented by shale intercalated with lenses of siltstone, which is preserved in the UNPD, LNPD, MPD and Cascades Developments. More specifically, shale bedrock of the Pietermaritzburg Formation is prominent in the south-western portion of the UNPD and south-eastern portion of the Cascades Development. Unweathered shale bedrock is preserved on the toe slopes of the MPD at depths of 20.00 m below natural ground level (NGL).

A continuous sequence of residual siltstone intercalated with sandy lenses of residual sandstone, caps the Pietermaritzburg Formation Shale bedrock. This sequence underlies the western and south eastern portion of the study site corresponding to the UNPD, LNPD, MPD and Cascades Developments.

On the higher slopes of the escarpment, the Pietermaritzburg Formation is conformably overlain by the more erosion resistant micaceous sandstones of the Vryheid Formation. The Vryheid Formation predominates the south-western region of the Town Bush Valley study site. The younger overlying Vryheid Formation has a shallow dip (1° - 5°) to the west and north-west (Price, 2006). During geological mapping undertaken for this particular study, it was observed that the bedrock of the Vryheid Formation generally trends in a north-west to south-east direction in the study area. Sandstone of the Vryheid Formation forms the basal bedrock unit of the WVD, with various intercalated sequences of siltstone (silty lenses) and shale preserved in the sandstone. More specifically, sandstone with siltstone intercalations (silty lenses) predominate the eastern portion of the WVD, at depths greater than 17.00 m below NGL.

2.3.2 Karoo dolerite intrusives

A review of the 1945 geological map compiled by the Geological Survey Office depict several sills that outcrop in the Town Hill Escarpment. These are not reflected on the more recent map versions by the Council for Geoscience in 2002. It is inferred that these once “thick” dolerite rock units have been masked by a combination of colluvial and fluvial processes. Colluvial processes have possibly resulted in the partial burial of these intrusives while fluvial processes have resulted in the erosion of these lineaments in the recent geologic past.

Some intrusions appear to be continuous and extend over large areas while others appear to be localised. Figure 2.11 illustrates a prominent dolerite sill located above the study area (1.7 km west), which characterises the typical elongated appearance of the dolerite sills in the Town Bush Valley.

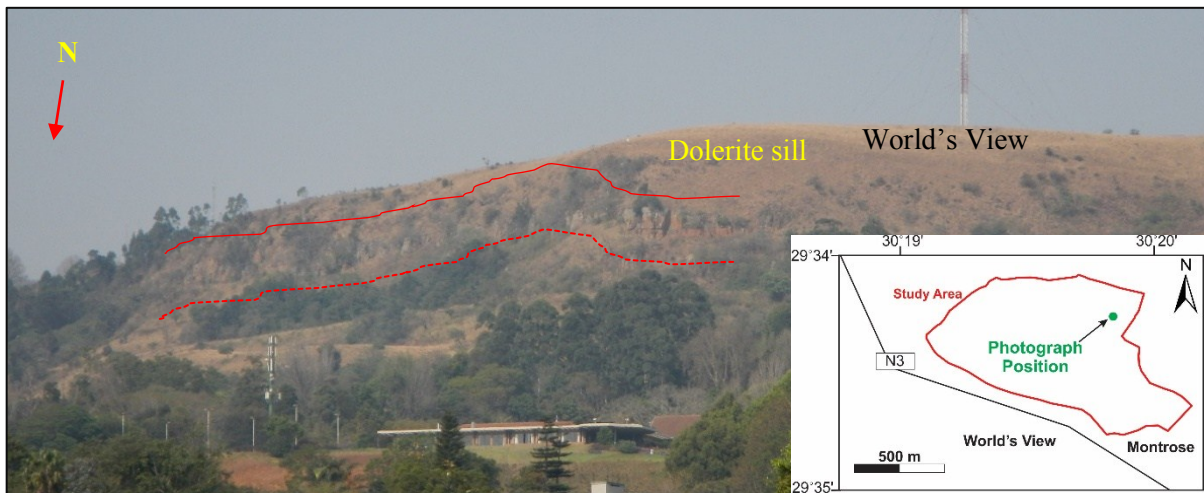


Figure 2.11: A dolerite sill observed from the Town Bush Valley looking towards World's View.

Borehole drilling investigations indicate residual dolerite horizons which are preserved in the north-western and south-eastern portion of the Town Bush Valley. The residual dolerite displays a coarse texture and is generally preserved in the study site as dolerite corestones in a clay matrix. This forms as a result of deep *in-situ* weathering processes operating on the dolerite bedrock over a period of geological time

Competent dolerite bedrock is preserved in the form of inclined sills in the Town Bush Valley. A dolerite sill trending in a north-west orientation underlies the southern region of the study site. Furthermore, a dolerite sill is also preserved in the south-western region, partially transecting the UNPD.

The north-eastern portion of the study site has two dolerite sill sequences positioned in the Cascades Development. They are inferred to have an irregular shape and the geological arrangement of the dolerite sill near the north-eastern boundary of the Cascades Development, suggests it intrudes the sedimentary rocks of the Pietermaritzburg Formation (Schreiner, 2005b).

2.3.3 Colluvial hillslope deposits

Thick colluvial and talus deposits mantle the hillslopes on the escarpment in Pietermaritzburg, with the term talus used to differentiate a coarse, immature colluvial variant (boulders, residual rock fragments) from the finer textured colluvial (gravel) deposit. These late Pleistocene to Holocene aged colluvial deposits are responsible for hillslope instability and deep donga erosion (Richards *et al.*, 2006). The unconsolidated colluvial deposits are restricted to the steep transportational mid-slopes and toe-slopes on the escarpment in Pietermaritzburg, which is often defined by outcropping sandstones of the Vryheid

Formation or dolerite. Richards *et al.* (2006) recognized that the thicknesses of pedogenically-altered colluvium or slope deposits in Pietermaritzburg are highly variable and range in thickness from 1.50 m to greater than 16.50 m. The basal deposits of the colluvium are typically referred to as talus which comprise a poor sorting array of large dolerite boulders (0.20 m to 1.50 m) and shale fragments within a sandy or silty matrix, derived from reworking of talus or finer textured colluvial deposits upslope (Richards *et al.*, 2006).

Soil profiling undertaken according to the South African Institute of Civil Engineering guidelines for soil logging (SAICE, 2002) indicates that the soil texture of the talus material is generally described as a silty sandy clay or silty clayey sand. Gravel to cobble sized shale and dolerite fragments form part of the soil matrix. More notable is the occurrence of boulder sized dolerite fragments in the soil texture which have been noted in various silt and clay matrixes, as illustrated in Figure 2.12.

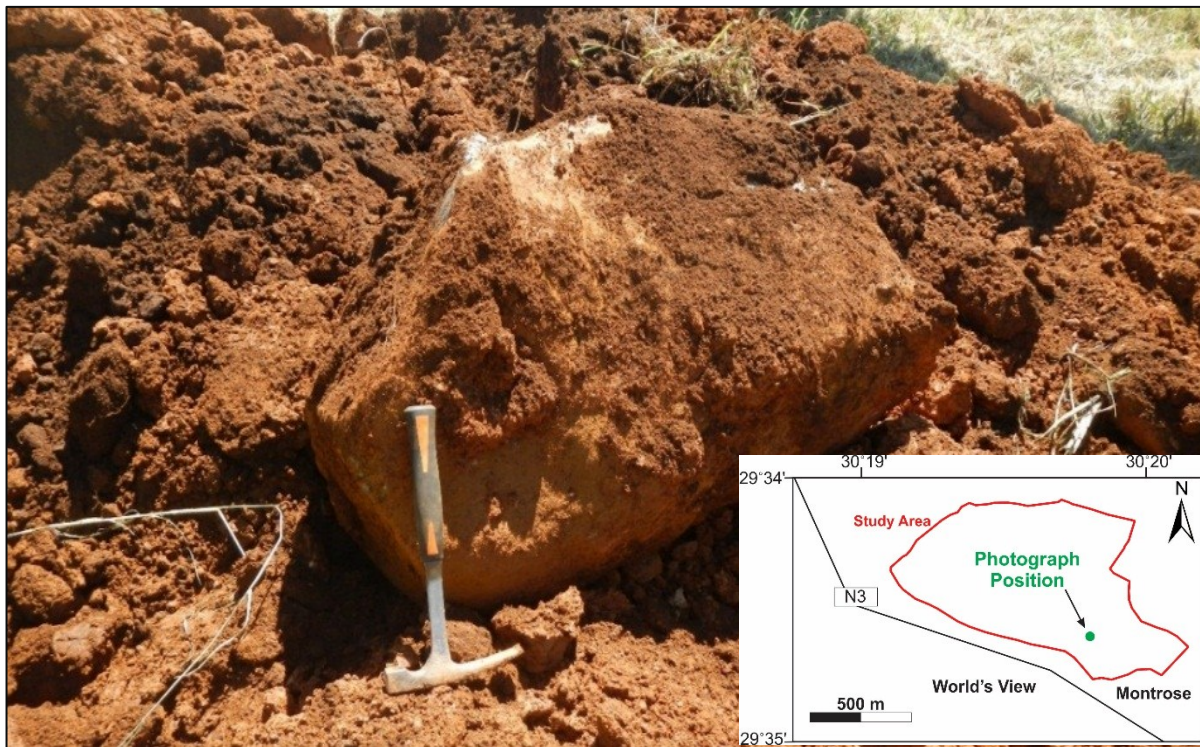


Figure 2.12: Boulders intersected in the talus horizon during trial pitting in the Montrose Park Development.

The high variability in the groundmass to fragment composition has resulted in the occurrence of numerous combinations of matrix supported or clast supported soil structures. The colluvial hillslope material includes talus deposits, which includes residual rock fragments preserved in their soil matrixes. The residual rock fragments and soils are derived from sandstone, siltstone and dolerite. These residual deposits are not seen as true residual soils, formed from *in-situ* weathering of bedrock, but large (> 6.00 m) rock fragments that are deposited as a result of the downslope movement of the soil. Richards *et al.* (2006) pointed out that the colluvium is derived by the erosion of older coarse talus, soils and

weathering profiles in bedrock, which accumulates through two transportational processes, namely mass movement and slope or sheetwash.

Based on the borehole profiles which is discussed in Chapter 5, the talus horizons of the MPD, UNPD, LNPD and Cascades Development generally extend to depths exceeding 21.00 m below NGL. Relatively, thicker talus deposits overlie the Cascades Development which are in the order of 12.00 m in thickness. The talus deposits forming the toe slopes of the Town Bush Valley are generally thicker than the talus soils forming the crest of the slope.

Topography is an important element in hillslope processes. Very steep terrain would result in material accumulating at the slope pediment but not much on the slope itself, and a flat terrain would result in localised talus deposition. The Town Hill Escarpment and slopes provide an initial steep terrain with progressively flatter slopes ideal for deep concentrations of talus (Price, 2006).

2.4 Hydrogeology

The hydraulic properties of the underlying soil and bedrock govern the way groundwater flows. It is important to differentiate the various aquifers and their hydraulic properties.

2.4.1 Aquifer Types

The nature and distribution of aquifers in a geological environment is controlled by the lithology and structure of the formations (Freeze & Cherry, 1979). The following types of aquifers occur in the study area:

Unconsolidated aquifer: The factors affecting the porosity of talus soil include particle size distribution, sorting, grain shape, degree of compaction, solution effects, mineralogical composition, particularly the presence of clay particles (Bell, 2007).

The talus material represents an unconfined aquifer system. The addition of grains of different sizes to such an assemblage lowers its porosity and this is directly proportional to the amount added (Bell, 2007). In a hummocky terrain, the presence of a basal aquifer system creates a highway for flow that infiltrates under the overlying local systems (Freeze & Cherry, 1979). Seepage is common in landslide debris and shallow depressions within hummocky topography are often filled with water (Richards *et al.*, 2006).

Intergranular fractured aquifer: The Sandstones of the Vryheid Formation represent a shallow aquifer system in the study area. The most common cementing material in sandstone bedrock is quartz, calcite and clay minerals (Freeze & Cherry, 1979). Freeze & Cherry (1979) suggests that the presence of small scale stratification in sandstone enables the permeability of very large samples to be uniformly anisotropic.

The shales and siltstones of the Vryheid Formation and Pietermaritzburg Formation represent a very low permeability, aquifer system in the study area. At depth, the shale aquifers are generally soft, with less fractures and a low permeability due to confining pressures. Typical values of hydraulic conductivity of intact shale samples tested in the laboratory rarely exceed 10^{-9} m/s and are commonly in the range of 10^{-12} to 10^{-10} m/s (Freeze & Cherry, 1979). Fractures in shale can impart a significant component of secondary porosity and permeability.

In igneous rocks, an appreciable amount of fracture permeability generally occurs within a couple of metres of the ground surface at a shallow depth.

Table 2.2 presents a summary of the various water bearing units present in the Town Bush Valley and their literature based hydraulic characteristics.

Table 2.2: General hydrogeological properties of water bearing units.

Lithology	Typical description	Water bearing unit (thickness)	Permeability range (k , Darcy) (Freeze & Cherry, 1979; Smith, 1990)	Hydraulic conductivity range (K , $m.s^{-1}$) (Freeze & Cherry, 1979)	Porosity range (n , %) (Freeze & Cherry, 1979)
Colluvial/ Talus deposit	Fine sandy, silty, clay with residual rock fragments and boulders	Aquifer (15-24 m)	10^2 to 10^{-2}	10^{-1} to 10^{-5}	35-50 (silty, sand)
Dolerite sill	Medium-coarse grained crystals	Aquifer (3-8 m)	10^0 to 10^{-3}	10^{-2} to 10^{-6}	0-10
Vryheid Formation	Fine grained sandstone,	Aquifer (20 m)	10^{-1} to 10^{-5}	10^{-4} to 10^{-8}	5-30
	Siltstone, shale	Aquifer (20m)	10^{-4} to 10^{-8}	10^{-7} to 10^{-11}	0-10
Pietermaritzburg Formation	Mudstone, shale, siltstone	Aquifer (200 m)	10^{-4} to 10^{-8}	10^{-7} to 10^{-11}	0-10

2.4.2 Hillslope hydrological processes and groundwater flow

Groundwater recharge can be defined as the entry into the saturated zone of water made available at the water-table surface, together with the associated flow away from the water table within the saturated zone (Freeze & Cherry, 1979).

Groundwater discharge can be defined as the removal of water from the saturated zone across the water-table surface, together with the associated flow towards the water table within the saturated zone (Freeze

& Cherry, 1979). Recharge and discharge areas in the study site is illustrated in Figure 2.13 (insets a, b, c). Groundwater flow is anticipated to flow through the unconsolidated talus material and along the talus and shale bedrock interface, representing an unconfined aquifer system.

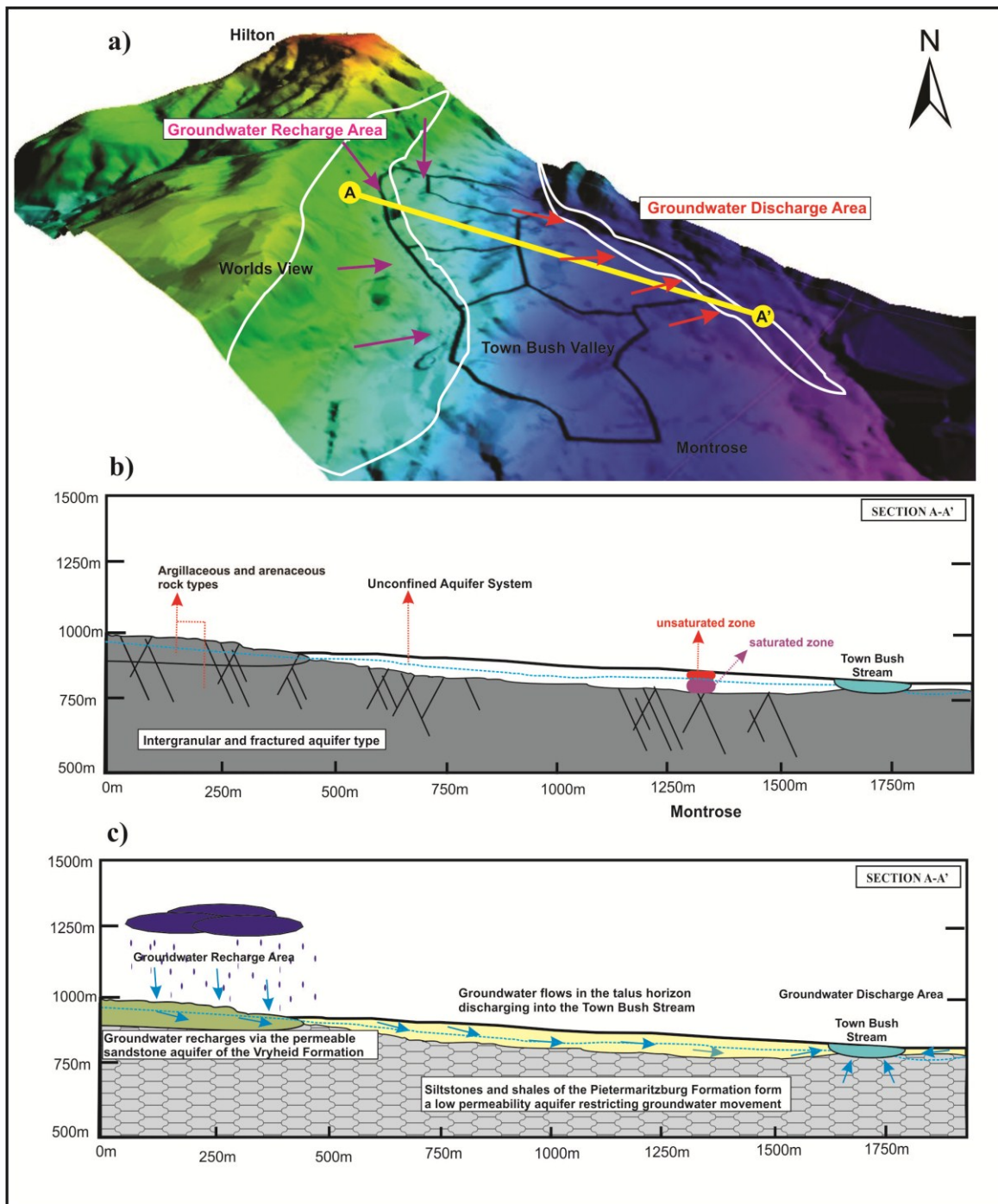


Figure 2.13: Town Bush Valley hillslope schematic presentation of groundwater flow.

Using points of measured groundwater levels, recorded mainly during the early spring season, contours were generated using the Surfer (version 8.0) software package. Figure 2.14 shows the interpolated groundwater table presented as depths below natural ground level. Figure 2.15 shows the interpolated groundwater flow directions which is presented as flow vectors.

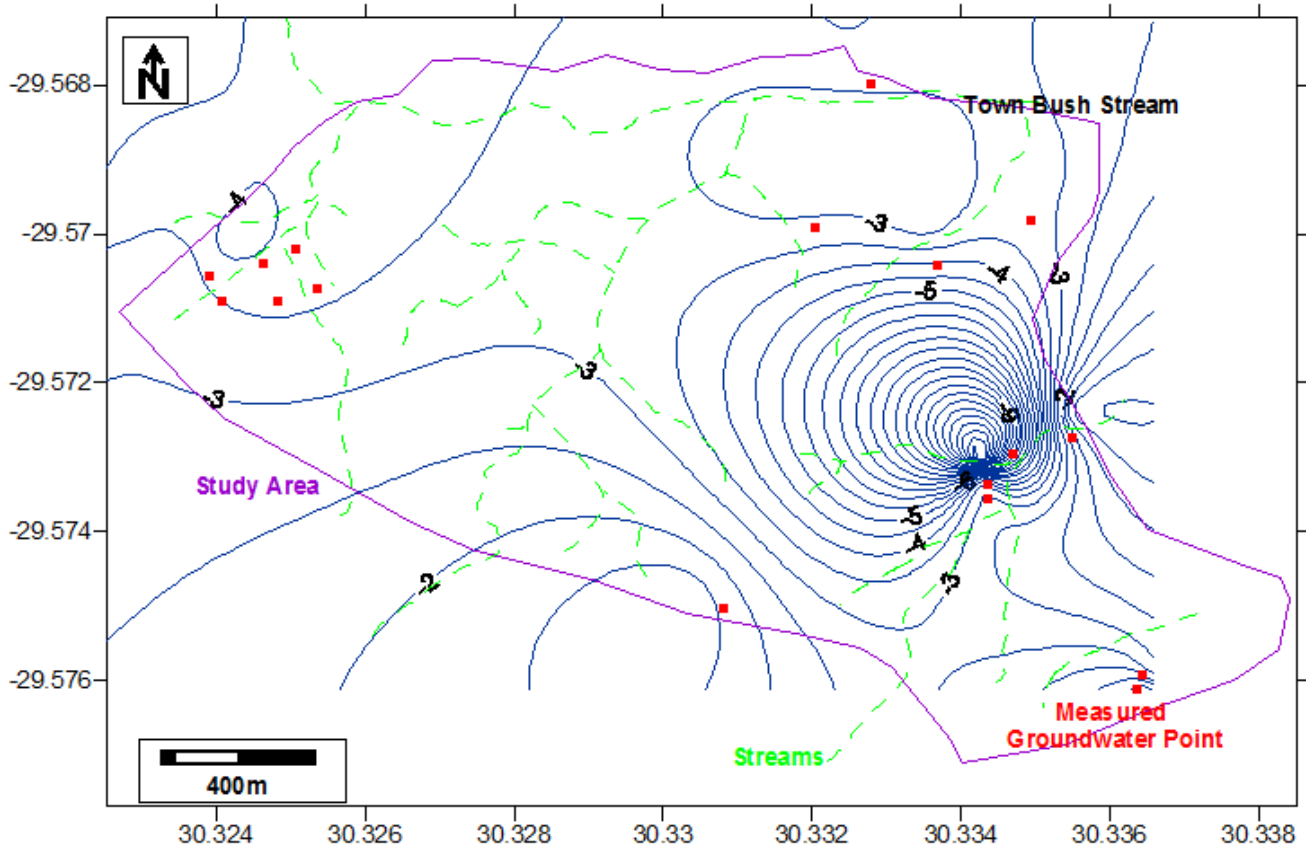


Figure 2.14: Contour map showing the depth to the groundwater table below natural ground level in Town Bush Valley.

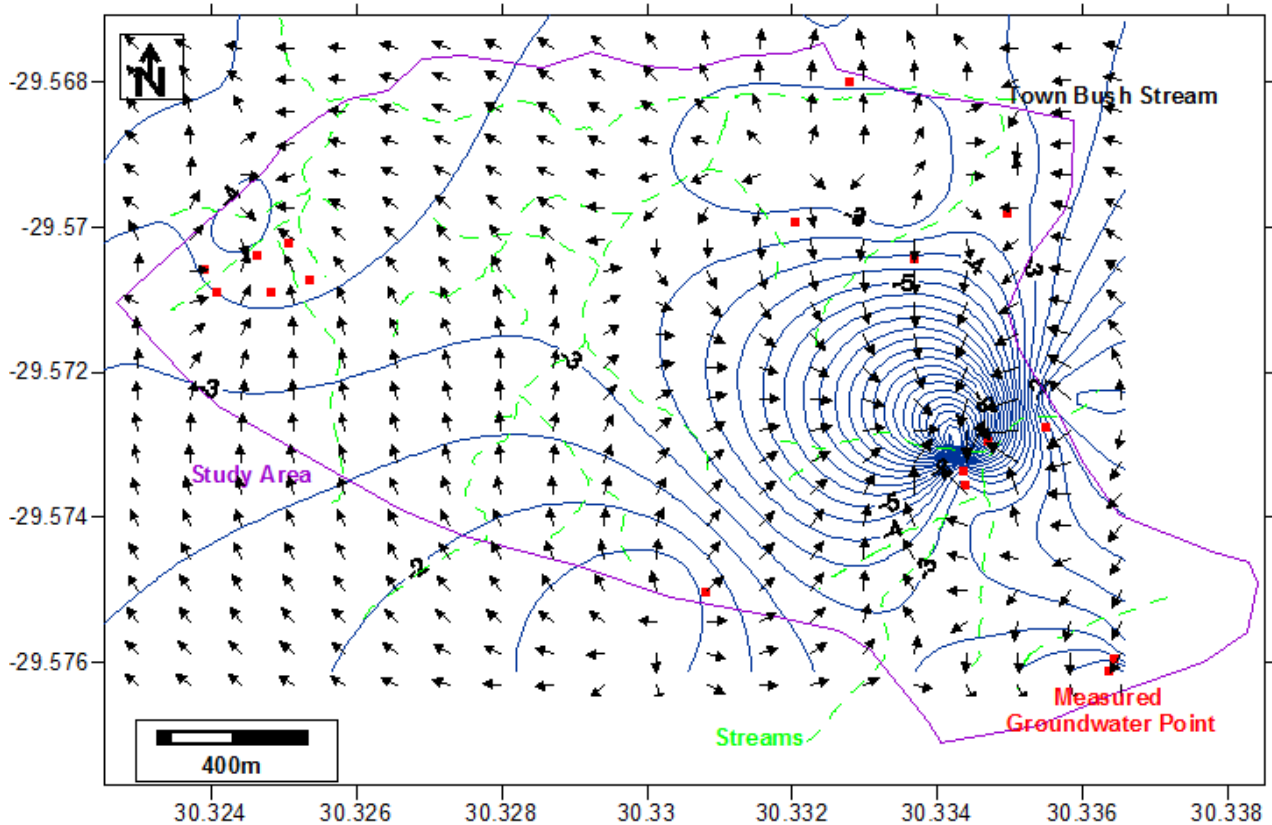


Figure 2.15: Vector map showing the localised groundwater flow regime in Town Bush Valley.

CHAPTER 3

LITERATURE REVIEW

3.1 Slope Stability Analysis

Slope stability analysis involves the application of mathematics to conditions of nature such as mass wasting processes (Cornforth, 2005). The process of slope development involves a complex set of interactions between soil and rocks on the one hand and the hydrological regime on the other (Bell & Maud, 1999). The index of slope stability is known as the factor of safety (FOS). This is defined by Duncan & Wright (2005), by Equation 1:

$$\text{FOS} = \frac{\text{Shear strength}}{\text{Shear stress}} \quad [3.1]$$

The FOS defines the stability of a slope and slope failure occurs if the shearing resistance of a potential failure surface is exceeded by shearing stress imposed on that failure surface (Duncan & Wright, 2005). When $\text{FOS} = 1.00$, a slope is at the point of failing because the resistance is in the exact state of balance with the destabilizing forces (Selby, 1982; Cornforth, 2005). Where $\text{FOS} < 1.00$ the slope is considered to be in a state of failure and where $\text{FOS} > 1.00$, the slope is considered to be stable (Selby, 1982).

Slope stability can be analysed using various methods such as the limit equilibrium method, limit analysis, finite difference method and finite element method (Budhu, 2000). Slope stability calculations need to be performed to ensure that the resisting forces are sufficiently greater than the forces tending to cause a slope to fail (Duncan & Wright, 2005). The calculations usually consist of computing a factor of safety value using one of several limit equilibrium procedures of analysis. These procedures of analysis employ the same definition of the factor of safety and compute the factor of safety using the equations of static equilibrium. The analyses of slope stability considers two numerical approaches namely a deterministic or probabilistic approach. The method of slope stability is linked to the approach taken and the results that are required.

3.1.1 Methods of slope stability analyses

Limit equilibrium procedures employ the FOS definition and compute it using the equations of static equilibrium. Uncertainty about shear strength is often the largest factor involved in slope stability analyses, and it is therefore logical that the factor of safety should be related directly to shear strength parameters (Duncan & Wright, 2005).

The factor of safety is obtained by inputting several parameters such as slope geometry, shear strength parameters, pore water pressure and external loads into an equation. The shear strength of soil is normally given by the Mohr-Coloumb failure criterion as shown in Equation 3.2 . A refinement of the

shear strength equation expressed in terms of the FOS defined in terms of total stresses (Equation 3.2) and effective stresses (Equation 3.3) is defined by Duncan & Wright (2005), as:

$$FOS = \frac{c + \sigma \tan\phi}{\tau} \quad [3.2]$$

$$FOS = \frac{c' + (\sigma - \mu) \tan\phi'}{\tau} \quad [3.3]$$

Where; c and ϕ are the cohesion and angle of friction respectively for the soil in terms of total stress, τ is the shear strength required for equilibrium and σ is the total normal stress on the shear plane. For effective stresses (Equation 3.3), μ is the pore water pressure, c' and ϕ' are the effective cohesion and effective angle of friction respectively for the soil.

The calculation of the factor of safety involves using one or more equations of static equilibrium calculation of the stresses for the analysed slope for which a factor of safety for each surface is determined. The factor of safety is assumed to be constant throughout a particular slip surface under analysis. If failure was to occur, the shear stress would be equal to the shear strength at all points along the failure surface and the assumption that the factor of safety is constant would be valid (Duncan & Wright, 2005).

Essentially there are two approaches in limit equilibrium analyses which satisfy static equilibrium. The first approach which are the single free-body procedures, considers equilibrium for the entire mass of the soil bounded beneath by an assumed slip surface and above the surface of the slope (Duncan & Wright, 2005). Such methods include the Infinite Slope Procedure and the Swedish Slip Circle Method. The second approach is known as the slice procedure, which involves dividing the soil mass into a number of vertical slices and equilibrium is computed for each individual slice (Duncan & Wright, 2005), such as, the Ordinary Method of Slices, the simplified Bishop Procedure and the Morgenstern & Price (1965) procedure.

In static equilibrium procedures, three static equilibrium conditions need to be satisfied which are equilibrium of forces in the vertical direction, equilibrium of forces in the horizontal direction and equilibrium of moments about any point. Different slope stability procedures make different assumptions since some satisfy all equilibrium procedures such as the Morgenstern & Price (1965) procedure, while others satisfy some equilibrium procedures such as the Bishops procedure. The problem of computing FOS is statically indeterminate, since there are more unknowns such as forces and the locations of forces, than the number of equilibrium equations. Thus, assumptions must be made in order to satisfy static equilibrium. For instance, two procedures may even satisfy the same equilibrium conditions but make different assumptions and therefore produce different values for the factor of safety (Duncan & Wright, 2005). Table 3.1 presents the applicability of various slope stability analysis procedures.

Table 3.1: Summary of slope stability analyses methods and conditions under which they apply.

Single free-body procedures	
Infinite Slope Procedure	This procedure can be used on both homogenous and non-homogenous soil. Also on slopes where the stratigraphy restricts the slip surface to shallow depths and parallel to the slope face (Duncan & Wright, 2005).
Swedish Circle Method	Applicable to slopes where the angle of friction is equal to zero and where relatively thick zones of weaker material are present. Also, where the slip surface can be approximated as a circle (Smith, 1990; Duncan & Wright, 2005; Knappet & Craig, 2012).
Slice procedures	
Circular slip surface procedures	
Ordinary Method of Slices	Applicable to non-homogenous slopes, where slip surfaces can be approximated by a circle. Convenient method for hand calculations but inaccurate for effective stress calculations with high pore water pressures.
Simplified Bishop Procedure	Applicable to non-homogenous slopes, where slip surfaces can be approximated by a circle. More accurate than the ordinary method of slices for high pore water pressures and is a convenient method for hand calculations (Duncan & Wright, 2005).
Non-circular slip surface procedures	
Spencer's Procedure (1967)	An accurate procedure applicable to virtually all slope geometries and soil profiles and is one of the simplest complete equilibrium procedures for calculating the factor of safety (Duncan & Wright, 2005).
Morgenstern & Price's (1965, 1967) Procedure	A rigorous and well-established procedure which provides added flexibility. It allows forces to vary across the slope and formulates equations of equilibrium by resolving equilibrium parallel to and normal to the base of the slice (Cornforth, 2005; Duncan & Wright, 2005). The procedure is based on limit equilibrium in which all boundary and equilibrium conditions are satisfied and in which the surface may be any shape (Knappet & Craig, 2012). It is applicable to virtually all slope geometries and soil profiles.
Simplified Janbu (1954, 1957)	Side forces are horizontal, there is no shear stress between slices. Correction factors must be applied to adjust the factor of safety value of F to more reasonable values (Duncan & Wright, 2005).

FOS determinations for rotational slides in drained soils involve dividing the soil mass into a series of slices. The forces acting on a slice are a combination of the total weight of the slice, total normal forces at the base, shear forces at the base, total normal forces on the sides and the shear forces on the sides of the slice (Knappet & Craig, 2012).

3.1.2 Deterministic approach in slope stability analysis

Deterministic models are widely used to understand and predict the occurrences of slope instability (Haneberg, 2000). In the field of engineering geology, the deterministic principle of calculating the stabilizing and driving forces to arrive at a FOS value has been the predominant method of slope stability analyses (Nilsen, 2000). A deterministic model is one in which there is an invariant causal relationship between the independent and dependent variables (Haneberg, 2000). A deterministic

approach in slope stability analysis is undertaken by using single values to represent a variable, such as the material's effective shear strength properties. The outcome of a deterministic analysis is based on the FOS value, if the $FOS > 1.00$ the slope will not fail, implying stable slope conditions (Nilsen, 2000). Conversely, if a value of $FOS \leq 1.00$ is obtained the slope will fail, implying unstable slope conditions

3.1.3 Probabilistic approach in slope stability analysis

It is widely recognised that the initial assessment of geotechnical parameters may not be accurate (Aleotti and Chowdhury, 1999). The ability to measure and simulate real-world variability is often limited in terms of time and money. In geological science, this is further complicated by the fact that the data sets may be fragmentary remains of a past event (Haneberg, 2004). Compared to a deterministic analysis, a probabilistic analysis takes into consideration the inherent variability and uncertainties into account in the analysis parameters (Sharma, 2016). Judgments are quantified within a probabilistic analysis by producing a distribution of outcomes rather than a single fixed value (Sharma, 2016).

Probabilistic methods in geotechnical engineering have been used for over 50 years but are regarded as being mathematical and difficult to learn by determinists who are used to the simple concept of safety factors (Gover, 2014). Analysis of slope stability comprises many uncertainties pertinent to lack of accurate geotechnical parameters, inherent spatial variability of geo-properties, change of environmental conditions, unpredictable mechanisms of failure, simplifications and approximations used in geotechnical models (Nilsen, 2000; Sharma, 2016). Aleotti & Chowdhury (1999), distinguished three systematic uncertainties in geotechnical engineering, which a probabilistic analysis is able to account for. Firstly a soil mass can only be investigated by a finite number of points. Secondly, the number of field and laboratory tests conducted to determine soil parameters is limited by financial and time constraints. Lastly, the testing equipment and methods may not be perfect.

A probabilistic approach in slope stability analysis recognizes that any earth structure has some probability of failure, however small, in contrast to a deterministic approach which alludes to the fact that failure cannot occur if $FOS > 1.00$ (Chowdhury, 1984). The recognition of uncertainties associated with the variability of geotechnical material parameters such as the cohesion and the angle of internal friction coupled with variable pore water pressures, has led to the development of methods of analysis within a probabilistic framework (Chowdhury, 1984). Other soil parameters used in a slope stability analysis equation include the unit weight, saturated unit weight, submerged unit weight and undrained cohesion (Das, 1994). Variability of some parameters such as the unit weight and geometrical parameters have an insignificant influence on stability and such parameters may be regarded as constant (Chowdhury, 1984). Slope stability of a natural slope is also dependent on fixed attributes such as the slope height and slope angle. The spatial and temporal variability of pore water pressures is important, but it is not reflected in the calculated values of the conventional deterministic FOS calculations (Aleotti & Chowdhury, 1999).

It is important to note that due to the uncertainty of input parameters, even if the $FOS \geq 1$, this does not imply that the probability of failure is equal to zero (Nilsen, 2000). If the concept of a deterministic approach is not understood it can cause a false impression of safety. In this way one can gain a better insight into aspects of slope stability and a keener appreciation of the risks associated with particular sites (Chowdhury, 1984).

The statistical parameters and calculation methods used during a probabilistic approach are expanded on in the following subsections below.

3.1.3.1 Mean, standard deviation and coefficient of variation

The mean is the average value calculated from a set of values (N) divided by the total number of values (x) (Montgomery & Runger, 2011). This can be represented by Equation 3.4:

$$\mu = \frac{\sum N}{x} \quad [3.4]$$

The standard deviation is a quantitative measure of the scatter of a variable (Montgomery & Runger, 2011). This can be represented by Equation 3.5:

$$\sigma = \sqrt{\frac{1}{N-1} \sum_1^N (x - x_{avg})^2} \quad [3.5]$$

Where; σ is the standard deviation, N is the number of measurements and x is the number of variables. The standard deviation is of great importance for the evaluation of variability in values (Lacasse & Nadim, 1996). The coefficient of variation is the standard deviation divided by the expected value of a variable (Montgomery & Runger, 2011). This is usually expressed as a percentage and is given by Equation 3.6:

$$COV = \frac{\sigma}{average\ value} \quad [3.6]$$

Reliability and probability of failure can be determined once the mean factor of safety and the coefficient of variation (COV) of the factor of safety have been determined. The value of the factor of safety can be calculated using conventional methods such as spreadsheets and computer software programs, while the value of COV can be determined using the Taylor series method (Gover, 2014). The COV is an indication of the percentage separation of the expected value of variable from the standard deviation. The COV gives the level of variability in material properties (Huvaj & Oguz, 2018). The higher the COV value the higher the dispersion of values around the mean value, increasing the degree of uncertainty (Huvaj & Oguz, 2018).

3.1.3.2 Probability of failure

The probability of failure (Pf) as defined by Aleotti & Chowdhury (1999), is a probability that the performance function has a value below the threshold value which is $FOS = 1.00$. Considering the FOS as the performance function, the probability of failure and can be defined by Equation 3.7:

$$Pf = P [FOS < 1.00] \quad [3.7]$$

Where; $P [FOS < 1.00]$ is the number of FOS values that have a $FOS \leq 1.0$ divided by the total number of FOS value obtained, which is expressed as a percentage.

The probability of success (P_s) or the reliability is therefore the complement of P_f (Aleotti & Chowhury, 1999). This can be defined by Equation 3.8:

$$P_s = 1 - P_f \quad [3.8]$$

In order to calculate the P_f , the probability distribution function (pdf) of the performance function is required (Aleotti & Chowhury, 1999). Probability distribution may be characterized using the mean and standard deviation. With reference to Equations 3.4, 3.5 and 3.7, the concept is illustrated in Figure 3.1.

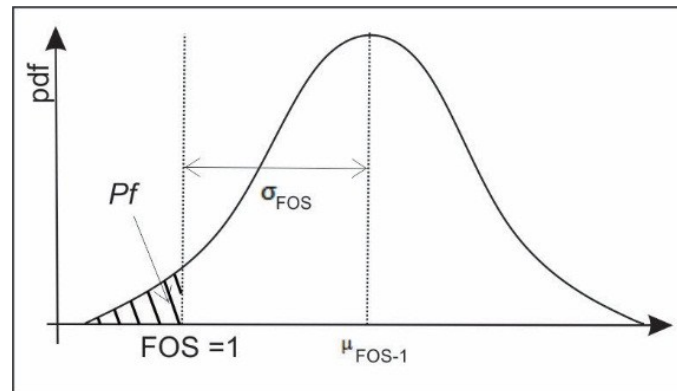


Figure 3.1: Probability distribution function (pdf) for the factor of safety (adapted from Gover, 2014).

3.1.3.3 Probability distribution functions

The probability distribution of a random variable x , is a description of the probabilities associated with the possible values of x (Montgomery & Runger, 2011). Distributions of soil properties must be determined based on available data and one can check whether a particular empirical distribution follows any well-known mathematical probability distribution function (Chowdhury, 1984). The most widely used distribution for a random variable is the normal distribution (Montgomery & Runger, 2011). Typical probability distributions functions are presented in Figure 3.2.

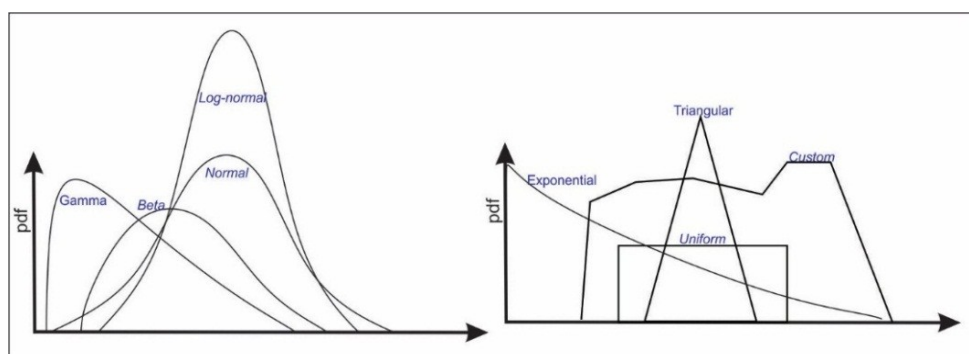


Figure 3.2: Probability distribution function types (adapted from Montgomery & Runger, 2011).

Lognormal distributions in which the logarithms of the random variables rather than the random variables themselves are normally distributed, are often used in geologic studies (Haneburg, 2000). Other distributions include the beta distribution which can take on a variety of shapes and the uniform

distribution in which all values have equal values. Haneburg (2000), stated that in many cases implicit assumptions are made that the data is normally distributed by calculating the mean, standard deviation, even when there is no reason to infer that the data were drawn from an underlying normal distribution.

3.1.3.4 Reliability index

The reliability index (β) is an alternative measure of safety which is linked to the probability of failure (Duncan & Wright, 2005). The value of β indicates the number of standard deviations which separate the mean FOS from the critical FOS = 1 (Duncan & Wright, 2005). The usefulness lies in the fact that the probability of failure and reliability are uniquely related to β (Duncan & Wright, 2005). The reliability index can be calculated assuming either a normal or lognormal distribution of the FOS results. Duncan & Wright, (2005) suggest that if the FOS values have a normal distribution Equation 3.9 can be used, for a lognormal distribution Equation 3.10 can be used.

$$\beta = \frac{\mu_{FOS-1}}{\sigma_{FOS}} \quad [3.9]$$

$$\beta_{LN} = \frac{\ln\left(\mu_{FOS-1}/\sqrt{1+COV_F^2}\right)}{\sqrt{\ln\left(\sqrt{1+COV_F^2}\right)}} \quad [3.10]$$

Where; β = normal reliability index; β_{LN} = lognormal reliability index; μ_{FOS-1} = mean FOS; σ_{FOS} = standard deviation of the FOS and COV_F = coefficient of variation.

The numerator gives the extent to which the average values are above the threshold value and the denominator reflects the dispersion from this average value (Aleotti & Chowhury, 1999). The reliability index combines the mean, standard deviation of the FOS to give an indication of consistency of the data. The reliability index is an alternative measure of stability that considers explicitly the uncertainties involved in stability analyses (Duncan & Wright, 2005).

Values near zero indicate that stability or instability is inferred with little confidence (Haneberg, 2004). The probability of failure computed using a reliability based approach, provides an added risk based dimension to complement the factor of safety. Factors of safety and reliability complement each other, and each has its own advantages and disadvantages, knowing the values of both is more useful than knowing either one by itself (Duncan & Wright, 2005).

3.1.3.5 Random variables

Haneberg (2000) defines a random variable as a variable that can take on a series of outcomes or realizations with a given probability of occurrence. Each parameter affecting slope stability may be regarded as a random variable with an associated *pdf* rather than as a constant (Chowdhury, 1984). The assessment of slopes is difficult because of many uncertainties, such as the variability of material properties over a site (Chowdhury, 1984; Bar & Heweston, 2018). Analysis of slope stability consists

of many uncertainties pertinent to lack of accurate geotechnical parameters, inherent spatial variability of geo-properties, change of environmental conditions, unpredictable mechanisms of failure, simplifications and approximations used in geotechnical models (Sharma, 2016). Soil material properties are highly variable and never well-understood since site investigations such as drilling, mapping and geotechnical testing sample only very small portions of the material (Bar & Heweston, 2018). Variability of some parameters such as unit weight and geometrical parameters have an insignificant influence on stability and such parameters may be regarded as constant (Chowdhury, 1984). Parameters such as shear strength and pore water pressures are desirable to consider as random variables (Chowdhury, 1984). The uncertainty associated with shear strength testing and the parameters derived thereof can be incorporated into a probabilistic model by letting the soil shear strength parameters vary over a realistic range of values (Haneburg, 2004). The reduction of uncertainties is achieved through the knowledge of probability theories and statistical analyses. Such approach to the modelling of uncertainty increases the confidence on the estimation of the corresponding likelihood of certain outcome (Haneburg, 2004).

3.1.3.6 Probabilistic approximation methods

Conventional deterministic approaches do not consider many uncertainties in their calculations quantitatively (Sharma, 2016). Decision making under uncertainty can be facilitated by using probabilistic approaches (Chowdhury, 1984). A probabilistic model is one in which one or more of the dependent variables exhibits some degree of random behaviour. The recent advances in computer statistical analyses software have added simplicity to these statistical tools.

Bar & Heweston (2018) have shown that the probability of failure is highly dependent on the method of modelling used. Aleotti & Chowdhury (1999) distinguished three commonly used probability calculation methods namely the, First Order Second Moment Method, Point Estimate Method and the Monte Carlo Simulation Method. Table 3.2, presents a summary of known approximation methods.

Table 3.2: Summary of various probabilistic approximation methods.

<p>First Order Second Moment (FOSM) Method - Uses the first terms of the Taylor series expansion to estimate the mean and variance of the performance function.</p>	<p>First Order Reliability Method (FORM) - Suited for complex slope stability analysis. The approach is based on a geometric interpretation of the reliability index</p>
<p>Second Order Moment Method (SOSM) - Uses the terms in the Taylor series up to the second order. The SOSM method is generally not a favoured method in geotechnical applications due to its honourous computations.</p>	<p>Low and Tang's (1997 & 2007) Approach Requires the normalization of random variables, this approach is generally regarded as being conceptually and computationally difficult.</p>
<p>Rosenblueth's Method – Point estimates are an approximate numerical integration approach. The expected value of any variable F is found by adding several terms (Chowdhury, 1984).</p>	<p>Monte Carlo Simulation – Involves the generation of random numbers and a value for the FOS associated with a set of random values of the basic stochastic variables (Chowdhury, 1984)</p>

3.1.3.7 Monte Carlo Simulation

The Monte Carlo method was developed in 1949 by John von Neumann and Stanislaw Ulam, wherein they designated the use of random sampling procedures for treating deterministic mathematical situations. The foundation of the Monte Carlo Simulation gained significance with the development of computers to automate the laborious calculation (Sharma, 2016). The Monte Carlo simulation involves the generation of random numbers and a FOS value associated with a set of random values of the basic stochastic variables (Chowdhury, 1984). After the generation of many FOS values, the *pdf* of the FOS is calculated. The *Pf* may be estimated from the generated distribution or directly from the relative frequencies with which the FOS was found to be $FOS \leq 1.00$ during the simulations (Sharma, 2016). During each pass, a random value from the distribution function for each parameter is selected and entered into the calculation, the concept is illustrated in Figure 3.3.

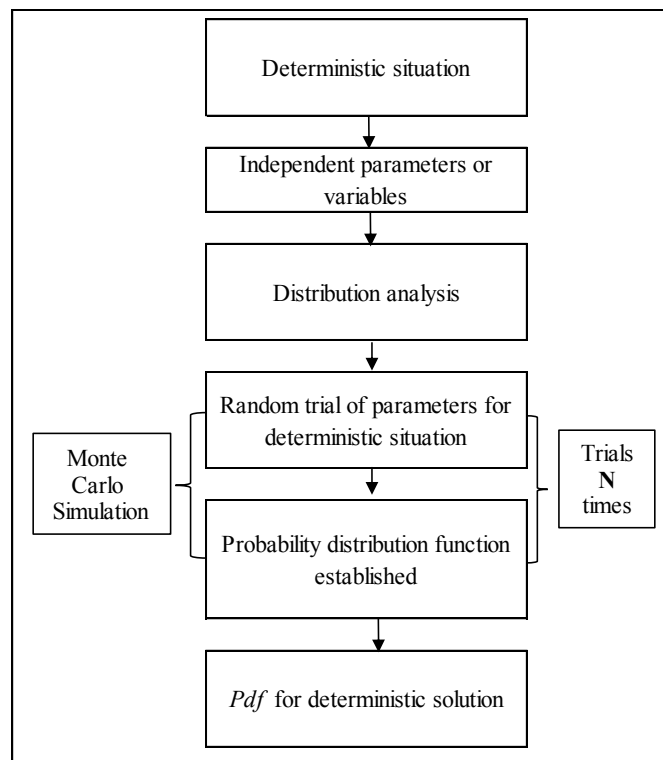


Figure 3.3: Steps involved in a Monte Carlo Simulation (Hutchinson & Bandalos, 1997).

The first step of a Monte Carlo simulation is to identify a deterministic model where multiple input variables are used to estimate a single value outcome. Step two requires that all variables or parameters be identified (Sharma, 2016). Step three requires that the probability distribution for each independent variable is established for the simulation model (Sharma, 2016). Step four requires that random trial processes are initiated to establish the *pdf* for the deterministic situation being modelled (Sharma, 2016). Sharma (2016) reasoned that the appropriate number of steps for an analysis is a function of the number of input parameters, the complexity of the modelled situation, and the desired precision of the output.

The Monte Carlo simulation is a popular method of slope stability risk analysis among engineers because of its simplicity.

3.2 Representation of pore water pressures

Depending on the seepage and groundwater conditions, several methods can be used to represent the pore water pressure in slope stability analyses. Several interpolation schemes have been developed to model seepage conditions such as the three and four-point interpolation scheme, spline interpolation and infinite element shape functions (Duncan & Wright, 2005). The spatial and temporal variation of pore water pressures is very important but is not reflected in the conventionally calculated factor of safety values (Aleotti & Chowhury, 1999).

Fast approximations of the pore water pressures can commonly be represented by the phreatic and potentiometric surfaces. Table 3.3 summarizes the various methods of pore water pressure representation.

Table 3.3: Summary of various pore water pressure representation methods.

<p>Flow Nets - When steady-state seepage conditions exist in a slope a graphical flow net solution can be used to determine the pore water pressures (Duncan & Wright, 2005). It involves determining the uppermost flow line which is the location of the line of seepage, and then constructing equipotential lines in the direction of flow.</p>	<p>Phreatic Surface - The phreatic surface offers a simple method to approximate the groundwater conditions. The phreatic surface represents a line of zero atmospheric pressure.</p>
<p>Piezometric surface - The piezometric surface may be represented by multiplying the pressure head, which is related to the vertical depth (H) Duncan & Wright, (2005). As defined by Equation 3.11:</p>	<p>When the pore water pressures are defined by the phreatic surface. Duncan & Wright (2005), defined that the pore water pressure may be represented by Equation 3.13 :</p>
$H = z + h_p \quad [3.11]$	$u = h_p \gamma_p \quad [3.13]$
<p>By the unit weight of water (γ_p) the product is defined by Duncan & Wright, (2005) by Equation 3.12:</p>	<p>Where, h_p is the pressure head, γ_p the unit weight of water.</p>
$u = H\gamma_p \quad [3.12]$	
<p>This representation is considered to be conservative compared to the phreatic surface (Duncan & Wright, 2005).</p>	

3.3 Conditions for Analyses

The physical and mechanical properties of soil often dictate the mechanism in which slopes can fail. It is imperative to understand the conditions and forces existing in a soil during dry, partially saturated

and saturated conditions. Furthermore, slope stability analyses are analysed either in terms of total stress or effective stress analyses (Bell, 2007).

3.3.1 Drainage conditions

Drainage conditions are considered in terms of the drained or undrained conditions. The definitions used in soil mechanics are related to the ease and speed with which water moves in or out of soil in comparison with the length of time that the soil is subjected to some change in load (Duncan & Wright, 2005). The shear strength of soil under undrained conditions is different to that under drained conditions. Under a given set of applied total stresses, in undrained loading excess pore water pressures are generated in the soil which change the effective stresses in the soil mass (Knappet & Craig, 2012). Under drained conditions excess pore pressures are zero as consolidation has already taken place (Knappet & Craig, 2012).

Therefore, for two identical samples of soil, which are subject to the same changes in the total stress but under different drainage conditions, the samples will have different internal effective stresses and therefore different strengths according to the Mohr-Coulomb criterion (Knappet & Craig, 2012).

The principle consideration in determining which condition is applicable is the rate at which the changes in total stress are applied in relation to the rate of dissipation of excess pore water pressures (Duncan & Wright, 2005; Knappet & Craig, 2012).

3.3.1.1 Undrained Conditions

Undrained condition occurs when there is no flow of water into or out of a soil mass in the length of time that the soil is subjected to some change in load (Duncan & Wright, 2005). Changes in the loads on the soil cause changes in the pore water pressures in the voids, as the water cannot move in or out in response to the tendency for the volume of voids to change (Duncan & Wright, 2005). Undrained conditions are representative of short-term conditions (Duncan & Wright, 2005).

The undrained strength can be expressed in terms of total stresses. An undrained slope stability analysis is performed using total shear strength parameters (Duncan & Wright, 2005). The total strength parameters are denoted by c_u and ϕ_u (Knappet & Craig, 2012).

3.3.1.2 Drained Conditions

Drained conditions occur when water is able to flow into or out of a mass of soil in the length of time that the soil is subjected to some change in load (Duncan & Wright, 2005). Under drained conditions, changes in the loads on the soil do not cause changes in the pore water pressures in the soil (Duncan & Wright, 2005). Water can move in or out of the soil freely when the volume of voids increases or decreases in response to the changing loads. Drained conditions are representative of long-term conditions (Duncan & Wright, 2005). If drainage conditions prevail where pore pressures are

controlled by hydraulic boundaries, or if the conditions at a site can reasonably be approximated by these conditions, an effective stress analysis is appropriate (Duncan & Wright, 2005).

A drained slope stability analysis is performed using, effective stress shear strength parameters (Duncan & Wright, 2005). Loading in the long-term implies conditions will be drained as such effective shear strength parameters (c' , ϕ') are used during slope stability analysis (Knappet & Craig, 2012).

3.4 Mechanical properties of Talus Material

3.4.1 Granular material

Soils such as gravel and sand are collectively referred to as granular soils and normally exhibit only an angle of friction component of strength (Smith, 1990). Granular materials, such as sands and gravels, are similar in terms of their properties (Duncan & Wright, 2005).

Measuring or estimating the drained strengths of granular material involves determining or estimating appropriate values of ϕ' . Typical friction values for granular soils are provided in Tables 3.4, 3.5 and 3.6.

Table 3.4: Typical friction angles for granular soils (Look, 2007).

Type	Description	ϕ'
Cohesion-less gravels	Very loose/loose	30°-34°
	Medium dense	34°-39°
	Dense	39°-44°
	Very dense	44°-49°
Cohesion-less sands	Very loose/loose	27°-32°
	Medium dense	32°-37°
	Dense	37°-42°
	Very dense	42°-47°
Cohesion-less sands	Loose – uniformly graded	27°-30°
	Loose – well graded	30°-32°
	Dense – uniformly graded	37°-40°
	Dense – well graded	40°-42°

Table 3.5: Typical friction angles for granular soils (Carter & Bentley, 1991).

Material	Loose (ϕ')	Dense (ϕ')
Uniform sand, round grains	27°	34°
Well-graded sand, angular grains	33°	45°
Sandy gravels	35°	50°
Silty sand	27°-33°	30°-34°
Inorganic silt	27°-30°	30°-35°

Table 3.6: Typical friction angles for granular soils (Budhu, 2000; Murthy, 2003; Das, 2006).

Soil Type	Description	ϕ'
Sand – rounded grains	Loose	27°-30°
	Medium dense	30°-35°
	Dense	35°-38°
Sand – angular grains	Loose	30°-35°
	Medium dense	35°-40°
	Dense	40°-45°
Mixtures of gravel and sand with fine grained soil	-	34°-48°

The most important factors governing values of ϕ' for granular soils are density, confining pressure, grain size distribution, strain boundary conditions, and the factors that control the amount of particle breakage during shear, such as the types of mineral and the size and shape of particles (Duncan & Wright, 2005). Particle shape influences the friction angle and can reduce the angle by about 4° (Look, 2007).

3.4.2 Silts

Silts display a broad range of material behaviour, non-plastic silts display similar behaviour to that of fine sands, whilst plastic silts display similar behaviour to clays (Duncan & Wright, 2005). Laboratory test procedures for silts can be conducted following the principles that have been established for testing clays (Duncan & Wright, 2005). Silts are moisture sensitive and compaction characteristics are similar to those for clays. Effective angle of internal friction values for non-plastic silts can be approximated based on clean sands. Table 3.7 illustrates typical values prescribed by Duncan & Wright (2005).

Table 3.7: Correlation of relative density with the angle of internal friction for clean sands (Duncan & Wright, 2005).

Density	Relative density (%)	ϕ'
Very loose	< 20	< 32°
Loose	20-40	32° - 35°
Medium	40-60	35° - 38°
Dense	60-80	38° - 41°
Very dense	> 80	41° - 45°

It is often difficult to determine whether silts will be drained or undrained under field loading conditions, thus it is beneficial to consider both drained and undrained conditions (Duncan & Wright, 2005).

3.4.3 Clays

The complex interactions with water and clays are responsible for a large percentage of slope stability problems. The undrained strengths of clays are important for short-term loading conditions, and drained

strengths are important for long-term conditions (Duncan & Wright, 2005). Depending on the loading and drainage conditions it is possible for a clay soil to exhibit purely frictional shear strength (Smith, 1990; Carter & Bentley, 1991). Index tests can be used with empirical correlations to estimate values of a range of strength properties. Such data be useful when high quality laboratory test data is unavailable and for providing additional data to support the results of such tests (Knappet & Craig, 2012).

Typical effective friction angles based on plasticity indices, are summarized in Tables 3.8 ($c' = 0$ kPa), 3.9 and 3.10 ($c' = 0$ kPa).

Table 3.8: Effective angle of friction values for normally consolidated clays (Duncan & Wright, 2005).

Plasticity index (%)	ϕ'
10	$33^\circ \pm 5$
20	$31^\circ \pm 5$
30	$29^\circ \pm 5$
40	$27^\circ \pm 5$
60	$24^\circ \pm 5$
80	$22^\circ \pm 5$

Table 3.9: Typical values for compacted clays (Duncan & Wright, 2005).

Plasticity index (%)	c' (kPa)	ϕ'
SM-SC	15	33°
SC	12	31°
ML	9	32°
CL-ML	23	32°
CL	14	28°
MH	21	25°
CH	12	19°

Table 3.10: Typical values for effective friction angles for normally consolidated clays (Carter & Bentley, 1991).

Unified Soils Classification System	ϕ'
SM	34°
SC	31°
ML	32°
CL	28°
MH	25°
CH	19°

The strength properties of clays are complex and subject to change over time through geological and geotechnical processes. These processes include consolidation, swelling, weathering, development of slickensides and creep (Duncan & Wright, 2005).

The strength properties of clays are sensitive to laboratory factors some of which are detailed in Table 3.11.

Table 3.11: Factors influencing clay strength.

Factor	Problems experiences	Mitigating techniques
Material disturbance	Reduces shear strengths measured in unconsolidated - undrained laboratory tests.	The recompression technique by Bjerum (1973) cited in Duncan and Wright (2005), involves consolidating the specimens to the <i>in-situ</i> field pressures.
		SHANSEP technique described by Ladd and Fooks (1974) and Ladd et. al. (1977), cited in Duncan and Wright (2005), involves consolidating the samples to the effective stresses that are higher than the <i>in-situ</i> stresses.
Anisotropy	Inherent Anisotropy - directional dependent stiffness and strength because of clay particles oriented perpendicular to the major principal strain direction during consolidation.	Laboratory tests to measure the undrained shear strength of clays should ideally be performed on completely undisturbed plane strain test specimens, tested under unconsolidated - undrained conditions or alternatively samples should be consolidated and sheared with stress orientations that simulate <i>in-situ</i> conditions
	Stress system - the magnitudes of the stresses during consolidation vary depending on the orientation of the planes on which they act, and the magnitudes of the pore pressures induced by undrained loading vary with the orientation of the changes in stress.	
Strain rate	Laboratory tests involve higher rates of strain than are typical for most field conditions. Slower loading results in lower undrained shear strengths of saturated clays.	Laboratory tests should ideally correct for strain rate effects or disturbance effects.

3.5 Review of the Engineering Geological Conditions at the Town Hill Escarpment

The micaceous sandstones of the Vryheid Formation are generally more competent in terms of their strength, durability and permeability in comparison to the shales of the Pietermaritzburg Formation (Price, 2006).

This geological arrangement, coupled with the relatively high rainfall of the area has led to numerous micro-relief structures in the form of slides and slumps, generally originating on the contact of the sequences. This has given rise to the hummocky or stepped topography that is evident on the slopes of the Town Hill Escarpment which was initially recognized by Maurenbrecher and Booth (1975) and later documented by investigations undertaken in the Town Bush Valley by Schreiner (2005a) and Price (2006). In Pietermaritzburg, small translational type slides involving both rock and colluvium generally occurs at the interface between colluvium and dipping shale beds (Richards *et al.*, 2006). The slides normally take the form of shallow, non-circular rotational slides resulting from the over-steepening of the sides with resultant sliding along the bedrock and colluvium interface (Richards *et al.*, 2006).

The thickness of the talus material blanketing the Town Hill Escarpment varies from very shallow (< 1.0 m) to an excess of 50 m in certain areas (Allen, 1981). Slope stability studies have been done in Pietermaritzburg on similar geology by Maurenbrecher (1973), Maurenbrecher and Booth (1975) and Maud (1985). More specifically, the areas of interest include Henly Hill, Town Hill (the Rickivy Landslide, Athlone Landslide, Ferncliffe Water Works), Northdale and the surrounding embankments of the N3 national highway located near World's View.

3.5.1 Geomorphological Description of the Town Bush Valley

The escarpment above Pietermaritzburg is about 300 m high and trends in an approximately north-westerly direction. A series of comparative aerial photographs are illustrated in Figure 3.4, spanning from 1967 to 2006.

Mass wasting processes operating in the Town Bush Valley was first recognized by Maurenbrecher and Booth (1975), who reported that the extensive areas of hummocky topography at the foot of the scarp slope represented in the 1939 aerial photograph shown in Figure 3.4, are zones of movement. These are illustrated by dotted lines in the 1939 aerial photograph and movement is anticipated to have taken place in a northerly direction with the colluvium derived from the escarpment itself (Maurenbrecher & Booth, 1975).

Richards *et al.* (2006) states that the mass movement and sheetwash processes contributed to crudely stratified sediment and large dolerite boulders, that infill some depressions preserved within the unconsolidated colluvium.

The 1967 aerial photograph shows distinct changes in the slope geomorphology. It is evident from the aerial photographs that the valley is still actively undergoing colluvial processes. The distinct hummocky topography evident in the 1939 (outlined in the black dotted lines) and the 1967 aerial photographs are less prominent in the 2006 aerial photograph.

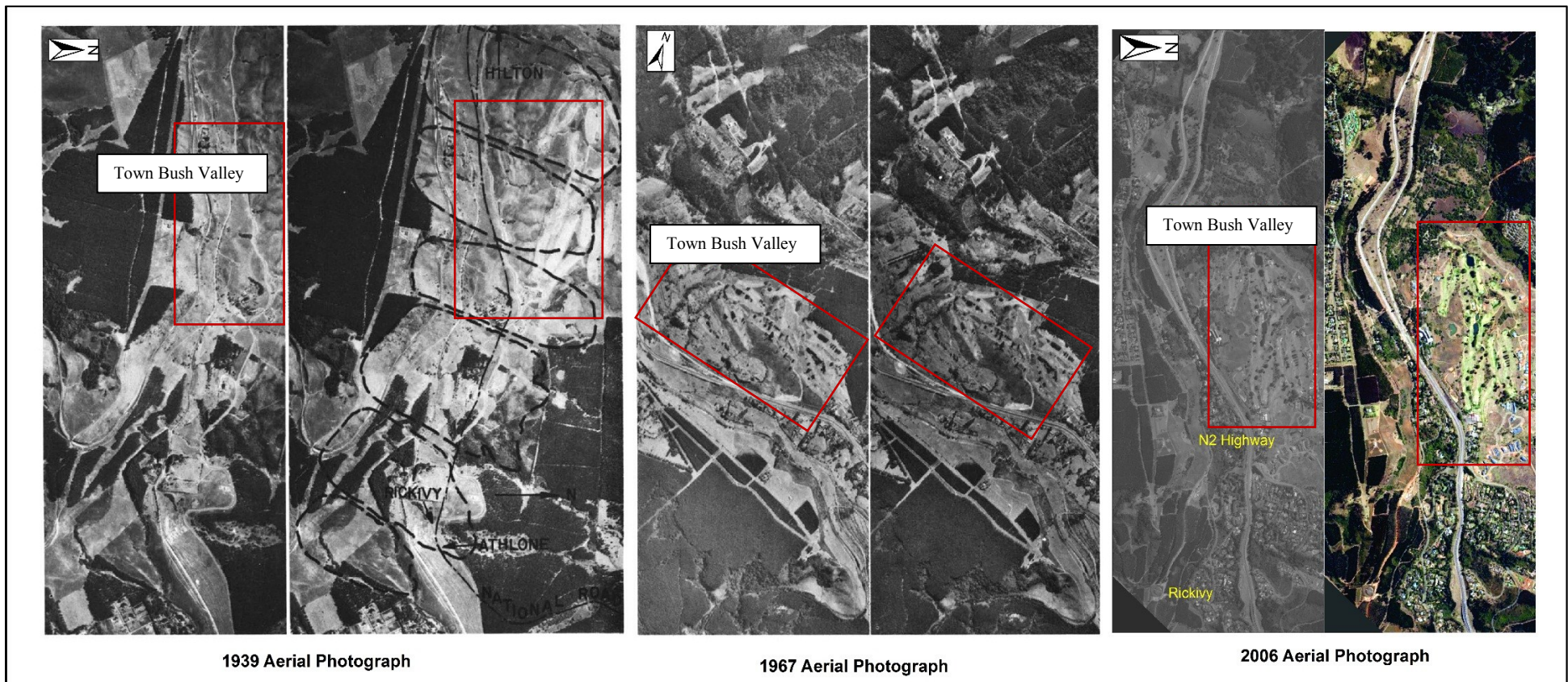


Figure 3.4: Comparative aerial photographs of the Town Bush Valley outlined in red spanning 67 years (adapted from Maurenbrecher and Booth, 1975).

3.5.2 Natural discontinuities in Town Bush Valley

Large scale fissures in the talus horizon of the Town Bush Valley were initially recognized by Price (2006) during investigations undertaken in the Cascades Development. These fissures were later documented by investigations undertaken by Singh (2015a), during site investigations in the Cascades Development and Montrose Park Development. These natural discontinuities are illustrated in Figure 3.5.

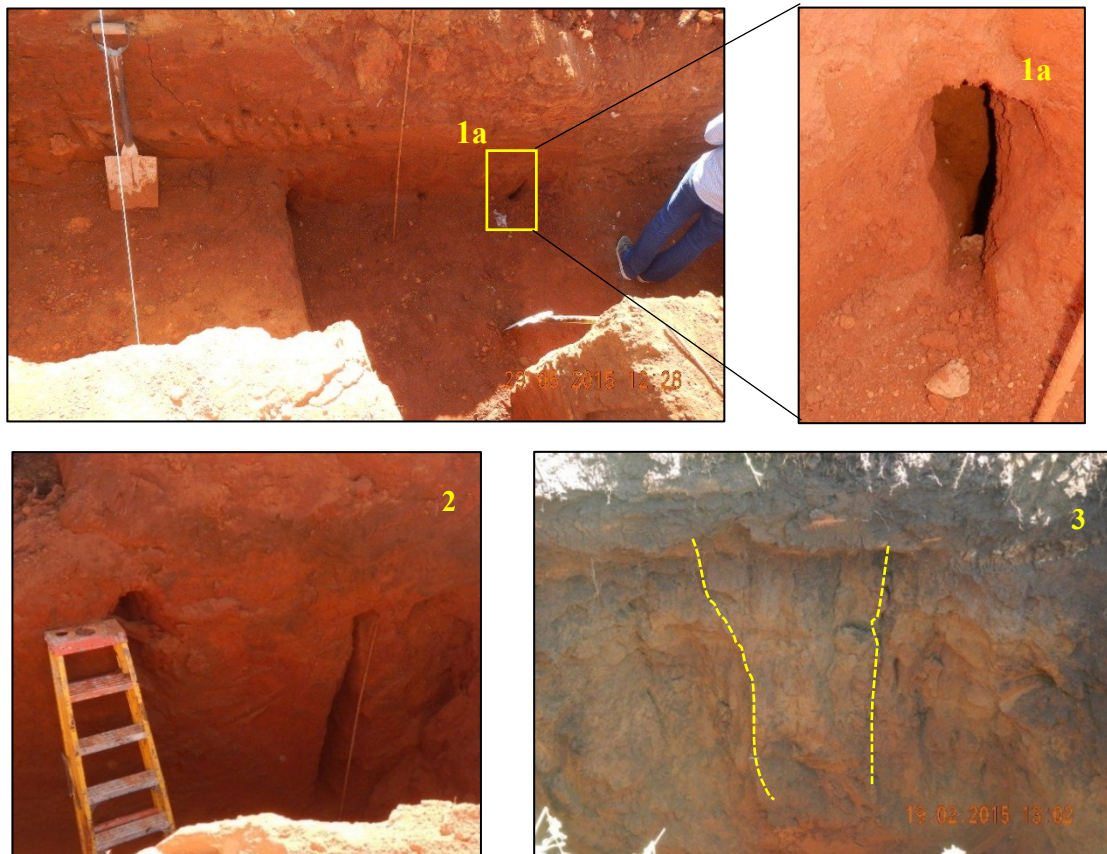


Figure 3.5: Fissures intersected in the Cascades Development (Photo 1a & 2) and MPD (Photo 3).

The relatively minor clay component of the talus material results in material behaviour that is less susceptible to shrink and swell cycles, resulting in fissures that appear to have remained open for a few years (Singh, 2015a). These fissures have widened over a period of geological time as a result of groundwater permeating laterally and horizontally over the fissure surfaces (Singh, 2015a).

3.5.3 Equilibrium Destabilising Forces

Slope instability is brought about by, either by a decrease in the shear strength of the soil or an increase in the shear stress required for equilibrium conditions (Duncan & Wright, 2005).

Table 3.12 summarizes some destabilizing forces, which are contributing factors in the case studies presented in the following sections.

Table 3.12: Destabilizing equilibrium conditions (Budhu, 2000; Duncan & Wright, 2005).

<u>Decrease in shear strength</u>	<u>Increase in shear stress</u>
<p>Increase pore water pressure - An increase in pore pressure brought about by rainfall reduces the stress shear strength. It is generally agreed that in most landslides, groundwater constitutes the most important single contributory cause.</p>	<p>Increase in loads - An increase in the load applied to a slope in the form of a surcharge load, means that shearing stresses are increased leading to a decrease in the stability of a slope. A surcharge load usual takes the form of a building development or fill. Loads placed at the crest add to the gravitational load.</p>
<p>Cracking - Tension cracks develop at the crest of a slope. These cracks are a result of tension in the soil, at the ground surface that exceeds the tensile strength of the soil.</p>	<p>Increase in soil weight due to an increase in water content - Increased volumes of water infiltration can increase the moisture content of the soil, thereby increasing the soil unit weight or its bulk density.</p>
<p>Shrink and swell cycles - Highly plastic clays, possess clay minerals that are subject to swell when in contact with water and shrink when dried out. Shrinkage may weaken the clay by developing desiccation cracks within it.</p>	<p>Excavation at the bottom of the slope - Earthworks which increase the steepness of the slope, resulting in an increase in the shear stresses acting on the slope, reducing stability. Similarly, undercutting in form of scouring from a stream at the base of a slope has the same effect.</p>
<p>Development of slickensides - Slickensides develop in highly plastic clays, in which plate-like clay particles tend to align themselves parallel to the direction of shear, resulting in distinct shear planes.</p>	<p>Drop in water level at the base of the slope - External water pressures acting on the lower part of a slope acts as a stabilizing force. If the water level drops, the stabilizing influence is reduced and the shear stresses within the soil increase.</p>
<p>Creep under sustained loads - Highly plastic clays deform continuously when subjected to sustained loads. The clays may fail under these loads even if the shear stresses are smaller than the short-term shear strength of the material.</p>	

3.5.4 Instability in roadworks

During construction of the N3 National Highway between 1957 to 1968, a series of landslides occurred along the section of the road aligned through the Town Hill Escarpment. In many cases, limited information is available about the landslides other than when and where they occurred (Maurenbrecher & Booth, 1975). During roadwork construction in 1957, the Montrose Cutting (Montrose Slide) failed on a deep-seated (2.0 m) talus failure plane (Maurenbrecher & Booth, 1975).

In 1967, further up the N3 near Hilton, a cutting failed after excessive rainfall, resulting in a landslide (Figure 3.6). Maurenbrecher & Booth (1975) emphasised that at the time of failure of the slopes, the

main cause of failure was deemed to be inadequate drainage and the possible contribution from naturally unstable subsoil was not mentioned.

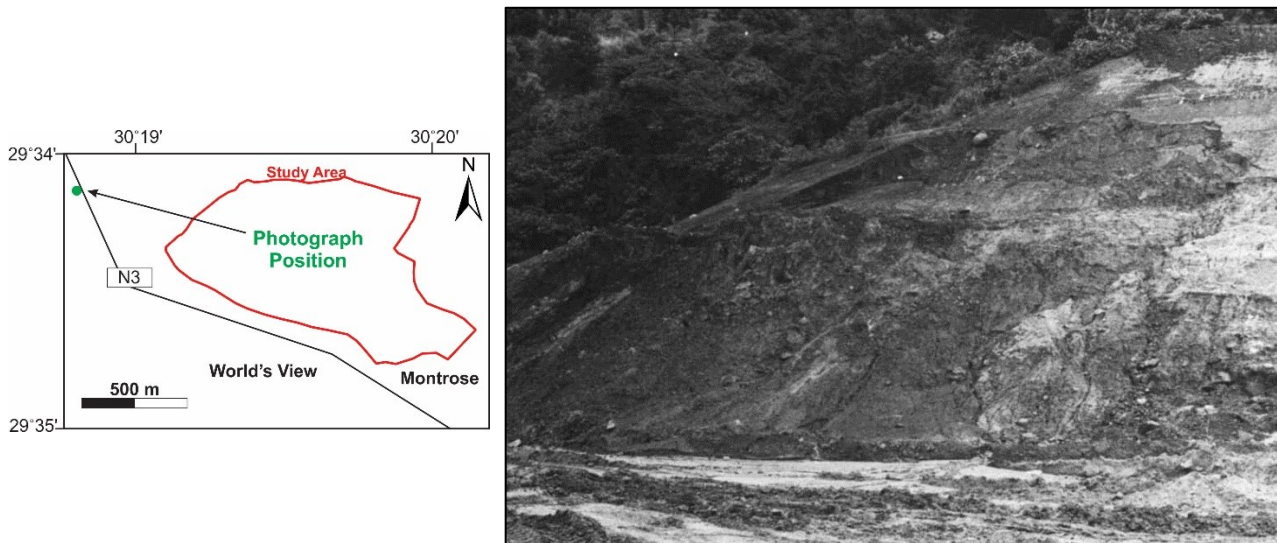


Figure 3.6: Cutting failure near Hilton in 1967 (adapted from Maurenbrecher and Booth, 1975).

In 2015, a large sinkhole developed in the southbound carriageway of the N3 Highway (Figure 3.7).

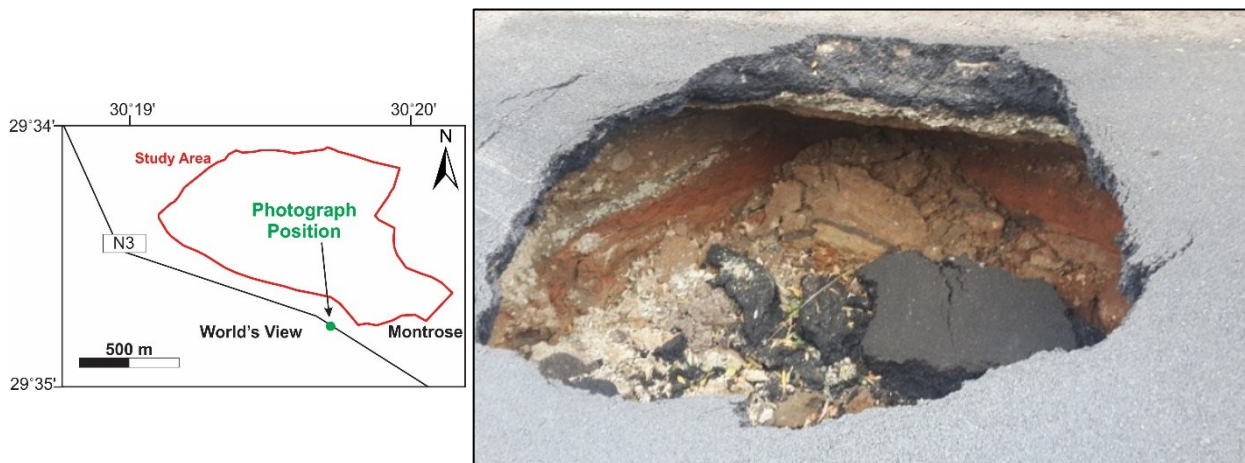


Figure 3.7: Sinkhole development in the N3 Highway in 2015.

During a site investigation conducted by the author, the subsurface cavity was deemed to have formed as a result of scouring action by a discontinuous drainage feature the formation of which is well documented by Allen (1981) and Singh (2016). As with the Montrose Slide and Hilton cutting failure, failure is attributed to poor drainage coupled with the talus soil. The latter is often less emphasised though it is a common trend in all case studies.

3.5.5 Northdale investigation

A deep auger hole investigation (12.0 m) was undertaken in 1979, in the suburb of Northdale, Pietermaritzburg. An auger hole advanced during the investigation intersected up to 10 m of intact shale, with an observed dip of 50°-70° into the slope. It was concluded that this seemingly intact shale block

was rotated backwards during sliding (Allen, 1981). Maurenbrecher and Booth (1975) pointed out that in some places, shale of the Ecca Group is known to be weathering *in-situ* and moving down slope.

3.5.6 Rickivy landslide

Arguable, the most documented historical geohazard problem in the Pietermaritzburg area is the zone of slope instability around Rickivy and Athlone below the World's View escarpment. Mass movement in the area started with failure of the Rickivy fill material during construction in 1957 (Maurenbrecher & Booth, 1975). In 1965, initial slumps resulted in minor damage which was rectified by resurfacing of the road. In 1969, cracking occurred and in early 1970, movement accelerated and continued until the end of the rainy season when movement ceased (Maurenbrecher & Booth, 1975). In 1971, the natural slope to the east of the fill failed resulting in a vertical displacement of about 2 m as shown in Figure 3.8.

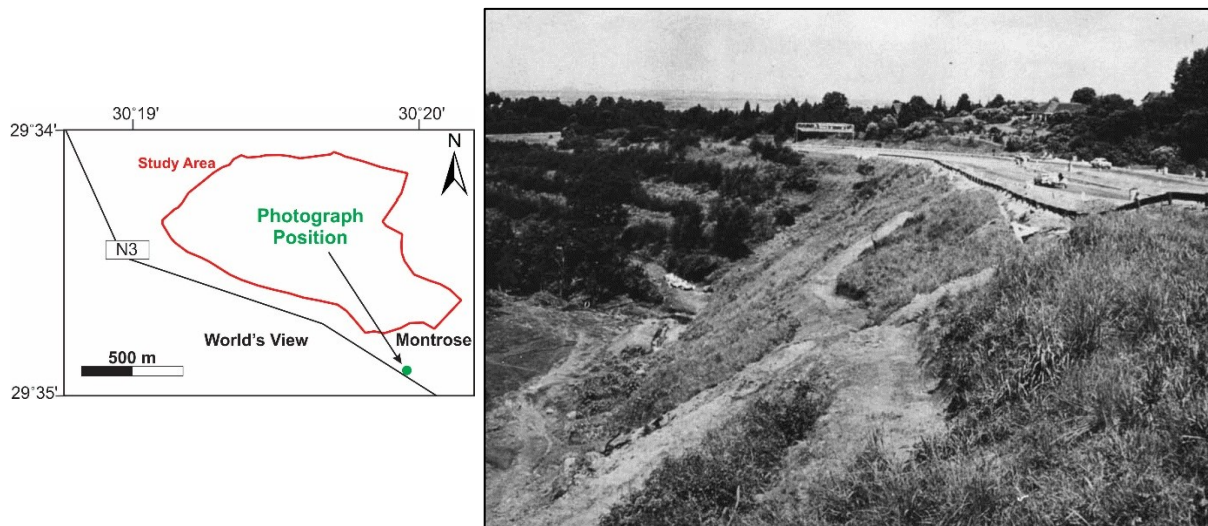


Figure 3.8: Rickivy embankment failure in 1970 (adapted from Maurenbrecher and Booth, 1975).

Geotechnical investigations undertaken on the Rickivy Embankment to establish the cause of failure concluded that the slip surface occurred in the *in-situ* talus below the fill material (borrowed talus material) as illustrated in Figure 3.9 (Maurenbrecher & Booth, 1975).

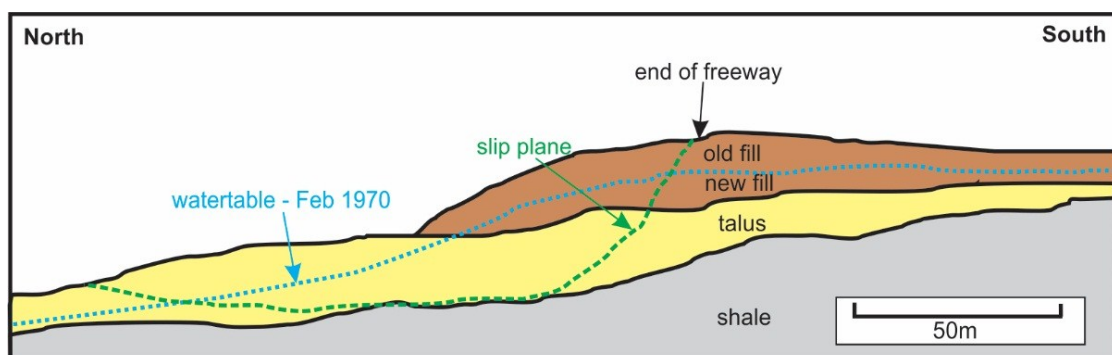


Figure 3.9: Cross-section of the Rickivy embankment (adapted from Maurenbrecher and Booth, 1975).

Allen (1981) pointed out that unless slip planes are specially sampled, unrealistically high shear strengths could result. Back analyses were undertaken on the Rickivy Embankment by Allen (1981), the results of the analyses concluded low effective shear strength values. Allen (1981) pointed out that results of laboratory shear tests can be misleading if the pre-existing slip planes have not been sampled as pre-existing slip planes have significantly low shear strength parameters as the material is in its residual state.

The Rickivy failure was due to failure on an existing slip surface in the subsoil, propagated further by the superimposition of fill material and high rainfall events (Maurenbrecher & Booth, 1975). It was suggested by Allen (1981) that initially the slip planes were discontinuous, but under the changed stress conditions caused by the embankment, progressive failure resulted in the slip planes becoming continuous (Allen, 1981).

3.5.6.1 Influence of pore water pressures

The Rickivy Embankment failed 12 years after construction. As pointed out in in Table 3.12, an increase in pore water pressures can result in an appreciable decrease in the shear strength of the soil.

Maurenbrecher and Booth (1975) suggested that the shear zones were originally discontinuous and that the new stress conditions following the imposition of the embankment loading caused progressive weakening between the zones. Once a continuous failure surface has developed, movement would have been controlled by changes in the pore-water pressures, since a relatively small increase in pore water pressure would be sufficient to reduce the factor of safety to unity (Maurenbrecher & Booth, 1975). Chowdhury (1984) pointed out that in clays excess negative pore water pressures are developed due to excavation and many years even several decades, before the pressures are fully dissipated. As positive pore water pressures increase to long-term equilibrium values, shear strength decreases in accordance with the principle of effective stress. Chowdhury (1984) reasoned that this may result in slope failure many years after the completion of an excavation.

3.5.7 Athlone slope failure

Following a heavy period of rainfall in 1971, vertical tension cracks marked the initiation of the Athlone slope failure as illustrated in Figure 3.10.

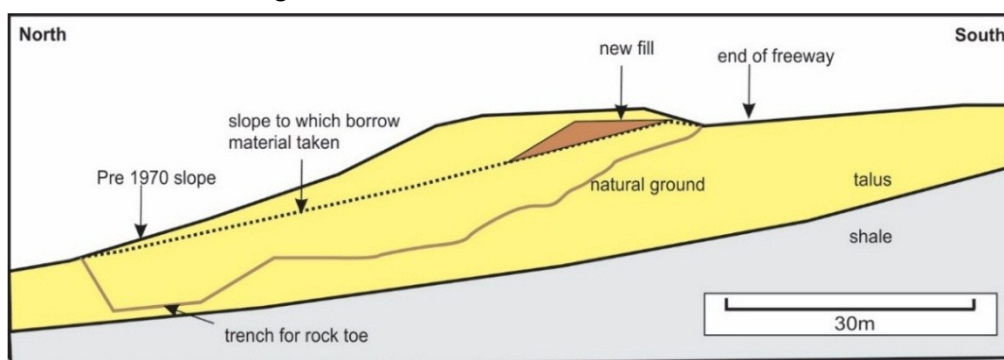


Figure 3.10: Cross-section of the Athlone slope failure (adapted from Maurenbrecher and Booth, 1975).

During the reconstruction phase of the failed slope multiple shear planes were observed by contractors as illustrated in Figure 3.11.

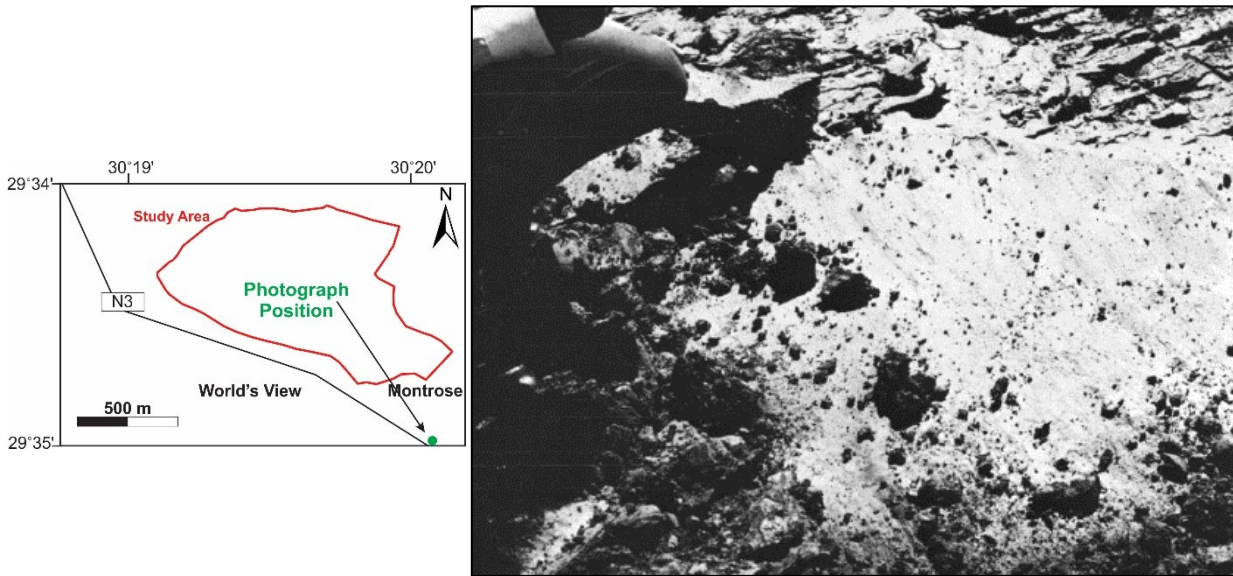


Figure 3.11: A shear plane on the Athlone Slope (adapted from Maurenbrecher & Booth, 1975).

3.6 Review of subsurface drilling, augering and trial pitting in Town Bush Valley

As mentioned in Chapter 2 the study area has been split into five village developments namely the World's View Development, Cascades Development, Upper National Park, Lower National Park and the Montrose Park Development.

The World's View Development was first investigated in October 2004 by Hadlow (2004) of Drennan Maud and Partners, in which six boreholes denoted BHD1 to BHD6 were drilled. Other geotechnical drilling investigations relevant to this study were conducted in 1993 by Hadlow (1993) of Drennan Maud and Partners, as part of the N3/Athlone circle to Hilton National Freeway upgrade during which four boreholes, denoted as BH1 to BH4 were drilled. Notable BH4 was inclined at 45° south in order to optimize data coverage. During the investigation, boreholes were drilled to depths ranging from 15.11 m (BHD2) to 36.58 m (BH1) below natural ground level (NGL).

The Upper National Park was originally investigated in June 2005 by Schreiner (2005e) of Jeffares and Green, in which six boreholes denoted BH1 to BH6 were drilled. Boreholes were drilled to depths ranging from 9.70 m (BH3) to 25.2 m (BH1) below NGL.

The Cascades Development was investigated in November 2005 by Schreiner (2005b) of Terratest, in which five boreholes, denoted BHV3/1 to BHV3/5 were drilled. Boreholes were drilled to depths ranging from 15.22 m (BHV3/4) to 26.62 m (BHV3/1) below NGL.

The Lower National Park was also investigated in November 2005 by Schreiner (2005a) of Jeffares and Green, in which two boreholes denoted BH4/1 and BHV4/2 were drilled. The rotary-core boreholes were drilled to depths ranging from 18.41 m (BHV4/1) to 23.95 m (BHV4/2). An air-percussion drilled borehole, was advanced to 132.0 m below NGL in May 2016 for groundwater abstraction. The data derived from the groundwater abstraction borehole provided bedrock levels.

The Montrose Park Development was investigated in September 2005 by Kujawa (2005) of Drennan, Maud and Partners, in which nine boreholes denoted D9 to D17 were drilled. In addition, nine auger holes were advanced during site investigations undertaken in 2006 by Schreiner (2006m), (2006n) of Terratest. Boreholes were drilled to depths ranging from 9.09 m (D11) to 23.25 m (D15) below NGL. The positions of the various boreholes, auger holes and trial pits excavated as part of this study are shown in Figure 3.12.

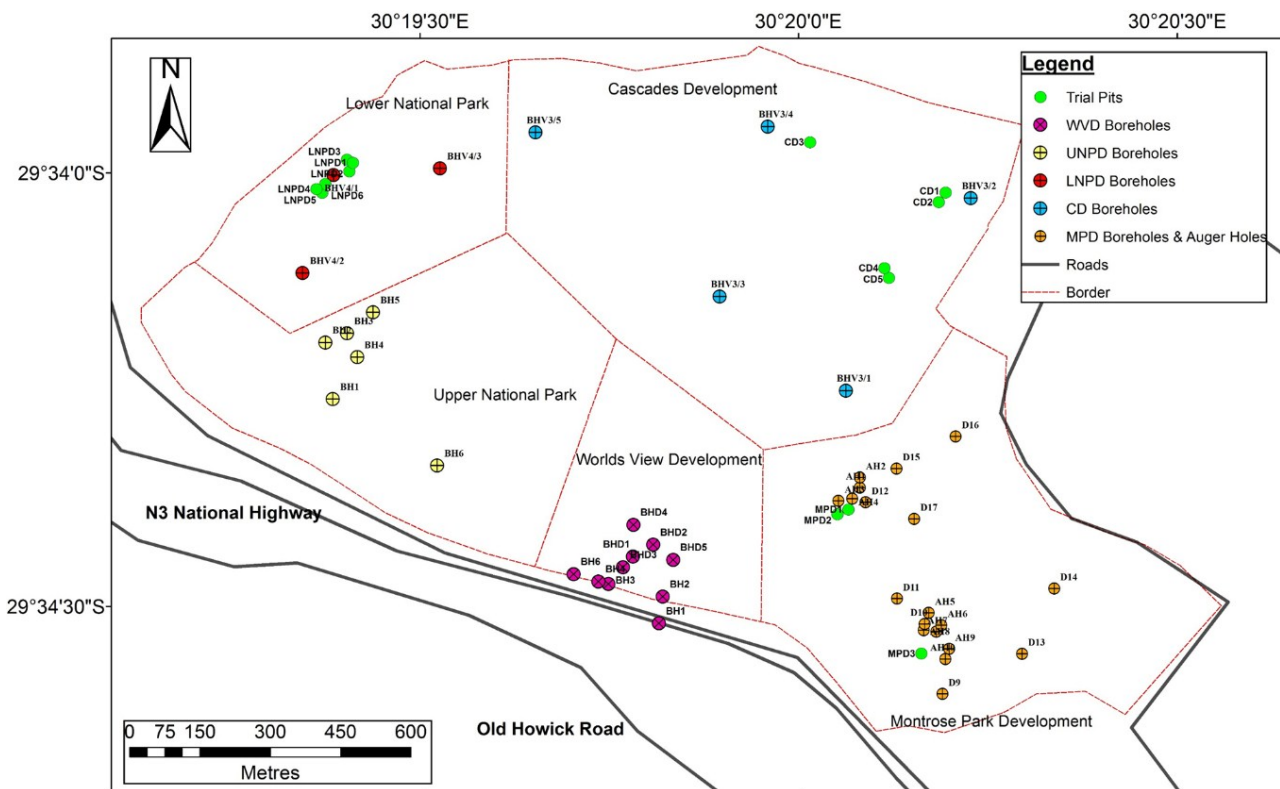
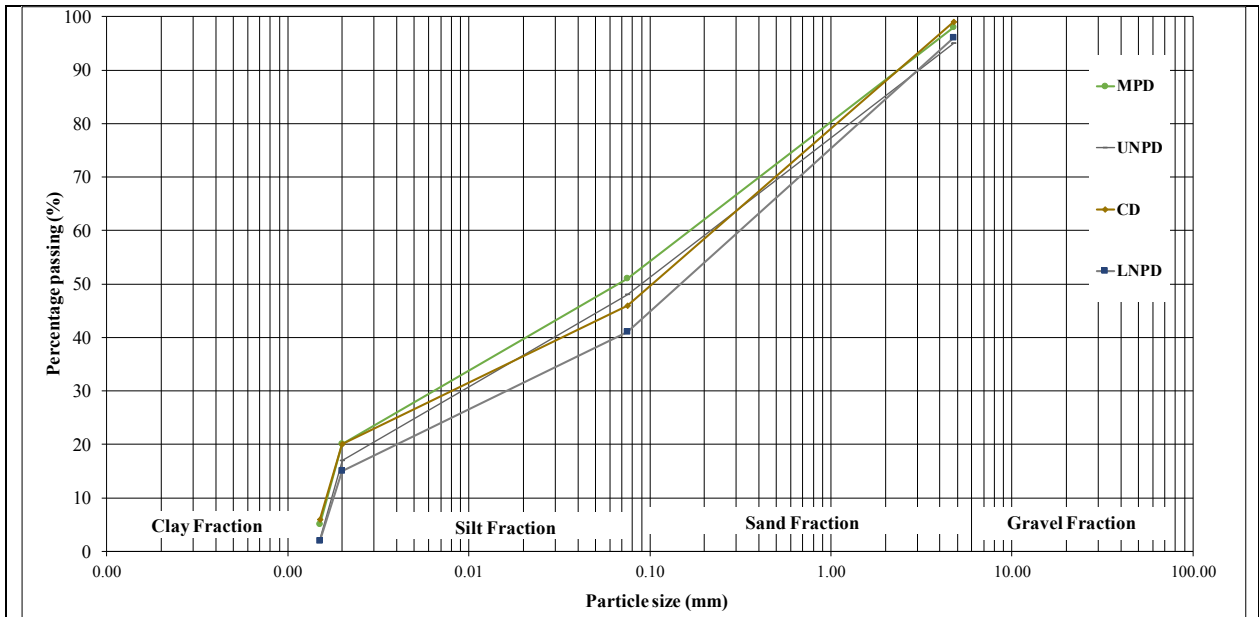


Figure 3.12: Location of the boreholes, auger holes and trial pits (from various sources).

3.6.1 Previous soil laboratory test results in the Town Bush Valley

A total of sixty-two consultant reports undertaken by Terratest Pty (Ltd) Consultants in the Town Bush Valley study area have been reviewed. From the review, a total of 119 laboratory tests were undertaken on the talus material and the average particle size distribution results are presented in Figure 3.13.



Sources:

Isherwood (2013); Ndela (2012); Schreiner, (2005c) to Schreiner, (2005d); Schreiner, (2006a) to Schreiner, (2006l); Schreiner, (2007a) to Schreiner, (2007e); Singh (2007a) to Singh (2007k); Singh (2008a) to Singh (2008e); Singh (2009a) to Singh (2009f); Singh (2010a) to Singh (2010e); Singh (2015b); Subrayen, (2013), Subrayen, (2014); Viviers, (2006), Viviers, (2007a) to Viviers, (2007c), Viviers, (2008a), Viviers, (2008b), Viviers, (2009), Viviers, (2011) & Vukea (2013).

Figure 3.13: Average particle size distribution curve for the Town Bush Valley talus material.

The test results indicate that the talus material comprises majority of sand sized particles, with a minor silt component. The results of previous shear strength tests conducted in the Town Bush Valley are summarized in Table 3.13.

Table 3.13: Previous shear strength test results obtained in the Town Bush Valley.

Location	x	Type of test	Depth	Material	c' (kPa)	ϕ' (°)	Source
WVD	1	CD	2.00 m	Talus - silty clay	0	22	Hadlow (2004)
WVD	1	CD	2.50 m	Talus - silty sandy clay	0	29	Hadlow (2004)
MPD	1	CD	2.50 m	Talus - sandy clay	8	28	Kujawa (2005)
MPD	1	CD	2.00 m	Talus - sandy clay	10	28	Kujawa (2005)

Where; x = number of samples; CD = Consolidated-drained shear box test

The shear strength test results indicate that the sampled talus material displays low c' values and high ϕ' values. The test results further indicate that the talus soils exhibit a high component of frictional strength. It is possible for a clay soil to exhibit purely frictional shear strength during shearing, due to the interparticle forces acting on each other (Smith, 1990; Carter & Bentley, 1991).

CHAPTER 4

METHODOLOGY

4.1 Scientific framework

The methodology applied and the analytical procedures used are critical to the intended outcomes of any study. This particular study involved desktop and fieldwork components in order to holistically evaluate the study site. The desktop component involved the collection, extraction and verification of data concluded from case studies and technical reports by various consultants, over the period from 1975 to 2016. Furthermore, previous geotechnical drilling and auger investigations conducted over the period from 2004 to 2015 are reviewed. In order to identify critical areas of slope instability, a digital elevation model was constructed and a review of available topographic maps, historic aerial imagery, geological maps and geotechnical maps was undertaken.

The fieldwork component for this study involved mapping geological, hydrogeological and drainage features. Trial pits were excavated in the study area and talus samples were retrieved for laboratory testing. A summary of the type of laboratory tests undertaken on the talus material and the test standards are presented in subsequent sections.

Understanding the factors which control the stability of slopes requires a sound knowledge of the shearing resistance of earth materials forming the slope (Chowdhury, 1984). The basic procedures used during shear strength testing is detailed with emphasis on the effective shear strength parameters which are representative of long-term slope stability. Cross-sections were constructed of various slopes using data collected from elevation data, subsoil profiles and groundwater levels. Cross-sections were orientated in order to optimally intersect data points.

Traditional slope stability analysis within a deterministic framework is limited by the use of single valued variables to assess the stability of a slope. The inherent variability and uncertainty of the parameters such as material properties and the groundwater table, which affect slope stability mean that slope stability analysis is best quantified using a probabilistic approach (Huvaj & Oguz, 2018). By adopting a probabilistic approach to deterministic models, the element of uncertainty and variability can be accounted for.

The general scientific processes followed in this study is presented in Figure 4.1.

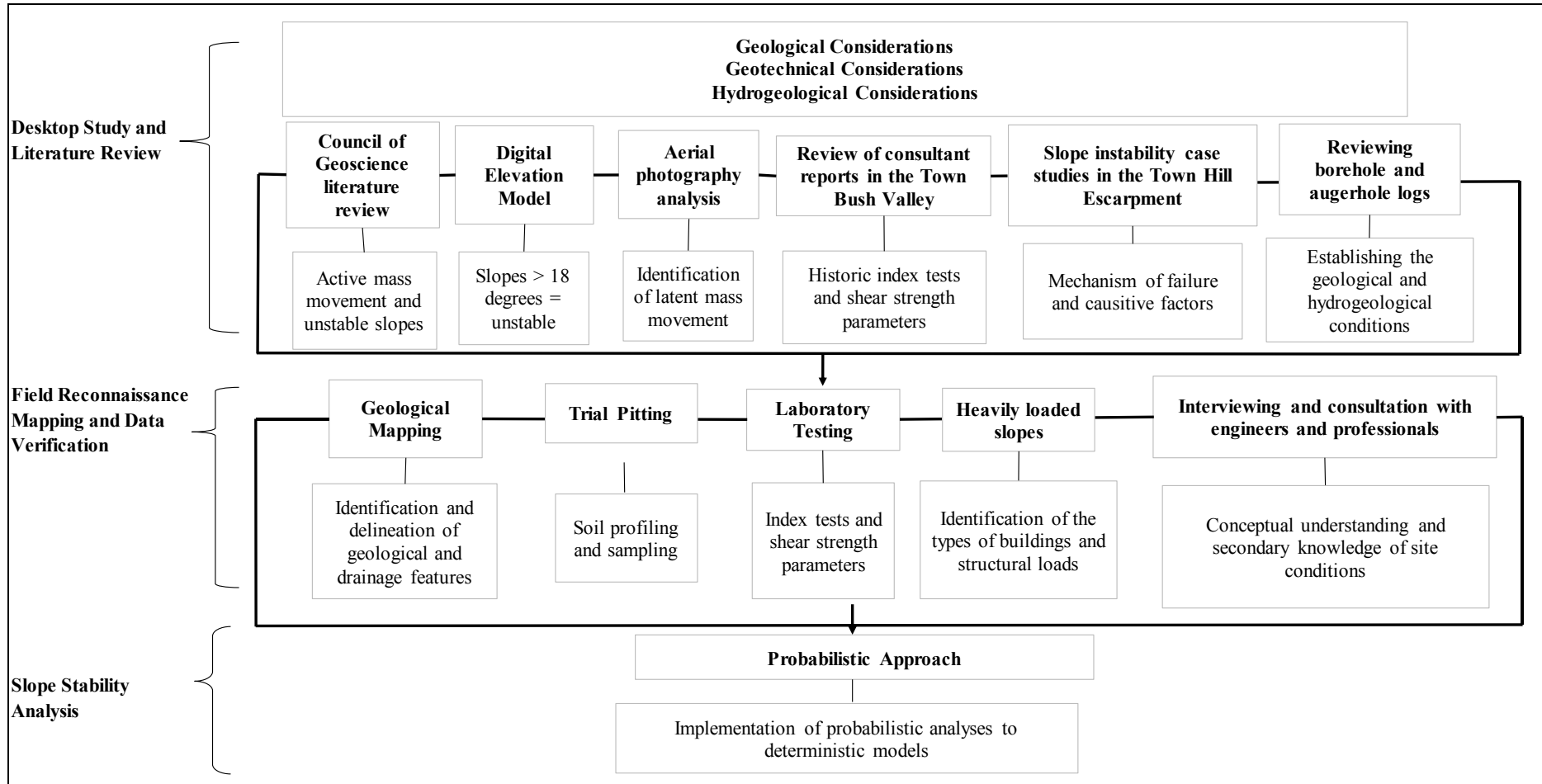


Figure 4.1: General flow chart indicating the scientific steps followed during the study.

4.2 Soil sampling

As part of this study, fourteen trial pits were advanced in the study area, from which thirteen samples were retrieved. Trial pits were profiled according to the guidelines for soil logging by the South African Institution of Civil Engineering (SAICE) (2002). Soil samples were taken from representative horizon and prepared according to Part 1 of the BS 1377 (1990a). The trial pits were excavated in areas where access was permissible. The positions wherein soil samples were taken are illustrated in Figure 2.

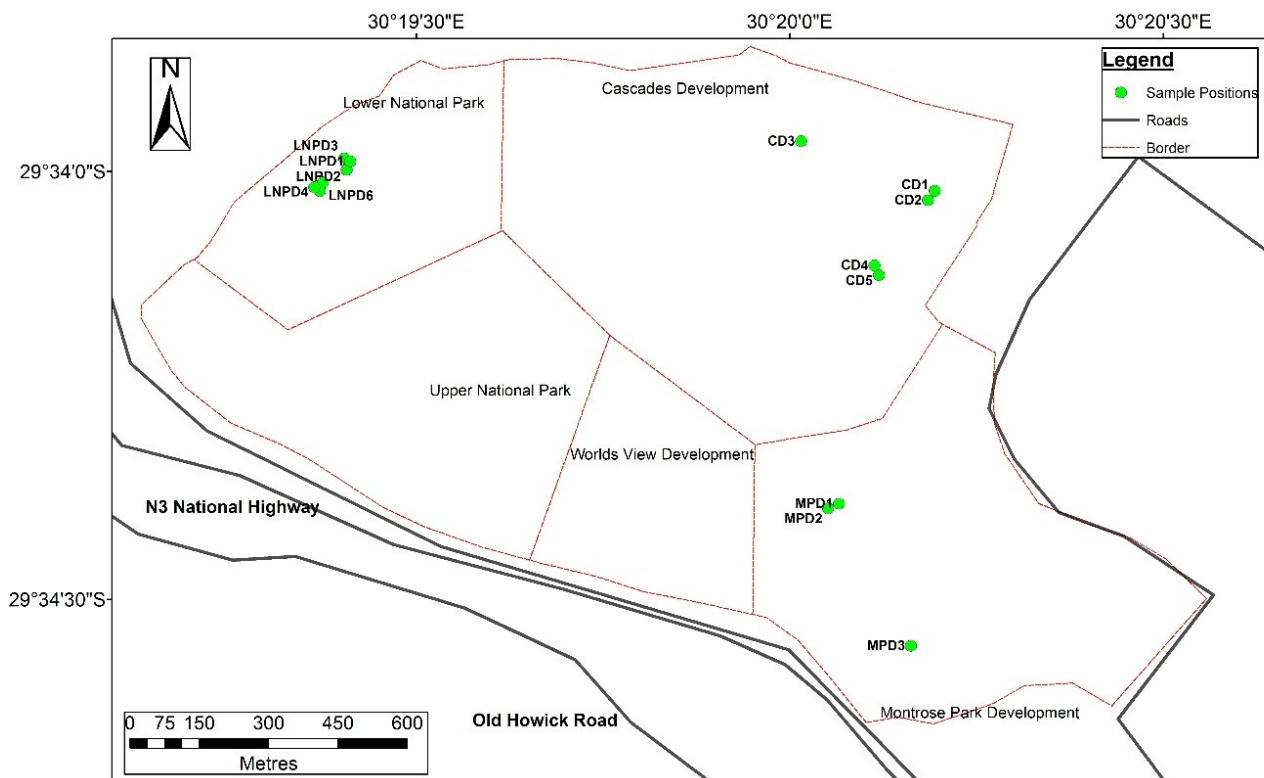


Figure 4.2: Soil sample positions in the Town Bush Valley.

4.2.1 Undisturbed sampling and *in-situ* density determination

Density determination involved pushing a metal cylinder of known dimensions into the *in-situ* soil and retrieving a column of soil, as illustrated in Figure 4.3. Samples were retrieved from sample positions MPD3 and LNP3.

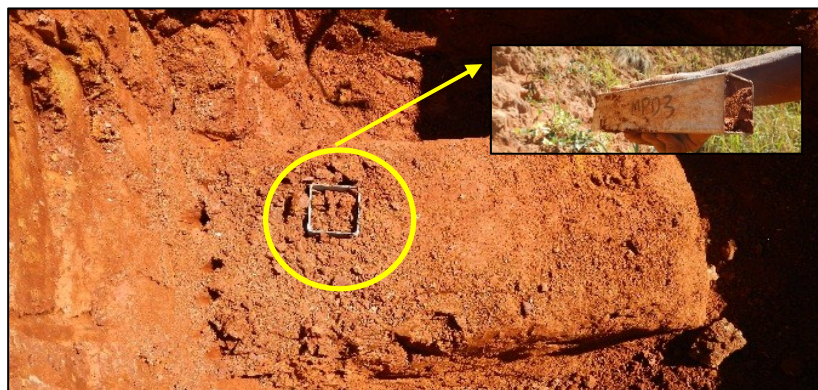


Figure 4.3: *In-situ* density retrieval from an undisturbed block at trial pit MPD3.

Two undisturbed block samples (LNP3 and MPD3) were taken from the talus material for density determination and triaxial testing (Figure 4.3). Undisturbed soil sampling was undertaken according to Part 1 of the BS 1377 (1990a), detailed soil sampling methodologies are provided in Appendix A1.

Density calculations involved determining the mass of the soil column in the cylinder. The equations used to determine the density, moisture content and other geotechnical parameters derived from moisture-density relationships are given in Appendix A1.

Undisturbed sampling involved the cutting of a block sample and the application of wax to the *in-situ* soil block in order to create a rigid mould and to preserve moisture at the *in-situ* condition as illustrated in Figure 4.4. The coated block was carefully extracted from the soil and transported to the laboratory for further testing.



Figure 4.4: Waxed soil block at trial pit MPD3.

4.3 Laboratory testing

During soil sampling, thirteen sample consignments were retrieved from trial pits for index testing and two carefully prepared undisturbed samples were submitted to the eThekweni Soils Laboratory for triaxial testing. Index testing was undertaken according to the South African Technical Methods for Highways (TMH), developed by the Council for Scientific Research (CSIR, 1986). The following test methods were applied:

- i. *Grading Analysis: TMH method A1 - Wet Preparation and sieve analysis of gravel, sand and soil samples;*
- ii. *Hydrometer Analysis: American Society for Testing Materials (ASTM)-D422-63 (1998) – Standard test method for Particle-size analysis of soils;*
- iii. *Liquid Limit: TMH method A2 – Determination of the liquid limit of soils by means of the flow curve method;*
- iv. *Plastic Limit: TMH method A3 – Determination of the plastic limit and plasticity index of soils;*
- v. *Linear Shrinkage: TMH method A4 – Determination of linear shrinkage of soils; and*
- vi. *Triaxial Testing: British Standards 1377: Part 8: 1990b – Consolidated Drained Triaxial Test*

4.3.1 Particle size analysis

The distribution of particle sizes or average grain diameter of coarse-grained soils (gravels and sands) is obtained by screening a known weight of the soil through a stack of sieves of progressively finer mesh size (Budhu, 2000). The screening process cannot be used for fine grained soils such as silts and clays, because of their small size (Budhu, 2000). A hydrometer analysis was undertaken to determine the distribution of the fine grained soil particles. The hydrometer test involves mixing a small amount of soil into a suspension and observing how the suspension settles over time (Budhu, 2000). The method uses the relationship between the velocity of the fall of a sphere in a dispersive fluid and viscosity of the fluid to classify the particles under different diameter categories (ASTM, 1998; Budhu, 2000). The grading curves obtained from particle size analysis can be used for a textural classification of the soil (Budhu, 2000; Murthy, 2003). The Unified Classification System (USCS) is one such classification system which separates the soil into two main categories. The first category is the coarse grained soils which is delineated if more than 50 % of the soil is finer than the 0.075 mm sieve aperture size. The second category is the fine grained soils which is delineated if more than 50 % of the soil is finer than 0.075 mm.

4.3.1.1 Grading analysis

The sieve analysis procedure firstly involved, quartering the sample by using a riffler. The material was then dry sieved through various sieve apertures. A known weight of dry soil is placed on the largest sieve and the stacked sieves are placed on a sieve shaker (Budhu, 2000). Calculations involved determining the percentages retained on each sieve which was then converted to a percentage passing the sieve. The grading analysis test culminated in the presentation of a particle-size distribution curve, which graphically illustrates the major soil particle sizes. Engineers have found it convenient to use a logarithm scale for representing the particle size distribution (Budhu, 2000; Knappet & Craig, 2012)

4.3.1.2 Hydrometer analysis

The hydrometer analysis firstly involved the dispersion of the soil fines passing the 2.00 mm sieve by using a dispersive agent. After several processes of soaking and dispersion, the soil slurry was transferred into a sedimentation cylinder. The sedimentation cylinder was inverted 30 times for 1 minute after which, the cylinder was laid to rest. Readings were taken by observing the top of the meniscus formed by the suspension and the hydrometer at various time intervals.

Calculations involved determining the equivalent particle diameter using Stoke's Law and the percentage of soil remaining in suspension. The grain size curve of the diameters of the particles and percentages smaller than the corresponding diameters were established (ASTM, 1998). The results of the test is the percentage of silt and clay in each sample.

4.3.2 Atterberg Limits Determination

The physical and mechanical behaviour of fine grained soils is linked to three states: brittle, plastic and fluid behaviour, the concept of which is shown in Figure 4.5 (Knappet & Craig, 2012).

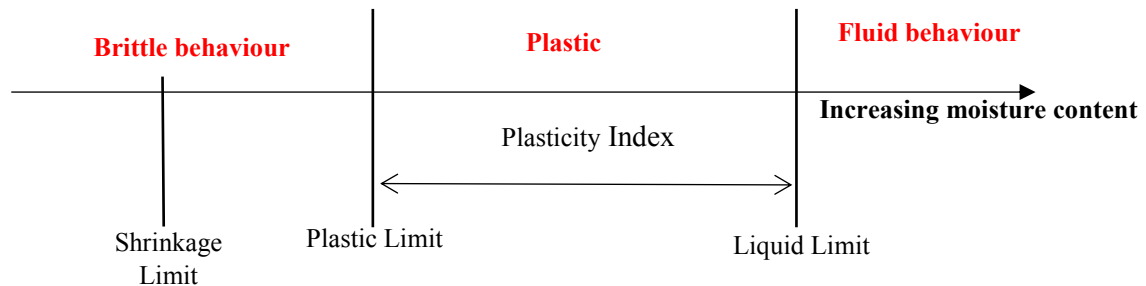


Figure 4.5: Changes in the soil state when water is added (adapted from Knappet & Craig, 2012).

The liquid limit is defined as the boundary between the liquid and plastic state which is dependent on the moisture content (TMH, 1986; Smith, 1990). The plastic limit is defined as the boundary between the plastic and semi-solid state which is dependent on the moisture content. The plasticity index of a soil is the numerical difference between the liquid limit and plastic limit of the soil and indicates the magnitude of the range of the moisture contents over which the soil is in a plastic condition (TMH, 1986). The water content at which the soil changes from a semi-solid to a solid is called the shrinkage limit (Budhu, 2000; Knappet & Craig, 2012).

4.3.2.1 Liquid limit

The liquid limit is the boundary at which soil behaviour changes from a plastic state to a liquid state (Knappet & Craig, 2012). The purpose of the test was to determine the number of taps taken for the faces of two soil portions to flow together over various moisture contents. Calculations involved plotting the moisture content verse number of taps and determining the moisture content at 25 taps, corresponding to the liquid limit of the soil.

4.3.2.2 Plastic limit

The purpose of the test was to establish the moisture content at which crumbling of soil threads of approximately 3 mm in diameter occurs (TMH, 1986; Budhu, 2000). Calculations involved establishing the percentage moisture content of the oven dried soil which corresponded to the plastic limit. The plasticity index was obtained by subtracting the plastic limit from the liquid limit.

The plasticity index is the range of water content within which a soil is plastic (Smith, 1990). Establishing the plastic index of soils, enables an understanding of the shrink and swell behaviour of the soil fines.

4.3.2.3 Linear shrinkage

The test involved oven drying a soil specimen in a shrinkage trough of known dimensions. Calculations involved measuring the percentage difference in the original wet length and dried length, to which a correction factor was applied.

4.3.3 Triaxial test

Consolidated-drained tests are carried out by consolidating the specimen under a confining pressure and allowing drainage during the compression stage (Head, 1998). The test has the advantage that drainage conditions can be controlled, enabling saturated soils of low permeability to be consolidated and pore water measurements to be made (Knappet & Craig, 2012). The rate of shearing must be slow enough to allow the complete dissipation of the resulting pore water pressure and to ensure that no excess pore water pressure develops (Head, 1998). A routine consolidated-drained triaxial test consists of three stages namely saturation, consolidation and compression. The typical layout of a triaxial pressure system with the ancillary apparatus is illustrated in Figure 4.6.

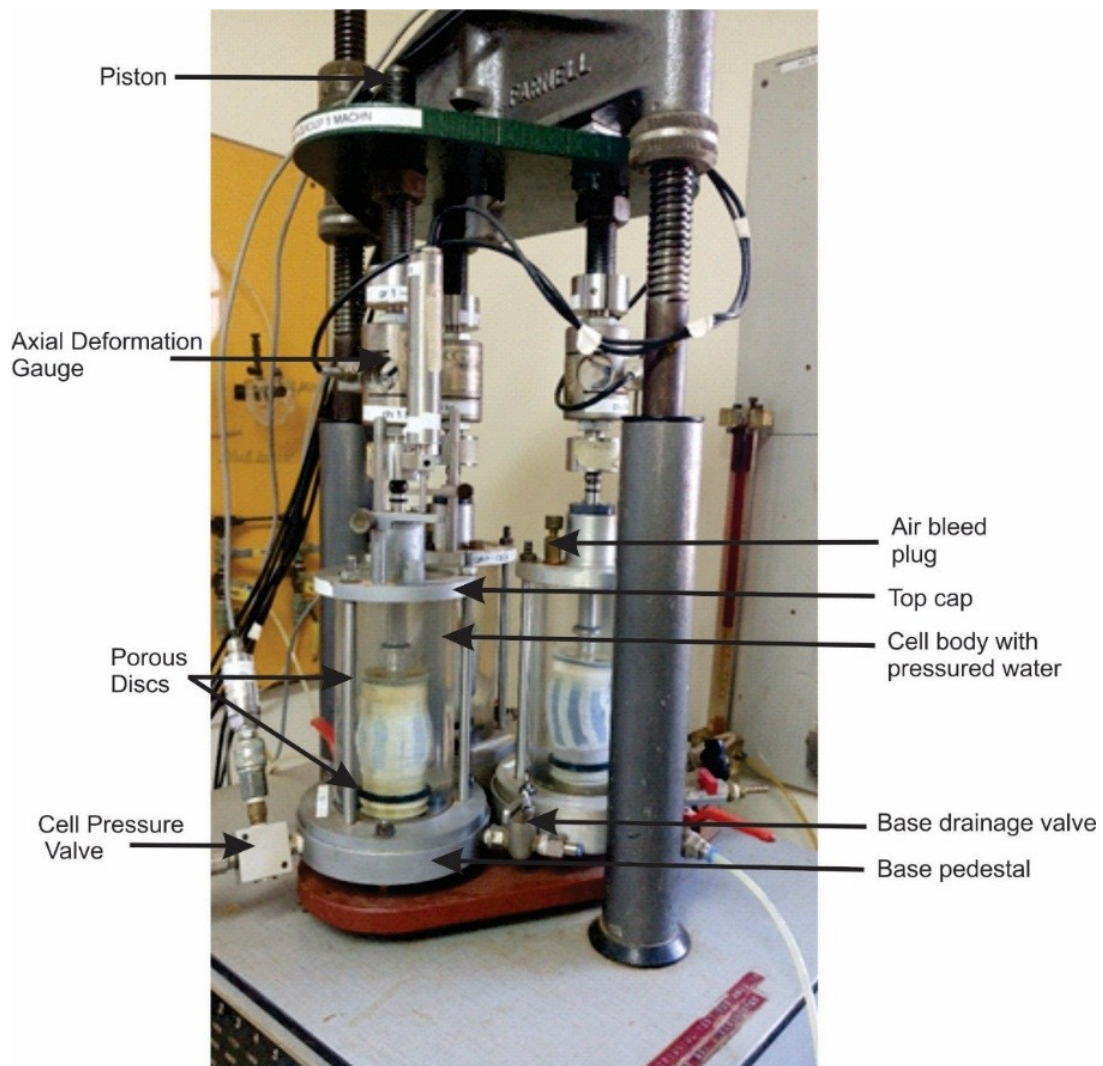


Figure 4.6: Typical triaxial system setup in a laboratory.

During the compression stage of a consolidated-drained triaxial test, the cell pressure is maintained constant while the specimen is sheared at a constant rate of axial deformation until failure occurs (Head, 1998). A detailed methodology is presented in Appendix A2, a summary of which is discussed below.

4.3.3.1 Saturation

The term saturation as a stage of the test which refers to way by which pore pressure in the specimen is increased so that air in the void spaces are eliminated (BS1377, 1990b; Head, 1998). The pore water pressure is increased in a controlled manner through the application of a back-pressure system and an increase in the cell pressure. The magnitude of the cell pressure increments must not exceed 50 kPa or the consolidation pressure during compression (Head, 1998). The time required for saturation depends on the type of soil and size of specimen as well as the initial degree of saturation (Head, 1998). Side drains were used during the saturation of the samples. The use of side drains in soils of low permeability can reduce the time required for saturation, but the pore water pressure response should be analysed with care (BS 1377, 1990b).

The pore water pressures were recorded using an automated transducer and the difference in pore water pressures were automatically calculated. The basic requirements for saturation is when the value of $B \geq 0.95$, then only is the specimen is considered saturated and consolidation can commence (BS 1377, 1990b).

4.3.3.2 Consolidation

During the consolidation stage of the triaxial test the specimen is consolidated under a confining cell pressure by allowing water to drain out into the back-pressure system (Budhu, 2000), so that pore water pressures gradually falls until it nearly equals the back pressure. Consolidation must be allowed to continue until at least 95 % of the excess pore pressure has dissipated (BS 1377, 1990b; Head, 1998). The use of side drains also shortens the consolidation time required for soils of low permeability.

Calculations involved determining the significant testing time and the rate of axial displacement. The data obtained during the consolidation phase was used to calculate a suitable rate of strain for the compression stage (BS 1377, 1990b). The rate of strain used during compression for this particular test was calculated to be 0.045 mm/min for the LNP3 sample and 0.045 mm/min for the MPD3 sample.

4.3.3.3 Compression

When equilibrium is achieved under the confining pressure shearing can commence. During the compression stage of a triaxial test the axial force is gradually increased until failure occurs, while the total confining pressure remains constant. During compression the rate of shearing is done at a slow rate to allow dissipation of the pore water pressures, so that the excess pore water pressures cannot build up and are kept at zero. During compression the deviator stress ($\sigma_1 - \sigma_3$) values and pore water pressure

values were plotted against the corresponding axial strains. Calculations involved plotting Mohr-circles and constructing a line representing the Mohr-Coulomb failure criterion for effective stresses. The results of which are presented in detail in Chapter 5.

4.4 Slope stability analyses

Slope stability analyses requires a sequence of input procedures, the basic phases used during slope stability analyses are presented in Figure 4.7.

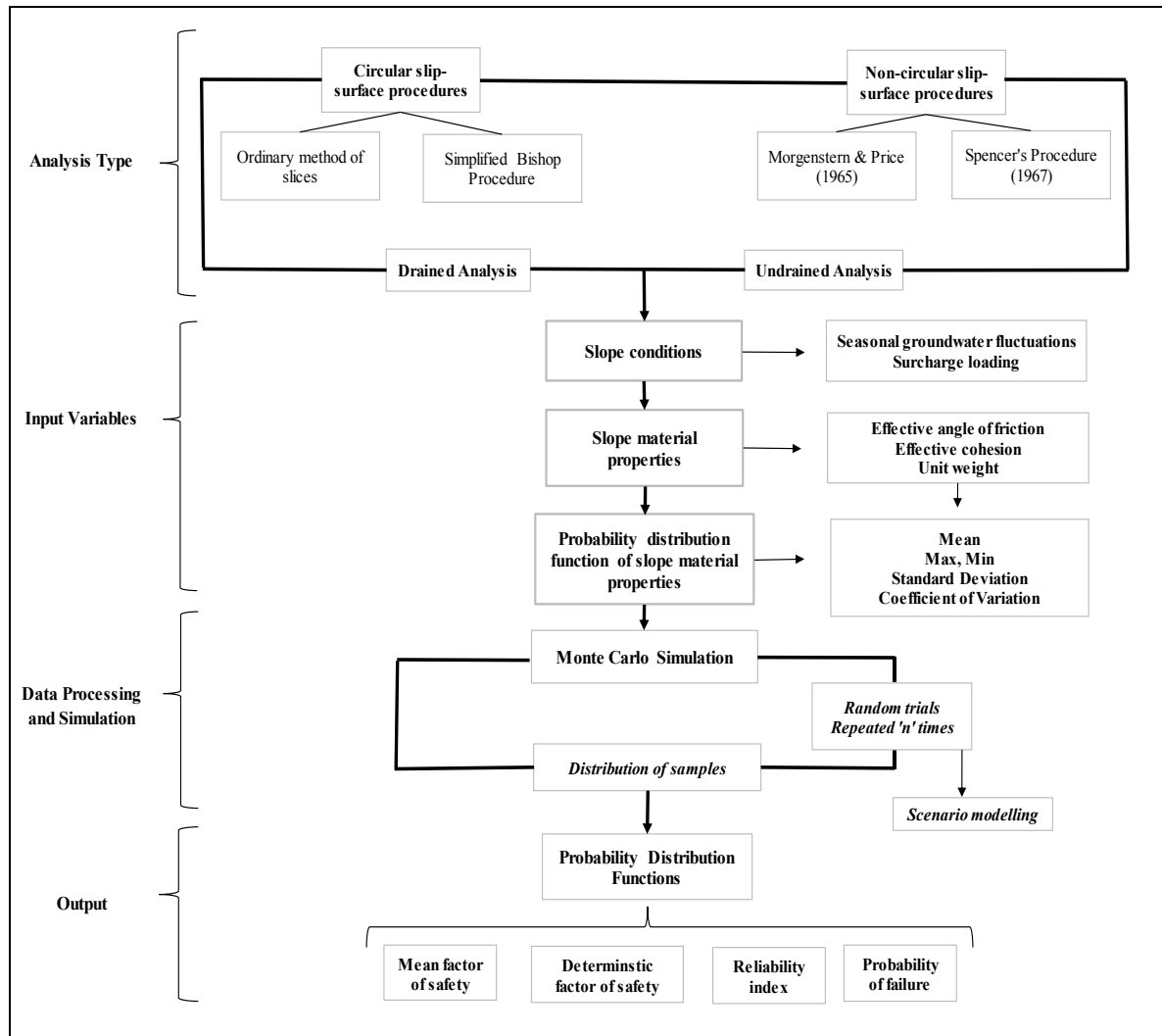


Figure 4.7: Flowchart illustrating the phases used during the probabilistic approach of slope stability analysis.

4.4.1 Selection of the method of analyses

The method chosen for the slope stability analysis was the Morgenstern and Price (1965) procedure. A rigorous and well-established procedure which provides added flexibility. It allows forces to vary across the slope and formulates equations of equilibrium by resolving equilibrium parallel to and normal to the base of the slice (Cornforth, 2005; Duncan & Wright, 2005). It is applicable to virtually all slope

geometries and soil profiles. The procedure is based on a limit equilibrium analysis in which all boundary and equilibrium conditions are satisfied and in which the geometry of the failure surface may be of any shape (Knappet & Craig, 2012). Long-term slope stability formed the basis for this study. This implies drained conditions are appropriate and as such the effective shear strength parameters (c' , ϕ') were used in the analyses.

Slope stability analyses were conducted using a limit equilibrium software package, Rocscience Inc. SLIDE (version 6.0). Rocscience SLIDE is a comprehensive two-dimensional (2D) slope stability program for soil or rock slopes. Material shear strengths, external loading, groundwater and support can be modelled in a variety of ways. Rocscience is a limit equilibrium software package in which automated search methods can determine the critical failure surface. The advancements in software allow for fast results and for statistical information to be incorporated into slope stability analyses (Bar & Heweston, 2018).

4.4.2 Selection of the cross-sections for analyses

Various lines of cross-section were considered and are presented in Figure 4.8. Cross-sections F-F' and G-G', were the slopes selected for slope stability analyses. A review of the various geological and aerial imagery suggest that these cross sections correspond to inclined slopes in which slope gradients exceed 18° . Furthermore, cross-sections F-F' and G-G' are aligned through closely spaced, heavily loaded structures that are proposed for development.

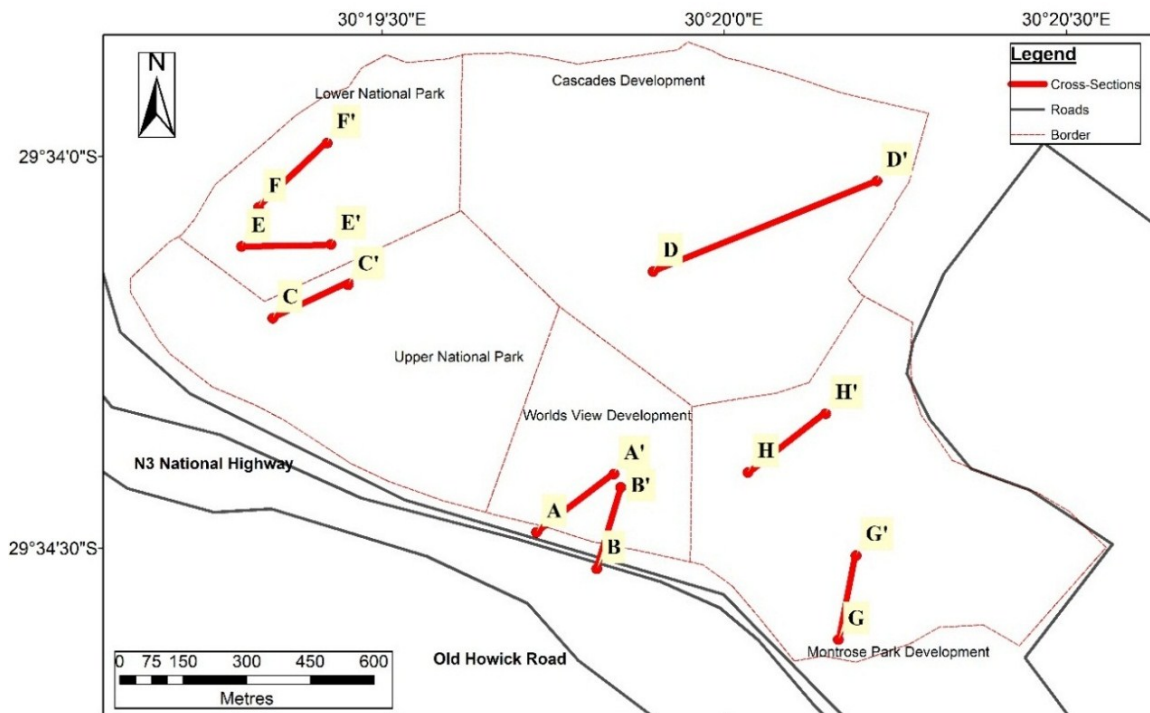


Figure 4.8: Lines of cross-section covering the WVD, MPD, UNPD, LNP and Cascades Development.

Cross-section F-F' is presented in Figure 4.9 and cross-section G-G' is presented in Figure 4.10.

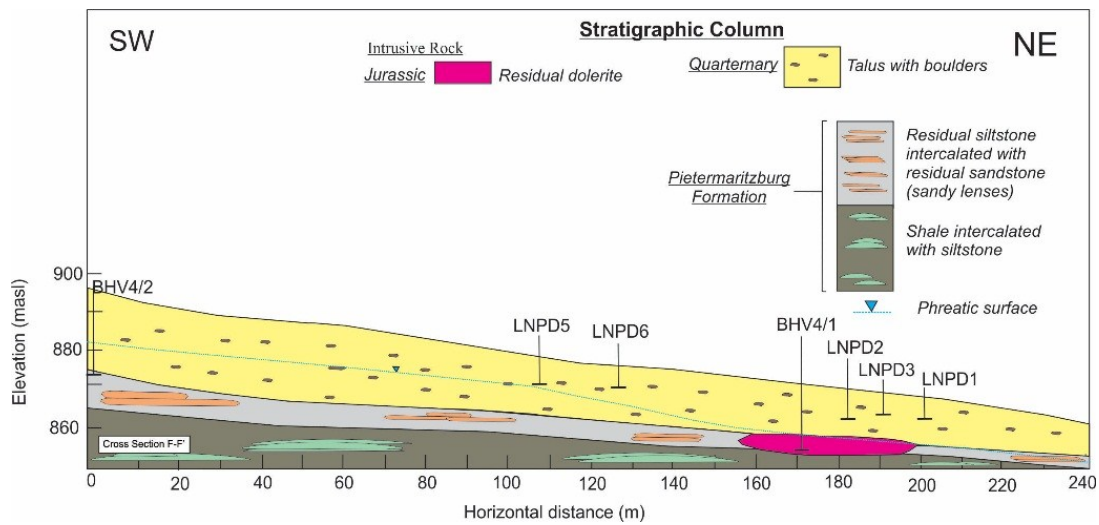


Figure 4.9: Cross-section F-F' of the LNPD used for the slope stability analyses.

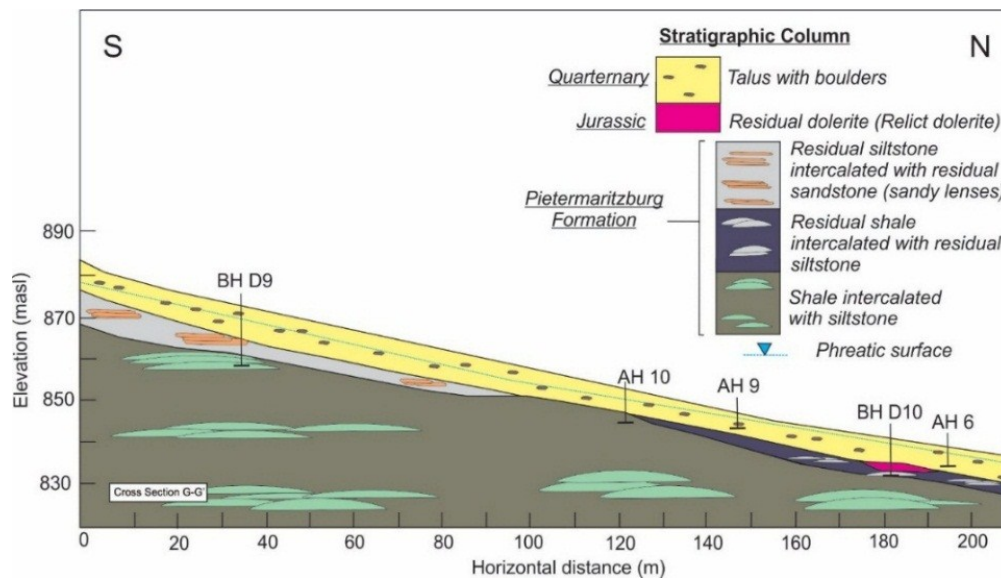


Figure 4.10: Cross-section G-G' of the MPD used for the slope stability analyses.

4.4.3 Representation of values

In this study, the effective shear strength parameters (c' , ϕ') of the talus material were the chosen random variables in the case of the probabilistic analysis. Variability of some parameters such as the unit weight and geometrical parameters has an insignificant influence on slope stability such parameters may be regarded as constants, parameters such as shear strength and pore water pressures are desirable to consider as random variables (Chowdhury, 1984).

The effective shear strength parameters were based on results from published and unpublished geotechnical reports, published geotechnical soil relationships, supplemented by soil survey data and laboratory testing done as part of this study. The data sets used can be found in Appendix A3.

Each parameter must be represented by a probability distribution function defined by its mean and standard deviation (Chowdhury, 1984; Lacasse & Nadim, 1996; Huvaj & Oguz, 2018). The effective shear strength parameters were defined by the mean and standard deviation and truncated at realistic minimum and maximum values as prescribed by Nilsen (2000) and Duncan & Wright (2005), that accurately represent the material properties and account for the variability in the effective shear strength parameters. Outlier values were removed in order to improve data quality and boost confidence. Lacasse & Nadim (1996) emphasised the importance of lumping together only consistent data sets during statistical analyses.

A histogram was used to determine the probability distribution function (*pdf*) of the random variables. A histogram relative frequency distribution is a compact summary of the data, in which the data is divided into a few class intervals or bins (Montgomery & Runger, 2011).

A lognormal distribution was selected for the effective shear strength parameters and was used during slope stability analyses. According to Huvaj & Oguz, (2018), a lognormal distribution is widely used and has been shown to perform well in probabilistic analyses.

The mean c' was calculated to be 0.5 kPa and a standard deviation of 0.9 kPa with a lognormal distribution as summarized in Table 4.1. The mean ϕ' was calculated to be 28.2° and a standard deviation of 1.8° with a lognormal distribution as summarized in Table 4.1.

Table 4.1: Statistical distribution of the random variables.

Random Variables - x = 38	c' (kPa)	ϕ'(°)
μ	0.5	28.2
σ	0.9	1.8
Min	0.0	22
Max	10	32
Probability Distribution Function	Lognormal	Lognormal
Where; x is the number of samples, μ is the mean, σ is the standard deviation.		

The unit weight and the groundwater table were not considered as random variables and were held constant. Limited shear strength data was available on the residual sedimentary horizons due to the lack of geotechnical tests conducted on the horizons. As a result, the effective shear strength parameters of the residual sedimentary horizons were held constant during slope stability analyses.

Lacasse & Nadim (1996), pointed out that unfortunately one is never able to gather enough subsurface data to get an exact picture of the variation of soil properties for an an engineering structure. The shear strength parameters for the residual sedimentary and residual dolerite horizons were based on the profile descriptions, which are discussed in Chapter 5, combined with theoretical values presented in the

various tables presented in Chapter 3. Table 4.2 summarizes the shear strength parameters used during analyses of the residual horizons.

Table 4.2: Effective shear strength parameters of the residual horizons.

Lithology	c' (kPa)	ϕ' (°)
Residual siltstone intercalated with residual sandstone	0	28
Residual Dolerite	0	31
Residual shale intercalated with residual siltstone	0	28

4.4.4 Representation of pore water pressures

Groundwater measurements concluded from investigations undertaken by consultants and presented in the course of this study provided a base map to construct a groundwater table contour map (Chapter 2, Figure 2.14). Due to limited records on temporal groundwater data, a realistic range of groundwater levels were incorporated during slope stability analysis. The measured groundwater table was defined using a slope-parallel phreatic surface during the analysis.

During slope stability analyses the phreatic surface was initially held constant at the measured groundwater table, the depth which corresponds to the measured groundwater table was defined in slope stability analyses as being 0.00 metres. The phreatic surface was then varied in order to simulate seasonal groundwater changes and determine its influence on the FOS. Increases (+ values) and decreases (- values) were made with reference to the measured groundwater table (0.00 m).

4.4.5 Probabilistic slope stability analyses

For a probabilistic approach in slope stability analyses, two types of analysis can be carried out namely, global minimum and overall slope stability analysis (Huvaj & Oguz, 2018). During this study the global minimum analysis method was used, for which a global minimum slip surface was generated. The global minimum slip surface is automatically generated by SLIDE and is the slip surface that has the lowest FOS value. Prior to slope stability analyses a sensitivity analysis was conducted on the effective shear strength parameters and is discussed in the following subsections.

Two conditions were considered during the slope stability analysis for each slope. Firstly, the stability of the natural slope (analysis 1) and the stability of the slope loaded (analysis 2). These two conditions were analysed under various scenarios. The slopes were analysed both deterministically and probabilistically which is discussed in the following subsections.

4.4.5.1 Sensitivity analysis

A sensitivity analysis was undertaken prior to slope stability analyses. A suite of carefully selected sensitivity analyses should be carried out in relation to the key input parameters that are expected to

influence slope stability analyses results (Bar & Heweston, 2018). As such, a sensitivity analysis was carried out to see the effect of the effective shear strength parameters on the FOS. The effective shear strength parameters were varied over their minimum and maximum range of values in order determine the input parameters sensitivity on the FOS. The results of the sensitivity analysis plot for the effective cohesion and effective angle of friction is discussed in Chapter 5.

4.4.5.2 Selection of scenarios and scientific procedures used during analyses

The procedure followed during slope stability analyses of the LNPD and MPD slopes entailed simulating various scenarios using a deterministic and a probabilistic approach. As mentioned previously two main conditions were analysed, the stability of the natural slope and the stability of the slope when it is loaded. Table 4.3 presents a detailed summary of the various analyses and scenarios considered.

Table 4.3: Baseline analyses and scenarios considered during slope stability analyses.

LNPD SLOPE					
ANALYSIS 1 – Global minimum search method					
Natural Slope Conditions	Deterministic	Deterministic	Deterministic	Deterministic and Probabilistic	
Phreatic Surface changes: -2.0 to +3.56 m	<i>Scenario 1</i> <i>Mean c' & φ'</i>	<i>Scenario 2</i> <i>Minimum c'</i> <i>Maximum φ'</i>	<i>Scenario 3</i> <i>Maximum c'</i> <i>Minimum φ'</i>	<i>Scenario 4</i> <i>Minimum range of c' & φ'</i>	
ANALYSIS 2 – Global minimum search method					
Loaded Slope Conditions (150 kPa)	Deterministic and Probabilistic				
Phreatic Surface changes: -2.0 to +1.50 m	<i>Mean c' & φ'</i>				
MPD SLOPE					
ANALYSIS 1 – Global minimum search method					
Natural Slope Conditions	Deterministic	Deterministic	Deterministic	Deterministic	Deterministic
Phreatic Surface changes: -2.0 to +1.50 m	<i>Scenario 1</i> <i>Mean c' & φ'</i>	<i>Scenario 2</i> <i>Minimum c'</i> <i>Maximum φ'</i>	<i>Scenario 3</i> <i>Maximum c'</i> <i>Minimum φ'</i>	<i>Scenario 4</i> <i>Minimum range of c' & φ'</i>	<i>Scenario 5</i> <i>Minimum c'</i> <i>Reduced φ'</i>
ANALYSIS 2 – Global minimum search method					
Loaded Slope Conditions (200 kPa)	Deterministic and Probabilistic				
Phreatic Surface changes: -2.0 to +1.50 m	<i>Mean c' & φ'</i>				

During analysis 1, the LNPD and MPD slopes were analysed deterministically at the natural slope conditions for scenario's 1 to 4. Various combinations of the effective shear strength parameters were analysed. The phreatic surface was lowered and then raised in 0.5 m increments in order to simulate seasonal groundwater changes. The negative value indicates the maximum depth the phreatic surface was lowered to, with 0.0 m being the measured groundwater level. The positive value indicates the maximum depth the phreatic surface was increased to, again with 0.0 m being the measured groundwater level. The scenarios were chosen in order to determine which conditions will produce a FOS = 1.00, under different phreatic surface heights.

Firstly, the mean effective shear strength parameters were used during scenario 1 which represents the average effective shear strength behaviour of the talus material. Haneberg (2000) pointed out that soils are best represented by their average values as it accounts for parameter uncertainty. Scenario 2 (minimum c' and maximum ϕ') and scenario 3 (maximum c' and minimum ϕ') were then run during slope analyses in order to determine the effective shear strength parameter's influence on the variability of the FOS results. Under the range of phreatic surface heights and effective shear strength parameter combinations, scenario's 1 to 3 did not attain a global minimum failure surface with a FOS = 1.00.

Scenario 4, was then undertaken using the minimum range of the effective shear strength parameters, which resulted in successfully identifying the global minimum failure surface which attained a FOS = 1.00. Once the critical phreatic surface height that gave a FOS = 1.00 was identified in scenario 4, a probabilistic analysis was then undertaken on the natural LNPD slope using the minimum effective shear strength parameters, at the critical phreatic surface, in order to determine the probability of failure of the slope at the worst-case scenario. The global minimum failure surface, is the surface on which a probabilistic analysis should be carried out (Huvaj & Oguz, 2018).

For the natural MPD slope, an additional deterministic scenario was required (scenario 5) as scenario's 1 to 4, did not attain a global minimum failure surface with a FOS = 1.00. This was achieved by systematically reducing the ϕ' value under various phreatic surfaces, until a FOS = 1.00 was obtained for the global minimum failure surface. Subsequently, following critical evaluation of scenario 5, a probabilistic analysis was not undertaken on the natural MPD using the corresponding effective shear strength parameters for the MPD slope. This was due to the low effective shear strength parameters obtained for scenario 5, which is discussed in detail in Chapter 5.

During analysis 2, the LNPD and MPD slopes were analysed probabilistically by applying a surcharge load to the slopes. The anticipated loads on the slopes are based on the size of the structures. For a double story structure a load of 150 kPa was used and for a triple storey configuration structure, a load of 200 kPa was used during slope stability analysis (Isherwood, C., pers. comm., 2015). The calculated loads are based on the deck sizes and the number of columns (Lotter, C., pers. comm., 2017). Only one

scenario was undertaken using the mean effective shear strength parameters. During analysis 2, the phreatic surface was lowered and then raised in order to determine which phreatic surface height produced a FOS = 1.00. The results culminated in determining amongst other parameters which is discussed below, the reliability index and probability of failure for the LNP and MPD slopes under loaded conditions.

The Monte Carlo Simulation was adopted during probabilistic analyses. Due to the long computational times of the Monte Carlo method a series of slope stability runs were undertaken to optimize the number of samples. This entailed ensuring that the results are converging to a conclusive result by varying the number of samples. The required number (N) of Monte Carlo runs was determined to be 10 000. At this number, the results were not influenced by the number of simulations. During slope stability analysis, 1 000 iterations were considered for each failure surface during convergence. A tolerance of 0.005 was set during convergence, which is the difference in factor of safety values between two successive iterations.

The parameters from a probabilistic slope stability analyses are the mean FOS(μ_{FOS-1}), the lognormal reliability index (β_{LN}) and the probability of failure (P_f). The mean factor of safety, obtained from the probabilistic analysis, is the average FOS of all of the FOS values calculated for the global minimum failure surfaces. The reliability index is an indication of the number of standard deviations which separates the mean FOS(μ_{FOS-1}) values from the critical FOS value which is a FOS= 1. The reliability index is calculated assuming either a normal or lognormal distribution for the FOS values.

In slope stability the probability of failure is the number of runs providing results of FOS < 1.00 divided by the total number of runs to find the probability of occurrence (Bar & Heweston, 2018). Important to note that the probability of failure gives a quantification of the likelihood of slope failure which is expressed as a percentage.

CHAPTER 5

RESULTS AND DISCUSSION

5.1 Introduction

This chapter presents the results from the geotechnical characterization of the study site and discusses the results obtained from the slope stability analyses.

Data in the form of engineering geological material descriptions from borehole, auger hole and trial pit records enables an understanding of the material and groundwater conditions prevailing on site. This chapter presents the results from subsurface investigations which includes borehole drilling and trial pitting. Cross-sections are presented of various slopes in the Town Bush Valley. Furthermore, the results of the various laboratory tests such as the index and shear strength tests is presented.

The results obtained from the deterministic and probabilistic slope stability analyses are presented and evaluated. The results of the probabilistic slope stability analyses along with the generated output functions are critically evaluated. The chapter culminates in an assessment of the probability of failure of selected slopes.

5.2 Geotechnical characterization of the Town Bush Valley

The geotechnical characterization of the Town Bush Valley involved the collection, assimilation and analysis of various data in order to understand the engineering properties of the material in the study area. Data in the form of engineering geological material descriptions from borehole, auger hole and trial pit records enable an understanding of the geotechnical properties of the material and the groundwater conditions prevailing on site.

5.2.1 Engineering geology descriptions of the material from boreholes, auger hole records and trial pitting

A detailed review of previous boreholes and auger holes undertaken by various consultants has been presented and discussed in Chapter 3 Section 3.6. Using the available subsurface information (borehole, auger hole, trial pit data) combined with the groundwater table contour map which is based on measured groundwater levels, eight geological cross-sections corresponding to lines A-A' to H-H' were constructed.

The lines of cross-section were chosen to intercept as many boreholes, auger holes and trial pit positions as illustrated in Figure 5.1.

In context of this chapter and for ease of reference, Figure 5.1 essentially combines the earlier Figure 3.12 and 4.8.

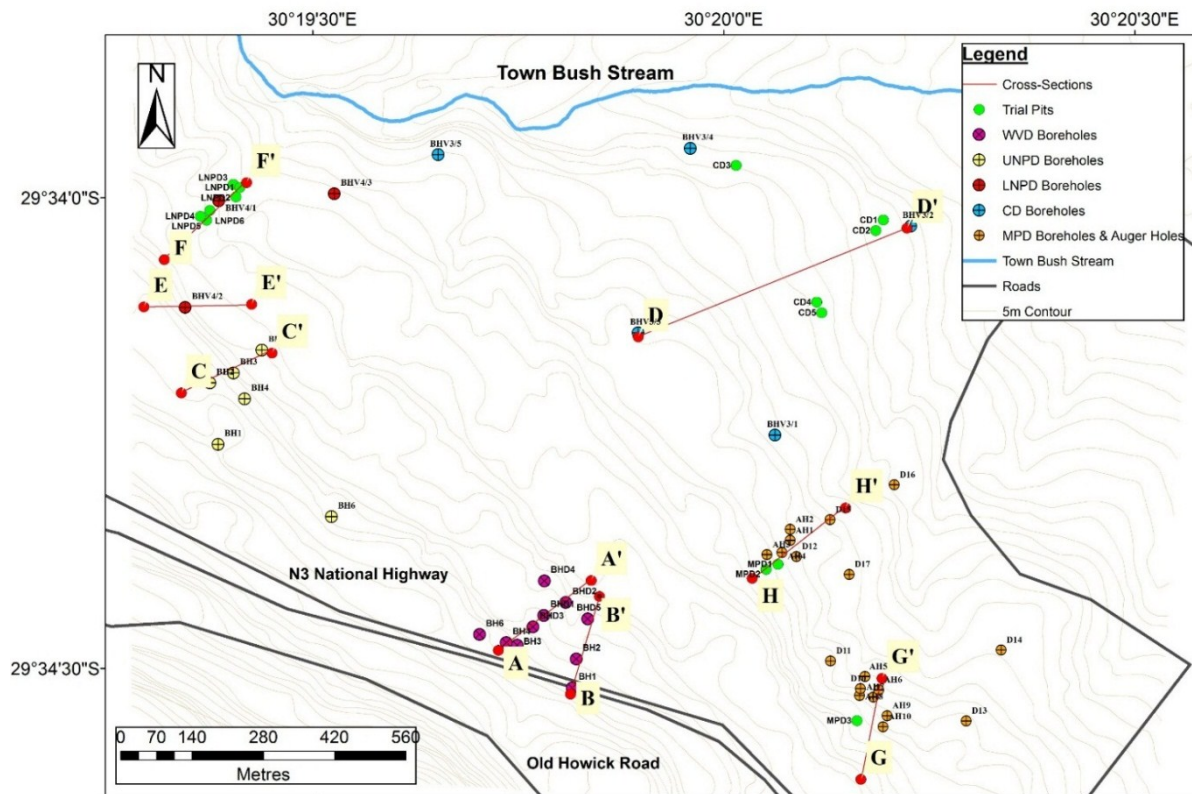


Figure 5.1: Location of lines of cross-section.

The cross-sections numbered A-A' to H-H', are presented in Figures 5.2 to 5.9. During reviewing of the borehole logs in some instances, due to the scarcity of data, the depth to bedrock was not proved. In the absence of bedrock levels, depths to bedrock were based on a combination of regional levels, the author's experience in the study site and conclusions and inferences drawn by previous consultants cited in Figure 3.13, Chapter 3. In the case of cross-section F-F', borehole BHV4/2 was extrapolated along the contour line in order to supplement subsurface data in the LNPB.

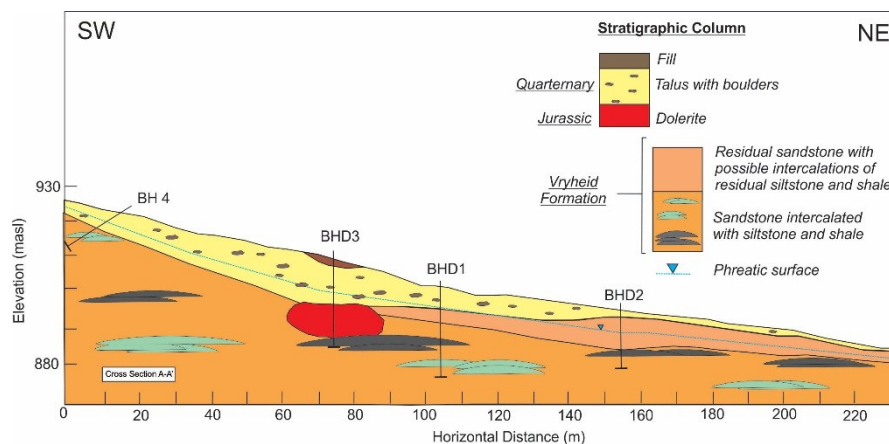


Figure 5.2: Geological cross-section A-A' of the WVD.

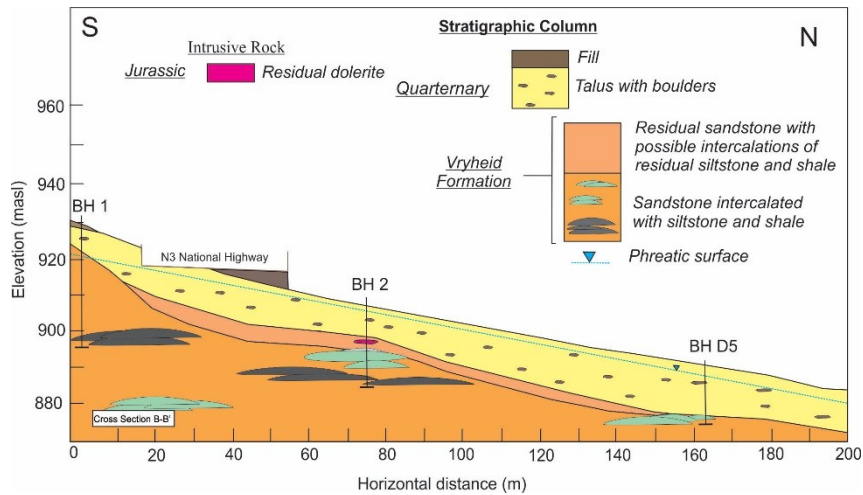


Figure 5.3: Geological cross-section B-B' of the WVD.

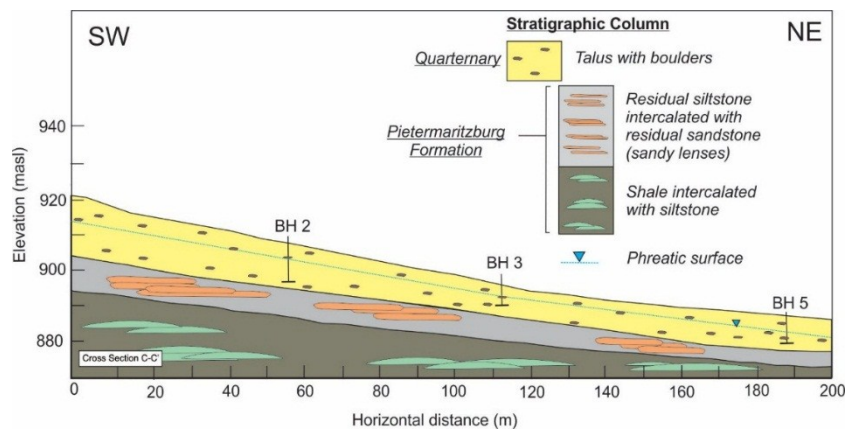


Figure 5.4: Geological cross-section C-C' of the UNPD.

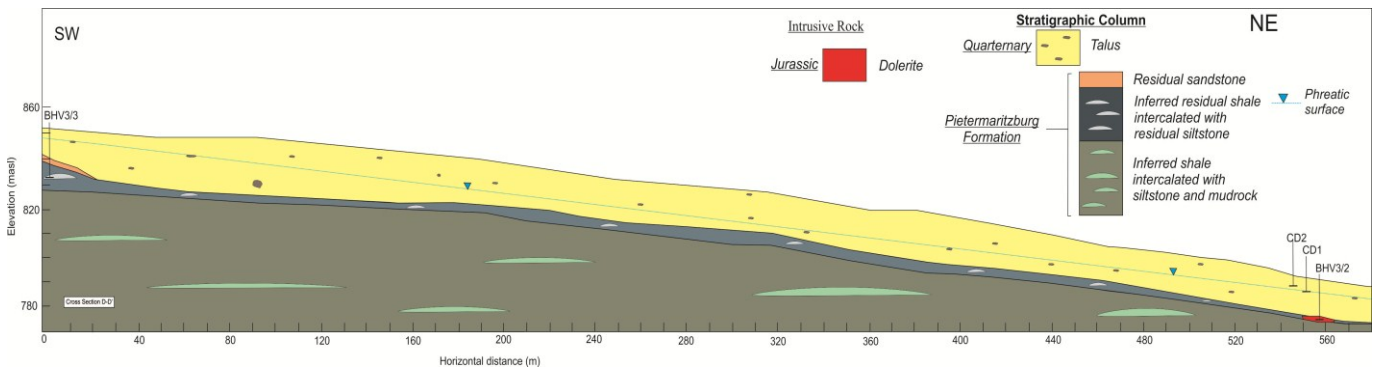


Figure 5.5: Geological cross-section D-D' of the Cascades Development.

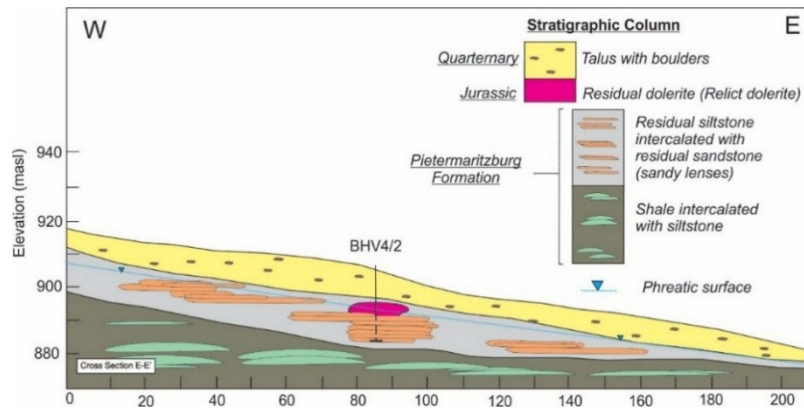


Figure 5.6: Geological cross-section E-E' of the LNPD.

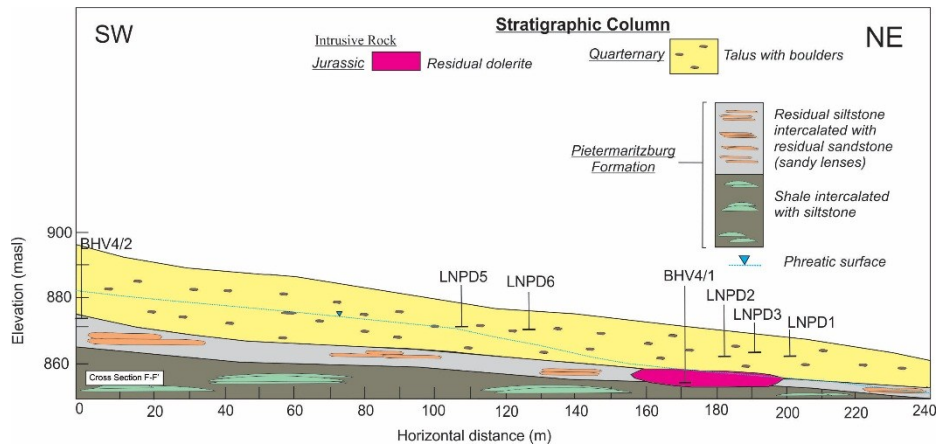


Figure 5.7: Geological cross-section F-F' of the LNPD.

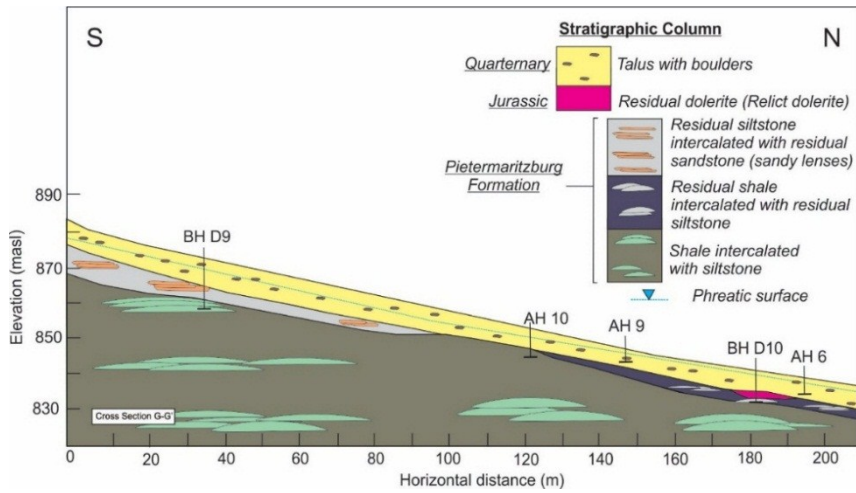


Figure 5.8: Geological cross-section G-G' of the MPD.

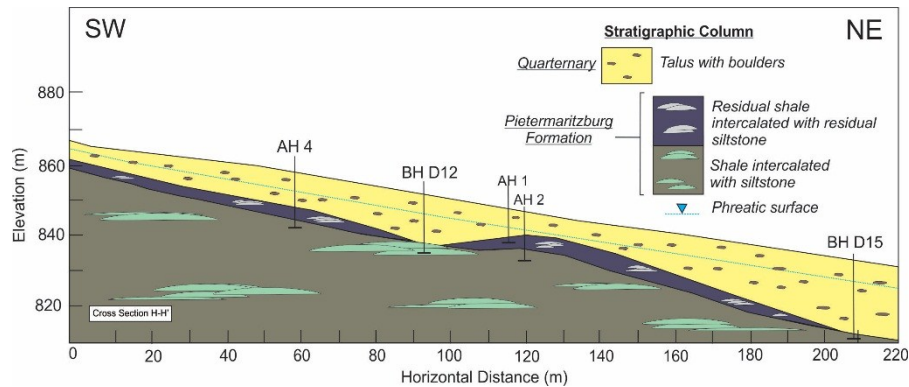


Figure 5.9: Geological cross-section H-H' of the MPD.

A summarized version of the logs is included in Appendix B1 with the complete logs presented in digital Appendix B1 (B1.1 to B1.5). A summary of the engineering geological descriptions of the material corresponding to the cross-sections in the Town Bush Valley is presented in Table 5.1, in accordance with the SAICE (2002). Furthermore, trial pitting was undertaken in the Cascades Development, LNP and MPD as part of this study in order to establish, assess and verify the geological and geotechnical properties of the talus material. The description of the trial pit profiles is presented in the subsequent sections.

Table 5.1: Generalized engineering geological descriptions.

Depth Range (metres below ground level)		Material	Generalized Engineering Descriptions
0	23.7	Talus	Slightly moist to moist, dark reddish brown, loose to medium dense, fissured and shattered, various proportions of boulder sized dolerite, shale and sandstone rock fragments in a silty clayey sand matrix.
6.9	18.4	Residual dolerite	Moist, reddish brown, soft to firm, fissured, sandy silty clay in a cobble to boulder sized dolerite fragment matrix.
0.9	17.8	Residual sandstone (intercalated with residual siltstone and shale). Vryheid Formation	Moist to very moist, yellowish-orange and light grey, soft to firm, intact to fissured, weathered sandstone fragments, sandy clay (residual sandstone). Intercalated with moist, grey mottled light brown, firm, fissured, siltstone fragments in a silty clay matrix (residual siltstone) and moist, dark olive and grey, firm, fissured, shale fragments in a silty clay matrix (residual shale).
8.2	10.6	Residual siltstone (intercalated with residual sandstone). Pietermaritzburg Formation.	Slightly moist, yellowish brown, streaked orange brown, firm, fissured, slightly silty clay (residual siltstone). Intercalated with slightly moist, yellowish orange, soft to firm, intact, fine grained sandy, silty clay (residual sandstone).
5	18.4	Residual shale (intercalated with residual siltstone). Pietermaritzburg Formation.	Slightly moist, reddish-brown mottled grey, firm to very stiff, intact, fine gravelly shale fragments in a sandy clayey, silt matrix (residual shale). Intercalated with slightly moist, greyish brown mottled orange brown, firm, fissured, occasional siltstone fragments in a fine grained sandy, clayey silt matrix (residual siltstone).
9.25	23	Dolerite	Orange brown mottled green grey and dark grey, moderately to slightly weathered, fine to medium grained, medium to widely jointed with clay and silt infill, hard rock strength.
7.76	36.6	Sandstone (intercalated with siltstone and shale). Vryheid Formation	Dark orangey brown, highly to completely weathered, medium to coarse grained, widely jointed, very soft to soft rock strength (sandstone bedrock). Intercalated with greyish, reddish brown, completely to highly weathered, fine grained, widely jointed, soft to medium rock strength (siltstone) and dark grey, slightly to highly weathered, very fine grained, thinly bedded, soft to medium rock strength (shale).
6.2	23.3	Shale (intercalated with siltstone). Pietermaritzburg Formation.	Dark grey to black, unweathered, fine grained, thinly bedded, widely fractured, soft to medium rock strength (shale). Intercalated with light greyish brown mottled orange brown, moderately to highly weathered, very fine grained, thinly bedded, widely fractured, soft rock strength (siltstone).

The World's View Development is underlain by weathered sandstone of the Vryheid Formation. Various bedrock units of siltstone and shale are noted in an intercalated sequence within the sandstone bedrock. The bedrock in-turn is overlain by Quaternary-aged residual soils and transported soils. The Cascades Development, UNPD, LNPDP and MPD is underlain by shales of the Pietermaritzburg Formation (intercalated with minor siltstone sequences). The bedrock is conformably overlain by residual sedimentary horizons of the Pietermaritzburg Formation. These residual sedimentary horizons are in-turn overlain by talus material. Schreiner (2005b) observed that during drilling investigations, a dolerite sill was intersected at BHV3/2 at a depth of 23.1 m below NGL, near the western boundary of the Cascades Development. Quaternary-aged talus deposits overlie the residual and bedrock sedimentary sequences. It is important to note that the borehole drilling data indicates that the talus soils on the toe slopes of the Town Bush Valley extend to depths in excess of 23.00 m below NGL (BHV3/2).

Schreiner (2005a) pointed out that a large amount of water loss was noted during rotary-core drilling investigations in the LNPDP. This was interpreted to indicate highly fissured soils, possibly due to relict joints in the residual sedimentary soils (Schreiner, 2005a).

The MPD is underlain by two residual sedimentary sequences; the upper sequence preserved on the higher slopes of the MPD consists of coarser residual siltstone with sandstone intercalations (sandy lenses) while the lower slopes are underlain by finer residual shale with siltstone intercalations. The transition between the two residual sequences (residual siltstone containing sandy lenses and residual shale with siltstone intercalation) lies near auger holes AH9 and AH10. However, the lithological boundary is covered by deep, talus deposits.

Three trial pits were excavated in the Cascades Development to depths ranging between 3.00 m (CD5) to 3.60 m (CD1), the profiles were logged according to SAICE (2002). A summary of the materials in the trial pit profiles are presented Table 5.2, with the complete set of logs presented in Appendix B1.

Table 5.2: Engineering geological descriptions, Cascades Development.

Lithology	Depth	Generalised descriptions from trial pits CD1-CD3
Colluvium (upper Talus)	0.00-1.00m	Moist, light reddish brown, loose, matrix supported, fine gravelly to cobble sized fragments, in a clayey fine sand matrix.
Talus	1.00-3.60m	Slightly moist, dark reddish-brown, soft to firm, matrix supported, completely weathered dolerite boulders, with residual sandstone rock fragments in a fine grained sandy, clayey, silt matrix. Dolerite boulders were noted to make 2 % by volume of the matrix

Six trial pits were advanced in the LNPDP to maximum excavation depths ranging between 3.00 m (LNPDP5/6) to 3.30 m (LNPDP2/4). A summary of the materials in the trial pit profiles is presented in Table 5.3 with the complete set of logs presented in Appendix B1.

Table 5.3: Engineering geological descriptions, LNP.

Lithology	Depth	Generalised descriptions from trial pits LNP1-LNP6
Colluvium (Upper Talus)	0.00- 0.90m	Slightly moist, khaki and light yellow occasionally blotched grey, soft to slightly firm, intact, clayey, sandy, silt with occasional boulders.
Talus	0.90- 3.10m	Slightly moist, orangey reddish-brown, soft to firm, fissured, completely weathered sandstone and dolerite boulders, with residual sandstone rock fragments in a fine to medium sandy, clay matrix. Dolerite boulders were noted to make 5 % by volume of the matrix.

Trial pitting in the LNP generally intersected similar profiles to the borehole logs presented in digital Appendix B1.4. In trial pit LNP1, residual siltstone and sandstone rock fragments were observed to form part of the matrix composition as illustrated in Figure 5.10 and 5.11.



Figure 5.10: Matrix supported talus profile intersected in trial pit LNP1.



Figure 5.11: Residual sandstone rock fragment preserved in the talus matrix (trial pit LNP2).

These residual rock fragments profiled in the talus deposits have been deposited as a result of mass wasting processes. The residual bedrock pieces are preserved as large fragments in the talus soils of the Town Bush Valley and are often mistaken as true residual soils.

Three trial pits were advanced in the MPD as part of this study. Trial pits were excavated to depths ranging between 4.40 m (MPD2) to 5.50 m (MPD3) and the profiles are summarized in Table 5.4 with the complete set of logs presented in Appendix B1. Photos taken during the site investigation are presented as Figure 5.12.

Table 5.4: Engineering geological descriptions, MPD.

Lithology	Depth	Generalised descriptions from trial pits MPD1-MPD3
Topsoil (Upper Talus)	0.00-1.00m	Slightly moist, dark reddish brown, soft, intact, silty, clayey, fine grained sand.
Talus	0.60-8.90m	Slightly moist, reddish brown, medium dense, matrix supported, fine gravelly to boulder sized fragments in a clayey, fine to medium sand matrix. Boulders were noted to make 10 % by volume of the matrix.



Figure 5.12: Excavator used during trial pitting (Photo 1), talus material intersected in trial pit MPD2 (Photo 2).

5.3 Results from laboratory testing

5.3.1 Grain Size Analysis and Atterberg Limits Determination

The grading of the particles has been classified according to the Unified Soils Classification method which grades the soil according to the following sieve apertures: gravel (75.00 mm - 4.75 mm), sand (4.75 mm - 0.075 mm), silt (0.075 mm - 0.002 mm) and clay (< 0.002 mm) (Carter & Bentley, 1991).

The particle size distribution (PSD) results are presented in Figure 5.13, with the full set of results presented in Appendix B2.

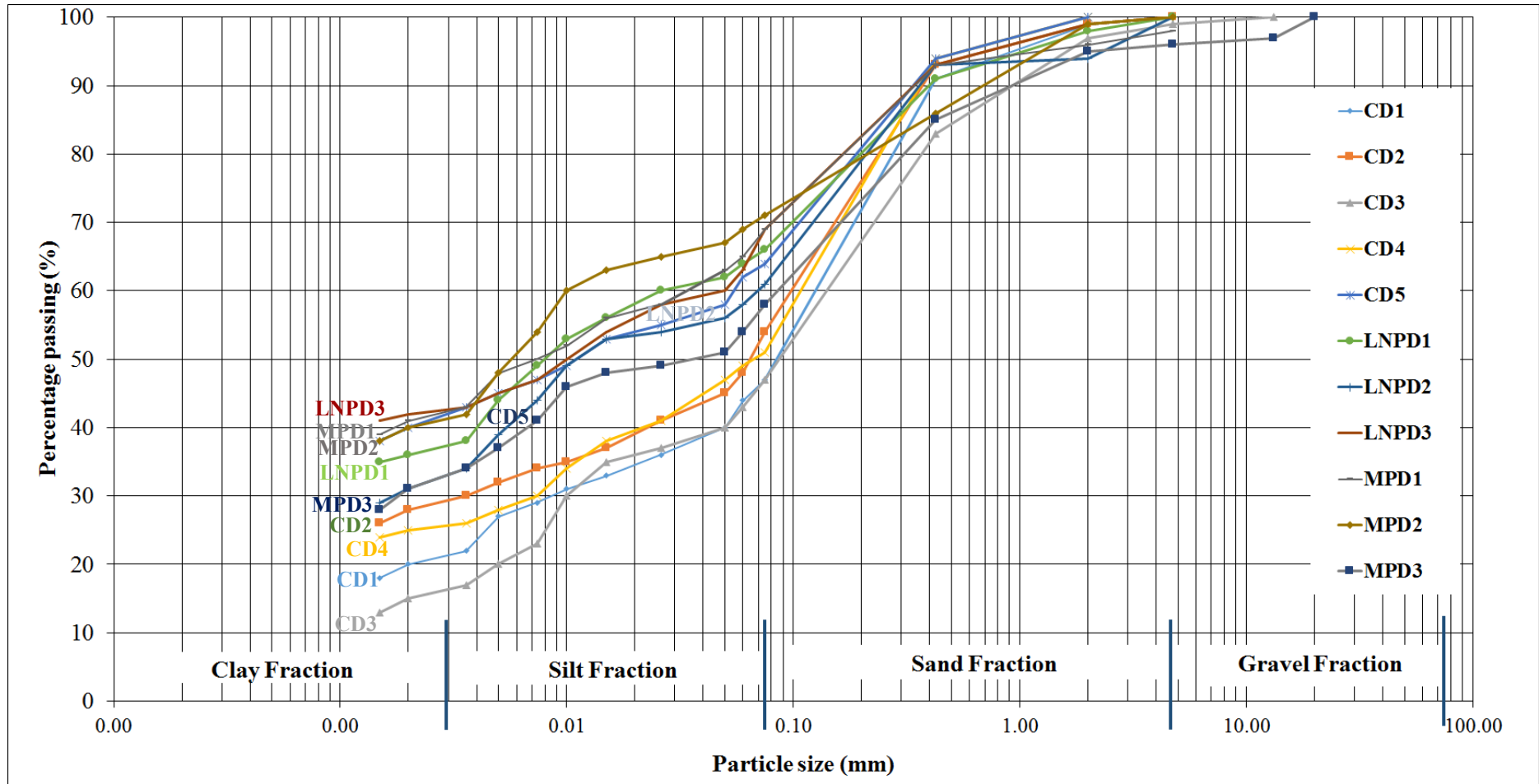


Figure 5.13: Particle size distribution curves for the talus material.

The PSD test results indicate that the talus material has a majority of sand component. Table 5.5 presents a summary of the index test results and calculated geotechnical parameters, the full set of results can be found Appendix B2.

Table 5.5: Summary of index properties for the talus material.

Sample Number	Depth (m)	Description	Atterberg Limits (%)				USCS
			W _L	W _P	I _P	LS	
CD1	1.00-3.00	silty sand	45	33	12	8	SM- silty, sand
CD2	1.00-3.00	clayey sand	49	30	19	10	CL- sandy, lean clay
CD3	2.00-3.00	silty sand	48	32	16	8.5	SM- silty, sand
CD4	0.30-3.30	silty sand	47	32	15	8	CL- sandy, lean clay
CD5	0.30-3.30	sandy clay	48	33	15	8	CL- sandy, lean clay
LNPD1	1.00-3.00	sandy clay	43	27	16	8.5	CL- sandy, lean clay
LNPD2	1.50-3.30	sandy clay	37	24	13	7	CL- sandy, lean clay
LNPD3	0.90-1.10	sandy clay	48	27	21	11	CL- sandy, lean clay
LNPD4	1.60-3.30	silty sand	37	19	18	9	SC- clayey sand
LNPD5	0.50-1.40	silty sand	45	27	18	7	SM- silty sand
MPD1	0.50-1.50	sandy clay	55	38	17	9	MH- sandy elastic silt
MPD2	0.50-1.50	silty clay	60	42	18	11	MH- elastic silt with sand
MPD3	4.30-4.50	clayey sand	46	29	17	9	CL- sandy lean clay
Geotechnical Parameter	Symbol	LNPD3				MPD3	
Moisture content	w	8.34 %				7.67 %	
Bulk density	ρ_b	1.23 g/cm ³				1.59 g/cm ³	
Dry density	ρ_d	1.14 g/cm ³				1.48 g/cm ³	
Void ratio	e	0.073				0.069	
Bulk unit weight	γ_b	24 kN/m ³				24 kN/m ³	
Saturated unit weight	γ_{sat}	25 kN/m ³				25 kN/m ³	
Dry unit weight	γ_d	24 kN/m ³				24 kN/m ³	
Effective unit weight	γ'	15 kN/m ³				15 kN/m ³	
Where; W _L is the liquid limit, W _P is the plastic limit, I _P is the plasticity index (I _P =W _L -W _P), LS is the linear shrinkage and USCS is the Unified Soils Classification System							

Dry densities values for both samples observed varied values for the talus material from the MPD and LNPD.

From Table 5.5, the Cascades Development PSD and index test results generally indicate that the talus soil has a majority of sand component with minor clay and silt portions. From historical PSD test results undertaken on the talus material which was obtained from Terratest and is presented in Chapter 3 Section 3.6, the Cascades Development grades as a silty, sand with mean particle sizes of 26 % and 53 % respectively. The tested Cascades Development samples (CD1- CD5) noted higher clay percentages, while the I_P's values were consistent with the range obtained during historical investigations (historical I_P values averaged 21 %).

The LNP, PSD test results indicate that the talus soils have a majority of sand sized particles with minor clay and silt portions. However, sample LNP3 graded as a sandy, clay which suggests the localized occurrence of a marginally higher clay concentrations in the upper metres of the talus horizon. The samples tested on the upper slopes of the LNP (samples LNP4 and LNP5) noted a higher sand portion in comparison to the lower slopes of the LNP (samples LNP1 and LNP2). The LNP samples generally noted higher clay portions in comparison with the historical data which was obtained from Terratest (historically the talus material graded as a silty, sand with average particle sizes of 24 % and 55 % respectively). The LNP sample's I_P and LS values are consistent with historical investigation results the latter noting average values of $I_P = 15 \%$ and $LS = 8 \%$.

The MPD, PSD test results indicate that the talus soils have nearly equal portions of sand, clay and silt. From historical test results which was obtained from Terratest, the MPD talus material grades as a silty, sand with mean particle sizes of 26 % and 47 % respectively. However, the MPD samples noted a higher silt and clay percentage. The average I_P of 21 % and LS of 10 % from previous MPD test results suggests that the samples are consistent with historical data.

In general, the samples tested are generally consistent with the historical laboratory data presented in Chapter 3 Section 3.6.

5.3.2 Triaxial test

A consolidated-drained triaxial test culminates in the compression stage Figure 5.14 and Figure 5.15 show the deviatoric stress and porewater pressure measurements plotted against axial strain for the three confining pressures (σ_3) corresponding to 100 kPa, 200 kPa and 300 kPa respectively for both samples tested.

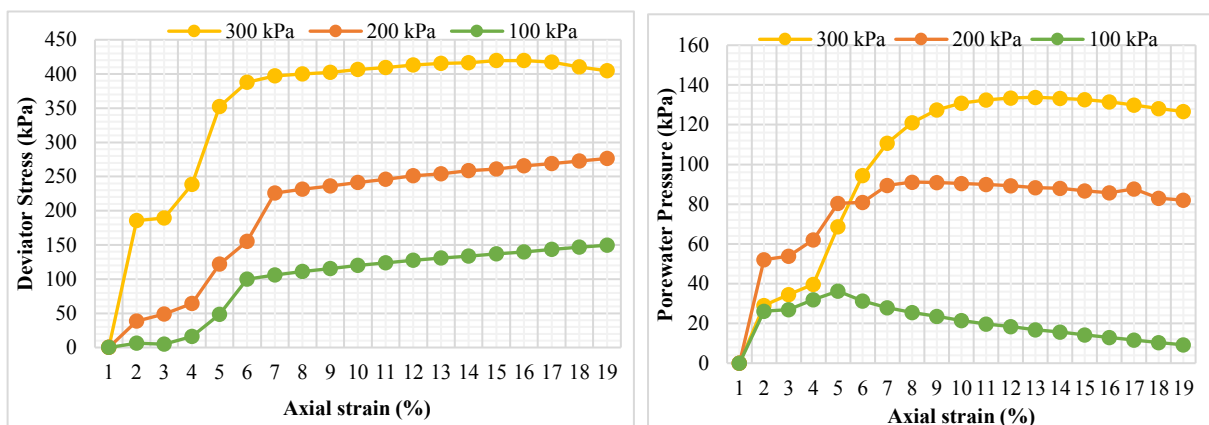


Figure 5.14: Sample LNP3 - Deviator stress (kPa) vs Axial strain (%) (left) and Pore water pressure (kPa) vs Axial strain (%) (right).

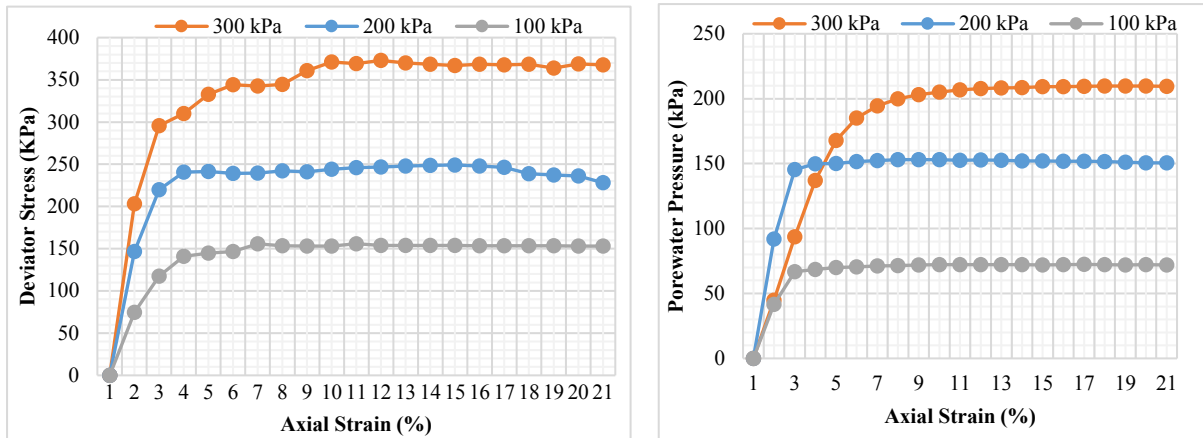


Figure 5.15: Sample MPD3 - Deviator stress (kPa) vs Axial strain (%) (left) and Pore water pressure (kPa) vs Axial strain (%) (right).

The deviator stress vs axial strain curves for the 100 kPa and 200 kPa cell pressures respectively show no pronounced peak even at high axial strain rates (17-20 %). Head (1998) reasoned that in soils in which the axial stress does not readily reach a maximum value, failure is deemed to have occurred when a 20 % axial strain has been reached. In the case of the talus test specimens, the maximum deviator stresses were taken at the maximum strains tested. Figure 5.16 illustrates barreling failure of the MPD and LNPD specimens. In a sample that fails completely by barreling failure there is no definite failure point as the deviator stress increases slightly with strain (Smith, 1990).



Figure 5.16: Barreling failure of specimens (Photo 1 - sample LNPD3; Photo 2 - LNPD specimen sets; Photo 3 - sample MPD3).

From the maximum deviator stress at failure, the major principal stress σ_1 was obtained and based on the pore water pressure at failure, the effective stress parameters for the major and minor principle stresses, σ_1' and σ_3' were obtained. The complete set of the raw data obtained during triaxial testing is presented in Appendix B3, a summary of these parameters are shown in Table 5.6.

Table 5.6: Triaxial test results of various samples for the talus material.

Sample	Confining pressure (kPa)	Deviatoric stress at failure (kPa)	Major principal stress (kPa)	Axial strain	Pore water pressure at failure (kPa)	Effective stress	
						σ_3'	σ_1'
LNPD3	σ_3	$\sigma_1 - \sigma_3$	σ_1	%	u	σ_3'	σ_1'
Specimen 1	100	164.8	264.8	18.85	0.16	99.84	264.64
Specimen 2	200	294.3	494.3	18.48	70.28	129.72	424.02
Specimen 3	300	419.5	719.5	8.83	132.65	167.35	586.85
MPD3	σ_3	$\sigma_1 - \sigma_3$	σ_1	%	u	σ_3'	σ_1'
Specimen 1	100	154.7	254.7	18.5	71.87	28.13	182.83
Specimen 2	200	249.2	449.2	11.6	152.1	47.9	297.1
Specimen 3	300	373	673	8.24	207.76	92.24	465.24

The effective stress parameters (σ_1' and σ_3') were used to construct Mohr-circle diagrams using the Rockscience Inc. software package RocData (version 3.0). Mohr-circles were constructed for the tested LNPD3 and MPD3 samples and tangents were drawn to the Mohr-circles from which the effective shear strength parameters, c' and ϕ' were obtained. The diagrams are illustrated in Figure 5.17 and 5.18 respectively. The tangent intersection with the Y-axis represents the effective cohesion value and the acute angle formed with the tangent and the effective cohesion value intercept, represents the effective angle of internal friction.

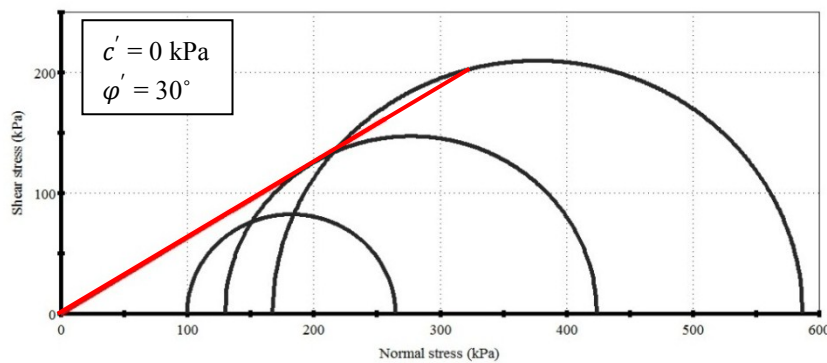


Figure 5.17: Mohr circles used to define the effective cohesion and effective angle of friction for sample LNPD3.

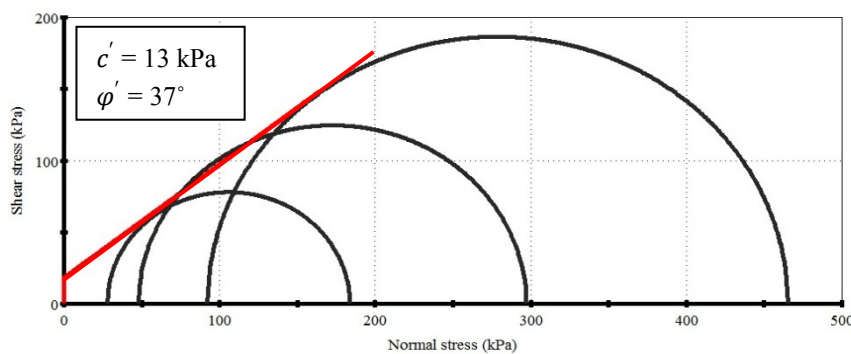


Figure 5.18: Mohr circles used to define the effective cohesion and effective angle of friction for sample MPD3.

Sample LNPD3 grades as a sandy clay and recorded a φ' of 30° and c' of 0 kPa. Index parameter correlations and unpublished shear strength parameters presented in Chapter 3 Section 3.4, indicates that the tested LNPD3 specimen falls within the upper limits of previous shear strength parameters obtained for talus material of the Town Bush Valley.

Sample MPD3 grades as clayey sand as the PSD results indicate the sample has nearly equal portions of clay, silt and sand. The values obtained for φ' and c' are 37° and 13 kPa respectively.

The high c' value can possibly be attributed to the presence of a clay lense in the talus material. The PSD test results indicate that the MPD3 sample has a 31 % clay fraction. The clay portion will display cohesive behaviour upon shearing, which has possibly resulted in the observed high c' value for the sample.

Based on previous test results presented in Table 3.13 (Chapter 3) and effective shear strength data in Appendix A3, on similar material. The MPD3 sample obtained very high φ' and c' values and was subsequently removed during the data truncation phase. Lacasse & Nadim (1996), emphasised that major uncertainties can arise relating to soil properties using statistical methods, as a result of inconsistent data populations.

5.4 Slope stability analyses of selected slopes in the Town Bush Valley

The LNPD and MPD slopes were analysed during slope stability analyses. The selection of the method of analyses, the representation of random variables and pore water pressures is discussed in Chapter 4 Sections 4.4.1 to 4.4.5.

The results of the slope stability analyses are sequentially presented and discussed in the following subsections. The results of the sensitivity analysis are firstly presented, leading to the results of the deterministic analyses which formed the basis for a probabilistic analysis.

The functions derived from a probabilistic analysis and the nomenclature used for the functions is detailed in Chapter 4 Section 4.4.5.2. It is important to note that the probabilistic framework for reliability analyses can offer much more than the replacement of the conventional FOS, by the probability of failure and the reliability index (Aleotti & Chowdhury, 1999).

Table 5.7 summarizes the values of the effective shear strength parameters and conditions used during deterministic and probabilistic slope stability analyses.

Table 5.7: Summarized analyses and scenarios considered for the LNPD and MPD slopes.

LNPD ANALYSIS 1 – Global minimum search method					
Natural Slope Conditions	Deterministic	Deterministic	Deterministic	Deterministic and Probabilistic	
Phreatic Surface changes: -2.0 to +3.56 m	<i>Scenario 1</i> Mean: $c' = 0.5$ kPa, $\phi' = 28.2^\circ$	<i>Scenario 2</i> $c' = 0$ kPa, $\phi' = 32^\circ$	<i>Scenario 3</i> $c' = 10$ kPa, $\phi' = 22^\circ$	<i>Scenario 4</i> Minimum: $c' = 0$ kPa, $\phi' = 22^\circ$	
LNPD ANALYSIS 2 – Global minimum search method					
Loaded Slope Conditions (150 kPa)	Deterministic and Probabilistic				
Phreatic Surface changes: -2.0 to +1.50 m	Mean: $c' = 0.5$ kPa, $\phi' = 28.2^\circ$				
MPD ANALYSIS 1 – Global minimum search method					
Natural Slope Conditions	Deterministic	Deterministic	Deterministic	Deterministic	Deterministic
Phreatic Surface changes: -2.0 to +1.50 m	<i>Scenario 1</i> Mean: $c' = 0.5$ kPa, $\phi' = 28.2^\circ$	<i>Scenario 2</i> $c' = 0$ kPa, $\phi' = 32^\circ$	<i>Scenario 3</i> $c' = 10$ kPa, $\phi' = 22^\circ$	<i>Scenario 4</i> Minimum: $c' = 0$ kPa, $\phi' = 22^\circ$	<i>Scenario 5</i> Minimum: $c' = 0$ kPa, $\phi' = 16^\circ$
MPD ANALYSIS 2 – Global minimum search method					
Loaded Slope Conditions (200 kPa)	Deterministic and Probabilistic				
Phreatic Surface changes: -2.0 to +1.50 m	Mean: $c' = 0.5$ kPa, $\phi' = 28.2^\circ$				

5.4.1 Sensitivity Analysis

The results of the sensitivity analyses for the effective cohesion and effective angle of friction is shown in Figure 5.19.

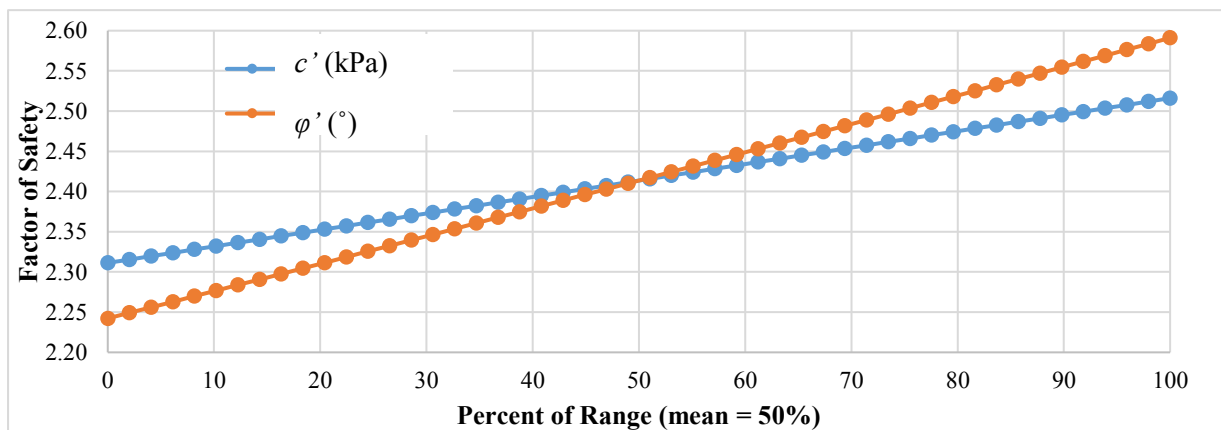


Figure 5.19: Sensitivity analysis for the effective cohesion and effective angle of friction.

From Figure 5.19, the ϕ' displays a steeper slope gradient in comparison to the c' values, over the 0-50 % range. The ϕ' slope continues its steep gradient over the 50-100 % range, which indicates greater FOS sensitivity to ϕ' values. The resultant output information from a sensitivity analysis contains information about both the FOS values and the sensitivity to change or reliability of the FOS results (Bar & Heweston, 2018).

The ranges used during a sensitivity analysis are very subject and conditioned by the experience of the practitioner (Haneberg, 2000). The use of meaningful sensitivity analyses is a key parameter which affects FOS results. The results of a sensitivity analysis are a proven solution for effectively calculating the probability of failure (Bar & Heweston, 2018).

5.4.2 Deterministic and probabilistic slope stability analyses for the LNPB slope

5.4.2.1 LNPB - analysis 1

As explained in Chapter 4 Section 4.4.5.2, the effective shear strength parameters were varied under different scenarios. The results of the four scenarios considered for analysis 1, is presented in Table 5.8.

Table 5.8: LNPB analysis 1, deterministic slope stability results.

LNPB Analysis 1		<i>Scenario 1</i>	<i>Scenario 2</i>	<i>Scenario 3</i>	<i>Scenario 4</i>
		<i>Mean: $c' = 0.5$ kPa, $\phi' = 28.2^\circ$</i>	<i>Min: $c' = 0$ kPa, Max: $\phi' = 32^\circ$</i>	<i>Max: $c' = 10$ kPa, Min: $\phi' = 22^\circ$</i>	<i>Both Min: $c' = 0$ kPa, $\phi' = 22^\circ$</i>
Season	Phreatic Surface (m)	Deterministic FOS	Deterministic FOS	Deterministic FOS	Deterministic FOS
Dry Season	- 2.00	2.39	2.64	2.30	1.71
	- 1.50	2.39	2.64	2.25	1.71
	- 1.00	2.37	2.59	2.2	1.71
	- 0.50	2.30	2.52	2.15	1.71
<i>Measured groundwater table</i>	0.00	2.26	2.45	2.09	1.71
Wet Season	+ 0.50	2.16	2.39	2.04	1.65
	+ 1.00	2.08	2.32	1.98	1.58
	+ 1.50	2.00	2.24	1.91	1.51
	+ 2.00	1.91	2.16	1.85	1.44
	+ 2.50	1.84	2.08	1.78	1.36
(extreme increases in the phreatic surface)	+ 3.00	1.69	1.94	1.71	1.25
	+ 3.50	1.48	1.66	1.63	1.06
	+ 3.56	1.42	1.55	1.62	1.00

At the measured groundwater table (0.0 m increase in the phreatic surface) using the average shear strength parameters the global minimum slip surface recorded a deterministic FOS of 2.26. Figure 5.20, illustrates the location of the global minimum failure surface.

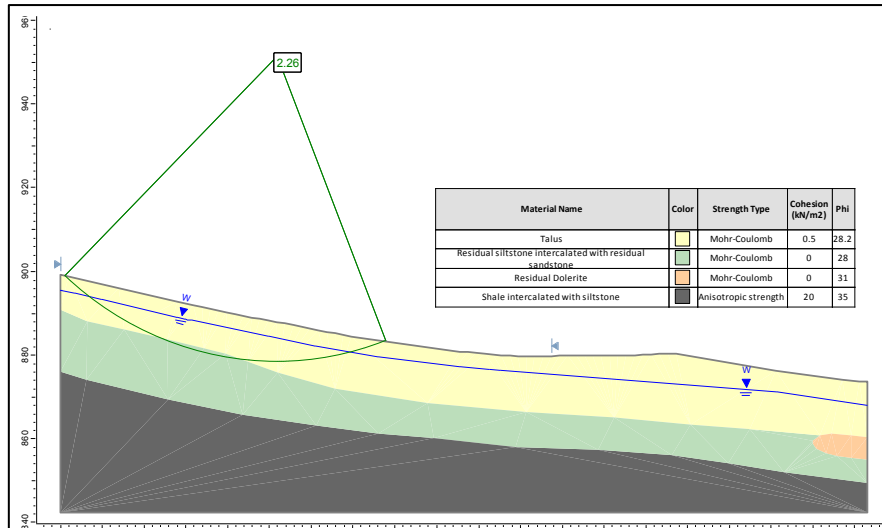


Figure 5.20: LNPd analysis 1 scenario 1, at the measured groundwater table.

The global minimum slip surface is primarily orientated through the talus material with the residual sedimentary horizon forming the base of the slip surface. The relatively high FOS = 2.23, implies stable slope conditions. A probabilistic slope stability analysis was then run on scenario 4, in order to determine the behaviour of the slope at the worst case scenario. The position of the global minimum failure surface is shown in Figure 5.21. The various functions related to the FOS is summarized in Table 5.9 and presented in Figure 5.22.

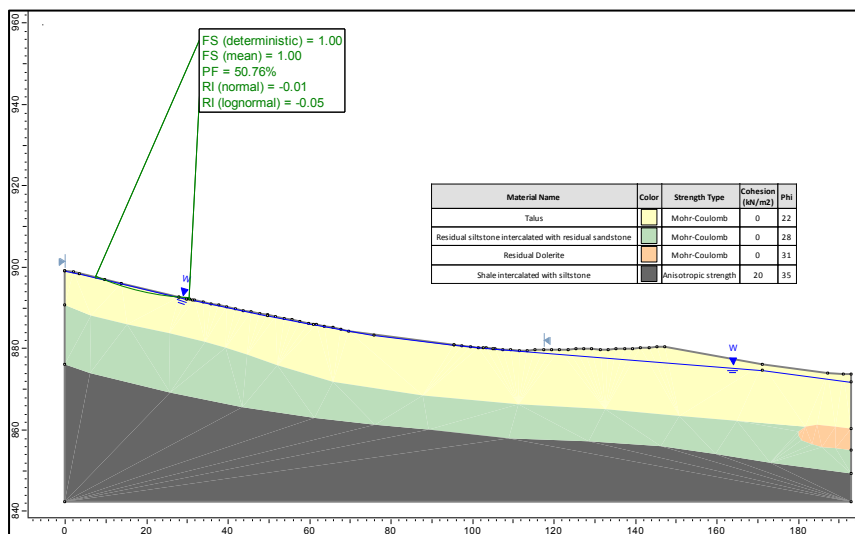


Figure 5.21: LNPd analysis 1 probabilistic analysis, at the maximum increase in the groundwater table using the minimum range of effective shear strength parameters.

Table 5.9: LNPd analysis 1 scenario 4, FOS functions at the maximum increase in the phreatic surface.

μ_{FOS-1}	σ	Min	Max	β	<i>pdf</i>	<i>P_f</i>
1.00	0.84	0.73	1.20	-0.01	Normal distribution	50.76 %

Where; μ_{FOS-1} is the mean factor of safety, σ is the standard deviation, Min is the minimum FOS, Max is the maximum FOS, β is the reliability index, *pdf* is the probability distribution function & *P_f* is the probability of failure.

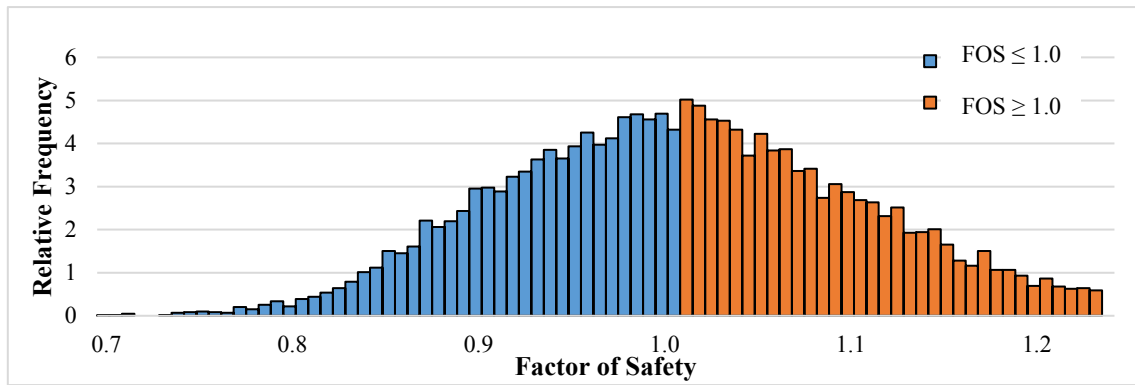


Figure 5.22: LNPD analysis 1 scenario 4, histogram of the relative frequencies for the FOS, at the maximum increase in the groundwater level.

From Table 5.8, scenarios 1 to 3 all indicate values for the $FOS > 1.40$, which lie above a $FOS = 1.00$. FOS values sharply decrease from the dry season to the wet season. The FOS of natural slopes may fluctuate widely from one season to another, being high in the dry season and low after rainfall (Chowdhury, 1984). Using the minimum effective shear strength parameters ($c' = 0$ kPa, $\phi' = 22^\circ$) scenario 4 was modelled, during which a $FOS = 1.00$ was obtained at a 3.56 m increase in the phreatic surface.

Using the average effective shear strength parameters (scenario 1) the results show that the slope is stable in its present form ($FOS = 2.26$ at a 0.0 m increase in the phreatic surface) under the range of phreatic surface conditions considered. An explanation for the observed high FOS values, can be attributed to the present geometry of the LNPD slope. As a localized convex feature is present on the lower section of the LNPD slope. The naturally occurring bulge on the toe has a possible stabilizing influence on the slope. The increased talus soil volume on the toe, can be a mitigating factor and resisting the formation of deep slip planes in the talus material.

Under conditions where a reduction in the effective shear strength parameters is brought about and the talus material is represented by the minimum recorded effective shear strength parameters (scenario 4), a value of $FOS = 1.00$ is obtained at a 3.56 m increase in the phreatic surface, which implies failure.

As shown in Table 5.9, a mean $FOS(\mu_{FOS-1}) = 1.00$ was obtained with a standard deviation of 0.84. The mean recorded FOS value obtained a small standard deviation with minimum and maximum FOS values recorded over a narrow range, implying a low variability in the FOS results.

The negative reliability index value indicates the number of standard deviations the mean $FOS(\mu_{FOS-1})$ lies below the critical value of $FOS = 1.00$. A value of $\beta = -2.0$, for example, would indicate that the calculated mean $FOS(\mu_{FOS-1})$ lies 2 standard deviations below the critical value of $FOS = 1.00$. The low β value ($\beta = -0.01$) correlates with the high Pf value which is discussed below however, the value indicates low reliability in the FOS value. The lower the reliability index the higher the degree of

uncertainty in the results obtained. The reliability index is an alternative measure of stability that considers explicitly the uncertainties involved in stability analyses (Duncan & Wright, 2005).

The histogram plot (Figure 5.22) for the simulations obtained for the FOS indicates a normal distribution.

Probabilistic slope stability analysis indicates a 50.8 % probability of failure for the global minimum slip surface at 3.56 m increase in the groundwater table. This implies that the slope has a 51 % of failure.

In concluding, under intense rainfall conditions where the phreatic surface rises to 3.56 m and where the talus material behaves in the minimum range of the recorded effective shear strength parameters, deterministic analyses indicate that the natural LNPD slope is unstable (FOS = 1.00) and probabilistic analyses indicates a 50.8 % possibility of failure occurring. The low reliability index value ($\beta = -0.01$) however, lowers the confidence in the Pf value (50.8 %) obtained.

5.4.2.2 LNPD – analysis 2

Slope stability modelling for analysis 2 was undertaken by applying two 150 kPa surcharge loads simulating double-storey structures on the slope using the average effective shear strength parameters.

The results obtained from the probabilistic slope stability analyses are presented in Table 5.10.

Table 5.10: LNPD analysis 2, summarized probabilistic slope stability analyses results.

LNPD Analysis 2		<i>Mean: $c' = 0.5 \text{ kPa}$, $\varphi' = 28.2^\circ$</i>				
Season	Phreatic Surface (m)	Deterministic FOS	$\mu_{\text{FOS-1}}$	β	β_{LN}	Pf (%)
Dry Season	- 2.00	1.00	0.99	-0.23	-0.23	64.61
	- 1.50	1.00	0.99	-0.20	-0.23	64.61
	- 1.00	1.00	0.99	-0.20	-0.23	64.61
	- 0.50	1.00	0.99	-0.20	-0.23	64.61
<i>Measured groundwater table</i>	0.00	1.00	0.99	-0.20	-0.23	64.61
Wet Season	+ 0.50	1.00	0.99	-0.20	-0.23	64.61
	+ 1.00	1.00	0.99	-0.20	-0.23	64.61
	+ 1.50	0.99	0.99	-0.20	-0.23	64.61

Where; $\mu_{\text{FOS-1}}$ is the mean factor of safety, β is the reliability index, β_{LN} is the lognormal reliability index & Pf is the probability of failure.

Figure 5.23, illustrates the location of the global minimum failure surface, at the measured groundwater level.

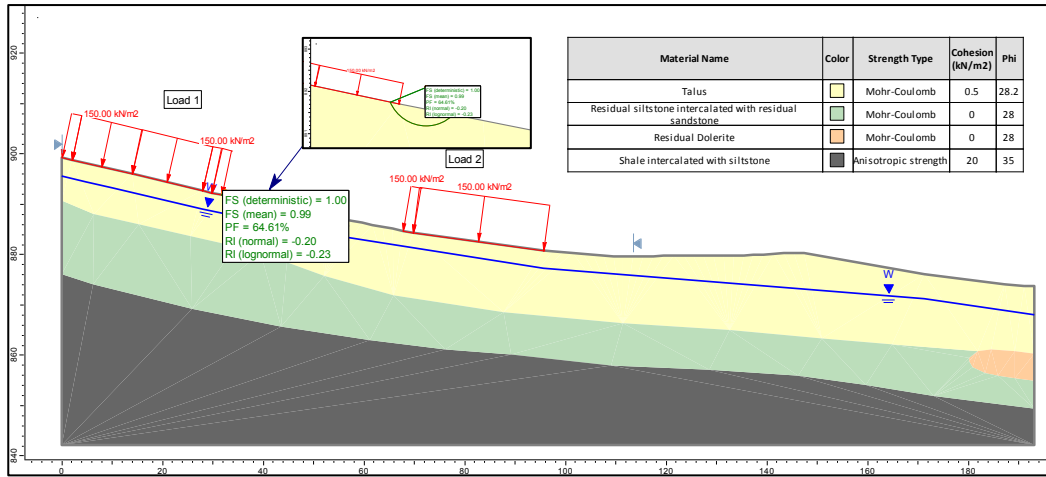


Figure 5.23: LNP analysis 2 probabilistic analysis, at the measured groundwater level using the mean effective shear strength parameters.

The global minimum slip surface is positioned in the talus material, located beneath load 1 at a shallow depth. The various parameters obtained from the probabilistic analyses are summarized in Table 5.11 and the distribution of the FOS is presented in Figure 5.24.

Table 5.11: LNP analysis 2, FOS functions at the measured phreatic surface.

μ_{FOS-1}	σ	Min	Max	β_{LN}	<i>pdf</i>	<i>Pf</i>
0.99	0.07	0.81	1.67	-0.23	Lognormal distribution	64.61 %

Where; μ_{FOS-1} is the mean factor of safety, σ is the standard deviation, Min is the minimum FOS, Max is the maximum FOS, β_{LN} is the lognormal reliability index, *pdf* is the probability distribution function & *Pf* is the probability of failure.

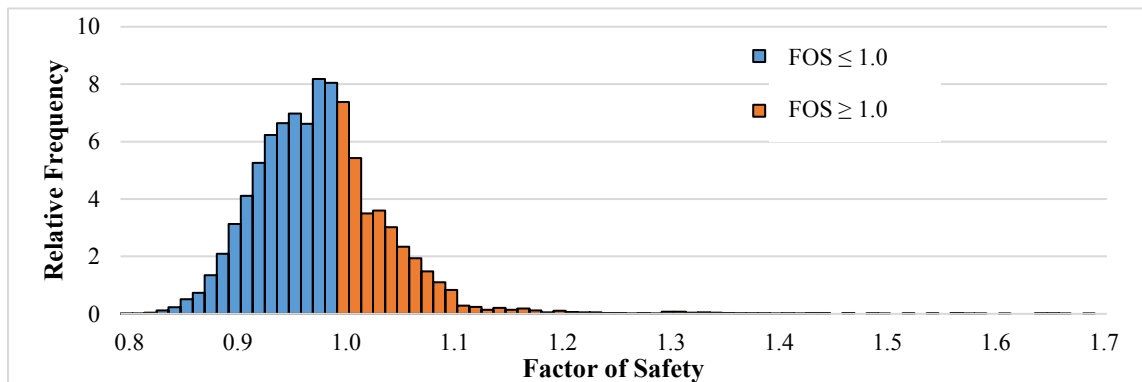


Figure 5.24: LNP analysis 2, histogram plot of the relative frequencies for the FOS, at the measured groundwater table.

From Table 5.10, the slope consistently obtained a mean FOS(μ_{FOS-1}) = 0.99 under the range of phreatic surface conditions considered which implies failure. The results show that the application of a load to the LNP slope will result in the formation of localized slip surfaces at the present groundwater table,

implying that the slope will fail. This highlights the influence of the application of surcharge loads to the LNPD slope, which is causative to slope failure.

From Table 5.11, a mean $FOS(\mu_{FOS-1}) = 0.99$ was obtained with a standard deviation of 0.07. The minimum recorded FOS value lies approximately 2 standard deviations below the mean value, implying a low variability in the minimum FOS value.

From Table 5.10, FOS values attaining a $FOS = 1.00$ also attained lognormal reliability index values of $\beta_{LN} < 1.0$. This implies a low degree of reliability in the results obtained over the corresponding phreatic surface heights analysed. The reliability index gives an indication of the degree of confidence one can afford to the FOS values. While, the FOS may be low a high reliability index value will increase the reliability in the FOS value obtained. Conversely, while the FOS value may be high a low reliability index will decrease the reliability in the FOS value.

From Table 5.11, although the negative β_{LN} value ($\beta_{LN} = -0.23$) correlates with the high Pf value, the very low β_{LN} value indicates low reliability in the FOS value. Chowdhury (1984), pointed out that a low reliability index values indicates less confidence in the FOS values obtained.

The histogram plot (Figure 5.24), indicates a lognormal distribution, with high relative frequencies recorded for FOS values over a narrow range between $0.9 \leq FOS \leq 1.10$, correlating with the low standard deviation value.

Probabilistic slope stability analysis indicates a 64.8 % probability of failure for the global minimum slip surface at the measured groundwater table (0.0 m).

In concluding, slope instability can be expected when the LNPD slope is loaded at the measured groundwater table. The problem of slope failure will be further exacerbated when the groundwater table rises, increasing the probability of slope failure. At the measured groundwater table, probabilistic analyses indicate a 64.8 % probability of slope failure occurring. The low reliability index value ($\beta = -0.23$) obtained however, lowers the confidence in the Pf value (64.8 %) obtained.

Our ability to simulate real world variability is limited by time and money, even if we could measure the value of variables with infinite precision the costs will be excessive (Haneberg, 2000). Analysis 2 of the LNPD slope has highlighted the benefits of a probabilistic approach. In which various probabilistic output functions have been obtained, to which a degree of reliability and confidence has been afforded.

As the analysis has shown a probabilistic approach is a useful tool in accounting for real world variability of parameters and uncertainty. The option to include the probabilistic approach as to supplement routine deterministic analyses should always be considered (Nilsen, 2000).

5.4.3 Deterministic and probabilistic slope stability analyses for the MPD slope

5.4.3.1 MPD – analysis 1

As discussed in Chapter 4 Section 4.4.5.2, five scenarios were considered for analysis 1 for the MPD slope and are presented in Table 5.12.

Table 5.12: MPD analysis 1 deterministic slope stability results.

MPD Analysis 1		Scenario 1	Scenario 2	Scenario 3	Scenario 4	Scenario 5
		Mean: $c' = 0.5 \text{ kPa}$, $\phi' = 28.2^\circ$	Min: $c' = 0 \text{ kPa}$, Max: $\phi' = 32^\circ$	Max: $c' = 10 \text{ kPa}$, Min: $\phi' = 22^\circ$	Both Min: $c' = 0 \text{ kPa}$, $\phi' = 22^\circ$	$c' = 0 \text{ kPa}$, $\phi' = 16^\circ$
Season	Phreatic Surface (m)	Deterministic FOS	Deterministic FOS	Deterministic FOS	Deterministic FOS	Deterministic FOS
Dry Season	- 2.00	2.69	2.93	2.64	1.89	1.35
	- 1.50	2.61	2.92	2.57	1.89	1.35
	- 1.00	2.51	2.82	2.50	1.89	1.35
	- 0.50	2.41	2.72	2.42	1.85	1.30
Measured groundwater table	0.00	2.32	2.60	2.33	1.74	1.24
Wet Season	+ 0.50	2.18	2.47	2.24	1.67	1.17
	+ 1.00	2.05	2.33	2.15	1.58	1.11
(extreme increase)	+ 1.50	1.91	2.19	2.05	1.40	1.00

Figure 5.25, illustrates the location of the global minimum failure surface obtained at the measured phreatic surface using the average shear strength parameters.

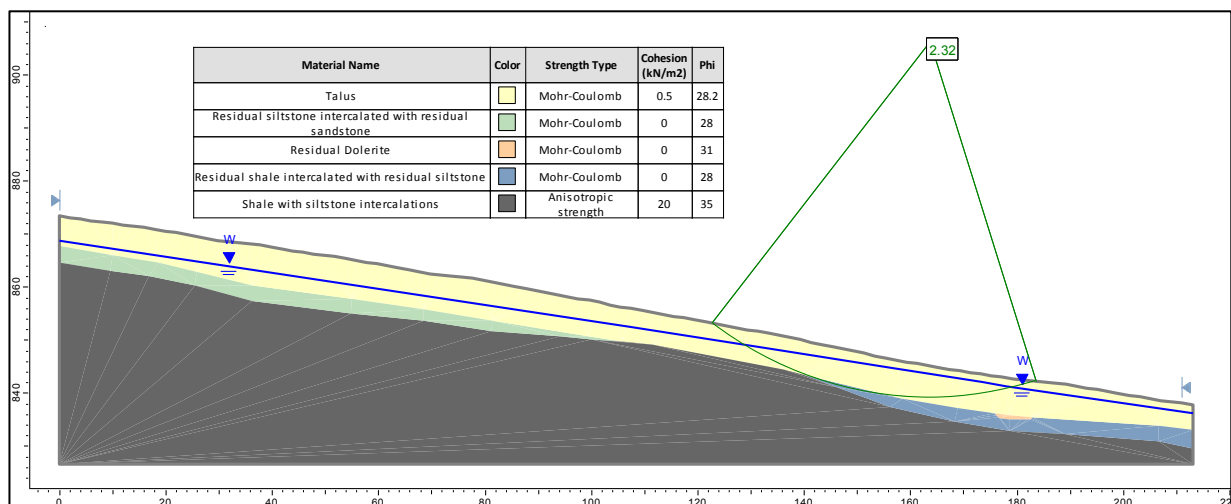


Figure 5.25: MPD scenario 1 analysis 1, at the measured groundwater table.

The global minimum slip surface is primarily orientated through the talus material with the residual sedimentary horizon and shale bedrock forming the base of the slip surface. The relatively high FOS = 2.32, implies stability. As explained in Chapter 4 Section 4.4.52, scenario 5 was conducted to establish the critical effective shear strength parameters that will result in slope failure. Figure 5.26, illustrates the location of the global minimum failure surface.

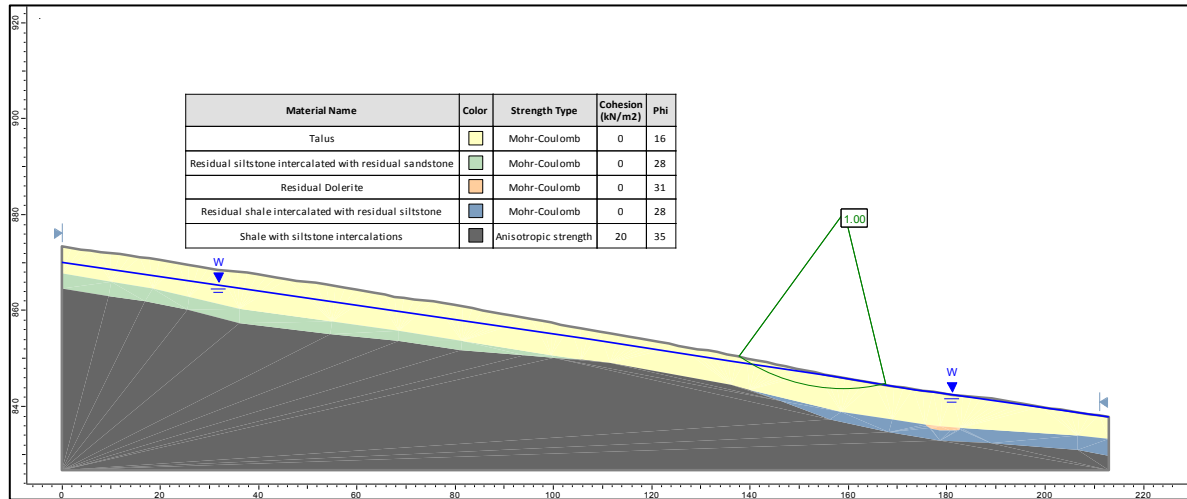


Figure 5.26: MPD analysis 1 scenario 5, at the maximum groundwater table.

From Table 5.12, scenarios 1 to 4 indicate values for the FOS > 1.00, over the range of phreatic surface heights considered. The FOS values gradually decreased from the dry to the wet season over the range of scenarios considered, highlighting the profound influence that an increase in pore water pressure has in reducing the shear strength of the talus material in the slope. Using the minimum effective shear strength parameters, a FOS = 1.40 was obtained at a 1.50 m increase in the phreatic surface. The use of average values has their own short-comings when conditions may be far from average (Haneberg, 2000). This situation can be mitigated by using conservative values to calculate the worst case FOS values (Haneberg, 2000). As such, scenario 5 was undertaken which concluded that a FOS = 1.00 was obtained at a 1.50 m increase in the phreatic height, using values of $c' = 0$ kPa and $\phi' = 16^\circ$ for the effective shear strength parameters.

The calculated ϕ' value lies approximately 3 standard deviations below the minimum ϕ' value defined in the study. A value of $c' = 0$ kPa, $\phi' = 16^\circ$, will only prevail under two conditions. Firstly, the value implies that the talus material of the MPD will have a majority of clay and will display shearing behaviour of a clay soil. Secondly, the low value possibly implies residual shear strength. If pre-existing discontinuities (shear planes) are present in the talus, this will result in a reduction of the peak shear strength to residual shear strength. Observations of distinct slickensided faces in the soil structure and residual shear strength test results would support these conditions which are shared by Allen (1981). However, limited records are available on these observations.

Using the average shear strength parameters, the analyses indicated that the slope is stable at the measured groundwater conditions (FOS = 2.32) even at a 1.50 m increase in the phreatic surface (FOS = 1.91). The observed high FOS value can be attributed to the present geometry of the slope and the uneven bedrock morphology. The latter of which has a convex curvature in the mid-slope region which can act as a stabilizing influence on the talus material. Minor geological details may remain undetected and thus the actual mode of failure may be different from the one assumed in the analysis (Chowdhury, 1984).

Based on the author's geological knowledge and engineering judgement a probabilistic slope stability analysis was not undertaken on scenario 5 for the following reasons. The ϕ' lies in the order of 3 standard deviations below the minimum range value (22°) of the ϕ' , considered during truncation of the random variables. As such the shear strength parameter values of $c' = 0$ kPa and $\phi' = 16^\circ$ concluded for scenario 5, were not deemed representative to conduct a probabilistic analysis. Engineering and significant judgement must be applied to representative scenarios before conducting a probabilistic approach (Bar & Heweston, 2018).

In concluding, under extremely wet conditions at a 1.50 m increase in the phreatic surface and where the talus effective shear strength parameters are reduced to values of $c' = 0$ and $\phi' = 16^\circ$, deterministic analyses indicate that the natural MPD slope will fail as a FOS = 1.00 is obtained.

5.4.3.2 MPD – analysis 2

Slope stability modelling for analysis 2 was undertaken by applying four 200 kPa surcharge loads simulating triple-storey structures on the slope. The results obtained from probabilistic slope stability analyses is presented in Table 5.13.

Table 5.13: MPD analysis 2, summarized probabilistic slope stability analyses results.

MPD Analysis 2		<i>Mean: $c' = 0.5$ kPa, $\phi' = 28.2^\circ$</i>				
Season	Phreatic Surface (m)	Deterministic FOS	$\mu_{\text{FOS-1}}$	β	β_{LN}	<i>Pf</i> (%)
Dry Season	- 2.00	1.19	1.24	2.23	2.24	0.30
	- 1.50	1.19	1.24	2.23	2.24	0.30
	- 1.00	1.19	1.24	2.23	2.24	0.30
	- 0.50	1.19	1.24	2.23	2.44	0.30
<i>Measured groundwater table</i>	0.00	1.19	1.24	2.23	2.44	0.30
Wet Season	+ 0.50	1.19	1.24	2.23	2.24	0.30
	+ 1.00	1.11	1.16	1.57	1.65	3.15
	+ 1.49	1.00	1.05	0.47	0.43	33.57
	+ 1.50	0.96	1.02	0.17	0.12	48.05

Where; $\mu_{\text{FOS-1}}$ is the mean factor of safety, β is the reliability index, β_{LN} is the lognormal reliability index & Pf is the probability of failure.

A deterministic FOS of 1.19 was recorded for the global minimum slip surface at the measured groundwater table. Figure 5.27, illustrates the location of the global minimum failure surface.

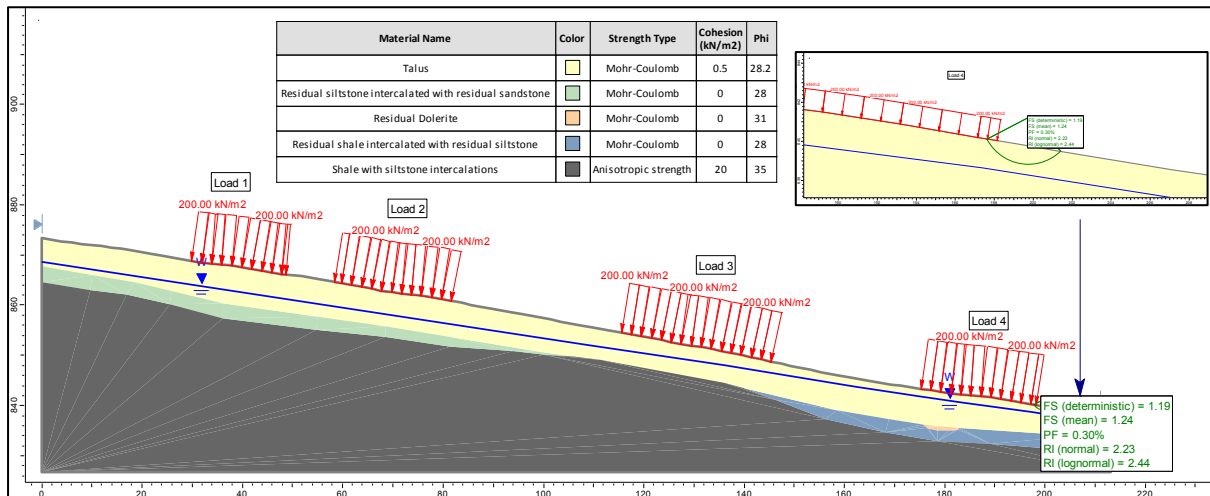


Figure 5.27: MPD analysis 2 probabilistic analysis, at the measured groundwater table using the mean effective shear strength parameters.

Probabilistic slope stability analyses were then undertaken by sequentially increasing the phreatic surface until a deterministic FOS of 1.00 was attained. At a 1.49 m increase in the phreatic surface the global minimum slip surface recorded a FOS = 1.00. Figure 5.28 illustrates the location of the global minimum failure surface.

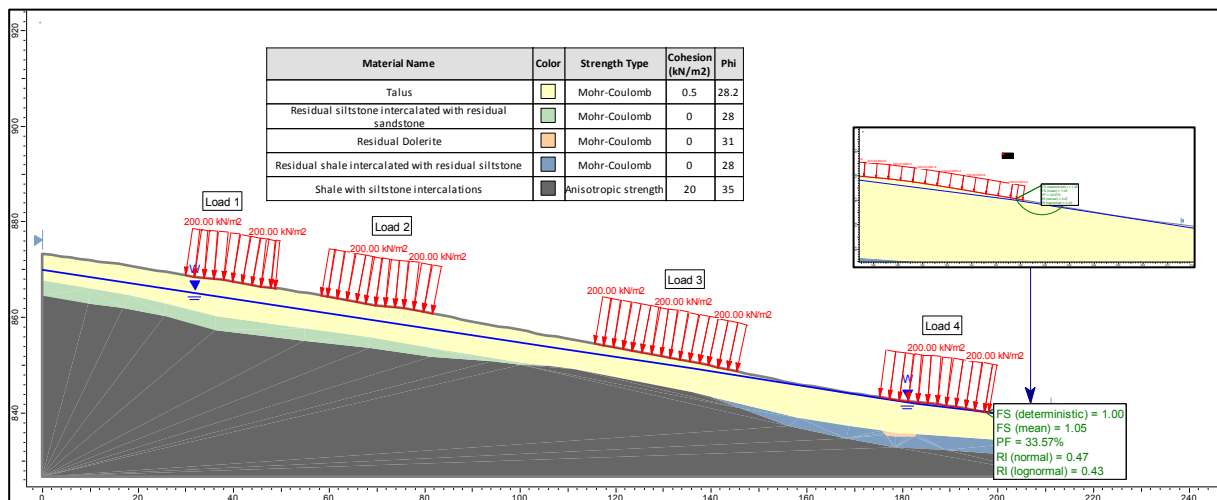


Figure 5.28: MPD analysis 2 probabilistic analysis, at the maximum increase in the groundwater table using the mean effective shear strength parameters.

The various parameters obtained from the probabilistic analyses are summarized in Table 5.14. Figure 5.29, illustrates the histogram plot obtained.

Table 5.14: MPD scenario 2 probabilistic parameters at a 1.49 m increase in the groundwater table.

μ_{FOS-1}	σ	Min	Max	β_{LN}	<i>pdf</i>	<i>Pf</i>
1.05	0.10	0.78	1.71	0.43	Lognormal	33.57 %

Where; μ_{FOS-1} is the mean factor of safety, σ is the standard deviation, Min is the minimum FOS, Max is the maximum FOS, β is the reliability index, β_{LN} is the lognormal reliability index, *pdf* is the probability distribution function & *Pf* is the probability of failure.

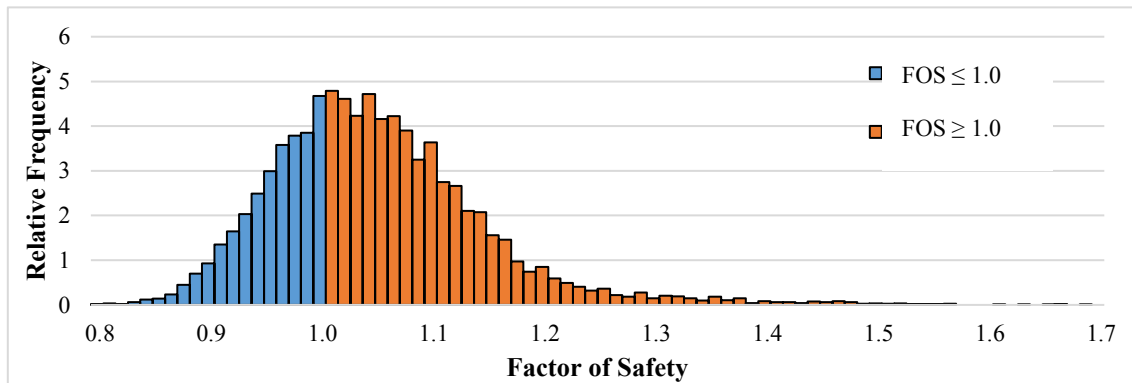


Figure 5.29: MPD analysis 2, histogram plot of the relative frequencies for the FOS, at the maximum increase in the groundwater table.

From Table 5.13, a deterministic FOS = 1.00 was obtained at a 1.49 m increase in the phreatic surface using the average shear strength parameters, implying slope instability. The slope obtained a mean FOS(μ_{FOS-1}) = 1.05 at a 1.49 m increase in the phreatic surface. In cases where the mean FOS(μ_{FOS-1}) \geq 1.00, values from the *Pf* show some element of failure. The high β values ($\beta > 2$) indicate reliability in the *Pf* values obtained.

The results show that the application of a load to the MPD slope will result in the formation of localized slip surfaces at a 1.49 m increase in the groundwater table, implying slope instability and an appreciable reduction in the FOS value with a degree of reliability. As with the LNP slope this highlights the influence of the application of surcharge loads to the MPD slope, which is causative to slope failure.

From Table 5.14, a mean FOS(μ_{FOS-1}) = 1.05 was obtained with a standard deviation of 0.10. The minimum recorded FOS values lies approximately 3 standard deviations below the mean FOS value, implying a low variability in the minimum FOS values. Although the maximum FOS value is representative of the results, it lies more than 5 standard deviations above the mean FOS value. This indicates very high variability in the upper range of FOS values. Lacasse & Nadim (1996), pointed out that if the variability is high it is important to consider whether the standard deviation arrived at a representative value given the range of values.

From Table 5.13, reliability indices decreased as the probability of failure and the phreatic surface increased. Higher probability of failure values correspond to lower reliability index values (Lacasse & Nadim, 1996). Notably, lognormal reliability index values of $\beta_{LN} > 1.5$ were attained for FOS > 1.00.

This implies a high degree of reliability in the Pf results obtained over the corresponding phreatic surface heights.

From Table 5.14, the lognormal reliability index value ($\beta_{LN} = 0.43$), indicates a low degree in confidence in the FOS value obtained. Studies by Chowdhury & Xu (1992), have shown that the reliability index value decreases as variation increases.

The histogram plot (Figure 5.29), indicates a lognormal distribution, with relatively high relative frequencies recorded over a broad range of FOS values between $0.9 \leq \text{FOS} \leq 1.1$. This variability is reflected in the minimum, maximum and standard deviation obtained for the FOS values in Table 5.14.

Probabilistic slope stability analysis indicates a 0.30 % probability of failure at the measured phreatic surface. A probabilistic approach recognizes that any earth structure has some probability of failure however small (Chowdhury, 1984). Furthermore, probabilistic slope stability analysis indicates a probability of failure of 33.6 % at a 1.49 m increase in the phreatic surface. The Pf values obtained are within the predicted range prescribed in the literature by Harr (1987) and Duncan & Wright (2005).

Thus, slope instability can be expected when the MPD slope is loaded and when the groundwater table rises by 1.49 m above the measured groundwater table. At a 1.49 m increase in the groundwater table probabilistic analyses indicates a probability of failure of 33.6 %. The reliability index value ($\beta = 0.43$) obtained however, indicates reduced confidence in the Pf value (33.6 %). In comparison to the higher reliability index values obtained during dry season slope stability analyses, for the corresponding Pf values obtained.

Analysis 2 of the MPD slope has highlighted the strengths and limitations of using a deterministic approach. Furthermore, the study indicates that a probabilistic approach is able to account for the element of uncertainty. For instance, by using the average effective shear strength parameters the effect of spatial variability is reduced. This is because the variability is averaged over a volume and only the averaged contribution to the uncertainty is of importance (Lacasse & Nadim, 1996). The study highlights the importance of probabilistic slope stability concepts to deterministic slope stability analysis. It gave a better insight into the performance of slopes in the Town Bush Valley. A probabilistic approach enables a study of reliability to be made under conditions of uncertainty, which enables decisions to be made about alternative designs (Chowdhury, 1984).

CHAPTER 6

CONCLUSIONS AND RECOMMENDATIONS

6.1 Conclusions

The main findings and conclusions drawn from the research on the geotechnical characterization and stability of the slopes of the Town Bush Valley, located around the greater Pietermaritzburg region of South Africa is presented. The purpose of the study was to evaluate the geotechnical properties and stability of critical sections of the Town Bush Valley and define factors that may compromise the stability of slopes. The study aimed at establishing the geological, hydrogeological and geotechnical conditions prevailing in the Town Bush Valley, an area in which limited scientific research has been undertaken.

The elevation in the study area ranges from 790 to 950 metres above mean sea level. The study area is situated on heterogeneous talus material, which is underlain at depth by shales of the Pietermaritzburg Formation and sandstones of the Vryheid Formation. The presence of deep talus horizons and residual sedimentary material were profiled in boreholes, auger and trial pit logs. Talus horizons at the MPD, UNPD, LNPD and Cascades Development extend to depths of 21.00 m below NGL.

A literature review of the critical geotechnical factors indicated that the study area has active mass movement and unstable slopes. The digital elevation model highlighted slopes in the Town Bush Valley which exceed 18° . The talus material appears to be formed from erosion of the Pietermaritzburg Formation. The talus accumulated and continues to accumulate over a period of geological time, promoted by the process of natural features in the Town Bush Valley such as incised palaeo-drainage channels, dolerite intrusions and slope geometry. The talus horizon is deepest at the toe of the slopes of the Town Bush Valley where the Cascades Development is located. The Town Hill Escarpment is actively undergoing large-scale geomorphological processes which were recognized as far back as 1939. Aerial photographic analysis indicated the presence of hummocky topography in the Town Hill Escarpment, indicating potential slope instability.

The hydrogeology of the study site indicates an unconfined aquifer system that is recharge along the high slopes of the Town Hill Escarpment. Groundwater circulates primarily through the unconsolidated talus horizon bounded by impermeable shale bedrock along the base.

The geotechnical characterization of the study area concluded that the talus material generally grades as a clayey sand. Two consolidated-drained triaxial tests were undertaken, which yielded a $c' = 0$ kPa, $\varphi' = 30^\circ$ and $c' = 13$ kPa, $\varphi' = 37^\circ$.

The Morgenstern and Price procedure was used during slope stability analyses. A deterministic and probabilistic approach was used during slope stability analyses. Two conditions were considered during the slope stability analysis of the LNPD and MPD slope. Firstly, the stability of the natural slope (analysis 1) and the stability of the slope with the application of a surcharge load (analysis 2). The effective shear strength parameters of the talus material were chosen as the random variables for the study, during probabilistic slope stability analyses. Monte Carlo Simulation method was the chosen probabilistic method. Various scenarios and groundwater conditions were considered during the analyses. Various functions were derived during probabilistic slope stability analyses, which allowed for an assessment of the values obtained. The results of the sensitivity analysis had indicated that the FOS values are sensitive to ϕ' values.

Analysis 1 of the LNPD slope indicated that at the measured phreatic surface and using the mean effective shear strength parameters, the slope is stable (FOS = 2.23) and continued to be stable under the range of phreatic surface conditions considered. Under conditions where the talus material behaves in the range of the minimum recorded effective shear strength parameters and at a 3.56 m increase in the phreatic surface, the natural LNPD slope is unstable (FOS = 1.00). Probabilistic analyses indicated a 50.8 % probability of failure, which is inferred with a low degree of confidence based on the reliability index. Analysis 2 of the LNPD slope indicated that under loaded (150 kPa) conditions, using the average shear strength parameters at the measured phreatic surface, the slope has a probability of failure of 64.6 %, which is inferred with a low degree of confidence based on the reliability index. LNPD slope stability modelling highlighted that a reduction in the FOS value will be brought about by loading the slope irrespective of seasonal changes in the groundwater table, which will result in slope failure.

Analysis 1 of the MPD slope indicated that at the measured phreatic surface and using the mean effective shear strength parameters, the slope is stable (FOS = 2.32) and continues to be stable even at the maximum increase in the phreatic surface (FOS=1.19). Under conditions where the effective shear strength parameters of the talus material are reduced to values of $c' = 0$ and $\phi' = 16^\circ$, the natural slope attains a FOS = 1.00 at the maximum phreatic surface. Analysis 2 of the MPD slope indicated that under loaded (200 kPa) conditions, using the average shear strength parameters at the measured phreatic surface the slope has probability of failure of 0.30 %, which is inferred with a high degree of confidence, based on the reliability index. At a 1.49 m increase in the phreatic surface (FOS = 1.00), a probability of failure of 33.6 % is obtained, which is inferred with a low degree of confidence based on the reliability index. MPD slope stability modelling highlighted the compounding influence of surcharge loads and a rise in the phreatic surface, which will result in a reduction in the FOS to unity and slope failure.

Thus, the slope stability analyses results have indicated that the application of surcharge loads in the form of structures to the LNPD and MPD slope, have a profound influence in reducing the FOS value

and this results in unstable slope conditions. The study indicated the importance of adopting a scenario based approach during deterministic and probabilistic slope stability modelling in order to identify initiating factors. The study has defined critical conditions that will initiate slope instability in the Lower National Park Development and the Montrose Park Development. The probabilistic approach to slope stability analyses was able to account for the uncertainty in soil properties. The study has highlighted the advantages of using probabilistic slope stability concepts to deterministic slope stability analysis. The probabilistic approach has given a better insight and understanding into the performance of the slopes in the Town Bush Valley.

6.2 Recommendations for further research

The study has highlighted the slope stability problems that will arise from applying structural loads to deep talus soils in the Town Bush Valley. In areas demarcated as having deep talus soils in the Town Hill Escarpment, it is recommended that a comprehensive geotechnical investigation be carried out. In order to assess the feasibility of the development prior to construction. It is further recommended that development restrictions be considered by the local Municipality, based on the outcomes of the pertaining geotechnical investigation.

The rate and scale at which mass wasting processes are operating on the Town Bush Valley is largely unknown. Furthermore, the degree of risk associated with founding on the talus material is an area of limited research. The first further area of research is to conduct a landslide hazard zonation map of the Town Hill Escarpment, focusing on areas of deep talus accumulation.

The construction of structures over zones of active talus soils is exponentially increasing in peripheral areas of Pietermaritzburg. Therefore, the second further area of research, is the design and performance of advanced geotechnical foundations that account for active earth pressures.

REFERENCES

- Allen, P. (1981). *Slope stability problems in the Pietermaritzburg area*. In: Symposium on the Engineering Geology of cities in South African. *Symposium on the Engineering Geology of Cities in South Africa*. Pretoria, South Africa, September 1981. Pretoria: Association of Engineering Geologists.
- Aleotti, P. & Chowdhury, R. (1999). Landslide hazard assessment: summary review and new perspectives, *Bulletin of Engineering Geology and the Environment*, **58**, pp 21-44.
- American Society for Testing and Materials, (1998). *ASTM D422-63 Standard test method for Particle-Size Analysis of Soils*. ASTM, West Conshohocken.
- Bar, N. and Heweston, A. (2018). Considerations for effectively using probability of failure as a means of slope design appraisal for homogenous and heterogeneous rock masses. *International Journal of Geological and Environmental Engineering*, **12**(2), pp 66-72.
- Bell, F.G. and Maud, R.R. (1999). Landslides associated with the colluvial soils overlying the Natal Group in the greater Durban region of Natal, South Africa. *Environmental Geology*, **39**(9), pp 1029-1038.
- Bell, F.G. (2007). *Engineering Geology*, 2nd Edition. Elsevier. Oxford, Great Britain.
- Botha, G.A. and Partridge, T.C. (2000). Colluvial deposits. In: Partridge T.C. and Maud, R.R. (Eds.), *The Cenozoic of Southern Africa*. Oxford University Press, New York, 88-99.
- Brink, A.B.A. (1983). *The Geology of South Africa: The Karoo Sequence Volume 3*, Building Publications: Cape Town.
- British Standards Institution, (1990a). *BS 1377 British Standard Methods of test for soils for civil engineering purposes, Part 1: General requirements and sample preparation*. B.S.I., London.
- British Standards Institution, (1990b). *BS 1377 British Standard Methods of test for soils for civil engineering purposes, Part 8: Shear strength test*. B.S.I., London.
- Budhu, M. (2000). *Soil Mechanics and Foundations*, 1st Edition. John Wiley & Sons Inc.: New York.
- Carter, M., and Bentley, S.P. (1991). *Correlations of Soil Properties*. Pentech Press Limited: London.
- Chevallier, L. and Woodford, A.C. (1999). Morpho-tectonics and mechanism of emplacement of the dolerite rings and sills of the western Karoo, South Africa. *S. Afr. J. Geol.*, **102**, pp 43-54.

- Chowdhury, R. N. (1984). Recent developments in landslide studies: Probabilistic methods, State of the art report–Session VII (a). *International symposium on landslides*, pp 209–228.
- Chowdhury, R. N. and Xu, D.W. (1992). Reliability index for slope stability assessment - two methods compared. *Reliability Engineering and System Safety*, **37**, pp 99-108.
- Cornforth, D.H. (2005). *Landslides in practice: investigation, analysis and remedial/preventative options in soils*. John Wiley & Sons Ltd.: Hoboken.
- Council for Geoscience. (2002). 2930CB Pietermaritzburg. *Geological Series*, 2930CB, 1:50 000, Pietermaritzburg: Council for Geoscience.
- Council for Geoscience. (2008). 2930CB Pietermaritzburg. *Geotechnical Series*, 2930CB, 1:50 000, Pretoria: Council for Geoscience.
- Council for Scientific and Industrial Research, (1986). *Standard Methods of Testing Road Construction Materials, Technical Methods for Highways*. CSIR, Pretoria.
- Courtillot, V. (1994). Mass extinctions in the last 300 million years: one impact and seven flood basalt?, *Israel J. Earth Sci.*, **43**, pp 255-266.
- Das, B.M. (1994). *Principles of Geotechnical Engineering*, PWS Publishing: Boston.
- Das, B.M. (2006). *Principles of Geotechnical Engineering*, 5th Edition, Thomson: Toronto.
- Department of Water and Sanitation. (2015). Department of Water and Sanitation site for spatial information. [online] Available at: http://www.dwa.gov.za/iwqs/gis_data/ [Accessed 10 June 2015].
- Du Toit, A.L. (1954). *The Geology of South Africa*. Oliver and Boyd, Edinburgh, 366.
- Duncan. J.M. and Wright, S.G. (2005). *Soil strength and slope stability*. Wiley & Sons: London.
- Duncan, A.R. and Marsh, J.S. (2006). The Karoo Igneous Province, South Africa. *S. Afr. J. Geol.*, **1**, pp 501-518.
- Fitch, F.J. and Miller, J.A. (1984). Dating Karoo igneous rocks by the conventional K-Ar and ⁴⁰Ar/³⁹Ar age spectrum methods. In: Erlank, A.J. (Ed.), *Petrogenesis of the Volcanic Rocks of the Karoo Province*. Special Publication Geological Society South Africa, **13**, pp 247-266.
- Freeze, R.A. and Cherry, J.A. (1979). *Groundwater*, 1st Edition. Prentice Hall Inc.: London.
- Gover, S.M. (2014). *A Review of Reliability-Based Slope Stability Analysis*. In: Proceedings of the 8th South African Young Geotechnical Engineers Conference, 8th South African Young

- Geotechnical Engineers Conference*. Stellenbosch, South Africa, 17, 18 & 19 September 2014. Pretoria: SAICE.
- Hadlow, M.J. (1993). *Upgrading the N3/3 between Athlone and Hilton*, Ref no: 7456. Drennan Maud and Partners, Durban.
- Hadlow, M.J. (2004). *Report to BCP Engineers on a Geotechnical Investigation of the Proposed Village I Development, Victoria Country Club, Pietermaritzburg*, Ref no: 16050. Drennan Maud and Partners, Durban.
- Haneberg, W.C. (2000). Deterministic and Probabilistic Approaches to Geologic Hazard Assessment. *Environmental and Engineering Geoscience*, **6**(3), pp 209-226.
- Haneberg, W.C. (2004). A Rational Probabilistic Method for Spatially Distributed Landslide Hazard Assessment. *Environmental and Engineering Geoscience*, **10**(1), pp 27-43.
- Harr, M.E. (1987). *Reliability-based design in civil engineering*. McGraw-Hill: New York.
- Head, K.H. (1998). *Manual of soil laboratory testing*, 2nd Edition. John Wiley & Sons Ltd.: Chichester.
- Hunter, D.R., Johnson, M.R., Anhaeusser, C.R., and Thomas, R.J. (2006). Introduction. In: Johnson, M.R., Anhaeusser, C.R., and Thomas, R.J. (Eds.), *The Geology of South Africa*, Geological Society of South Africa, Johannesburg/ Council for Geoscience, Pretoria, pp 1-7.
- Hutchinson, S. and Bandalos, D. (1997). A Guide to Monte Carlo Simulation Research for Applied Researchers. *Journal of Vocational Education Research*, **22**, pp 233-245.
- Huvaj, N. and Oguz, E.H. (2018). Probabilistic Slope Stability Analysis: A Case Study. *Sakarya University Journal of Science*, **22**(5), pp 1458-1465.
- Isherwood, C. (2013). *Victoria Country Club Estate, Plot 9527 and Plot 9528 consolidated, Geotechnical Investigation Report*, Ref no:4000006/9527-9528. Terratest, Pietermaritzburg.
- Isherwood, C. (2015). *A detailed analysis of the loading conditions at the Town Bush Valley*. [conversation] (Personal communication, January-September 2015).
- Jennings J.E., Brink, A.B.A., Williams A.A.B. (1973). *Revised Guide to Soil Profiling for Civil Engineering Purposes in South Africa*, **15**. Pretoria: SAICE (1973).
- Johnson. M.R. (1991). Sandstone petrography, provenance and plate tectonic setting in Gondwana context of the south eastern Karoo-basin, *South African Journal of Geology*, **94**, pp 137-154.

- Johnson, M.R., Hunter, D.R., Anhaeusser, C.R., and Thomas, R.J. (2006). Sedimentary rocks in the Karoo Supergroup. In: Johnson, M.R., Anhaeusser, C.R., and Thomas, R.J. (Eds.), *The Geology of South Africa*, Geological Society of South Africa, Johannesburg/ Council for Geoscience, Pretoria, pp 461-499.
- Knappet, J.N. and Craig, R.F. (2012). *Craig's Soil Mechanics*, 8th Edition, Spon Press: London.
- Kujawa, T. (2005). *Report to Riel Associates on a Geotechnical Investigation of the Proposed Village 5 Development, Victoria Country Club, Pietermaritzburg*, Ref no: 16050. Drennan Maud and Partners, Durban.
- Lacasse, S. and Nadim, F. (1996). *Uncertainties in characterising soil properties*. In: Geotechnical Special Publication. *Uncertainty in the geological environment: from theory to practice*. Madison: ASCE.
- Landman, K. (2002). *Gated communities in South Africa: building bridges or barriers*. In: Sustainable Development Network. *International Conference on Private Urban Governance*. Mainz, Germany, 6-9 June 2012, Pretoria: CSIR.
- Le Blanc Smith, G. (1980). *Genetic stratigraphy and palaeoenvironmental control on coal distribution in the Witbank Basin coalfield*. Ph.D. thesis (unpublished), University of Witwatersrand, Johannesburg.
- Look, B.G. (2007). *Handbook of Geotechnical Investigation and Design Tables*. Taylor & Francis: London.
- Lotter, C. (2017). *A review of the of the loading conditions at the Town Bush Valley*. [conversation] (Personal communication, January-September 2015).
- Low, B.K. and Tang, W.H. (1997). Efficient reliability evaluation using spreadsheet. *Journal of Engineering Mechanics*, **123**(7), pp 749-752.
- Low, B.K. and Tang, W.H. (2007). Efficient spreadsheet algorithm for First-order Reliability Method. *Journal of Engineering Mechanics*, **133**(12), pp 1378-1387.
- Maud, R.R. (1981). *The engineering geology of the city of Pietermaritzburg*. In: Symposium on the Engineering Geology of cities in South African. *Symposium on the Engineering Geology of Cities in South Africa*. Pretoria, South Africa, September 1981. Pretoria: Association of Engineering Geologists.

- Maud, R.R. (1985). Talus on Pietermaritzburg Shale Formation. *In: Brink, A.B.A. Engineering Geology of Southern Africa, Post-Gondwana Deposits, Building Publications, Pretoria, pp 167-170.*
- Maurenbrecher, P.M. (1973). Instability of a Road Embankment at Rickivy, Pietermaritzburg. *The Civil Engineer in South Africa*, **15**, pp 218-224.
- Maurenbrecher, P.M. and Booth, A.R., (1975). Some Slope Stability Problems in Soils Derived From the Eccas Shales of Natal, South Africa. *Engineering Geology*, **10**, pp 99-121.
- Montgomery, D.C. and Runger, G.C (2011). *Applied Statistics and Probability for Engineers*. John Wiley & Sons, Inc: Asia.
- Morgenstern, N.R. and Price, V. (1965). The analysis of the stability of general slip surfaces. *Geotechnique*, **15** (1), pp 79–93.
- Murthy, V.N.S. (2003). *Geotechnical Engineering: Principles and Practices of Soil Mechanics and Foundation Engineering*. Marcel Dekker, Inc.: Basel.
- Ndela, G. (2012). *Geotechnical Investigation Report for Plots 9984 & 9985, Village 4 at the Victoria Country Club Estate*, Ref no:400006/9984-9985. Terratest, Pietermaritzburg.
- Nilsen, B. (2000). New trends in rock slope stability analysis. *Bulletin of Engineering Geology and Environment*, **5**, pp 173-178.
- Partridge, T.C., Botha. G.A. and Haddon I.G. (2006). Cenozoic Deposits of the Interior, South Africa. *S. Afr. J. Geol.*, **1**, pp 591-602.
- Price, G.V. (2006). *Victoria Country Club Estate: Village 3 Independent Engineering Geological Appraisal*, Ref no: Terreco_Tgt122_gvp. Terreco, Gonubie.
- Chevallier, L. and Woodford, A.C. (1999). Morpho-tectonics and mechanism of emplacement of the dolerite rings and sills of the western Karoo, South Africa. *S. Afr. J. Geol.*, **102**, pp 43-54.
- Richards, N.P., Botha, G.A., Schoeman, P., Clarke, B.M., Kota, M.W. and Ngcobo, F.W. (2006). Engineering geological mapping in Pietermaritzburg, South Africa: Constraints on development. *IAEG 2006*, **407**, pp 1-11.
- Rosenfeld, C.L. (1994). The Geomorphological Dimensions of Natural Disasters. *Geomorphology*, **10**, pp 27-26.
- SA Explorer. (2015). Pietermaritzburg Climate. [online] Available at: <http://www.saexplorer.co.za/south-africa/climate/pietermaritzburgclimate.asp> [Accessed 10 October 2015].

- SAICE (South African Institute of Civil Engineering). (2002). *Guidelines for Soil and Rock Logging in South Africa*, 2. Pretoria: AEG, SAICE and SAIEG (1990).
- Schreiner, H.D. (2005a). *Report to Riel Associates Project Development and Management, Victoria Country Club, Village 4, Geotechnical Investigation Report*, Ref no:16-1055. Jeffares and Green, Pietermaritzburg.
- Schreiner, H.D. (2005b). *Geotechnical Investigation Report, Village 3 at the Victoria Country Club Estate*. Jeffares & Green, Pietermaritzburg.
- Schreiner, H.D. (2005c). *Geotechnical Investigation Report for Plot 9205, Village 2 at the Victoria Country Club Estate*, Ref no:16-1230/3/HDS. Terratest, Pietermaritzburg.
- Schreiner, H.D. (2005d). *Geotechnical Investigation Report for Plot 9212, Village 2 at the Victoria Country Club Estate*, Ref no:16-1230/5/HDS. Terratest, Pietermaritzburg.
- Schreiner, H.D. (2005e). *Geotechnical Investigation Report, Village 2 at the Victoria Country Club Estate*, Ref no:16-1055/HDS. Jeffares & Green, Pietermaritzburg.
- Schreiner, H.D. (2006a). *Geotechnical Investigation Report for Plot 9216, Village 2 at the Victoria Country Club Estate*, Ref no:16-1230/22. Terratest, Pietermaritzburg.
- Schreiner, H.D. (2006b). *Geotechnical Investigation Report for Plot 9217, Village 2 at the Victoria Country Club Estate*, Ref no:16-1230/24. Terratest, Pietermaritzburg.
- Schreiner, H.D. (2006c). *Geotechnical Investigation Report for Plot 9219, Village 2 at the Victoria Country Club Estate*, Ref no:16-1230/21. Terratest, Pietermaritzburg.
- Schreiner, H.D. (2006d). *Geotechnical Investigation Report for Plot 9222, Village 2 at the Victoria Country Club Estate*, Ref no:16-1230/23. Terratest, Pietermaritzburg.
- Schreiner, H.D. (2006e). *Geotechnical Investigation Report for Plot 9335, Village 3 at the Victoria Country Club Estate*, Ref no:16-1230/15. Terratest, Pietermaritzburg.
- Schreiner, H.D. (2006f). *Geotechnical Investigation Report for Plot 9344, Village 3 at the Victoria Country Club Estate*, Ref no:16-1230/15a. Terratest, Pietermaritzburg.
- Schreiner, H.D. (2006g). *Geotechnical Investigation Report for Plot 9365, Village 3 at the Victoria Country Club Estate*, Ref no:16-1230/10. Terratest, Pietermaritzburg.
- Schreiner, H.D. (2006h). *Geotechnical Investigation Report for Plot 9355, Village 5 at the Victoria Country Club Estate*, Ref no:16-1230/17. Terratest, Pietermaritzburg.
- Schreiner, H.D. (2006i). *Geotechnical Investigation Report for Plot 9554, Village 5 at the Victoria Country Club Estate*, Ref no:16-1230/18. Terratest, Pietermaritzburg.

- Schreiner, H.D. (2006j). *Geotechnical Investigation Report for Plot 9583, Village 5 at the Victoria Country Club Estate*, Ref no:16-1230/18. Terratest, Pietermaritzburg.
- Schreiner, H.D. (2006k). *Geotechnical Investigation Report for Plot 9474, Village 3 at the Victoria Country Club Estate*, Ref no:16-1230/16. Terratest, Pietermaritzburg.
- Schreiner, H.D. (2006l). *Geotechnical Investigation Report for Plot 9879, Village 3 at the Victoria Country Club Estate*, Ref no:16-1230/10. Terratest, Pietermaritzburg.
- Schreiner, H.D. (2006m). *Geotechnical Investigation Report for Plot 9555, Village 5 at the Victoria Country Club Estate*, Ref no:16-1230/17. Terratest, Pietermaritzburg.
- Schreiner, H.D. (2006n). *Geotechnical Investigation Report for Plot 9561, Village 5 at the Victoria Country Club Estate*, Ref no:16-1230/19. Terratest, Pietermaritzburg.
- Schreiner, H.D. (2007a). *Geotechnical Investigation Report for Plot 9358, Village 3 at the Victoria Country Club Estate*, Ref no:16-1230/28. Terratest, Pietermaritzburg.
- Schreiner, H.D. (2007b). *Geotechnical Investigation Report for Plot 9298, Village 4 at the Victoria Country Club Estate*, Ref no:16-1230/43. Terratest, Pietermaritzburg.
- Schreiner, H.D. (2007c). *Geotechnical Investigation Report for Plot 9566, Village 5 at the Victoria Country Club Estate*, Ref no:16-1230/35. Terratest, Pietermaritzburg.
- Schreiner, H.D. (2007d). *Geotechnical Investigation Report for Plot 9572, Village 5 at the Victoria Country Club Estate*, Ref no:16-1230/32. Terratest, Pietermaritzburg.
- Schreiner, H.D. (2007e). *Geotechnical Investigation Report for Plot 9576, Village 5 at the Victoria Country Club Estate*, Ref no:16-1230/30. Terratest, Pietermaritzburg.
- Selby, M.J. (1982). *Hillslope Materials & Processes*. Oxford University Press: New York.
- Sharma, R.K. (2016). *Reliability Analysis of Slope Stability using Monte Carlo Simulation and Comparison with Deterministic Analysis*. In: Proceedings of the International Conference on Computational Methods, 7th International Conference on Computational Methods. Berkeley, USA, 1-4 August 2016, USA: Scientech Publisher llc.
- Singh, K. (2015a). *VCCE Plot 9366 & Plot 9367*, Ref no:400006 (VCCE)_9366/9367. Terratest, Pietermaritzburg.
- Singh, K. (2015b). *Victoria Country Club Estate Plot 94770, Village 3, Pietermaritzburg*, Ref no: 400006(VCCE)9470. Terratest, Pietermaritzburg.

- Singh, K. (2016). *Victoria Country Club Estate Groundwater Flow at Plot 9284 and Plot 9285*, Ref no:400006 (VCCE)_9284/9285. Terratest, Pietermaritzburg.
- Singh, R. (2006a). *Geotechnical Investigation Report for Plot 9342, Village 3, Victoria Country Club Estate*, Ref no:16-1230/26. Terratest, Pietermaritzburg.
- Singh, R. (2006b). *Geotechnical Investigation Report for Plot 9372, Village 3, Victoria Country Club Estate*, Ref no:16-1230/20. Terratest, Pietermaritzburg
- Singh, R. (2007a). *Geotechnical Investigation Report for Plot 9201, Village 2, Victoria Country Club Estate*, Ref no:400006/66. Terratest, Pietermaritzburg.
- Singh, R. (2007b). *Geotechnical Investigation Report for Plot 9324, Village 3, Victoria Country Club Estate*, Ref no:16-1230-53. Terratest, Pietermaritzburg.
- Singh, R. (2007c). *Geotechnical Investigation Report for Plot 9355, Village 3, Victoria Country Club Estate*, Ref no:16-1230-36. Terratest, Pietermaritzburg.
- Singh, R. (2007d). *Geotechnical Investigation Report for Plot 9360, Village 3, Victoria Country Club Estate*, Ref no:16-1230-28. Terratest, Pietermaritzburg.
- Singh, R. (2007e). *Geotechnical Investigation Report for Plot 9362, Village 3, Victoria Country Club Estate*, Ref no:16-1230-28a. Terratest, Pietermaritzburg.
- Singh, R. (2007f). *Geotechnical Investigation Report for Plot 9562, Village 5, Victoria Country Club Estate*, Ref no:16-1230-42. Terratest, Pietermaritzburg.
- Singh, R. (2007g). *Geotechnical Investigation Report for Plot 9375, Village 3, Victoria Country Club Estate*, Ref no:16-1230-44. Terratest, Pietermaritzburg.
- Singh, R. (2007h). *Geotechnical Investigation Report for Plot 9383, Village 3, Victoria Country Club Estate*, Ref no:16-1230-9383. Terratest, Pietermaritzburg.
- Singh, R. (2007i). *Geotechnical Investigation Report for Plot 9388, Village 3, Victoria Country Club Estate*, Ref no:16-1230-45. Terratest, Pietermaritzburg.
- Singh, R. (2007j). *Geotechnical Investigation Report for Plot 9405, Village 3, Victoria Country Club Estate*, Ref no:16-1230-9405. Terratest, Pietermaritzburg.
- Singh, R. (2007k). *Geotechnical Investigation Report for Plot 9523, Village 3, Victoria Country Club Estate*, Ref no:16-1230-9523. Terratest, Pietermaritzburg.

- Singh, R. (2008a). *Geotechnical Investigation Report for Plot 9345, Village 3, Victoria Country Club Estate*, Ref no:16-1230-47. Terratest, Pietermaritzburg.
- Singh, R. (2008b). *Geotechnical Investigation Report for Plot 9352, Village 3, Victoria Country Club Estate*, Ref no:16-1230-51. Terratest, Pietermaritzburg.
- Singh, R. (2008c). *Geotechnical Investigation Report for Plot 9563, Village 5, Victoria Country Club Estate*, Ref no:16-1230-52. Terratest, Pietermaritzburg.
- Singh, R. (2008d). *Geotechnical Investigation Report for Plot 9568, Village 5, Victoria Country Club Estate*, Ref no:16-1230-50. Terratest, Pietermaritzburg.
- Singh, R. (2008e). *Geotechnical Investigation Report for Plot 9858, Village 3, Victoria Country Club Estate*, Ref no:16-1230-60. Terratest, Pietermaritzburg.
- Singh, R. (2009a). *Geotechnical Investigation Report for Plot 9201, Village 2, Victoria Country Club Estate*, Ref no:400006/66. Terratest, Pietermaritzburg.
- Singh, R. (2009b). *Geotechnical Investigation Report for Plot 9263, Village 4, Victoria Country Club Estate*, Ref no:400006/69. Terratest, Pietermaritzburg.
- Singh, R. (2009c). *Geotechnical Investigation Report for Plot 9976, Village 4, Victoria Country Club Estate*, Ref no:400006/68. Terratest, Pietermaritzburg.
- Singh, R. (2009d). *Geotechnical Investigation Report for Plot 9976, Village 4, Victoria Country Club Estate*, Ref no:400006/70. Terratest, Pietermaritzburg.
- Singh, R. (2009e). *Geotechnical Investigation Report for Plot 9385, Village 3, Victoria Country Club Estate*, Ref no:16-1230-67. Terratest, Pietermaritzburg.
- Singh, R. (2009f). *Geotechnical Investigation Report for Plot 9533, Village 3, Victoria Country Club Estate*, Ref no:400006-65. Terratest, Pietermaritzburg.
- Singh, R. (2010a). *Geotechnical Investigation Report for Plot 9214, Village 2, Victoria Country Club Estate*, Ref no:400006/72. Terratest, Pietermaritzburg.
- Singh, R. (2010b). *Geotechnical Investigation Report for Plot 9231, Village 2, Victoria Country Club Estate*, Ref no:400006/77. Terratest, Pietermaritzburg.
- Singh, R. (2010c). *Geotechnical Investigation Report for Plot 9333, Village 3, Victoria Country Club Estate*, Ref no:400006/71. Terratest, Pietermaritzburg.

- Singh, R. (2010d). *Geotechnical Investigation Report for Plot 9281, Village 4, Victoria Country Club Estate*, Ref no:400006/73. Terratest, Pietermaritzburg.
- Singh, R. (2010e). *Geotechnical Investigation Report for Plot 9864, Village 3, Victoria Country Club Estate*, Ref no:400006/74. Terratest, Pietermaritzburg.
- Subrayen, P. (2013). *Victoria Country Club Estate, Plot 9363, Geotechnical Investigation Report*, Ref no:400006/9363. Terratest, Pietermaritzburg.
- Subrayen, P. (2014). *Victoria Country Club Estate, Plot 9473, Geotechnical Investigation Report*, Ref no:400006/9473. Terratest, Pietermaritzburg.
- Smith, G.N. (1990). *Elements of Soil Mechanics*, 6th Edition. BSP Professional Books: London.
- South African Weather Service (SAWS). (2015). *Rainfall and climatic data for Cedara weather station (02394820)* [spreadsheet]. SAWS, Ref no: CLS-Disclosure-001898. Cedara weather station, Pietermaritzburg.
- Stark, T. D., and Eid, H. T. (1993). Modified Bromhead ring shear apparatus, *ASTM. Geotechnical Testing Journal*, **16**(1), pp 100–107.
- Storey, B.C., Alabaster, T. and Pankhurst, R.J. (Eds.) (1992). Magmatism and the causes of Continental Break-up. *Spec. Publ. Geol. Soc. Lond.*, **68**, 404.
- TMH (Technical Methods for Highways). (1986). *Standard Methods for Road Construction Materials. Technical Methods for Highways*, **2**. Pretoria: National Transport Commission. Committee of State Road Authorities.
- Viviers, K. (2006). *Geotechnical Investigation Report for Plot 9205, Village 2, Victoria Country Club Estate*, Ref no:16-1230/27. Terratest, Pietermaritzburg.
- Viviers, K. (2007a). *Geotechnical Investigation Report for Plot 9325, Village 3, Victoria Country Club Estate*, Ref no:16-1230/36. Terratest, Pietermaritzburg.
- Viviers, K. (2007b). *Geotechnical Investigation Report for Plot 9291, Village 4, Victoria Country Club Estate*, Ref no:16-1230/31. Terratest, Pietermaritzburg.
- Viviers, K. (2007c). *Geotechnical Investigation Report for Plot 9577, Village 5, Victoria Country Club Estate*, Ref no:16-1230/30. Terratest, Pietermaritzburg.
- Viviers, K. (2008a). *Geotechnical Investigation Report for Plot 9205, Village 2, Victoria Country Club Estate*, Ref no:16-1230/54. Terratest, Pietermaritzburg.

- Viviers, K. (2008b). *Geotechnical Investigation Report for Plot 9855, Village 3, Victoria Country Club Estate*, Ref no:16-1230/9855. Terratest, Pietermaritzburg.
- Viviers, K. (2009). *Geotechnical Investigation Report for Plot 9374, Village 2, Victoria Country Club Estate*, Ref no:16-1230/63. Terratest, Pietermaritzburg.
- Viviers, K. (2011). *Geotechnical Investigation Report for Plot 9382, Village 3, Victoria Country Club Estate*, Ref no:4000006/80. Terratest, Pietermaritzburg.
- Vukea, N. (2013). *Geotechnical Investigation Report for Plot 9983, Village 4, Victoria Country Club Estate*, Ref no:400006/9983. Terratest, Pietermaritzburg.
- Watkeys, M.K. (2006). Gondwana Break-up: A South African Perspective, South Africa. In: Johnson, M.R., Anhaeusser, C.R., and Thomas, R.J. (Eds.), *The Geology of South Africa*, Geological Society of South Africa, Johannesburg/ Council for Geoscience, pp 531-539.
- Weinert, H.H. (1980). *The natural road construction materials of Southern Africa*. National Institute for Transport and Road Research: Pretoria.

APPENDICES

SOIL SAMPLING

Undisturbed sampling and *in-situ* density determination

An undisturbed block was retrieved from the subsoil for triaxial testing and for the determination of *in-situ* density. Two soil blocks (30cm x 30cm x 30cm), were prepared.

Apparatus

- Candle wax and matches
- Gas burner
- Soil lathe
- Brush
- Steel pot
- Cling wrap
- Aluminium foil
- Two metal cylinders of known dimensions

Methodology

Procedure *in-situ* density

- Push the metal cylinder into the undisturbed block, until the cylinder is fully embedded.
- Carefully cut the soil away from the metal cylinder using a soil lathe, so the cylinder can be removed.
- The metal cylinder containing the soil, is then wrapped in cling wrap for the determination of moisture content and *in-situ* density

Procedure undisturbed sampling

- Melt pieces of wax candle in a steel pot using a gas burner.
- The molten wax is applied to all walls of the soil block until evenly coated.
- A soil lathe is used to cut the waxed block from the *in-situ* bottom soil, until a clean removal by hand is possible.
- The newly exposed underside should be levelled, prior to the application of molten wax.
- After the wax has cooled to a hard coating, the orientation of the sample should be annotated on the block walls.
- The block is then wrapped in cling wrap and foil.

GEOTECHNICAL EQUATIONS

Moisture Content (%) $w = \left(\frac{m_2 - m_3}{m_3 - m_1} \right) 100\%$

Where; m_1 = mass of container, m_2 = mass of wet soil + container, m_3 = mass of dry soil + container

Bulk Density (g/cm³) $\rho_b = \frac{\text{mass}(g)}{(\text{length})(\text{breadth})(\text{height})(\text{mm})} = \frac{(1000)m}{(l)(b)(h)(\text{mm})}$

Dry density (g/cm³) $\rho_d = \frac{100\rho_b}{100+w}$

Specific Gravity (G_s) $G_s = \frac{\rho_s}{\rho_w}$

Where; ρ_s is the density of solid particle is assumed to be 2.65, ρ_w is the density of water 1g/cm³

Void ratio (e) $e = \frac{\rho_s - \rho_d}{\rho_d}$

Degree of saturation (S_r) $S_r = \frac{w \cdot G_s}{e}$

Bulk unit weight (γ_b) $\gamma_b = \frac{G_s + S_r \cdot e}{e + 1} \cdot \gamma_w$

Where; γ_w is the unit weight of water 9.81 kN/m³

Saturated unit weight (γ_{sat}) $\gamma_{sat} = \frac{G_s + e}{e + 1} \cdot \gamma_w$

Dry unit weight (γ_d) $\gamma_d = \frac{G_s}{e + 1} \cdot \gamma_w = \frac{\gamma}{1 + w}$

Effective unit weight (γ') $\gamma' = \gamma_{sat} - \gamma_w = \frac{G_s - 1}{e + 1} \cdot \gamma_w$

TRIAXIAL TESTING

Triaxial Testing – BS 1377: Part 8:1990

Apparatus

- Undisturbed specimen prepared according to BS 1377: Part 1: 1990
- Triaxial cell
- Loading piston
- Cylindrical cell body
- Cell base of corrosion-resistant rigid material
- Specimen top cap of light weight impermeable corrosion-resistant material
- On-off valves
- Tubular material
- 4No. rubber o-rings
- Membrane stretcher
- O-ring stretcher
- Rigid porous discs
- Side drains

Pressure systems and ancillary apparatus

- Cell pressure system and a back pressure system
- Calibrated pressure gauge
- Calibrated pore water pressure measuring device
- Glass burette
- Timing device
- Compression test apparatus
- Machine capable of applying axial deformation with calibrated displacement transducer
- Calibrated force-measuring device

Saturation

Requirements

- Water applied from the back-pressure must be de-aerated.
- Magnitude of cell pressure increments must not exceed 50 kPa or the consolidation pressure during compression.
- The difference between the cell pressure and back pressure shall not be greater than the desired effective test pressure or 20 kPa whichever is less.

Procedure

- Ensure that the back pressure valve is closed and then apply the first increment of cell pressure, allow pore water pressures to reach equilibrium.
- Increase the cell pressure by 50 kPa and then allow the pore water pressure to steady before recording the value.
- Calculate the change in pore water pressure (Δu) resulting from the increase in cell pressure, calculate the value of the pore pressure coefficient B by the following equation:

$$B = \frac{\Delta u}{50}$$

- If $B \geq 0.95$, the specimen is considered saturated and consolidation can commence.

Consolidation

Procedure

- Increase the confining pressure (σ_3) and adjust the back pressure as required, to give a difference equal to the required effective consolidation pressure ($\sigma_3' = \sigma_3 - u$).
- Allow the pore water pressure to steady before recording the value.
- Record the reading of the volume-change indicator at time zero, start the consolidation process by opening the back pressure valve.
- Record readings of the volume-change indicator at suitable time intervals, readings may be taken at other time intervals as long as the square-root time/compression curve can be plotted.
- Allow consolidation to continue until there is no significant volume change and at least 95% of the excess pore pressures have been dissipated.
- When consolidation is complete, the volume-change indicator and pore pressure readings are recorded and the total volume change is calculated (ΔV_c) during consolidation.

Calculation and Plotting

- Calculate the dimension of the specimen after consolidation using the following equations:

$$\text{Volume:} \quad V_c = V_0 - \Delta V_c$$

$$\text{Area:} \quad A_c = A_0 \left[1 - \frac{2 \Delta V_c}{3 V_0} \right]$$

$$\text{Length:} \quad L_c = L_0 \left[1 - \frac{1 \Delta V_c}{3 V_0} \right]$$

Where; V_c (cm^3) is the consolidated volume, V_0 (cm^3) is the original specimen volume, ΔV_c (cm^3) is the change in volume as a result of water draining out, A_c (mm^2) is the consolidated area of cross-section, A_0 (mm^2) is the original area of cross-section, L_c (mm) is the consolidated length, L_0 (mm) is the original specimen length.

- The measured volume change is plotted against the square-root time
- A line is drawn which best fits the early portion of the graph, after which a horizontal line is drawn through the final point on the graph. The point where these lines intersect is read off and the value of square-root time, denoted by $\sqrt{t_{100}}$, and calculate the time intercept of this point t_{100} .
- The significant testing time in the compression test is calculated from equation:

$$t_r = F t_{100}$$

Where; $F = 1.8$ based on 95% dissipation of excess pore pressure induced by shear

- The rate of axial displacement to be applied to the specimen is calculated from equation:

$$d_r = \frac{\epsilon_f \times L_0}{t_f}$$

Where; ϵ_f is the estimated significant strain interval (assumed to be 20%), L_c (mm) is the consolidated length and t_f (min) is the significant testing time.

Compression

Requirements

- The triaxial cell should be seated on the compression machine, with the loading piston brought within a short distance of the specimen top cap.
- The compression machine should be set to but not exceeding the axial displacement rate.
- The axial deformation gauge should be adjusted so it can measure deformation of at least 25% of the specimen length thereafter zeroed.

- Ensure the back pressure valve is closed and the cell pressure valve and valve to the pore pressure measuring device are open.
- Record initial readings for the compression stage (deformation gauge, proving ring, pore pressure, cell pressure, time).
- The soil specimens were consolidated under confining pressures of 100 kPa, 200 kPa and 300 kPa.

Procedure

- Apply compression to the specimen and start the timer.
- Record sets of readings for the deformation gauge, force device and pore pressure at intervals during the test.
- The deviator stress ($\sigma_1 - \sigma_3$) is plotted against axial strain and the pore pressure is plotted against axial strain.
- Continue the test until one of the following occurs: maximum deviator stress; maximum effective principal stress ratio; constant shear stress and constant pore pressure.
- At the end of the test stop the compression, close the pore pressure valve and then systematically dismantle the triaxial machine.

Calculations

- For each set of readings the axial strain (ϵ) is calculated by:

$$\epsilon = \frac{\Delta L}{L_c}$$

Where; L_c (mm) is the consolidated length, ΔL_o (mm) is the change in length during compression as per the deformation gauge.

- Area (mm^2) of cross-section of the specimen is given by:

$$A = \frac{A_c}{1-\epsilon}$$

Where; A_c is the initial area of the specimen normal to the axis at the start of compression.

- Applied axial stress ($\sigma_1 - \sigma_3$) in kPa is given by:

$$(\sigma_1 - \sigma_3) = \frac{(R-R_0)C_r}{A} 1000$$

Where; R = proving ring reading, R_0 = initial proving ring reading, C_r = calibration factor

- A membrane correction factor and a drain correction factor should be factored to the deviator stress, the corrected deviator stress is given by equation:

$$(\sigma_1 - \sigma_3) = (\sigma_1 - \sigma_3)_m - \sigma_{mb} - \sigma_{dr}$$

While the major principal stress is given by equation:

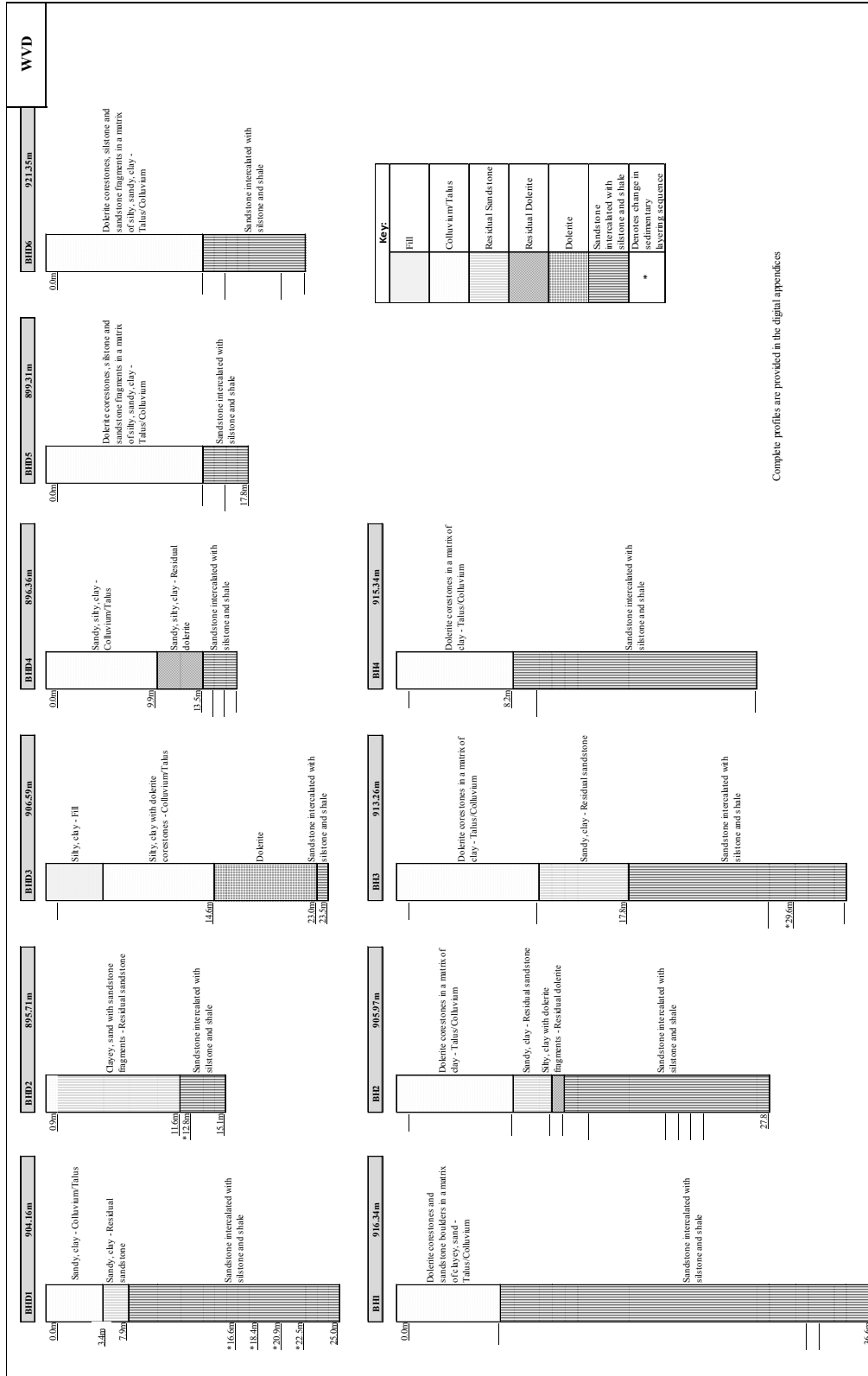
$$\sigma_1 = (\sigma_1 - \sigma_3) + \sigma_3$$

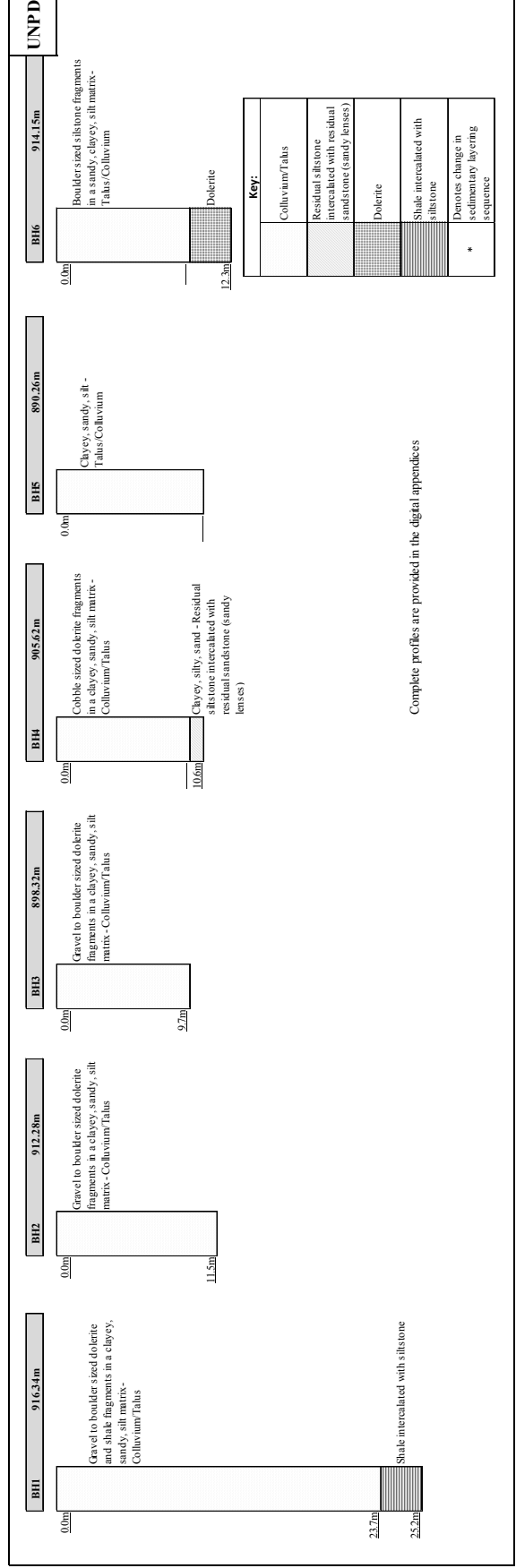
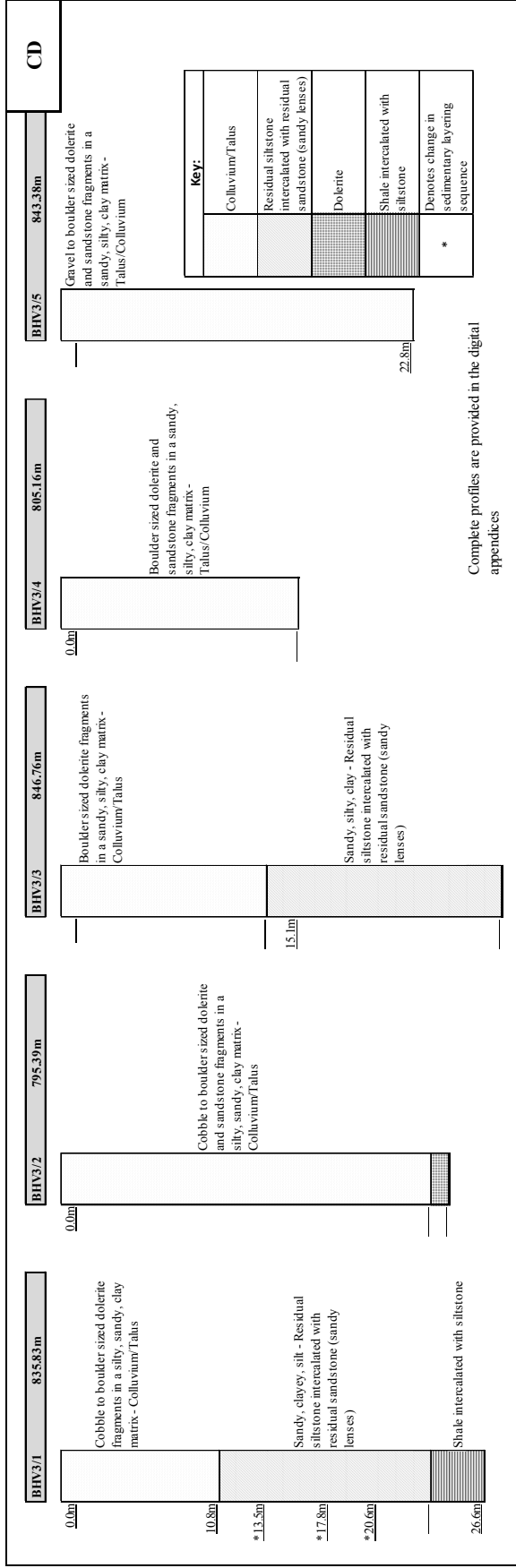
Where; σ_{mb} = membrane correction factor, σ_{dr} = side drain correction factor, σ_3 = cell confining pressure.

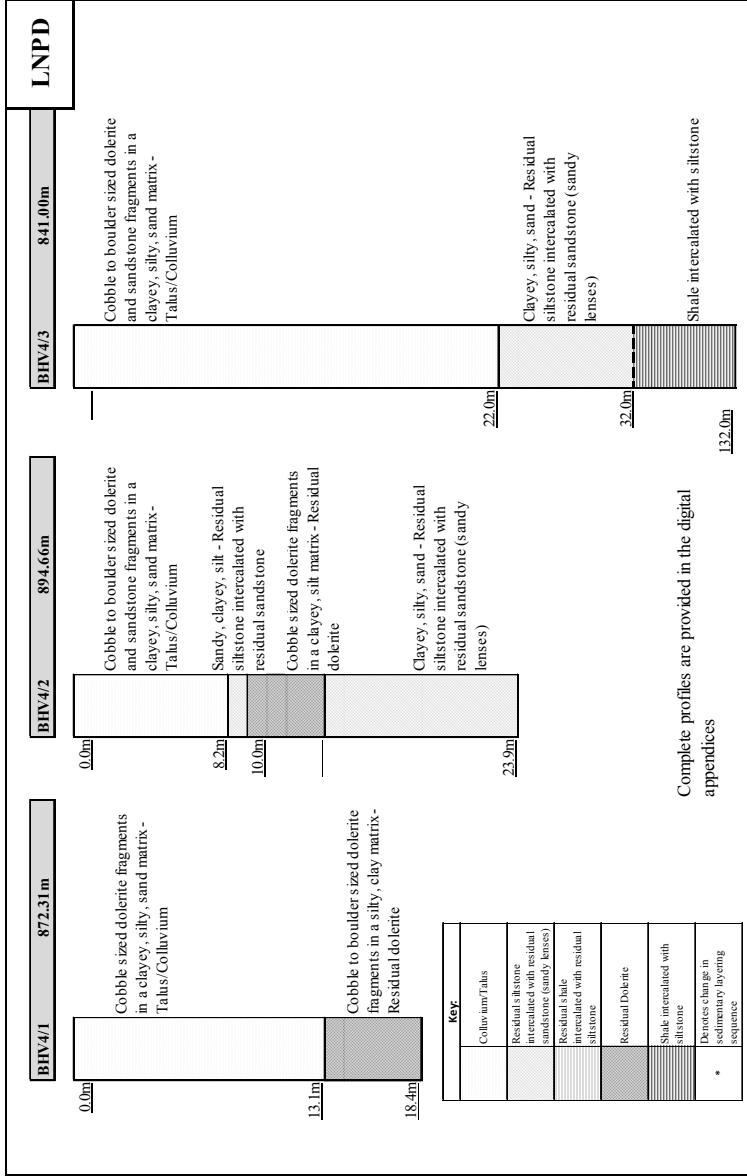
EFFECTIVE SHEAR STRENGTH PARAMETER DATA SETS

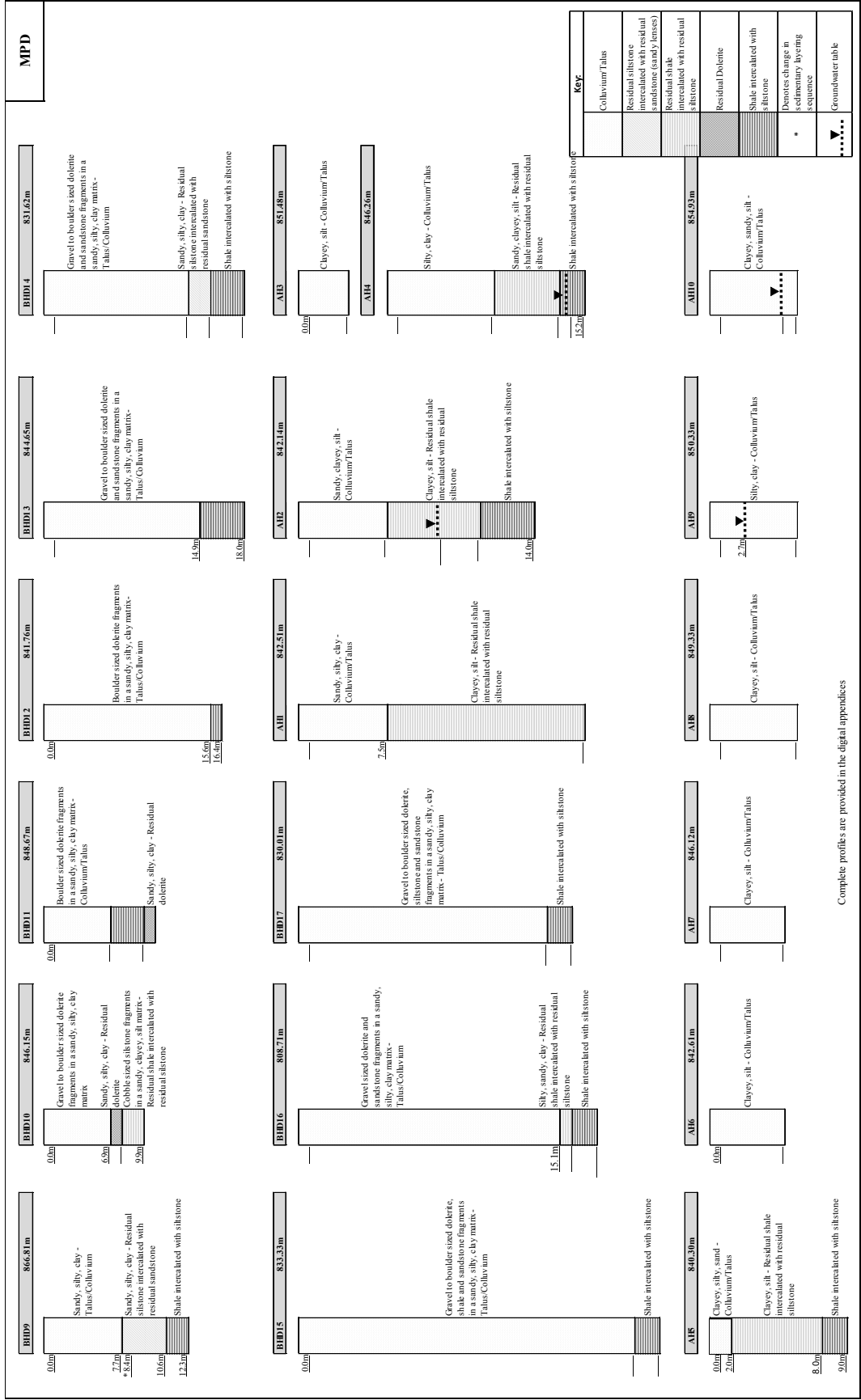
$x = 38$					
c'	ϕ'	<i>Source</i>	c'	ϕ'	<i>Source</i>
0	27	Carter and Bentley (1991)	0	30	LNPD
0	28	Carter and Bentley (1991)	0	22	Hadlow (2004)
0	29	Carter and Bentley (1991)	0	29	Hadlow (2004)
0	30	Carter and Bentley (1991)	8	28	Kujawa (2005)
0	31	Carter and Bentley (1991)	10	28	Kujawa (2005)
0	32	Carter and Bentley (1991)	0	24	Allen (1981)
0	28	Carter and Bentley (1991)	0	25	Allen (1981)
0	28	Carter and Bentley (1991)	0	26	Allen (1981)
0	28	Carter and Bentley (1991)	0	27	Allen (1981)
0	28	Carter and Bentley (1991)	0	28	Allen (1981)
0	28	Carter and Bentley (1991)	0	29	Allen (1981)
0	28	Carter and Bentley (1991)	0	30	Allen (1981)
0	31	Carter and Bentley (1991)	0	31	Allen (1981)
0	25	Carter and Bentley (1991)	0	32	Allen (1981)
0	28	Carter and Bentley (1991)			
0	24	Duncan and Wright (2005)			
0	25	Duncan and Wright (2005)			
0	26	Duncan and Wright (2005)			
0	27	Duncan and Wright (2005)			
0	28	Duncan and Wright (2005)			
0	29	Duncan and Wright (2005)			
0	30	Duncan and Wright (2005)			
0	31	Duncan and Wright (2005)			
0	32	Duncan and Wright (2005)			

ABBREVIATED BOREHOLE AND AUGER HOLES
COMPLETE TRIAL PIT LOGS









Complete profiles are provided in the digital appendices

KEY

[Pattern]	Colluvium/Talus
[Pattern]	Residual silstone intercalated with residual sandstone (sandy lenses)
[Pattern]	Residual shale intercalated with residual silstone
[Pattern]	Residual Dolerite
[Pattern]	Shale intercalated with silstone
[Pattern]	Denotes change in sedimentary layering sequence
[Pattern]	Groundwater table

Scale: 1:1000

0.00

1.00

3.60

Slightly moist, reddish dark brown, soft to firm, matrix supported, fine gravely fragments in a fine to coarse grained SANDY, CLAYEY, SILT matrix. COLLUVIUM

Slightly moist, dark reddish-brown, soft to firm, matrix supported, completely weathered dolerite boulders, with residual sandstone rock fragments in a fine grained SANDY, CLAYEY, SILT matrix. Dolerite boulders were noted to make 2% by volume of the matrix. Talus.

Slightly moist, dark reddish-brown, soft to firm, intact, completely weathered dolerite boulders, with residual sandstone rock fragments in a fine grained SANDY, CLAYEY, SILT matrix. Dolerite boulders were noted to make 2% by volume of the matrix. Talus.

NOTES

- 1) E.O.H at 3.60m- no refusal.
- 2) No groundwater seepage encountered.
- 3) SAMPLE taken: 1.00--3.00m.
- 4) No sidewall collapse.

CONTRACTOR :
MACHINE : VOLVO TLB
DRILLED BY : K. SINGH
PROFILED BY : K. SINGH
TYPE SET BY : K. SINGH
SETUP FILE : STANDARD.SET

INCLINATION :
DIAM :
DATE : 2013 to 2015
DATE : 30/06/2016 20:16
TEXT : ..ices\ANNEX\ICD\CDTPs.txt

ELEVATION :
X-COORD : 29d3401.8"S
Y-COORD : 30d2011.7"E
HOLE No: CD1

Scale: 1:1000

0.00

0.80

3.30

Slightly moist, dark orangey-brown, loose, fissured, SILTY, fine grained SAND. Colluvium.

Slightly moist, dark pinkish-reddish brown, medium dense, matrix supported, sparse dolerite boulders with residual sandstone rock fragments in a silty, CLAYEY, fine to medium SAND matrix. Boulders were noted to make 2% by volume of the matrix. Talus.

Slightly moist, dark pinkish-reddish brown, medium dense, matrix supported, sparse dolerite boulders with residual sandstone rock fragments in a silty, CLAYEY, fine to medium SAND matrix. Boulders were noted to make 2% by volume of the matrix. Talus.

NOTES

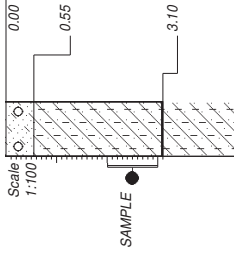
- 1) E.O.H at 3.30m - no refusal.
- 2) No groundwater seepage encountered.
- 3) SAMPLE taken: 1.00--3.30m.
- 4) No sidewall collapse.

CONTRACTOR :
MACHINE : VOLVO TLB
DRILLED BY : K. SINGH
PROFILED BY : K. SINGH
TYPE SET BY : K. SINGH
SETUP FILE : STANDARD.SET

INCLINATION :
DIAM :
DATE : 2013 to 2015
DATE : 30/06/2016 20:16
TEXT : ..ices\ANNEX\ICD\CDTPs.txt

ELEVATION :
X-COORD : 29d3402.6"S
Y-COORD : 30d2011.3"E
HOLE No: CD2

Scale : 1:100



NOTES

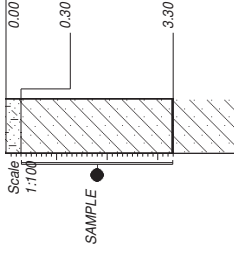
- 1) E.O.H at 3.10m - no refusal.
- 2) No groundwater seepage encountered.
- 3) SAMPLE taken: 2.00--3.00m.
- 4) No sidewall collapse.

CONTRACTOR :
MACHINE : VOLVO TLB
DRILLED BY : K. SINGH
PROFILED BY : K. SINGH
TYPE SET BY : K. SINGH
SETUP FILE : STANDARD.SET

INCLINATION :
DIAM :
DATE : 2013 to 2015
DATE : 30/06/2016 20:16
TEXT : ..ces\ANNEX\ICD\CDTPs.txt

ELEVATION :
X-COORD : 29d33°58.08"S
Y-COORD : 30d20°0.94"E

Scale : 1:100



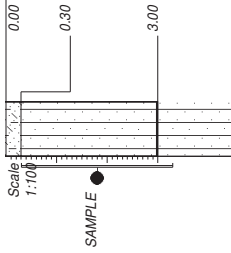
NOTES

- 1) E.O.H at 3.30m - no refusal.
- 2) No groundwater seepage encountered.
- 3) SAMPLE taken: 0.30--3.30m.
- 4) No sidewall collapse.

CONTRACTOR :
MACHINE : VOLVO TLB
DRILLED BY : K. SINGH
PROFILED BY : K. SINGH
TYPE SET BY : K. SINGH
SETUP FILE : STANDARD.SET

INCLINATION :
DIAM :
DATE : 2013 to 2015
DATE : 30/06/2016 20:16
TEXT : ..ces\ANNEX\ICD\CDTPs.txt

ELEVATION :
X-COORD : 29 34°06.9"S
Y-COORD : 30 20°06.3"E



Slightly moist, dark brown, loose, intact, clayey, silty SAND with rootlets. Colluvium.

Slightly moist, reddish orange-brown blotched yellow-brown, soft to firm, intact, sandy, SILT. Talus.

Slightly moist, reddish orange-brown blotched yellow-brown, soft to firm, intact, sandy, SILT. Talus.

NOTES

- 1) E.O.H at 3.00m - no refusal.
- 2) No groundwater seepage encountered.
- 3) SAMPLE taken: 0.30--3.30m.
- 4) No sidewall collapse.

CONTRACTOR :
MACHINE : VOLVO TLB
DRILLED BY : K. SINGH
PROFILED BY : K. SINGH
TYPE SET BY : K. SINGH
SETUP FILE : STANDARD.SET

INCLINATION :
DIAM :
DATE : 2013 to 2015
DATE : 30/06/2016 20:16
TEXT : ..ces\ANNEX\ICD\CDTPs.txt

ELEVATION :
X-COORD : 29 34'07.6" S
Y-COORD : 30 20'06.6" E

HOLE No: CD5

○ ○ ○	GRAVELLY	{SA03}
●●●●	SAND	{SA04}
●●●●	SANDY	{SA05}
	SILT	{SA06}
- - - - -	SILTY	{SA07}
/ / / / /	CLAY	{SA08}
- - - - -	CLAYEY	{SA09}
□	DISTURBED SAMPLE	{SA38}

Name ●

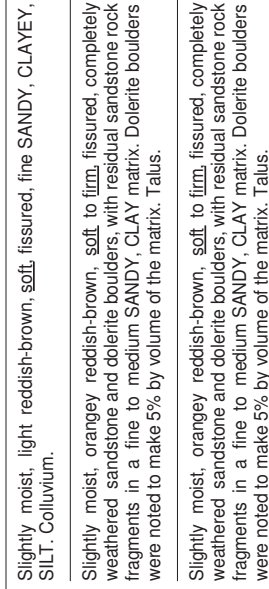
CONTRACTOR :
MACHINE :
DRILLED BY :
PROFILED BY :
TYPE SET BY : K. SINGH
SETUP FILE : STANDARD.SET

INCLINATION :
DIAM :
DATE :
DATE : 30/06/2016 20:16
TEXT : ..ces\ANNEX\ICD\CDTPs.txt

ELEVATION :
X-COORD :
Y-COORD :
Y-COORD :

LEGEND
SUMMARY OF SYMBOLS

Scale :
1:1000



NOTES

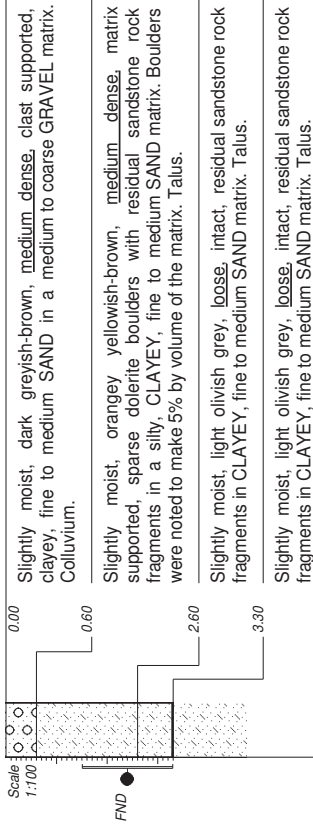
- 1) E.O.H at 3.10m- no refusal.
- 2) No groundwater seepage encountered.
- 3) No sidewall collapse.

CONTRACTOR :
MACHINE : VOLVO TLB
DRILLED BY : K.SINGH
TYPE SET BY : K.SINGH
SETUP FILE : STANDARD.SET

INCLINATION :
DIAM :
DATE : 20/04/2015
DATE : 30/06/2016 20:30
TEXT : ...ces\ANNEX\LNPD\LNPD1.txt

ELEVATION :
X-COORD : 29d33'58.7"S
Y-COORD : 30d19'24.3"E
HOLE No: LNPD1

Scale :
1:1000



NOTES

- 1) E.O.H at 3.30m- no refusal.
- 2) No groundwater seepage encountered.
- 3) SAMPLE taken: FND IND 1.50--3.30m.
- 4) No sidewall collapse.

CONTRACTOR :
MACHINE : VOLVO TLB
DRILLED BY : K.SINGH
TYPE SET BY : K.SINGH
SETUP FILE : STANDARD.SET

INCLINATION :
DIAM :
DATE : 20/04/2015
DATE : 30/06/2016 20:30
TEXT : ...ces\ANNEX\LNPD\LNPD1.txt

ELEVATION :
X-COORD : 29d34'00.7"S
Y-COORD : 30d19'24.0"E
HOLE No: LNPD2

Scale :
1:1000

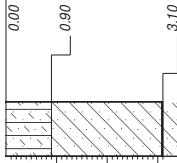
Slightly moist, light reddish brown, soft, fissured, fine SANDY, CLAYEY, SILT. Colluvium.

Slightly moist, orangey reddish-brown, soft to firm, fissured, completely weathered sandstone and dolerite boulders, with residual sandstone rock fragments in a fine to medium SANDY, CLAY matrix. Dolerite boulders were noted to make 5% by volume of the matrix. Talus.

Slightly moist, orangey reddish-brown, soft to firm, fissured, completely weathered sandstone and dolerite boulders, with residual sandstone rock fragments in a fine to medium SANDY, CLAY matrix. Dolerite boulders were noted to make 5% by volume of the matrix. Talus.

NOTES

- 1) E.O.H at 3.10m- no refusal.
- 2) No groundwater seepage encountered.
- 3) No sidewall collapse.



CONTRACTOR :
MACHINE : VOLVO TLB
DRILLED BY : K.SINGH
TYPE SET BY : K.SINGH
SETUP FILE : STANDARD.SET

INCLINATION :
DIAM :
DATE : 20/04/2015
DATE : 30/06/2016 20:30
TEXT : ..ces\ANNEX\LNPD\LNPD.txt

ELEVATION :
X-COORD : 29d33'58.7"S
Y-COORD : 30d19'24.3"E

Scale :
1:1000

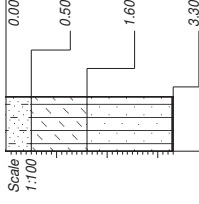
Slightly moist, dark brown, loose, intact, SILTY, fine SAND with roots. Colluvium.

Slightly moist, khaki brown, soft, intact, slightly sandy, CLAYEY, SILT with rock pieces of khaki stained black on joints. Talus.

Slightly moist, red brown, soft, intact, slightly clayey, fine grained SANDY, SILT. Talus.

NOTES

- 1) No ground water seepage.
- 2) No Refusal.



CONTRACTOR :
MACHINE : VOLVO TLB
DRILLED BY : K.SINGH
TYPE SET BY : K.SINGH
SETUP FILE : STANDARD.SET

INCLINATION :
DIAM :
DATE : 20/04/2015
DATE : 30/06/2016 20:30
TEXT : ..ces\ANNEX\LNPD\LNPD.txt

ELEVATION :
X-COORD :
Y-COORD :

Scale: 1:1000

**NOTES**

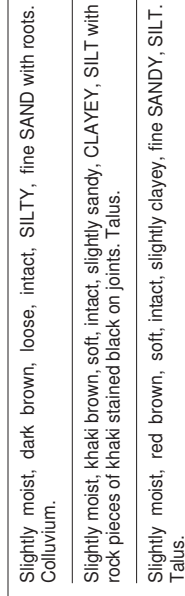
- 1) No ground water seepage.
- 2) No Refusal.

CONTRACTOR :
MACHINE : VOLVO TLB
DRILLED BY : K.SINGH
PROFILED BY : K.SINGH
TYPE SET BY : K.SINGH
SETUP FILE : STANDARD.SET

INCLINATION :
DIAM :
DATE : 20/04/2015
DATE : 30/06/2016 20:30
TEXT : ..ces\ANNEX\LNPD\LNPD.txt

ELEVATION :
X-COORD :
Y-COORD :

Scale: 1:1000

**NOTES**

- 1) No ground water seepage.
- 2) No Refusal.

CONTRACTOR :
MACHINE : VOLVO TLB
DRILLED BY : K.SINGH
PROFILED BY : K.SINGH
TYPE SET BY : K.SINGH
SETUP FILE : STANDARD.SET

INCLINATION :
DIAM :
DATE : 20/04/2015
DATE : 30/06/2016 20:30
TEXT : ..ces\ANNEX\LNPD\LNPD.txt

ELEVATION :
X-COORD :
Y-COORD :

JOB NUMBER: 000

	GRAVEL	{SA02}
	SAND	{SA04}
	SANDY	{SA05}
	SILT	{SA06}
	SILTY	{SA07}
	CLAY	{SA08}
	CLAYEY	{SA09}
	DISTURBED SAMPLE	{SA38}

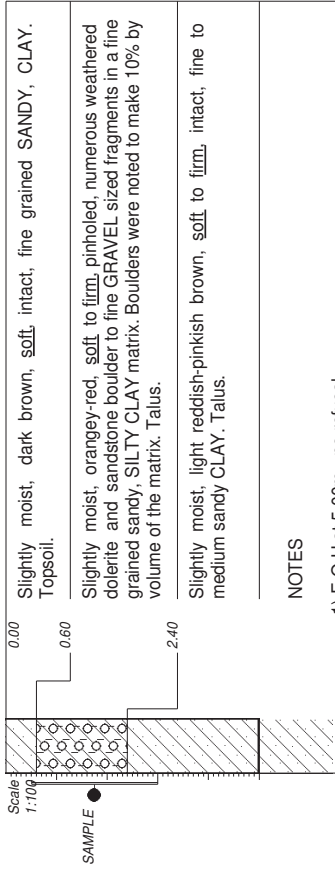
Name ●

CONTRACTOR :
 MACHINE :
 DRILLED BY :
 PROFILED BY :
 TYPE SET BY : K. SINGH
 SETUP FILE : STANDARD.SET

INCLINATION :
 DIAM :
 DATE :
 DATE : 30/06/2016 20:30
 TEXT : ..ces\ANNEX\LNPD\LNPD.txt

ELEVATION :
 X-COORD :
 Y-COORD :

LEGEND
SUMMARY OF SYMBOLS



NOTES

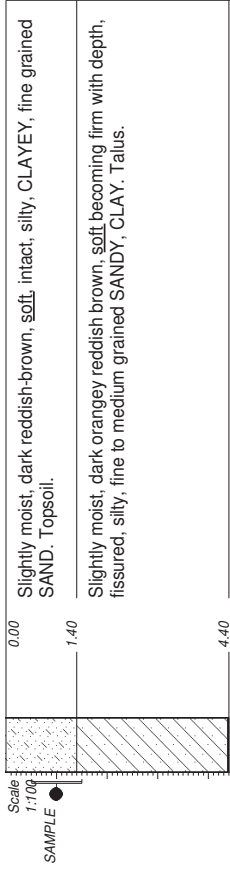
- 1) E.O.H at 5.00m - no refusal.
- 2) No groundwater seepage encountered.
- 3) SAMPLE taken: 0.5--3.00m.
- 4) No sidewall collapse.

CONTRACTOR :
MACHINE : Hyundai Rolex 305LC-71 21t Exc.
DRILLED BY : K.SINGH
PROFILED BY : K.SINGH
TYPE SET BY : K.SINGH
SETUP FILE : STANDARD.SET

INCLINATION :
DIAM :
DATE : 10/03/2015
DATE : 30/06/2016 20:38
TEXT : ..es\ANNEX\B\MPD\MPDTPFS.txt

ELEVATION :
X-COORD :
Y-COORD :

HOLE No: MPD1



NOTES

- 1) E.O.H at 4.40m- no refusal.
- 2) No groundwater seepage encountered.
- 3) SAMPLE taken 0.50--1.50m.
- 4) No sidewall collapse.

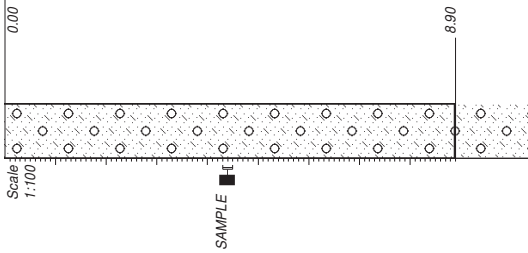
CONTRACTOR :
MACHINE : Hyundai Rolex 305LC-71 21t Exc.
DRILLED BY : K.SINGH
PROFILED BY : K.SINGH
TYPE SET BY : K.SINGH
SETUP FILE : STANDARD.SET

INCLINATION :
DIAM :
DATE : 10/03/2015
DATE : 30/06/2016 20:38
TEXT : ..es\ANNEX\B\MPD\MPDTPFS.txt

ELEVATION :
X-COORD : 29 34'24.71" S
Y-COORD : 30 20'03.12" E

HOLE No: MPD2

Slightly moist, reddish brown, medium dense, matrix supported, fine GRAVELLY to boulder sized fragments in a CLAYEY, fine to medium grained SAND matrix. Talus.



Slightly moist, reddish brown, medium dense, matrix supported, fine GRAVELLY to boulder sized fragments in a CLAYEY, fine to medium SAND matrix. Talus.

NOTES

- 1) Cutting Exposure.
- 2) No groundwater seepage encountered.
- 3) Undisturbed SAMPLE taken: 4.30--4.50m.
- 4) No sidewall collapse.

CONTRACTOR :
MACHINE : Hyundai Rolex 305LC-71 21t Exc.
DRILLED BY : K.SINGH
PROFILED BY : K.SINGH
TYPE SET BY : K.SINGH
SETUP FILE : STANDARD.SET

INCLINATION :
DIAM :
DATE : 10/03/2015
DATE : 30/06/2016 20:38
TEXT : ..es\ANNEX\B\MPD\MPDTPS.txt

ELEVATION :
X-COORD : 29 34'33.60"S
Y-COORD : 30 20'9.50"E

HOLE No: MPD3

	GRAVEL	{SA02}
	GRAVELLY	{SA03}
	SAND	{SA04}
	SANDY	{SA05}
	SILTY	{SA07}
	CLAY	{SA08}
	CLAYEY	{SA09}
	UNDISTURBED SAMPLE	{SA37}
	DISTURBED SAMPLE	{SA38}

Name

Name

CONTRACTOR :
MACHINE :
DRILLED BY :
PROFILED BY :
TYPE SET BY : K.SINGH
SETUP FILE : STANDARD.SET

INCLINATION :
DIAM :
DATE :
DATE : 30/06/2016 20:38
TEXT : ..es\ANNEX\B\MPD\MPDTPS.txt

ELEVATION :
X-COORD :
Y-COORD :

LEGEND
SUMMARY OF SYMBOLS

DIGITAL APPENDIX B1.1 TO B1.5

COMPLETE BOREHOLE AND AUGER HOLE LOGS

COMPACT DISC FORMAT

**DISC APPENDED
TO BACK COVER**

LABORATORY TESTING DATA

MOISTURE CONTENT AND DENSITY CALCULATIONS									
Point Sample No.	Depth (m)	Mass of wet soil + container (m ₂)	Mass of dry soil + container (m ₃)	Mass of container (m ₁)	Mass of moisture (m ₂ -m ₃)	Mass of dry soil (g)	Moisture content (%)	Bulk density (g/cm ³)	Dry density (g/cm ³)
LNPD3	1.00	1104.88	1058.23	499.14	46.65	599.09	8.34	1.23	1.14
MPD3	4.30	1345.64	1285.36	499.69	60.28	785.67	7.67	1.59	1.48

SIEVE, HYDROMETER ANALYSIS, ATTERBERG LIMITS TEST RESULTS															Test results obtained from Soilco. Laboratories Pietermaritzburg				
TRIAL PIT NUMBER:	DEPTH (m):	CD1	CD2	CD3	CD4	CD5	LNPDI	LNPDI	LNPDI	LNPDI	LNPDI	LNPDI	LNPDI	LNPDI	LNPDI	MPD1	MPD2	MPD3	
		1.00-3.00	1.00-3.00	2.00-3.00	0.30-3.30	0.30-3.00	1.0-3.0	0.15-3.30	0.90-1.10	1.60-3.30	0.50-1.40	0.50-1.50	0.50-1.50	0.50-1.50	0.50-1.50	0.50-1.50	0.50-1.50	0.50-1.50	0.50-1.50
	20.0mm			100															100
	14.0mm	100	100	99			100	100	100	100	100	100	100	100	100	100	100	100	97
	4.75mm	99	99	97	100		98	94	99	99	99	99	99	99	99	99	99	99	96
	2.00mm	91	93	83	94		91	85	93	85	86	93	85	85	93	98	98	85	85
	0.425mm	47	54	47	51		64	66	69	39	43	69	39	43	69	71	58	58	58
	0.075mm																		
	0.060mm	44	48	43	49		62	64	63	36	41	65	36	41	65	69	54	54	54
	0.050mm	40	45	40	47		58	62	60	34	38	63	34	38	63	67	51	51	51
	0.026mm	36	41	37	41		55	60	58	26	31	58	26	31	58	65	49	49	49
	0.015mm	33	37	35	38		53	56	54	20	24	56	20	24	56	63	48	48	48
	0.010mm	31	35	30	34		49	53	50	19	22	52	19	22	52	60	46	46	46
	0.0074mm	29	34	23	30		47	49	44	17	21	50	17	21	50	54	41	41	41
	0.002mm	27	32	20	28		45	44	39	15	19	48	15	19	48	48	37	37	37
	0.0036mm	22	30	17	26		43	38	34	15	17	43	15	17	43	42	34	34	34
	0.0020mm	20	28	15	25		40	36	31	14	16	41	14	16	41	40	31	31	31
	0.0015mm	18	26	13	24		38	35	29	12	14	39	12	14	39	38	28	28	28

SIEVE APERTURE (% PASSING)		HYDROMETER ANALYSIS		ATTERBERG LIMITS	
Liquid Limit (W _L) %	45	49	48	47	46
Plastic Limit (W _P) %	33	30	32	32	29
Plasticity Index (I _p) %	12	19	16	15	17
Linear Shrinkage (L _S) %	8	10	8.5	8	9
Equivalent PI %	10.9	17.7	13.3	14.1	14.4
Classification (Group Index)	A-7.5(3)	A-7.5(9)	A-7.5(4)	A-7.5(5)	A-7.6(9)

CONSOLIDATED UNDRAINED TRIAXIAL TEST

Results adapted from: THEKWINI SOILS LAB. CC

REF. NO. 8132

LAB. NO. 6070

Sigma 1 $\sigma_1 = (\sigma_1 - \sigma_3) + \sigma_3$

Effective sigma 1 $\sigma'_1 = \sigma_1 - u$

Effective sigma 3 $\sigma'_3 = \sigma_3 - u$

Position : MPD3

Depth : 4.30-4.50

100 kPa										200 kPa										300 kPa									
Inputs										Inputs										Inputs									
L (cm)	8.1	Lo(cm)	8	Moisture content before (%)	25.7	Moisture content after (%)	25.7	L (cm)	8.1	Lo(cm)	7.96	Moisture content before (%)	25	Moisture content after (%)	25.4	L (cm)	0	Lo(cm)	7.89	Moisture content before (%)	25.4								
Ao(cm ²)	11.52	117.5	66.83	158.8	58.8	2.18	33.9	Ao(cm ²)	11.95	219.7	145.5	309.9	109.9	2.10	32.7	Ao(cm ²)	10.87	203.2	44.94	101.6	1.68								
Vo(cm ³)	93.32	89.92	68.37	170.4	70.4	2.41	185.1	Vo(cm ³)	96.76	240.6	149.8	320.3	120.3	2.20	1780	Vo(cm ³)	85.63	309.9	136.99	455.0	2.03								
Proving Ring	2.8	69.85	172.3	72.3	2.45	11.81	147.3	Proving Ring	2.8	241.6	150.1	320.8	120.8	2.21	1424	Proving Ring	2.8	332.7	167.96	466.4	2.11								
Dry density (kg/m ³)	1473	70.5	173.4	73.4	2.47	11.81	1473	Dry density (kg/m ³)	1473	319.6	151.53	319.6	119.6	2.20	1424	Dry density (kg/m ³)	2.8	344.2	185.18	472.1	2.15								
Sigma 3 100										Sigma 3 200										Sigma 3 300									
Area at test	11.24	0	0	0	0	0	0	Area at test	11.53	0	0	0	0	0	0	Area at test	10.87	0	0	0	0								
% Strain	0.75	74.5	41.51	137.3	37.3	1.75	11.3	% Strain	0.64	146.8	91.82	273.4	73.4	1.73	10.94	% Strain	0.68	203.2	44.94	101.6									
Deviator Stress (Kpa)	11.52	2.4	117.5	66.83	158.8	58.8	2.18	Deviator Stress (Kpa)	219.7	219.7	145.5	309.9	109.9	2.10	11.01	Deviator Stress (Kpa)	295.7	203.2	44.94	101.6									
Pore Water Pressure (kPa)	0	0	0	0	0	0	0	Pore Water Pressure (kPa)	0	0	0	0	0	0	0	Pore Water Pressure (kPa)	0	0	0	0									
$[\sigma_1 - \sigma_3]/2$	5.76	1.2	58.76	79.4	79.4	29.4	1.09	$[\sigma_1 - \sigma_3]/2$	5.76	109.9	72.9	154.9	54.9	1.05	5.43	$[\sigma_1 - \sigma_3]/2$	147.85	101.6	22.47	50.8									
σ_1/σ_3	1.0	1.0	1.0	1.0	1.0	1.0	1.0	σ_1/σ_3	1.0	1.0	1.0	1.0	1.0	1.0	1.0	σ_1/σ_3	1.0	1.0	1.0	1.0									
11.51	3.22	140.8	68.37	170.4	70.4	2.41	185.1	11.78	2.12	219.7	145.5	309.9	109.9	2.10	32.7	11.01	1.31	295.7	44.94	101.6	1.68								
11.71	4.04	144.6	69.85	172.3	72.3	2.45	11.81	11.98	2.9	240.6	149.8	320.3	120.3	2.20	11.09	11.18	2.03	309.9	136.99	455.0	2.03								
11.81	4.85	146.8	70.5	173.4	73.4	2.47	11.81	11.98	3.71	241.6	150.1	320.8	120.8	2.21	11.18	11.18	2.83	332.7	167.96	466.4	2.11								
11.92	5.69	157.7	71.27	177.9	77.9	2.56	11.92	12.08	4.52	239.1	151.53	319.6	119.6	2.20	11.26	11.26	3.52	344.2	185.18	472.1	2.15								
12.02	6.49	153.4	71.54	176.7	76.7	2.53	12.02	12.29	6.12	242.3	152.95	321.2	121.2	2.21	11.37	11.37	4.38	342.5	194.38	471.3	2.14								
12.13	7.32	153.2	71.92	176.6	76.6	2.53	12.13	12.39	6.92	241	152.95	320.5	120.5	2.21	11.46	11.46	5.15	344.6	199.95	472.3	2.15								
12.24	8.14	153.1	72.19	176.6	76.6	2.53	12.24	12.5	7.73	244.1	153.01	323.1	123.1	2.22	11.55	11.55	5.93	361	203.2	480.5	2.20								
12.33	8.83	155.9	72.08	176.0	76.0	2.56	12.33	12.59	8.41	245.9	153.67	325.0	125.0	2.23	11.65	11.65	6.7	371.1	205.19	485.6	2.24								
12.44	9.63	153.7	72.14	176.9	76.9	2.54	12.44	12.7	9.18	246.8	152.73	323.4	123.4	2.23	11.75	11.75	7.49	369.3	206.71	485.6	2.24								
12.55	10.42	153.7	72.3	176.9	76.9	2.54	12.55	12.7	9.18	246.8	152.73	323.4	123.4	2.23	11.84	11.84	8.24	373	207.76	486.5	2.24								
12.67	11.24	153.7	72.3	176.9	76.9	2.54	12.67	12.93	10.8	247.6	152.44	323.9	123.9	2.24	11.94	11.94	8.99	370	208.27	485.0	2.23								
12.78	12.06	153.9	72.03	177.0	77.0	2.54	12.78	13.05	11.6	249.2	152.15	324.3	124.3	2.24	12.06	12.06	9.87	368.5	208.61	484.3	2.23								
12.9	12.86	153.6	72.3	176.8	76.8	2.54	12.9	13.17	12.4	247.8	151.87	323.9	123.9	2.24	12.18	12.18	10.73	366.9	209.16	483.5	2.22								
13.02	13.68	153.5	72.36	176.8	76.8	2.54	13.02	13.29	13.2	246.2	151.75	323.1	123.1	2.23	12.28	12.28	11.51	368.4	209.37	483.2	2.23								
13.14	14.48	153.5	72.19	176.8	76.8	2.54	13.14	13.41	13.99	238.6	151.47	319.3	119.3	2.19	12.39	12.39	12.28	367.7	209.41	483.9	2.23								
13.27	15.28	153.6	71.97	176.8	76.8	2.54	13.27	13.54	14.79	237.3	151.01	318.7	118.7	2.19	12.51	12.51	13.13	368.4	209.66	484.2	2.23								
13.4	16.09	153.2	72.14	176.6	76.6	2.53	13.4	13.66	15.58	236	150.67	318.0	118.0	2.18	12.61	12.61	13.79	363.8	209.75	481.9	2.21								
13.53	16.9	153.1	72.03	176.6	76.6	2.53	13.53	13.79	16.37	228.2	150.67	314.1	114.1	2.14	12.74	12.74	14.68	368.8	209.7	484.4	2.23								
13.66	17.71	152.9	71.92	176.5	76.5	2.53	13.66	13.93	17.17	224.4	150.67	312.2	112.2	2.12	12.86	12.86	15.47	367.8	209.58	483.9	2.23								
13.79	18.5	154.7	71.87	177.4	77.4	2.55	13.79	14.06	17.98	221	150.27	310.5	110.5	2.11	12.97	12.97	16.22	367	209.41	483.5	2.22								
13.93	19.32	154.4	71.76	177.2	77.2	2.54	13.93	14.2	18.8	215.2	150.21	307.6	107.6	2.08	13.11	13.11	17.93	365.4	208.86	482.7	2.22								
14.07	20.12	152	71.81	176.0	76.0	2.52	14.07	14.35	19.59	211.5	150.21	305.8	105.8	2.06	13.24	13.24	17.93	366	208.9	483.0	2.22								
								14.35	19.59	211.5	150.21	305.8	105.8	2.06	13.36	13.36	18.62	367.5	208.68	483.8	2.23								
															13.49	13.49	19.42	368.7	207.93	484.4	2.23								

APPENDIX B

APPENDIX B1

BOREHOLE, AUGER HOLE AND TRIAL PIT LOGS

APPENDIX B1.1: WORLDS VIEW DEVELOPMENT

APPENDIX B1.2: UPPER NATIONAL PARK DEVELOPMENT

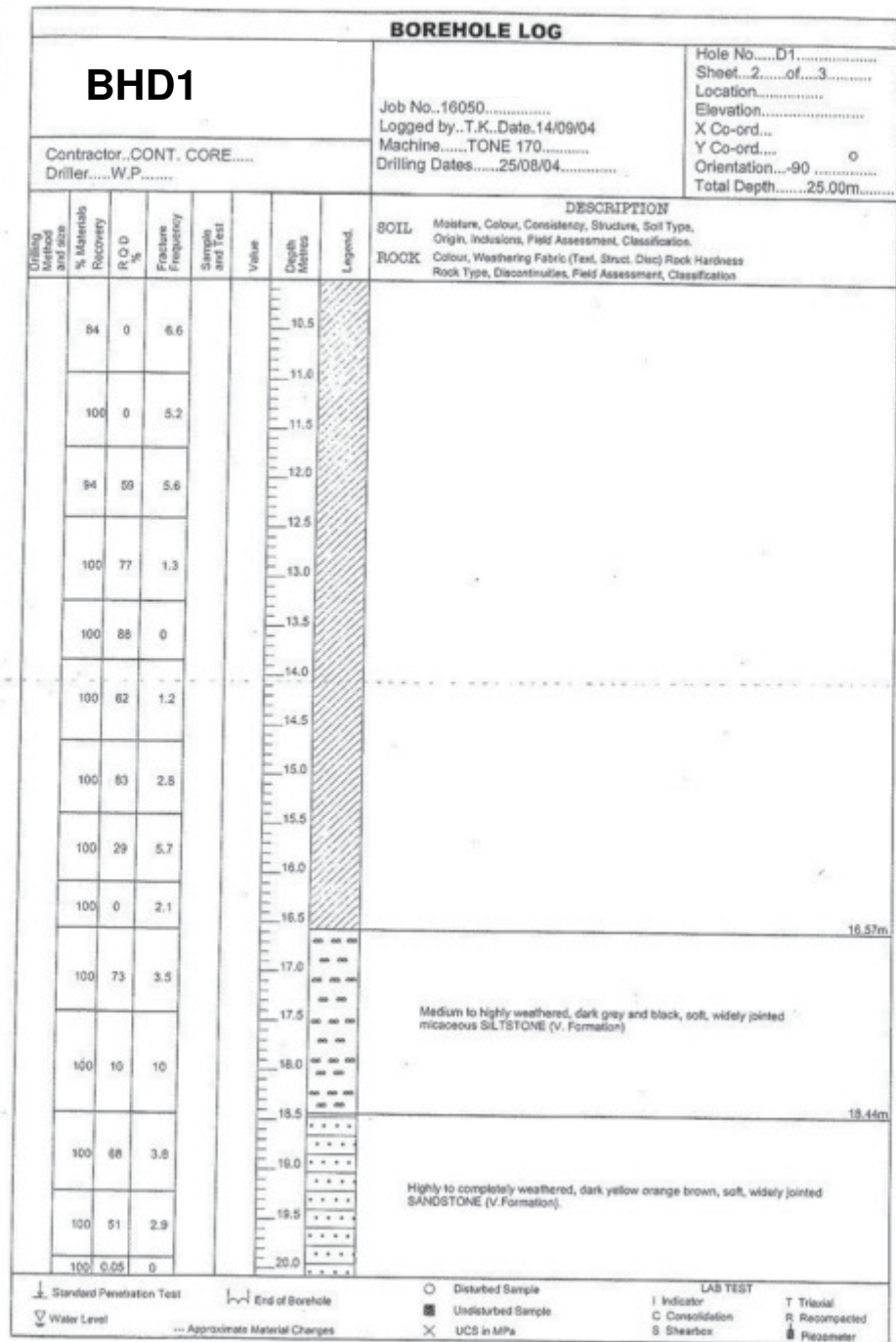
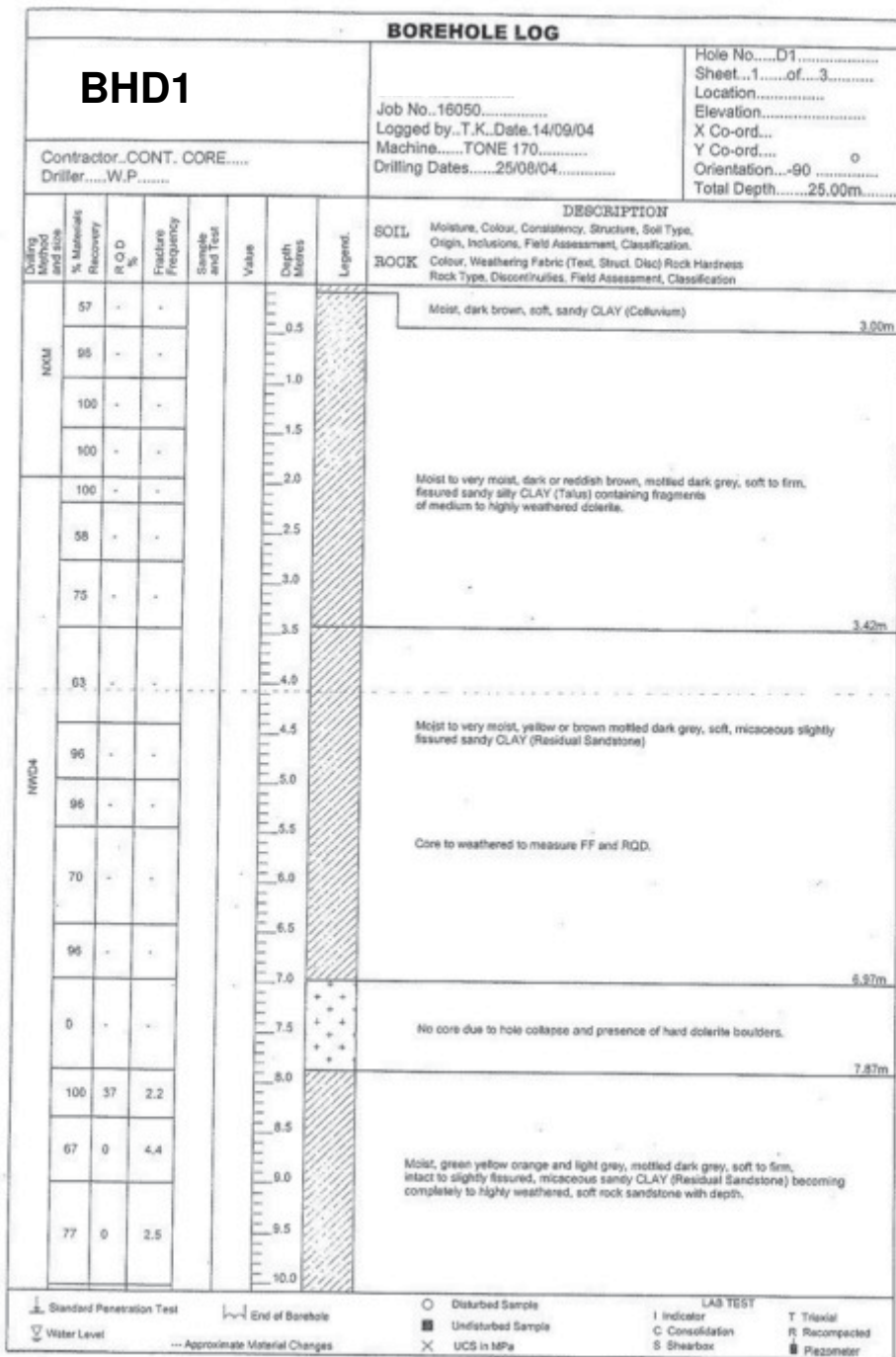
APPENDIX B1.3: CASCADES DEVELOPMENT

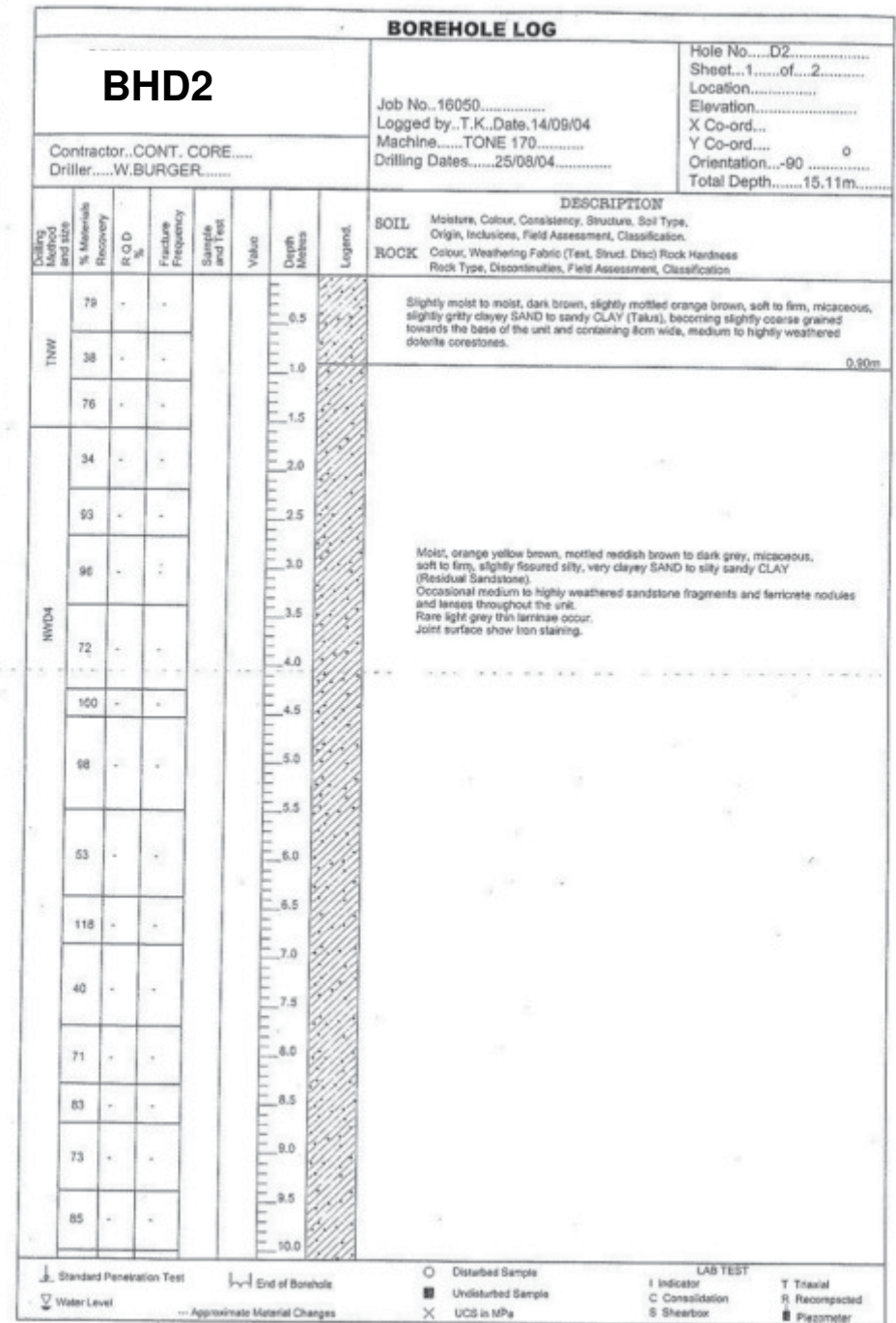
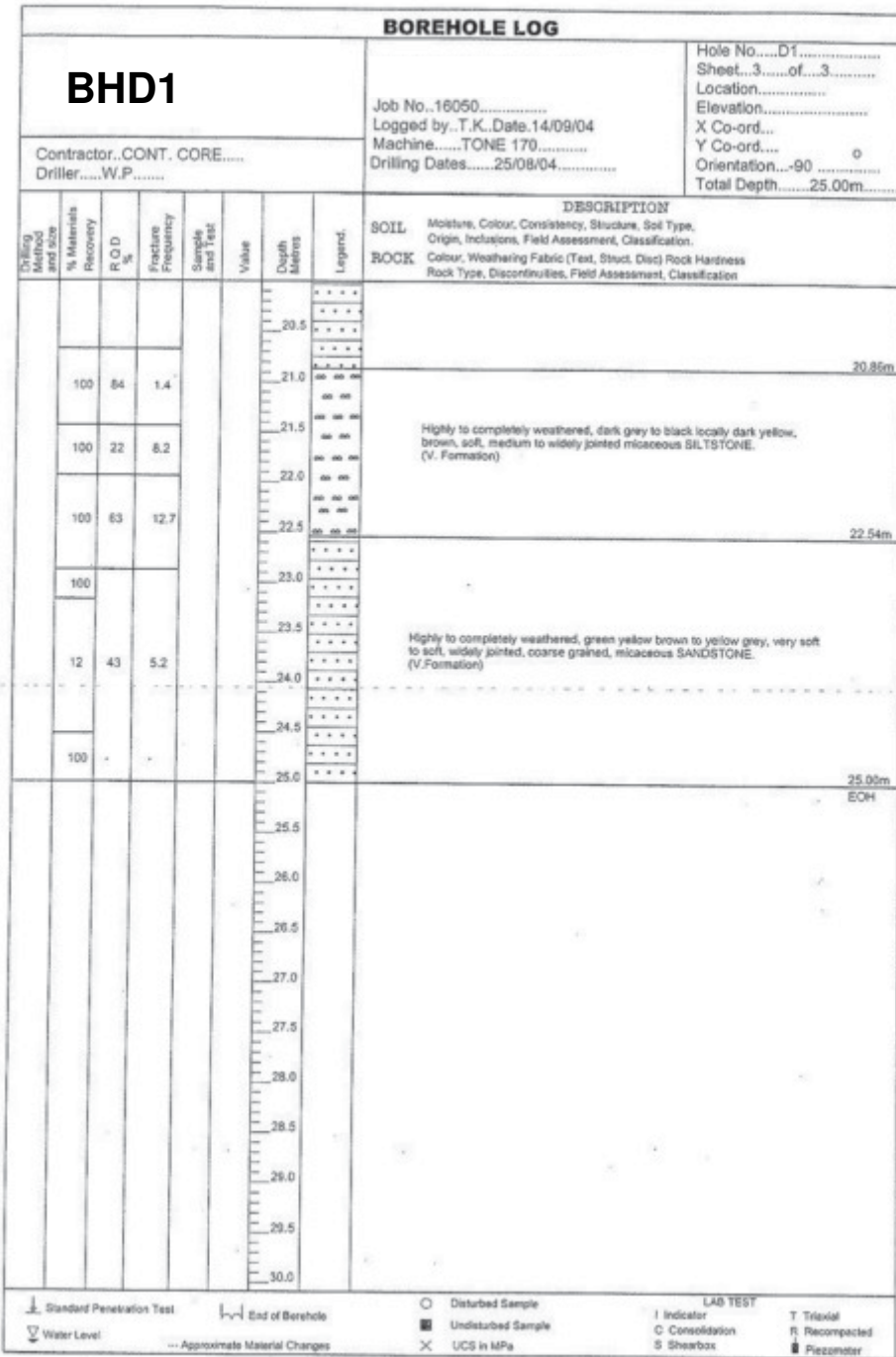
APPENDIX B1.4: LOWER NATIONAL PARK DEVELOPMENT

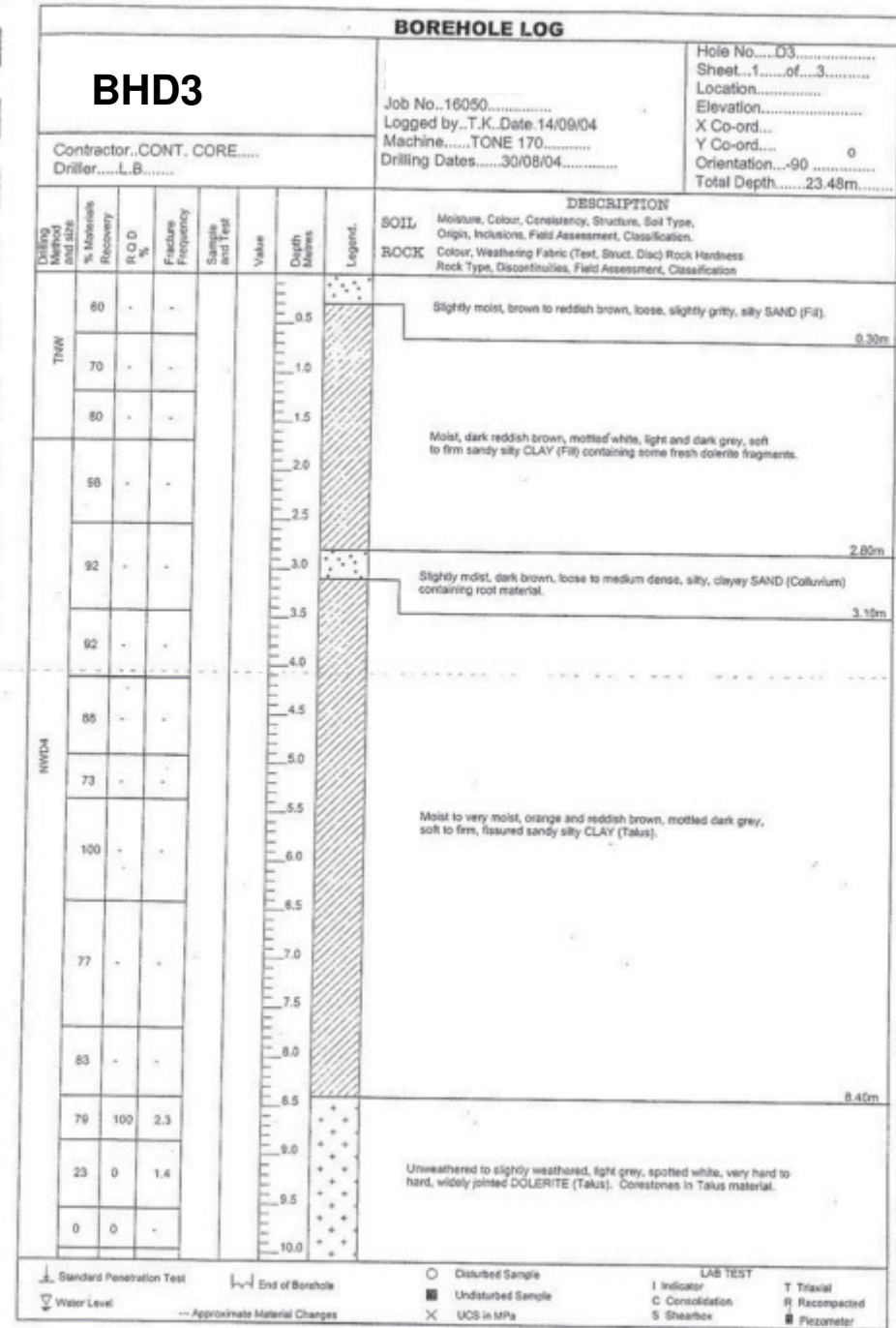
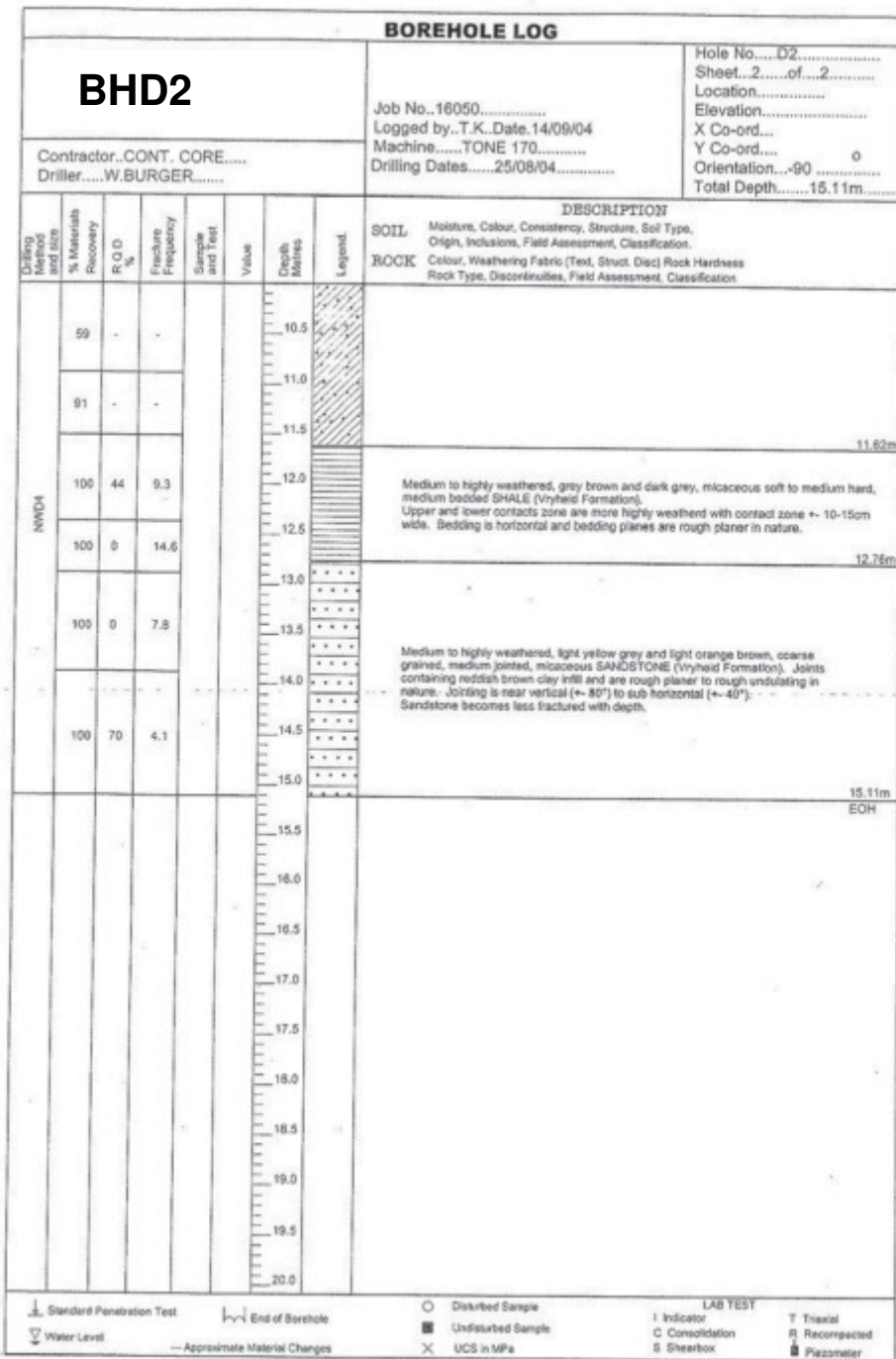
APPENDIX B1.5: MONTROSE PARK DEVELOPMENT

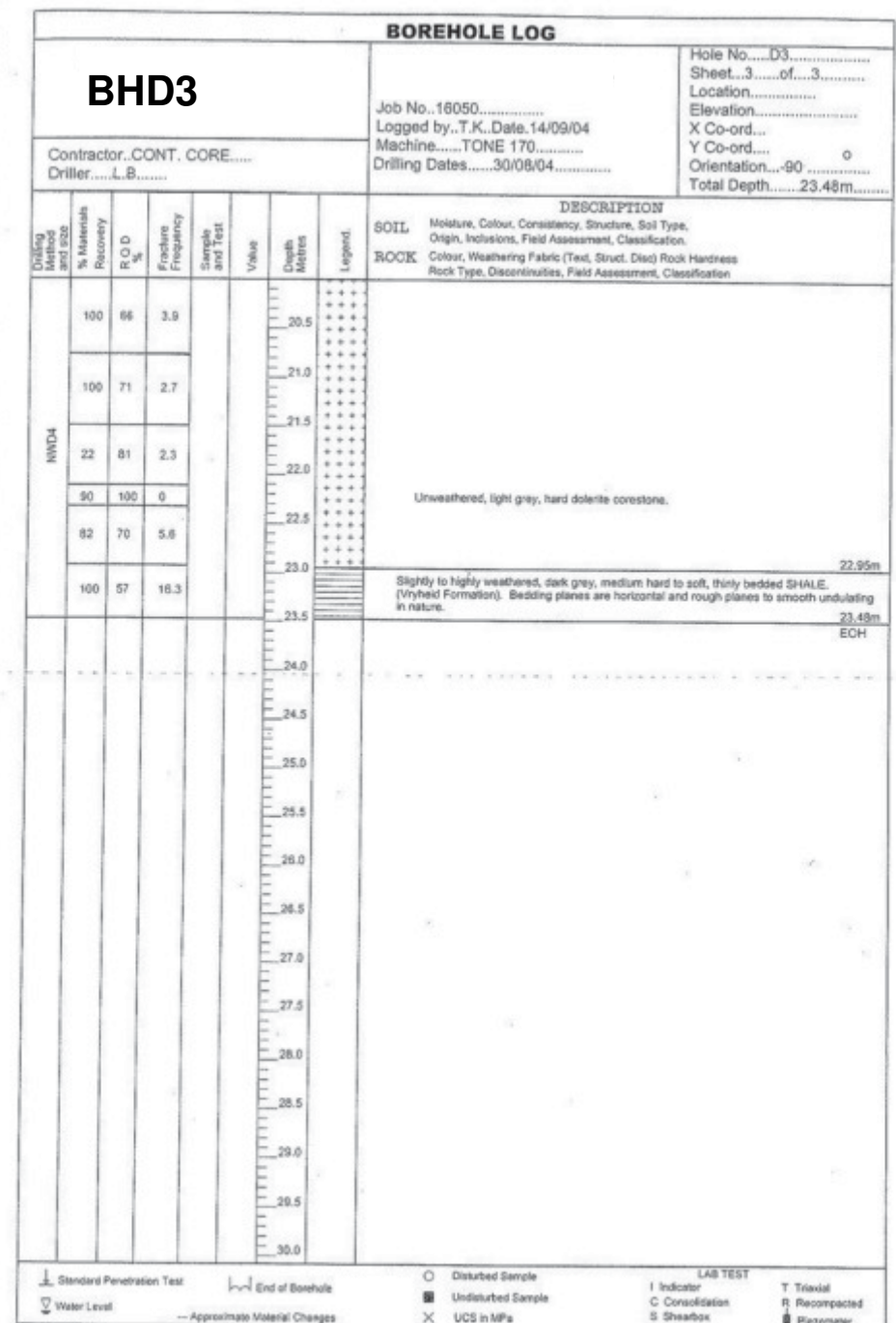
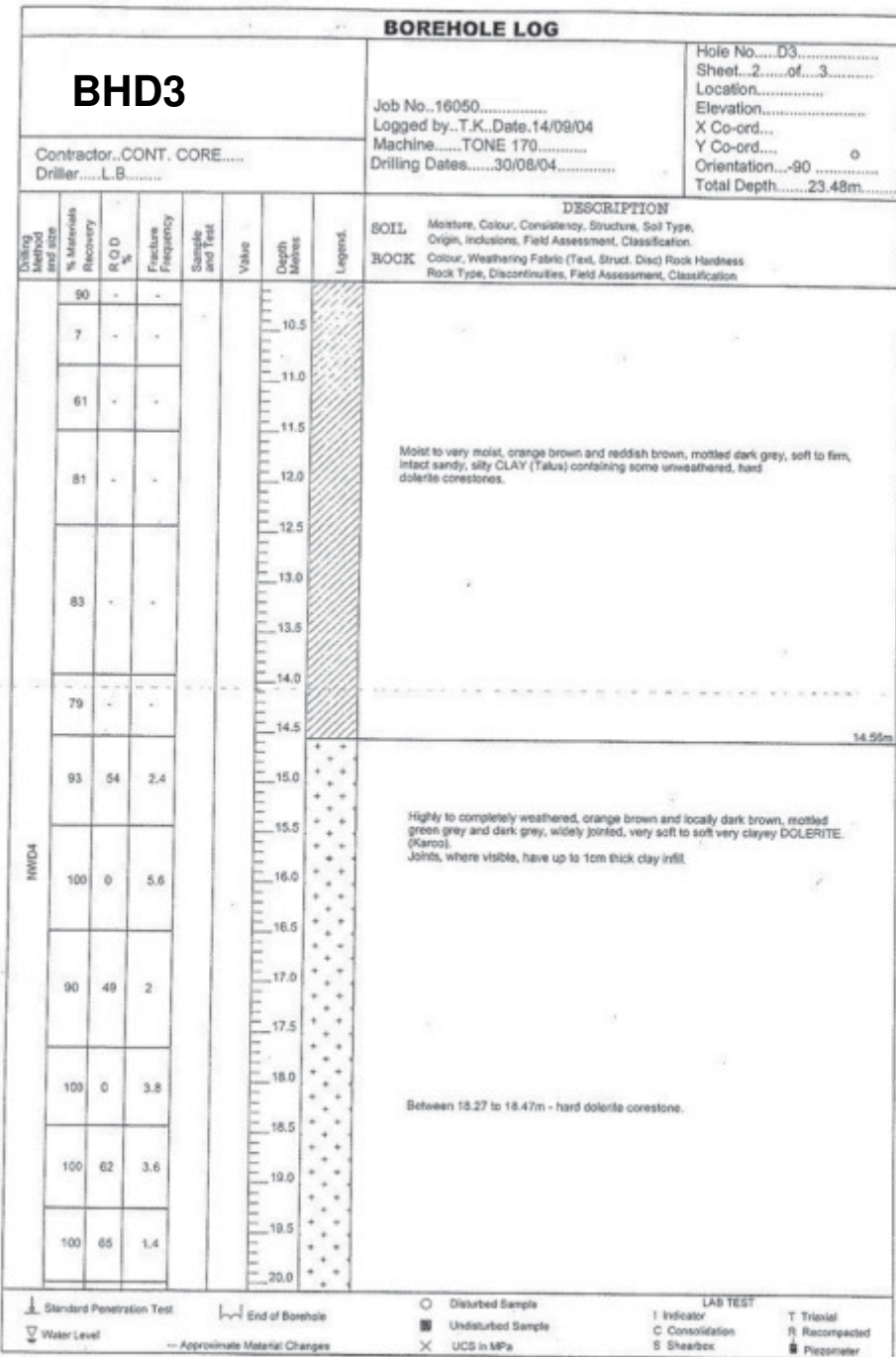
APPENDIX B1.1

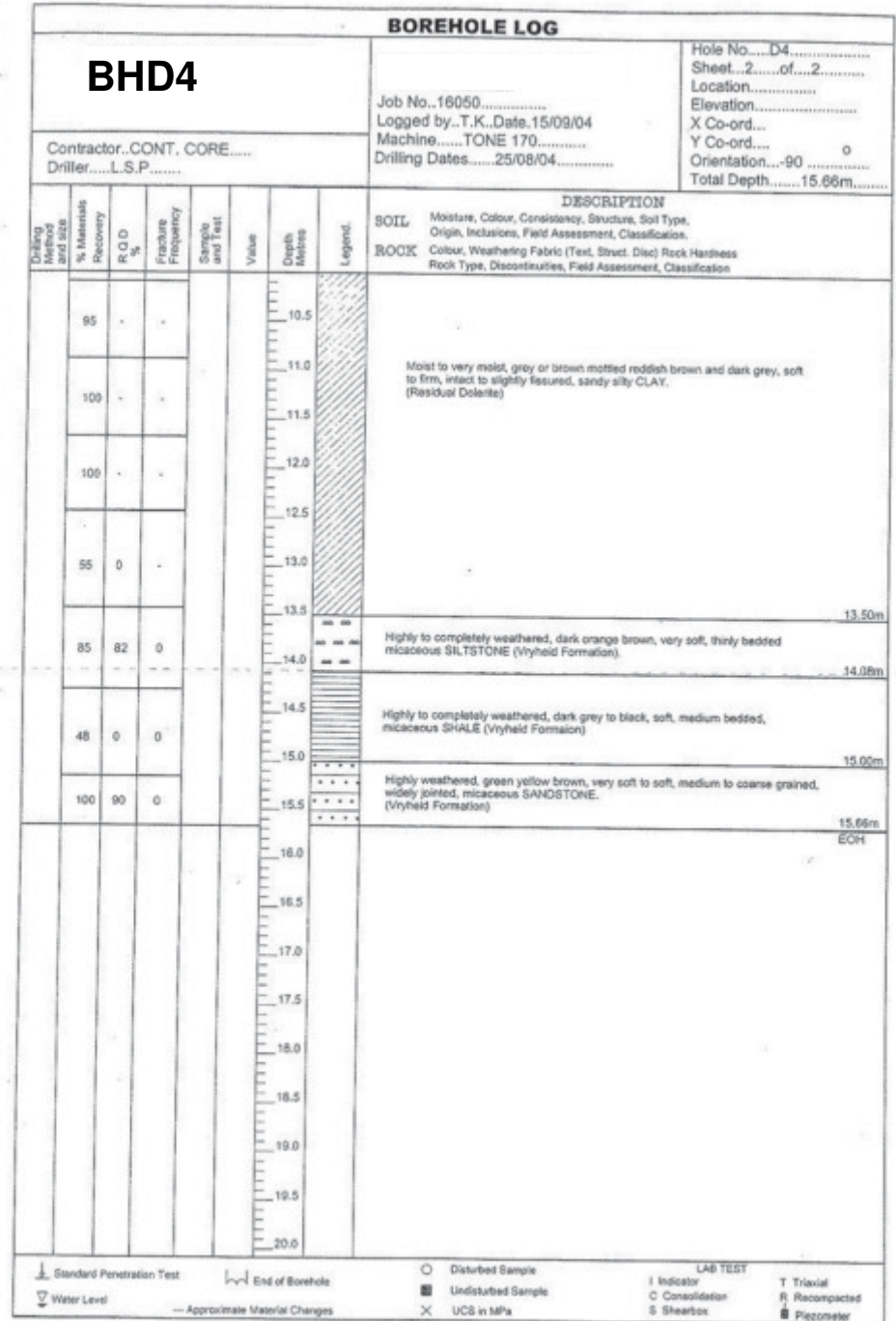
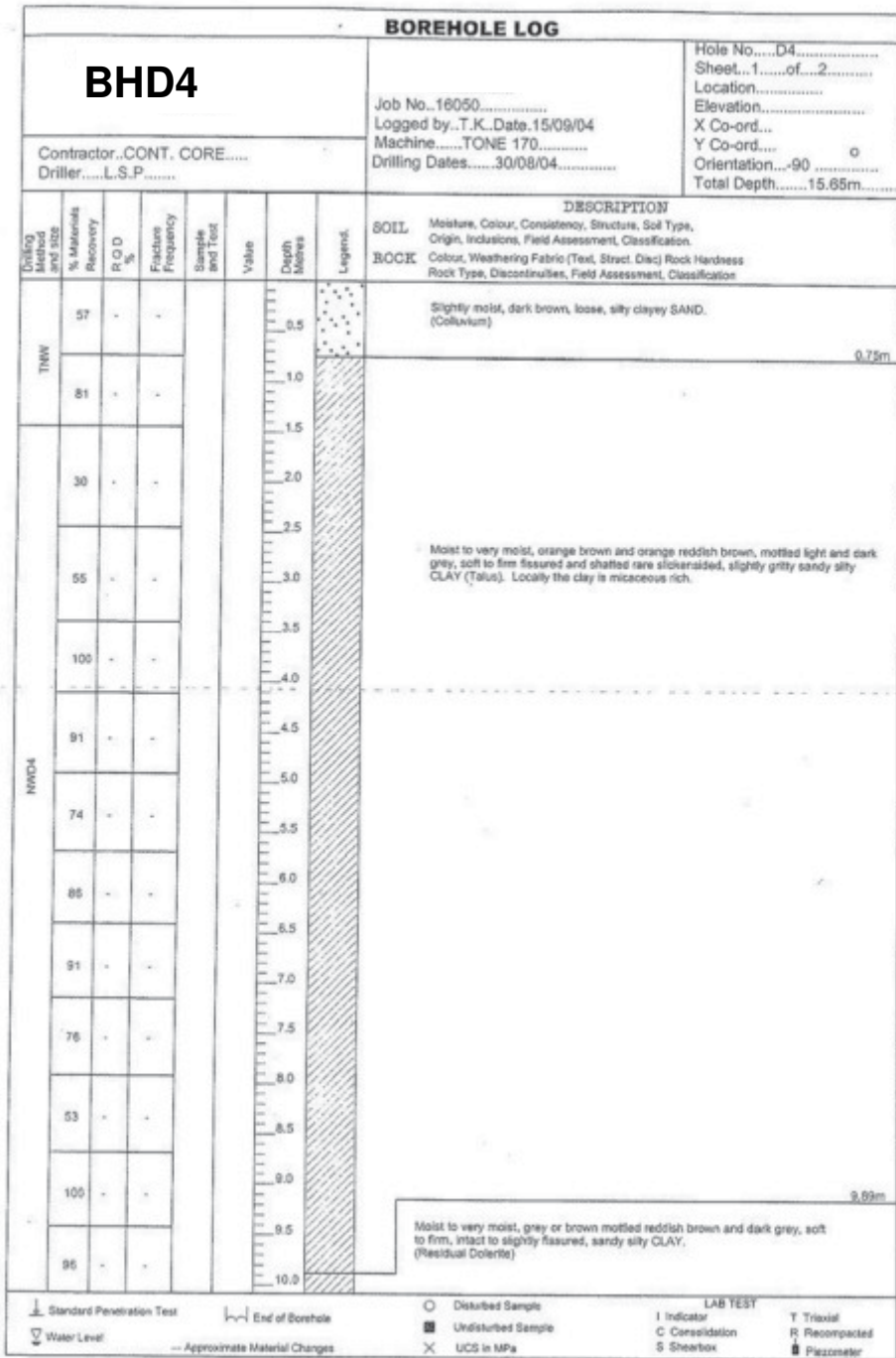
WORLDS VIEW DEVELOPMENT

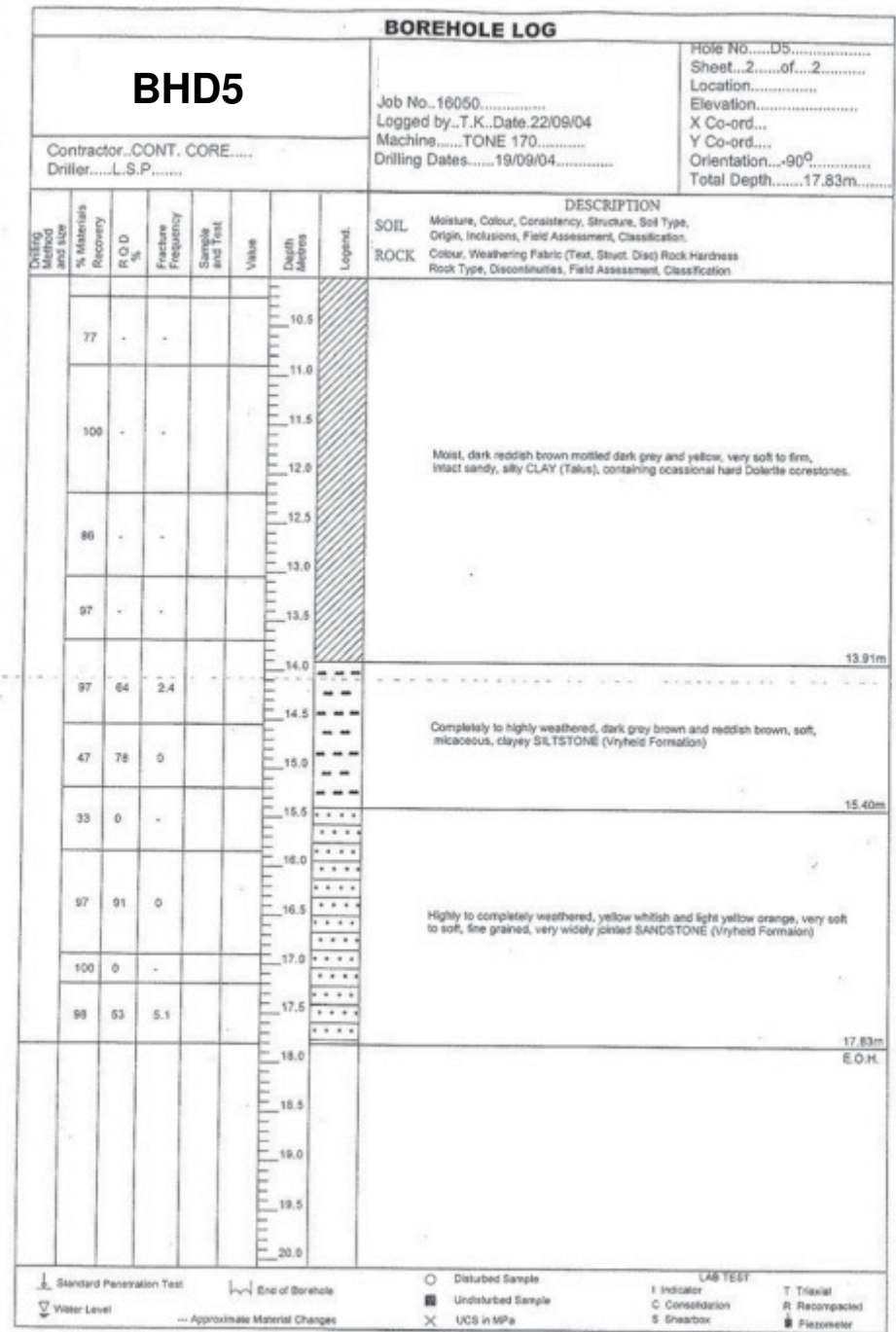
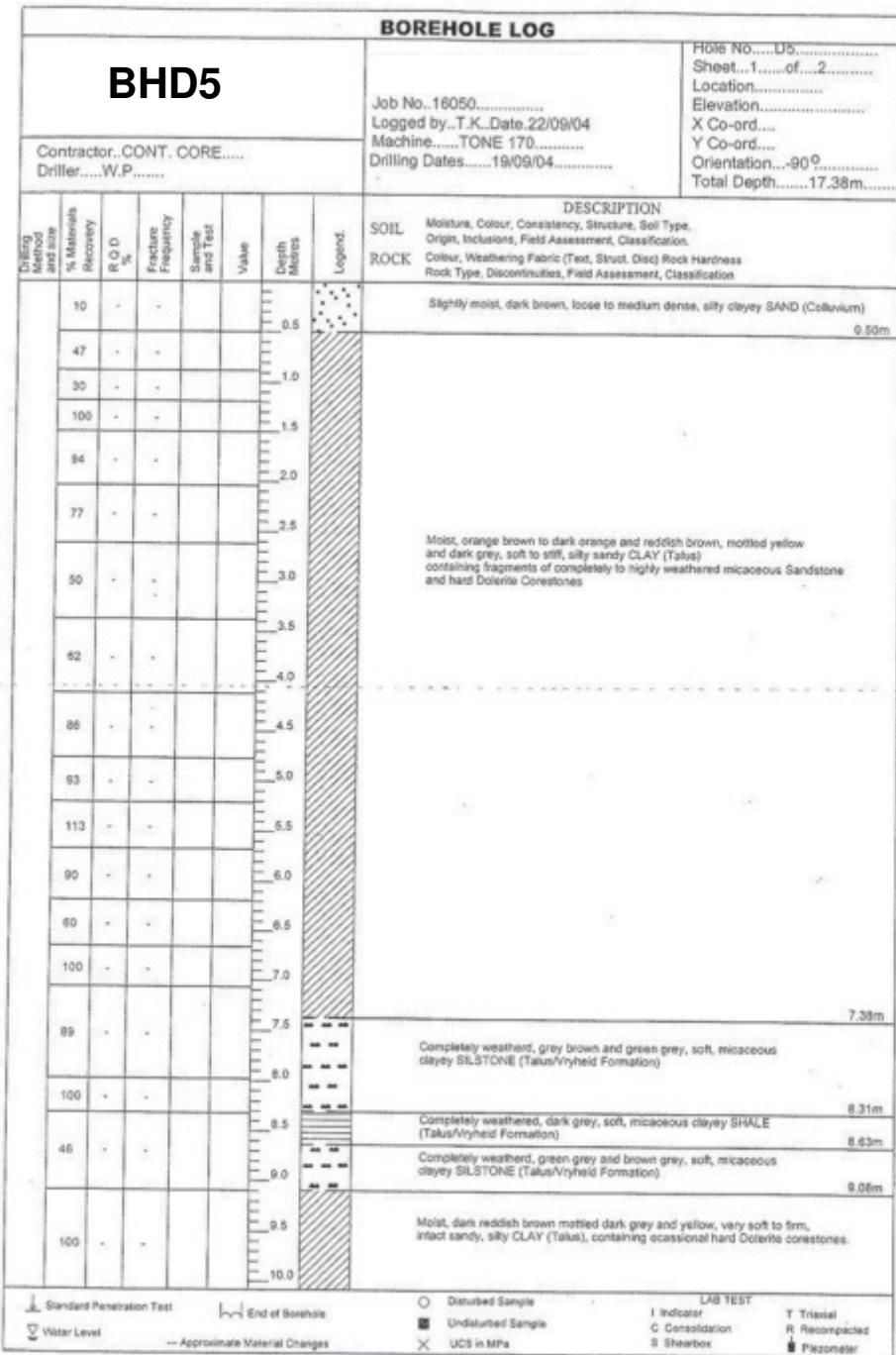


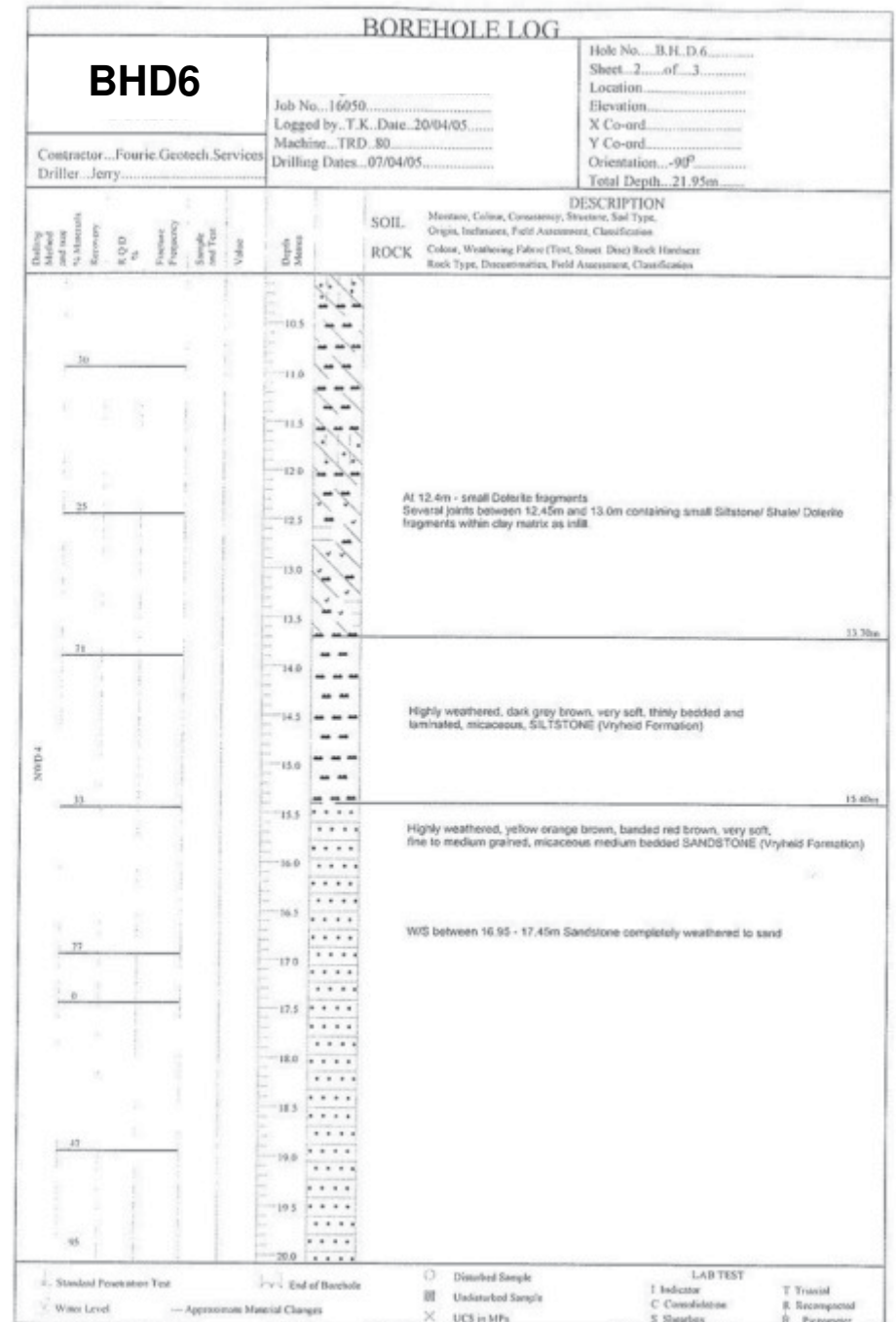
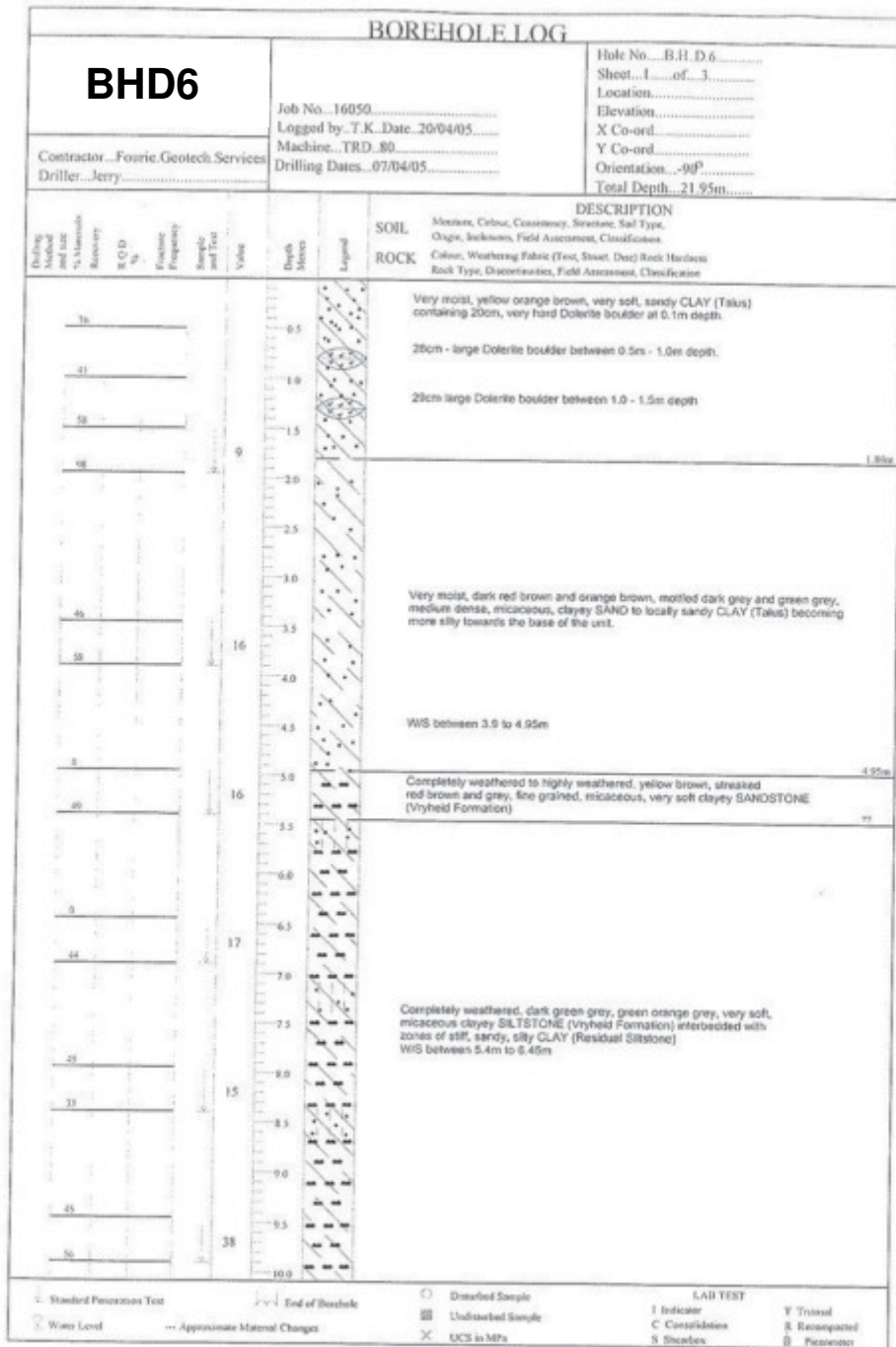


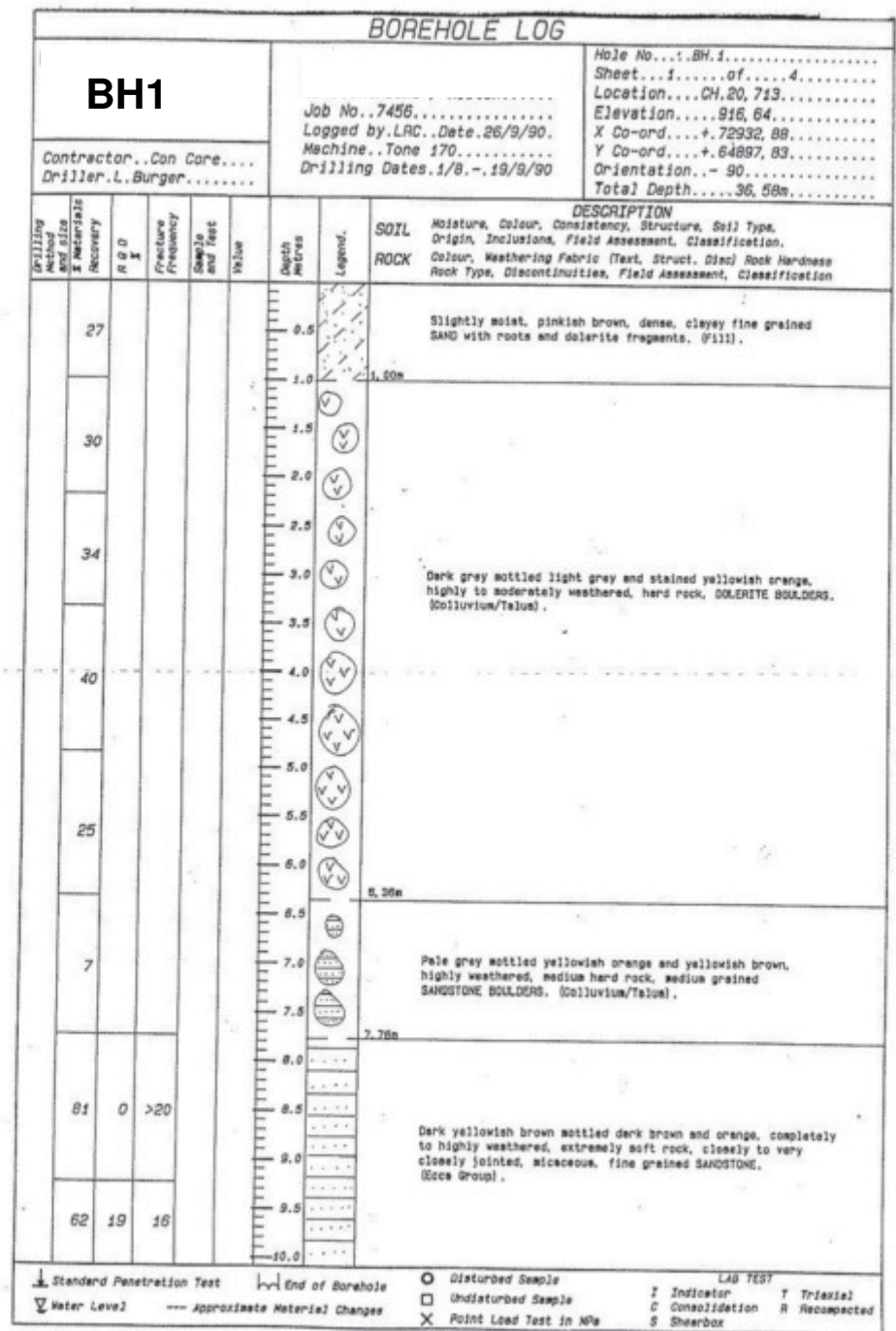
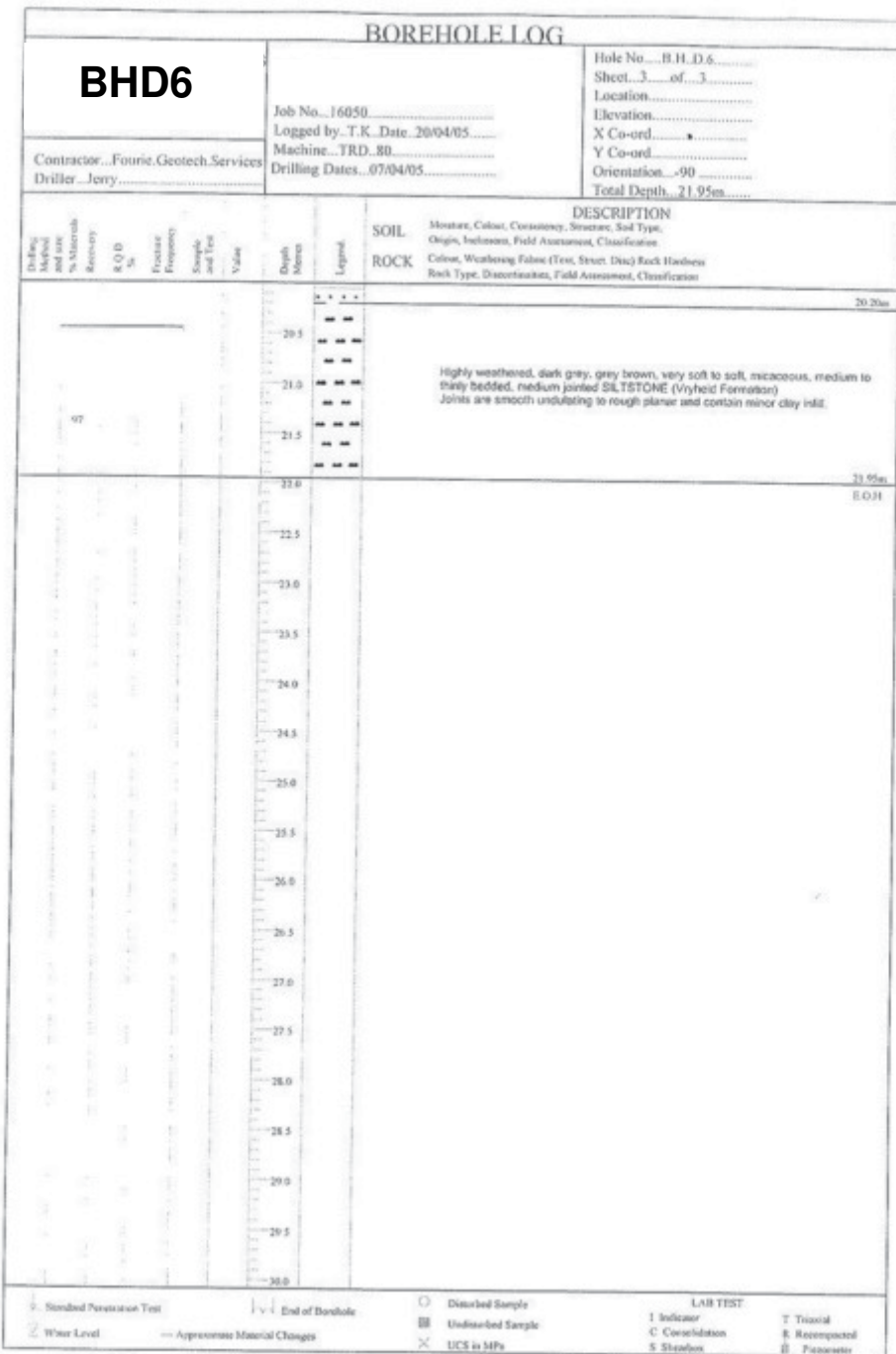


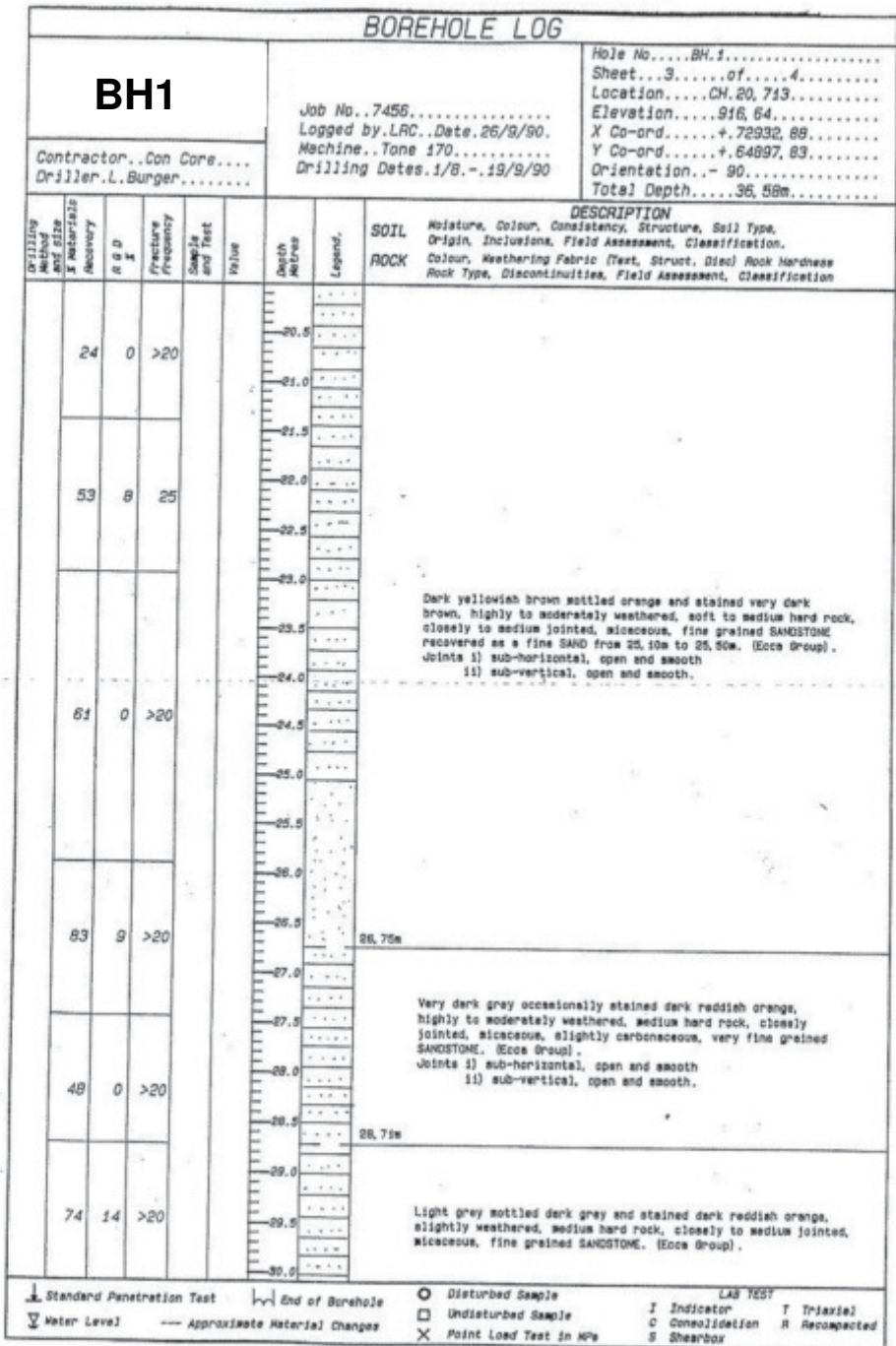
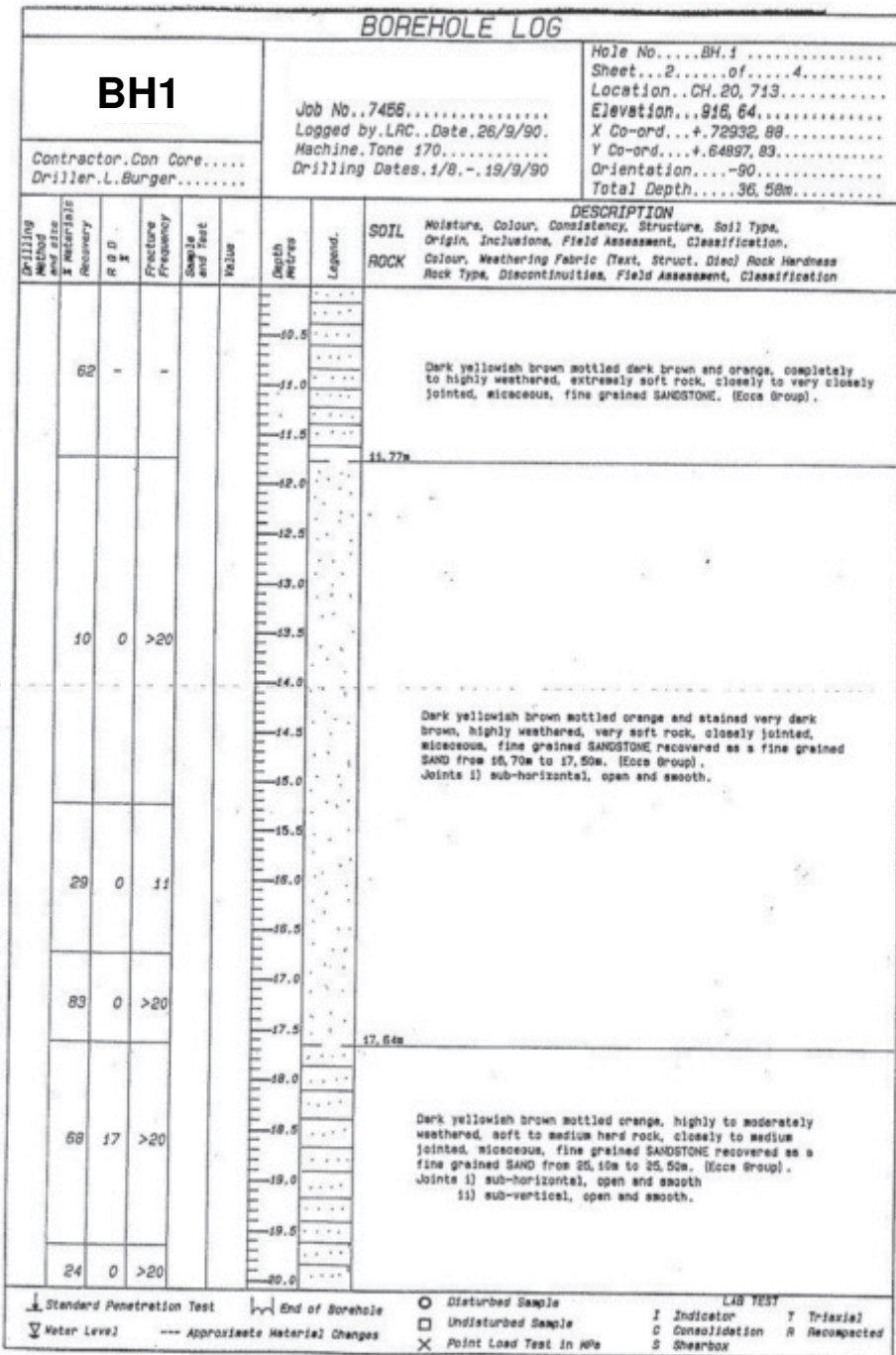


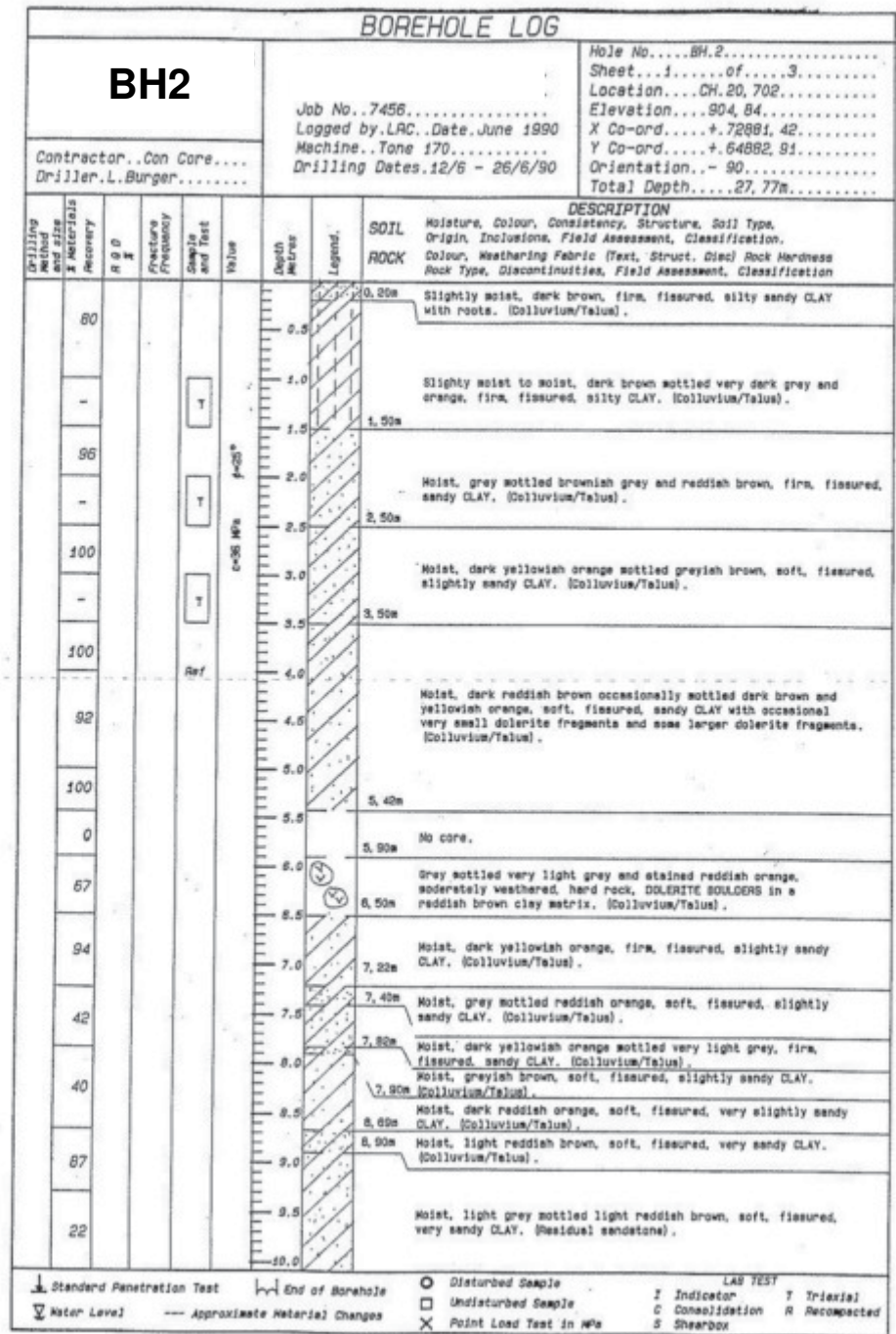
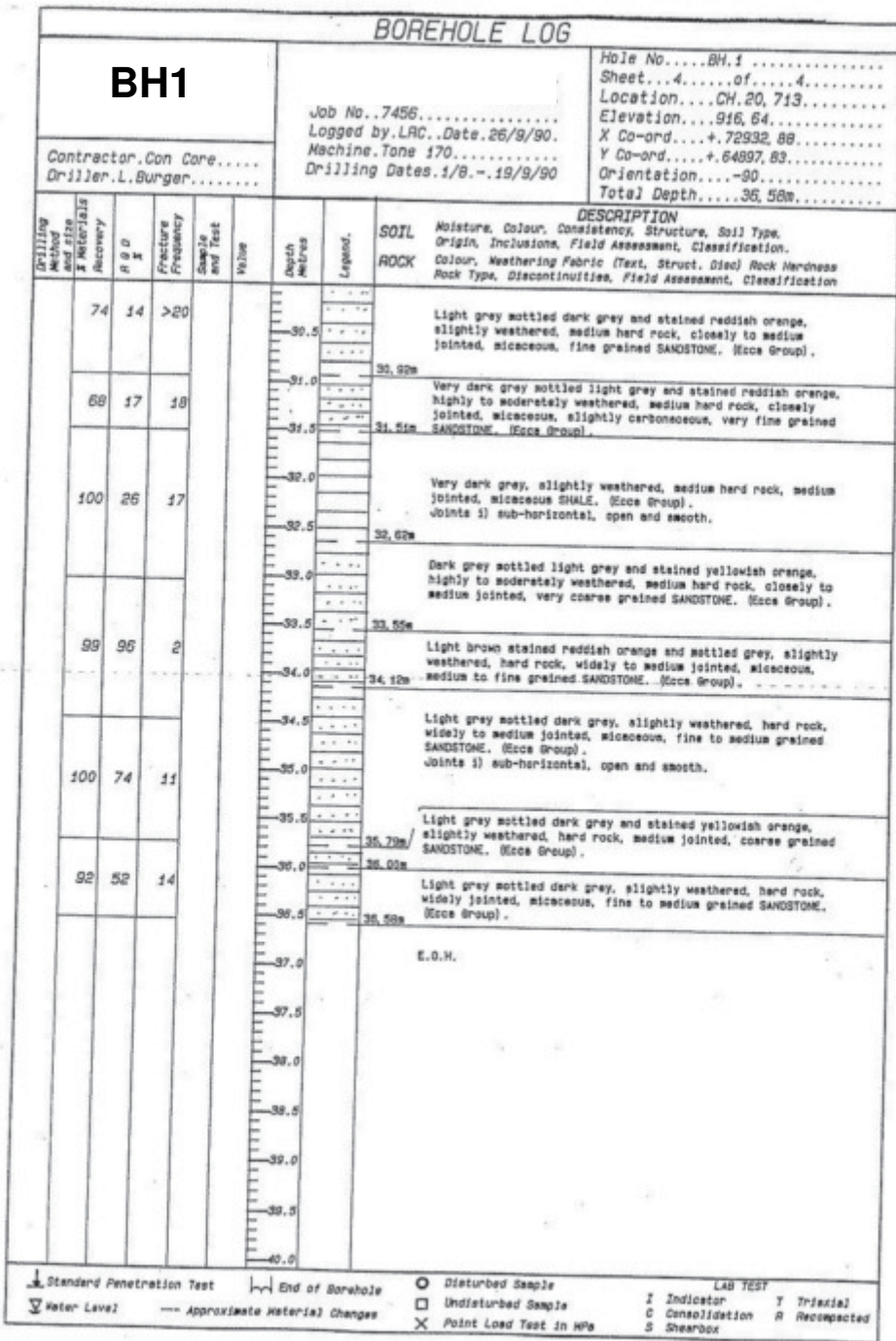










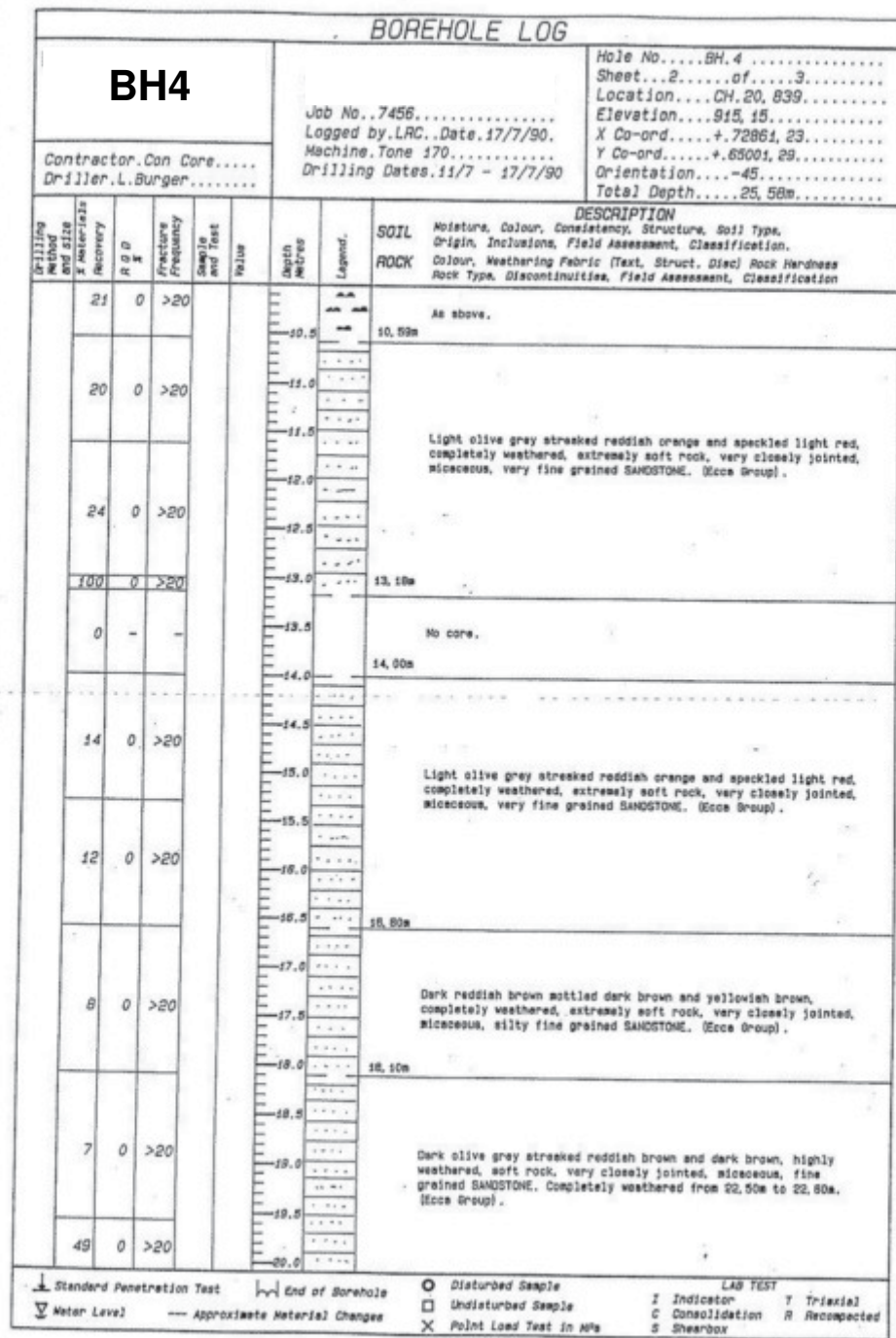
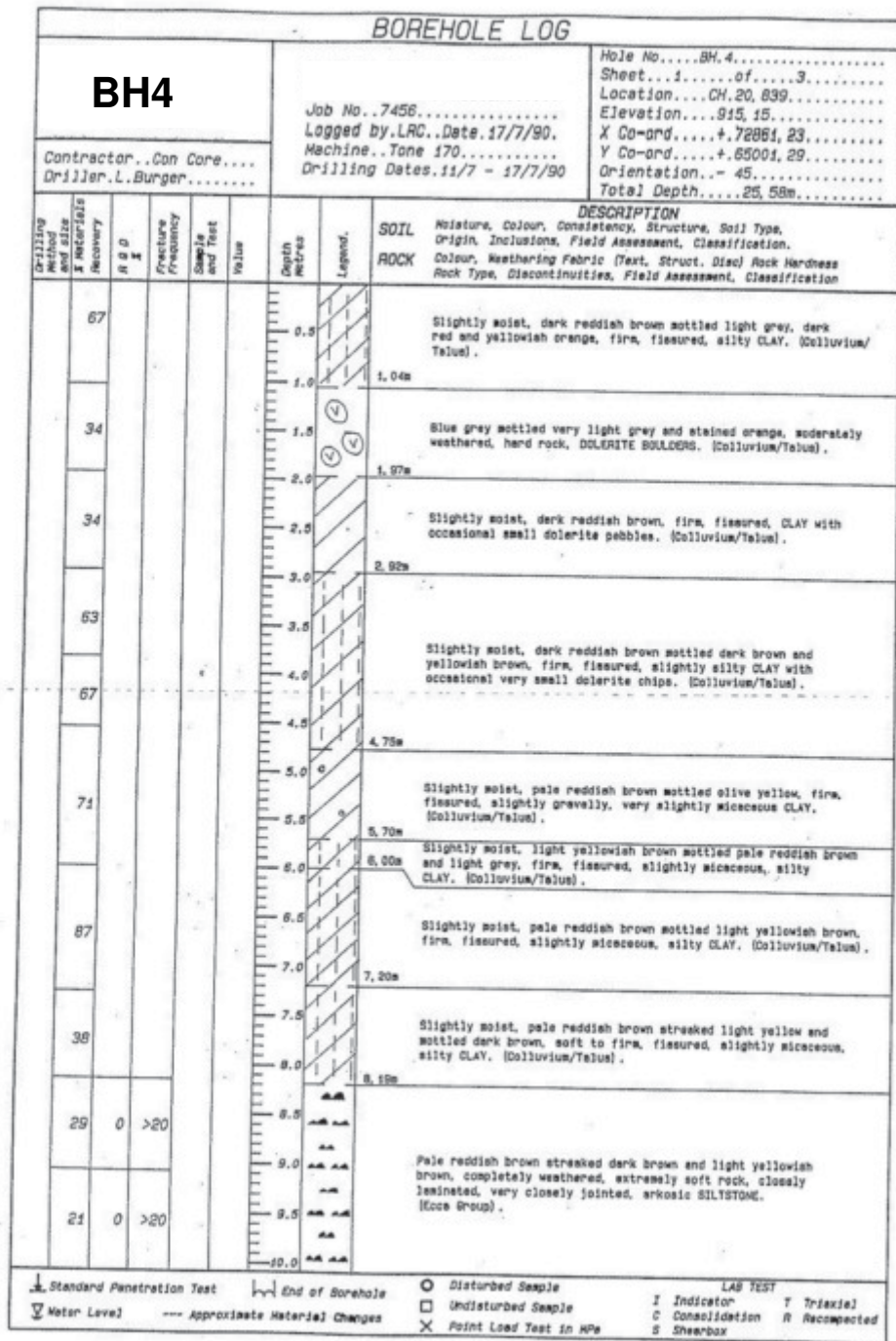


BOREHOLE LOG									
BH2			Job No. 7456 Logged by LAC, Date June 1990 Machine, Tone 170 Drilling Dates 12/6 - 26/6/90			Hole No. BH.2 Sheet 2 of 3 Location CH. 20, 702 Elevation 904.84 X Co-ord. +72881.42 Y Co-ord. +64882.91 Orientation 90 Total Depth 27.77m			
Contractor Con Core Driller L. Burger									
Drilling Method and size of Materials Recovery	R R R	Fracture Frequency	Sample and Test	Value	Depth Metres	Legend	DESCRIPTION		
							SOIL	ROCK	
							Moisture, Colour, Consistency, Structure, Soil Type, Origin, Inclusions, Field Assessment, Classification.		
							Colour, Weathering Fabric (Text, Struct. Disc) Rock Hardness Rock Type, Discontinuities, Field Assessment, Classification		
22					10.5	10.50m	Moist, light grey mottled pale reddish brown, soft, fissured, very sandy CLAY. (Residual dolerite).		
					11.0	11.10m	Moist, reddish brown and very dark grey mottled red and olive, firm, fissured, silty CLAY with occasional dolerite and siltstone fragments. (Residual dolerite).		
47					11.5	12.30m	Light yellowish brown streaked dusky red and very dark grey, completely weathered, extremely soft rock, very closely jointed, micaceous, fine grained SANDSTONE. (Ecca Group).		
					12.0	12.30m			
33					12.5	13.50m	Moist, grey mottled light brown, firm, fissured, silty CLAY with moderately weathered, dark grey siltstone fragments. (Residual siltstone).		
					13.0	13.50m			
					13.5	15.30m	Pale red and yellowish brown streaked reddish orange and olive, completely weathered, extremely soft rock, very closely jointed, micaceous, slightly sandy SILTSTONE. (Ecca Group).		
41					14.0	15.30m			
					14.5	15.30m			
					15.0	15.30m			
24					15.5	16.9m	Pale grey streaked reddish brown, completely weathered, extremely soft rock, very closely jointed, micaceous, SILTSTONE. (Ecca Group).		
					16.0	16.9m			
					16.5	16.9m			
					17.0	16.9m			
66					17.5	17.70m	Pale grey streaked reddish brown and olive, completely weathered, very soft rock, very closely jointed, micaceous, SILTSTONE. (Ecca Group).		
					18.0	17.70m			
					18.5	19.0m	Dark olive and grey, completely to highly weathered, soft rock, micaceous, SHALE fragments in a brown, silty CLAY matrix. (Residual shale).		
					19.0	19.0m			
57	10	23			19.5	19.07m	Dark grey, slightly weathered, hard rock, medium jointed, micaceous, SHALE. (Ecca Group). Joints i) sub-horizontal, open and smooth.		
					19.0	19.07m			
					19.5	19.80m	Moist, brown, dense, intact, silty medium to coarse grained SAND. (Residual sandstone).		
					19.0	19.80m			
72	0	>20			19.5	19.80m	Dark grey, moderately weathered, hard rock, closely jointed, micaceous, SHALE. Completely weathered from 20.00m to 20.10m. (Ecca Group).		
					19.0	19.80m			

Standard Penetration Test End of Borehole Disturbed Sample LAB TEST
 Water Level Approximate Material Changes Undisturbed Sample I Indicator T Triaxial
 Point Load Test in MPa Consolidation R Recompacted S Shearbox

BOREHOLE LOG									
BH2			Job No. 7456 Logged by LAC, Date June 1990 Machine, Tone 170 Drilling Dates 12/6 - 26/6/90			Hole No. BH.2 Sheet 3 of 3 Location CH. 20, 702 Elevation 904.84 X Co-ord. +72881.42 Y Co-ord. +64882.91 Orientation 90 Total Depth 27.77m			
Contractor Con Core Driller L. Burger									
Drilling Method and size of Materials Recovery	R R R	Fracture Frequency	Sample and Test	Value	Depth Metres	Legend	DESCRIPTION		
							SOIL	ROCK	
							Moisture, Colour, Consistency, Structure, Soil Type, Origin, Inclusions, Field Assessment, Classification.		
							Colour, Weathering Fabric (Text, Struct. Disc) Rock Hardness Rock Type, Discontinuities, Field Assessment, Classification		
					20.10m		As above.		
					20.5		Moist, light grey and dark grey, medium dense, intact, medium and coarse grained SAND. (Residual sandstone).		
					20.90m				
	100	72	12		21.0	21.50m	Light grey and dark grey stained yellowish brown, slightly weathered, hard rock, medium jointed, micaceous, fine to medium grained SANDSTONE. (Ecca Group).		
	87	87	1		21.0	21.40m			
					21.5	21.40m	Yellowish brown mottled light grey and dark grey, slightly to moderately weathered, hard rock, medium jointed, micaceous, medium grained SANDSTONE. (Ecca Group).		
					22.0	21.40m			
	74	67	4		22.0	22.0m	Light grey and dark grey, slightly weathered, hard rock, medium jointed, micaceous, fine grained SANDSTONE. (Ecca Group).		
					22.5	22.0m			
					23.0	22.5m	Light grey stained very dark grey and orange brown, slightly to moderately weathered, hard rock, medium jointed, micaceous, medium grained SANDSTONE. (Ecca Group). Joints i) sub-horizontal, open and smooth ii) sub-vertical, closed, stained very dark grey and with FeO.		
	100	83	6		23.0	23.30m			
					23.5	23.30m	Light grey mottled very dark grey, slightly weathered, hard rock, medium jointed, micaceous, fine grained SANDSTONE with occasional FeO staining on joint planes. (Ecca Group). Joints i) sub-horizontal, open and rough ii) sub-horizontal, closed with FeO staining.		
					24.0	24.30m			
	99	78	1		24.0	24.30m			
					24.5	24.30m			
					25.0	24.30m			
					25.5	24.30m			
					26.0	24.30m	Dark grey, slightly weathered, hard rock, medium to widely jointed, micaceous, very fine grained SANDSTONE. (Ecca Group). Joints i) sub-horizontal, open and rough.		
					26.5	24.30m			
					27.0	24.30m			
					27.5	24.30m			
					27.5	27.77m			
					28.0		E.O.H.		
					28.5				
					29.0				
					29.5				
					30.0				

Standard Penetration Test End of Borehole Disturbed Sample LAB TEST
 Water Level Approximate Material Changes Undisturbed Sample I Indicator T Triaxial
 Point Load Test in MPa Consolidation R Recompacted S Shearbox



BOREHOLE LOG

BH4

Hole No. BH.4
 Sheet ... 3 of 3
 Location ... CH. 20, 839
 Elevation ... 915, 15
 X Co-ord ... + 72851, 23
 Y Co-ord ... + 65001, 29
 Orientation ... - 45
 Total Depth ... 25, 58m

Contractor ... Con Core ...
 Driller ... L. Burger

Job No. 7456
 Logged by LAC .. Date 17/7/90 ..
 Machine .. Tone 170
 Drilling Dates 11/7 - 17/7/90

Drilling method used	Material Recovery	R B M	Fracture Frequency	Sample and Test	Value	Depth Metres	Legend	DESCRIPTION	
								SOIL	ROCK
	49	0	>20			20.5			
	13	0	>20			22.0		Dark olive grey streaked reddish brown and dark brown, highly weathered, soft rock, very closely jointed, micaceous, fine grained SANDSTONE. Completely weathered from 22, 50m to 22, 80m. (Ecca Group).	
	27	0	>20			24.0		24, 10m	
	79	0	>20			25.0		Dark olive streaked dark brown and stained dark reddish orange, highly to moderately weathered, medium hard rock, very closely jointed, micaceous, fine grained SANDSTONE. (Ecca Group).	
						25, 58m		E.O.H.	

↓ Standard Penetration Test h End of Borehole ○ Disturbed Sample LAB TEST
 ▽ Water Level --- Approximate Material Changes □ Undisturbed Sample I Indicator T Triaxial
 X Point Load Test in MPa C Consolidation R Recompact S Shearbox

UPPER NATIONAL PARK DEVELOPMENT

HOLE No: BH1
Sheet 1 of 2

JOB NUMBER: 000

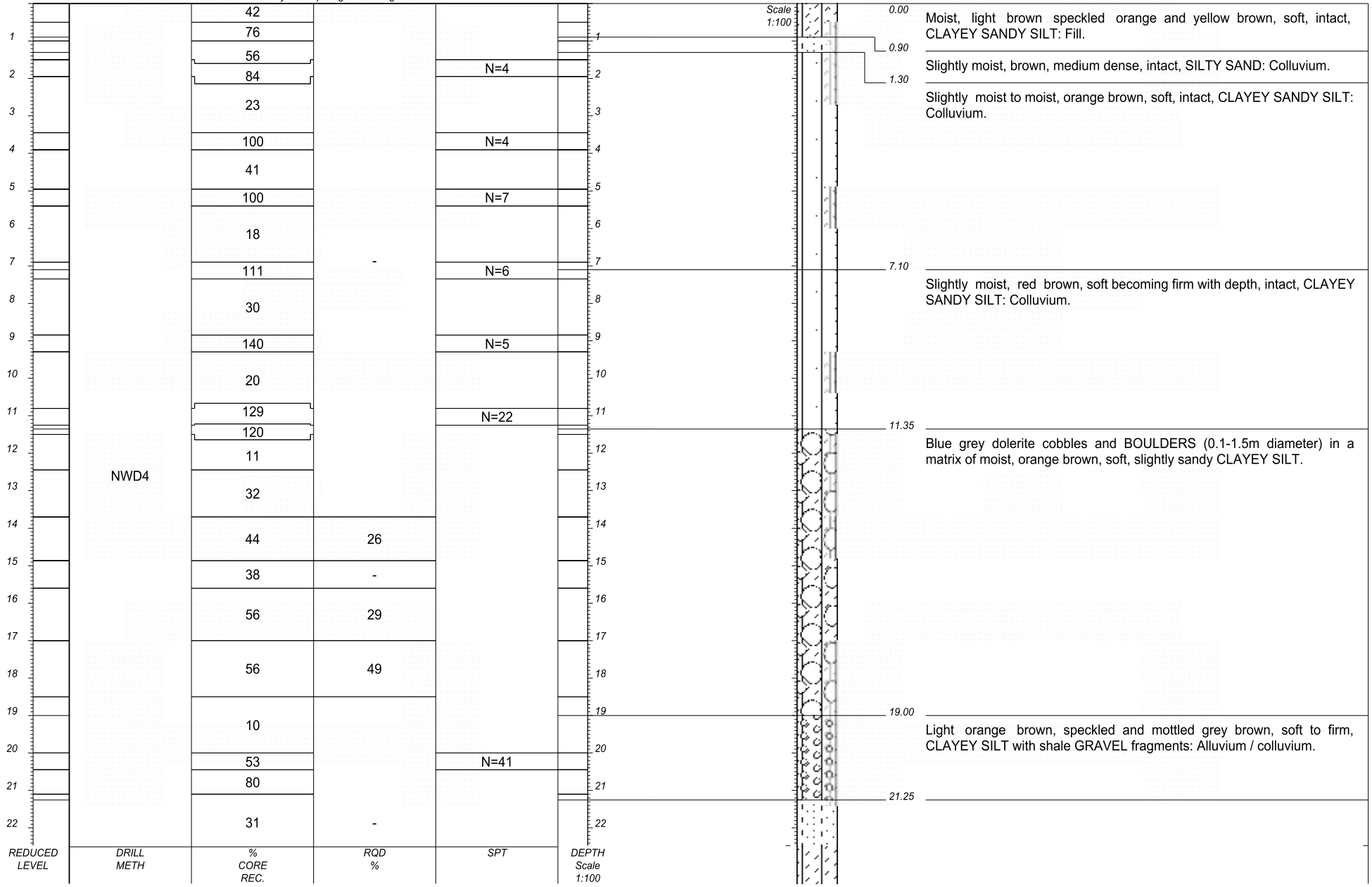
ROCK FABRIC MF -massive BF -bedded FF -foliated CF -cleaved SF -schistose GF -gneissose LF -laminated	GRAIN SIZE FG -fine grained MG -medium grain CG -coarse grain	JOINT ROUGHNESS SLJ-slickensided SJ -smooth RJ -rough	ROCK HARDNESS EHR-extremely hard rock VHR-very hard rock HR -hard rock MHR-medium hard rock SR -soft rock VSR-very soft rock
	JOINT SPACING VCJ-very close spacng CJ -close spacing MJ -medium spacing WJ -wide spacing VWJ-very wide spacng	JOINT SHAPE CUR-curvilinear PLA-planar UND-undulating STE-stepped IRR-irregular	



Upper National Park Development

HOLE No: BH1
Sheet 1 of 2

JOB NUMBER: 000



HOLE No: BH1
Sheet 2 of 2

JOB NUMBER: 000

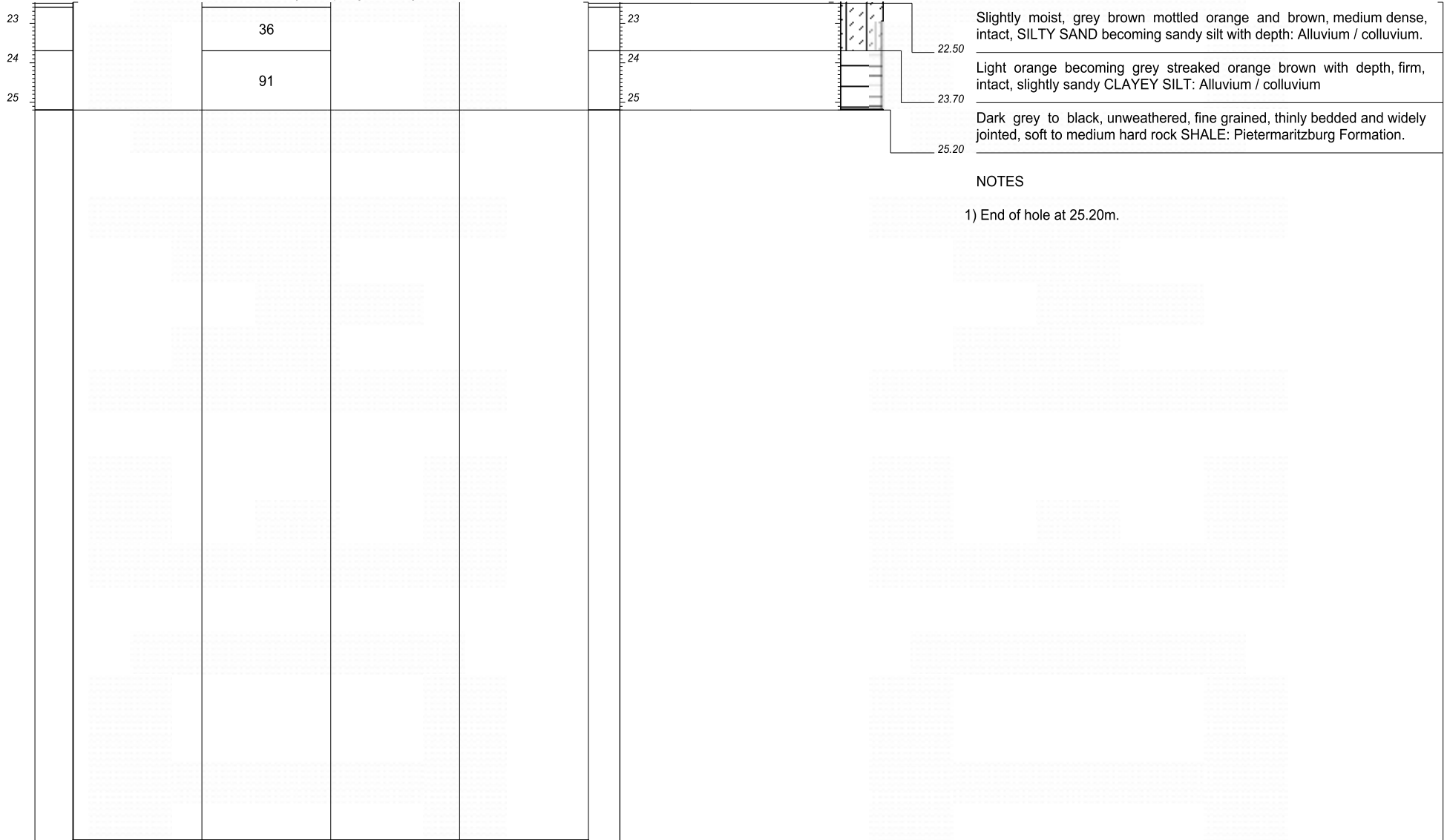
ROCK FABRIC MF -massive BF -bedded FF -foliated CF -cleaved SF -schistose GF -gneissose LF -laminated	GRAIN SIZE FG -fine grained MG -medium grain CG -coarse grain	JOINT ROUGHNESS SLJ-slickensided SJ -smooth RJ -rough	ROCK HARDNESS EHR-extremely hard rock VHR-very hard rock HR -hard rock MHR-medium hard rock SR -soft rock VSR-very soft rock
	JOINT SPACING VCJ-very close spacg CJ -close spacing MJ -medium spacing WJ -wide spacing VWJ-very wide spacng	JOINT SHAPE CUR-curved/linear PLA-planar UND-undulating STE-stepped IRR-irregular	



Upper National Park Development

HOLE No: BH1
Sheet 2 of 2

JOB NUMBER: 000



Slightly moist, grey brown mottled orange and brown, medium dense, intact, SILTY SAND becoming sandy silt with depth: Alluvium / colluvium.

Light orange becoming grey streaked orange brown with depth, firm, intact, slightly sandy CLAYEY SILT: Alluvium / colluvium

Dark grey to black, unweathered, fine grained, thinly bedded and widely jointed, soft to medium hard rock SHALE: Pietermaritzburg Formation.

NOTES

1) End of hole at 25.20m.

REDUCED LEVEL	DRILL METH	% CORE REC.	RQD %	SPT	DEPTH Scale 1:100	CONTRACTOR :	INCLINATION : VERTICAL	ELEVATION :
						MACHINE :	DIAM : NWD4	X-COORD :
						DRILLED BY :	DATE : MARCH 2005	Y-COORD :
						PROFILED BY : S. BOK	DATE : MARCH 2005	
						TYPE SET BY : S.BOK	DATE : 24/04/2017 11:41	
						SETUP FILE : A3.SET	TEXT : ..NEXBIUNPD161055BH's.txt	

HOLE No: BH1

HOLE No: BH2
Sheet 1 of 1

JOB NUMBER: 000

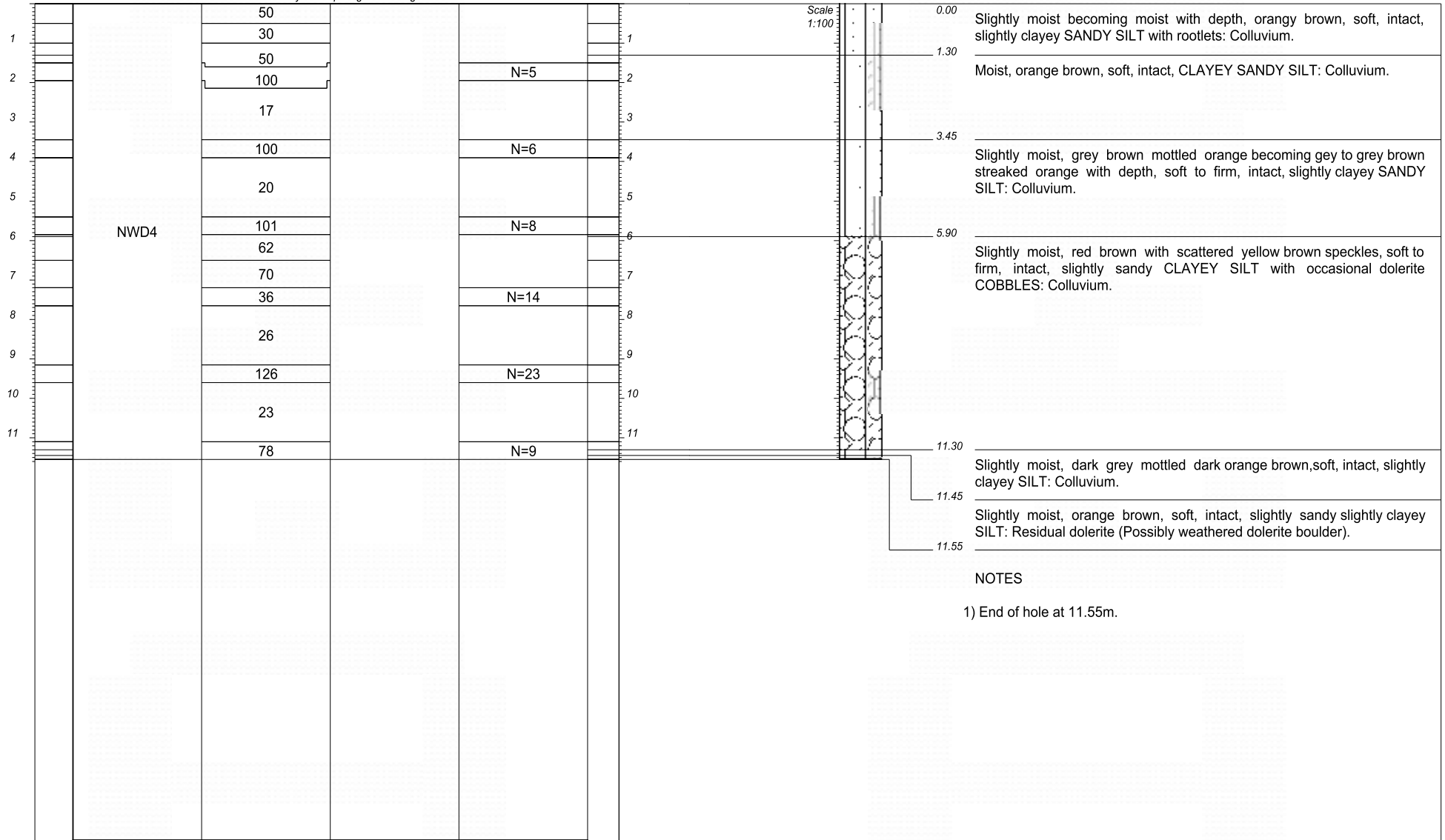
ROCK FABRIC MF -massive BF -bedded FF -foliated CF -cleaved SF -schistose GF -gneissose LF -laminated	GRAIN SIZE FG -fine grained MG -medium grain CG -coarse grain	JOINT ROUGHNESS SLJ-slickensided SJ -smooth RJ -rough	ROCK HARDNESS EHR-extremely hard rock VHR-very hard rock HR -hard rock MHR-medium hard rock SR -soft rock VSR-very soft rock
	JOINT SPACING VCJ-very close spacg CJ -close spacing MJ -medium spacing WJ -wide spacing VWJ-very wide spacng	JOINT SHAPE CUR-curved/linear PLA-planar UND-undulating STE-stepped IRR-irregular	



Upper National Park Development

HOLE No: BH2
Sheet 1 of 1

JOB NUMBER: 000



NOTES
1) End of hole at 11.55m.

CONTRACTOR :	INCLINATION :	ELEVATION :
MACHINE :	DIAM : NWD4	X-COORD :
DRILLED BY :	DATE : MARCH 2005	Y-COORD :
PROFILED BY : S. BOK	DATE : MARCH 2005	
TYPE SET BY : S.BOK	DATE : 24/04/2017 11:41	
SETUP FILE : A3.SET	TEXT : ..NEXB\UNPD\161055BH's.txt	

HOLE No: BH2

HOLE No: BH3
Sheet 1 of 1

JOB NUMBER: 000

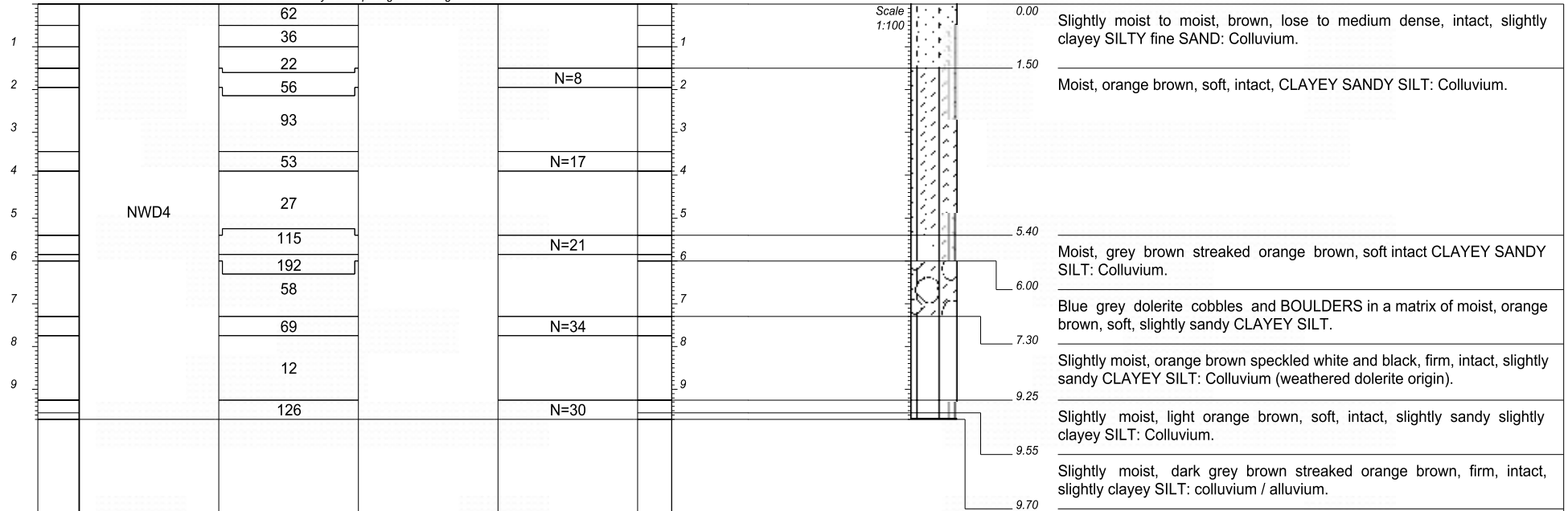
ROCK FABRIC MF -massive BF -bedded FF -foliated CF -cleaved SF -schistose GF -gneissose LF -laminated	GRAIN SIZE FG -fine grained MG -medium grain CG -coarse grain	JOINT ROUGHNESS SLJ-slickensided SJ -smooth RJ -rough	ROCK HARDNESS EHR-extremely hard rock VHR-very hard rock HR -hard rock MHR-medium hard rock SR -soft rock VSR-very soft rock
	JOINT SPACING VCJ-very close spacg CJ -close spacing MJ -medium spacing WJ -wide spacing VWJ-very wide spacng	JOINT SHAPE CUR-curvilinear PLA-planar UND-undulating STE-stepped IRR-irregular	



Upper National Park Development

HOLE No: BH3
Sheet 1 of 1

JOB NUMBER: 000



NOTES
1) End of hole at 9.7m.

CONTRACTOR :	INCLINATION :	ELEVATION :
MACHINE :	DIAM : NWD4	X-COORD :
DRILLED BY :	DATE : MARCH 2005	Y-COORD :
PROFILED BY : S. BOK	DATE : MARCH 2005	
TYPE SET BY : S.BOK	DATE : 24/04/2017 11:41	
SETUP FILE : A3.SET	TEXT : ..NEXB\UNPD\161055BH's.txt	

HOLE No: BH3

HOLE No: BH4
Sheet 1 of 1

JOB NUMBER: 000

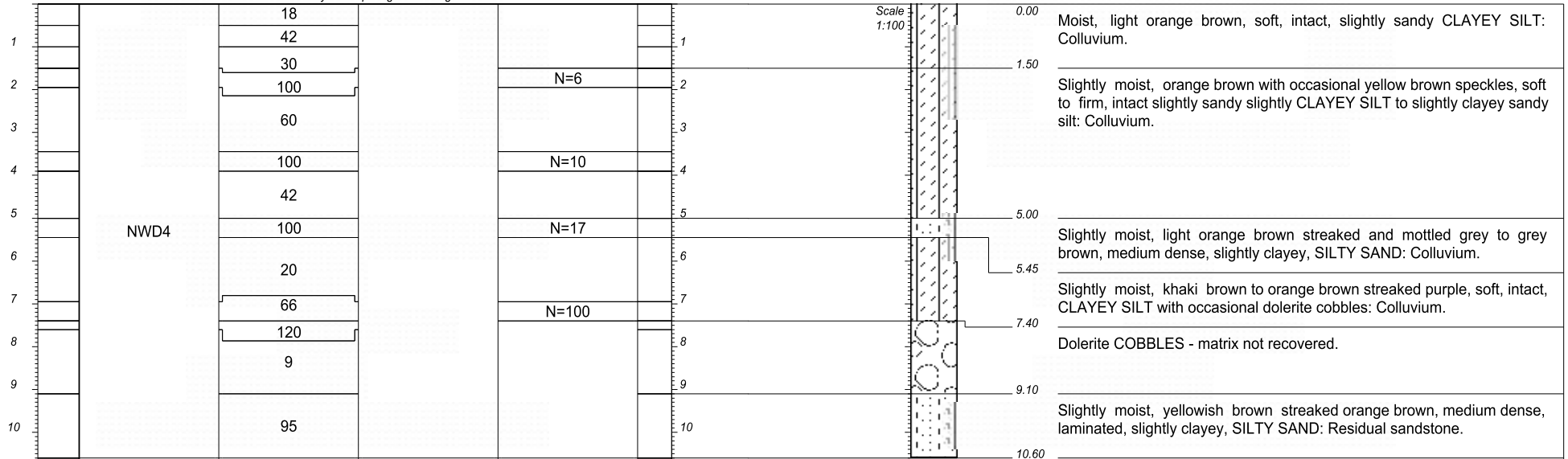
ROCK FABRIC MF -massive BF -bedded FF -foliated CF -cleaved SF -schistose GF -gneissose LF -laminated	GRAIN SIZE FG -fine grained MG -medium grain CG -coarse grain	JOINT ROUGHNESS SLJ-slickensided SJ -smooth RJ -rough	ROCK HARDNESS EHR-extremely hard rock VHR-very hard rock HR -hard rock MHR-medium hard rock SR -soft rock VSR-very soft rock
	JOINT SPACING VCJ-very close spacg CJ -close spacing MJ -medium spacing WJ -wide spacing VWJ-very wide spacng	JOINT SHAPE CUR-curvilinear PLA-planar UND-undulating STE-stepped IRR-irregular	



Upper National Park Development

HOLE No: BH4
Sheet 1 of 1

JOB NUMBER: 000



NOTES
1) End of hole at 10.6m.

CONTRACTOR :	INCLINATION :	ELEVATION :
MACHINE :	DIAM : NWD4	X-COORD :
DRILLED BY :	DATE : MARCH 2005	Y-COORD :
PROFILED BY : S. BOK	DATE : MARCH 2005	
TYPE SET BY : S.BOK	DATE : 24/04/2017 11:41	
SETUP FILE : A3.SET	TEXT : ..NEXBIUNPD\161055BH's.txt	

HOLE No: BH4

HOLE No: BH5
Sheet 1 of 1

JOB NUMBER: 000

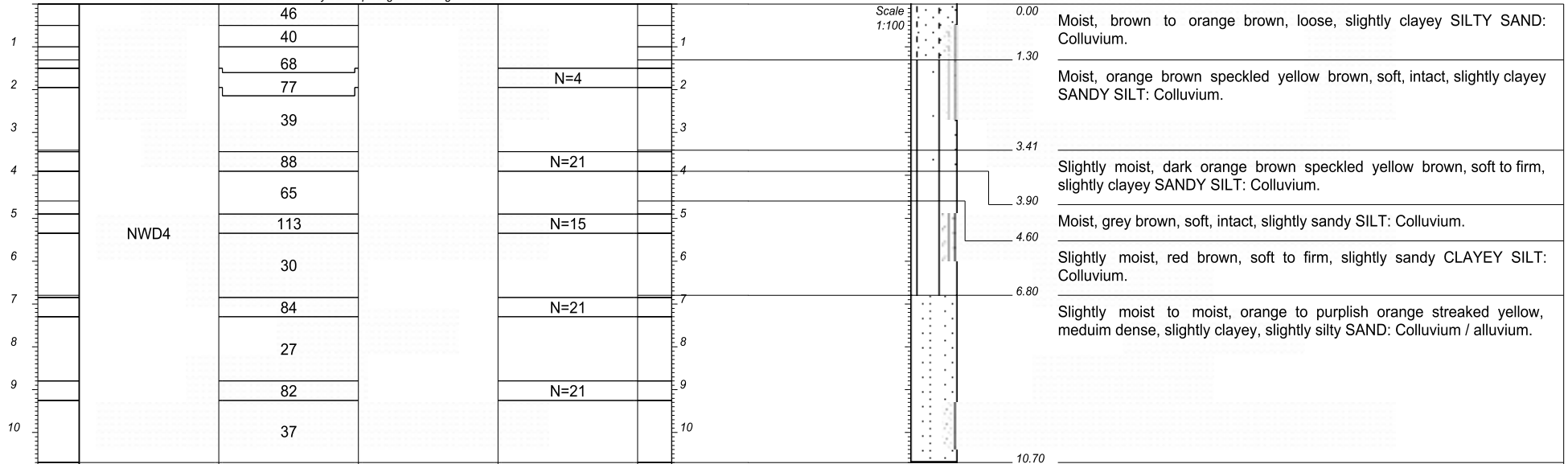
ROCK FABRIC MF -massive BF -bedded FF -foliated CF -cleaved SF -schistose GF -gneissose LF -laminated	GRAIN SIZE FG -fine grained MG -medium grain CG -coarse grain	JOINT ROUGHNESS SLJ-slickensided SJ -smooth RJ -rough	ROCK HARDNESS EHR-extremely hard rock VHR-very hard rock HR -hard rock MHR-medium hard rock SR -soft rock VSR-very soft rock
	JOINT SPACING VCJ-very close spacg CJ -close spacing MJ -medium spacing WJ -wide spacing VWJ-very wide spacng	JOINT SHAPE CUR-curved/linear PLA-planar UND-undulating STE-stepped IRR-irregular	



Upper National Park Development

HOLE No: BH5
Sheet 1 of 1

JOB NUMBER: 000



NOTES
1) End of hole at 10.7m.

REDUCED LEVEL	DRILL METH	% CORE REC.	RQD %	SPT	DEPTH Scale 1:100	CONTRACTOR : MACHINE : DRILLED BY : PROFILED BY : S. BOK	INCLINATION : DIAM : NWD4 DATE : MARCH 2005 DATE : MARCH 2005	ELEVATION : X-COORD : Y-COORD :
						TYPE SET BY : S.BOK SETUP FILE : A3.SET	DATE : 24/04/2017 11:41 TEXT : ..NEXBIUNPD1161055BH's.txt	HOLE No: BH5

HOLE No: BH6
Sheet 1 of 1

JOB NUMBER: 000

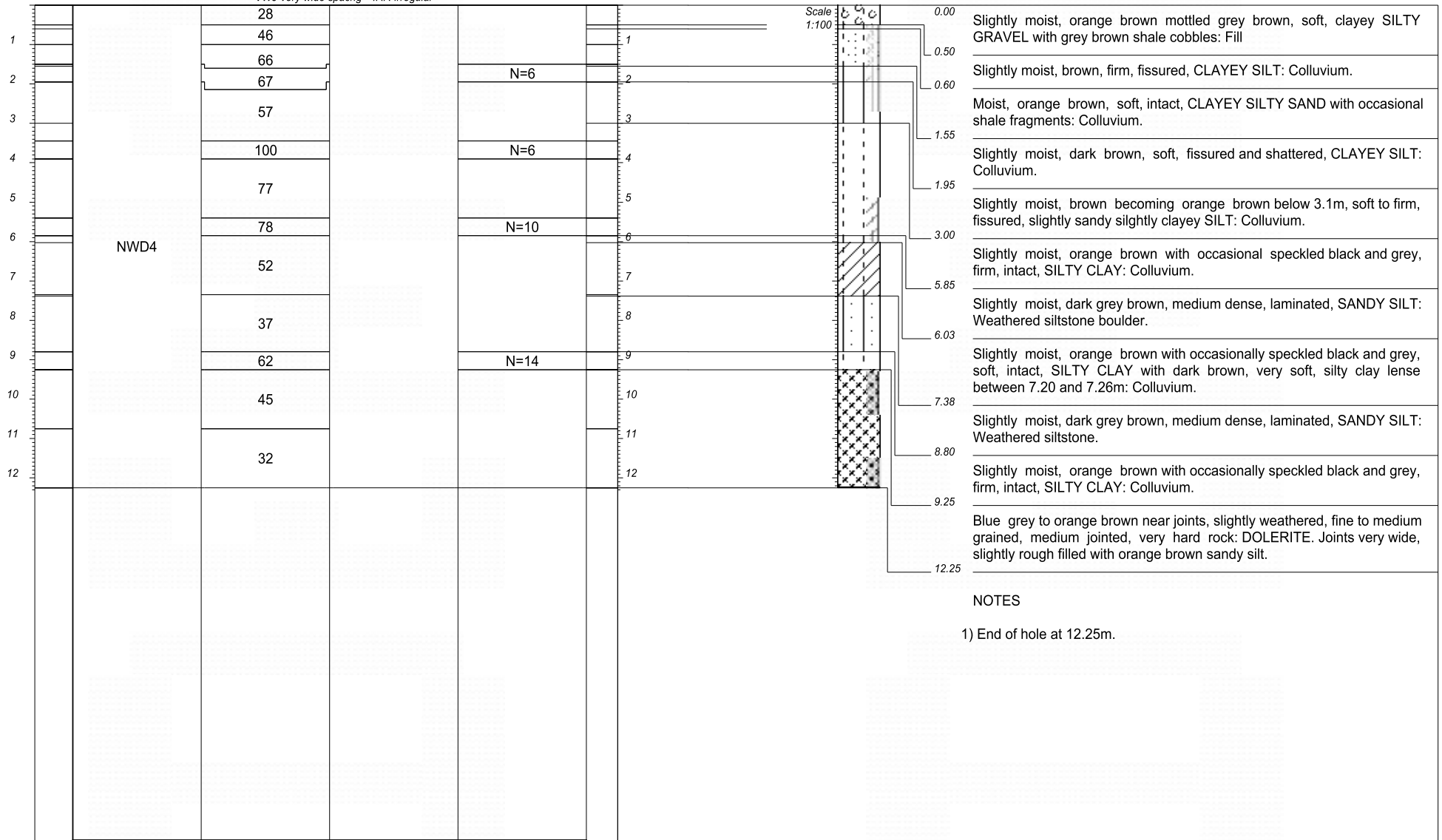
ROCK FABRIC MF -massive BF -bedded FF -foliated CF -cleaved SF -schistose GF -gneissose LF -laminated	GRAIN SIZE FG -fine grained MG -medium grain CG -coarse grain	JOINT ROUGHNESS SLJ-slickensided SJ -smooth RJ -rough	ROCK HARDNESS EHR-extremely hard rock VHR-very hard rock HR -hard rock MHR-medium hard rock SR -soft rock VSR-very soft rock
JOINT SPACING VCJ-very close spacg CJ -close spacing MJ -medium spacing WJ -wide spacing VWJ-very wide spacng	JOINT SHAPE CUR-curvilinear PLA-planar UND-undulating STE-stepped IRR-irregular		



Upper National Park Development

HOLE No: BH6
Sheet 1 of 1

JOB NUMBER: 000



NOTES
1) End of hole at 12.25m.

CONTRACTOR :	INCLINATION :	ELEVATION :
MACHINE :	DIAM : NWD4	X-COORD :
DRILLED BY :	DATE : MARCH 2005	Y-COORD :
PROFILED BY : S. BOK	DATE : MARCH 2005	
TYPE SET BY : S.BOK	DATE : 24/04/2017 11:41	
SETUP FILE : A3.SET	TEXT : ..NEXB\UNPD\161055BH's.txt	

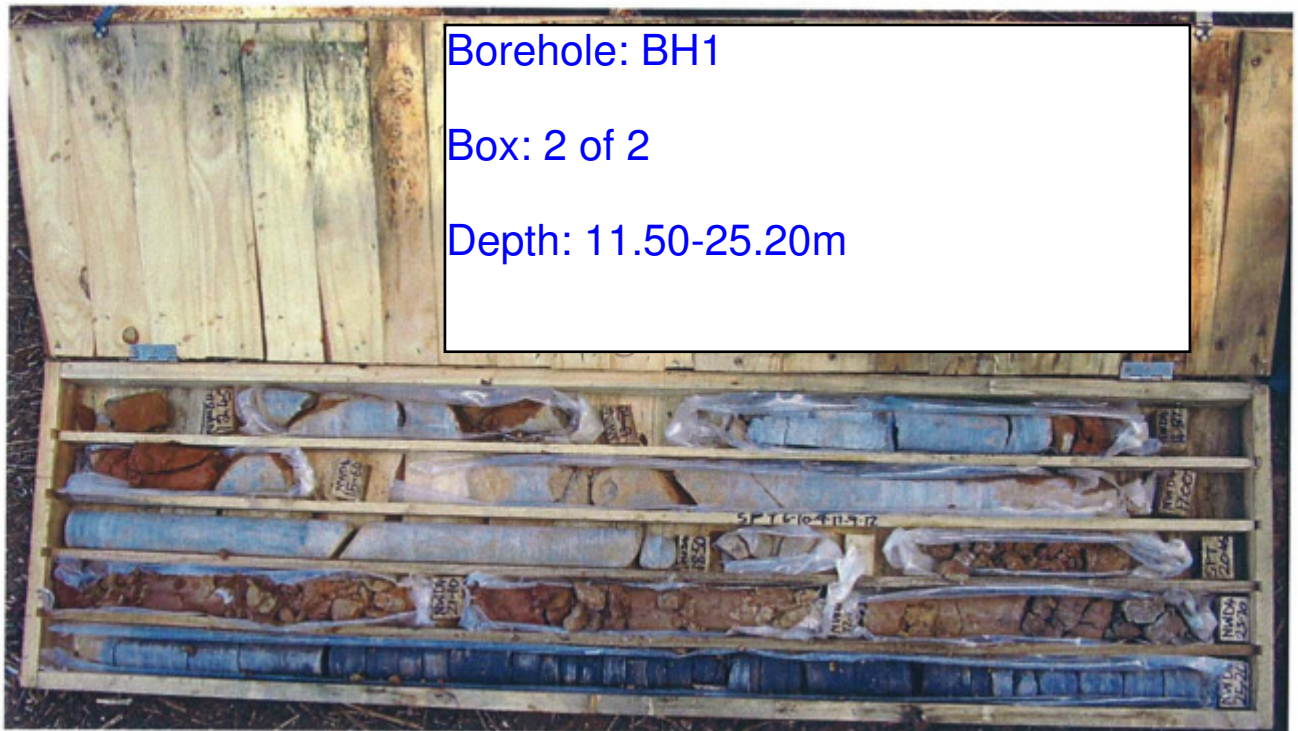
HOLE No: BH6

	BOULDERS	{SA01}
	GRAVEL	{SA02}
	SAND	{SA04}
	SANDY	{SA05}
	SILT	{SA06}
	SILTY	{SA07}
	CLAY	{SA08}
	CLAYEY	{SA09}
	SHALE	{SA12}
	DOLERITE	{SA18}{SA42}

CONTRACTOR :
MACHINE :
DRILLED BY :
PROFILED BY :
TYPE SET BY : S.BOK
SETUP FILE : A3.SET

INCLINATION :
DIAM :
DATE :
DATE :
DATE : 24/04/2017 11:41
TEXT : ..NEXBIUNPD\161055BH's.txt

ELEVATION :
X-COORD :
Y-COORD :
LEGEND
SUMMARY OF SYMBOLS



Borehole: BH2

Box: 1 of 1

Depth: 0.00-11.55m

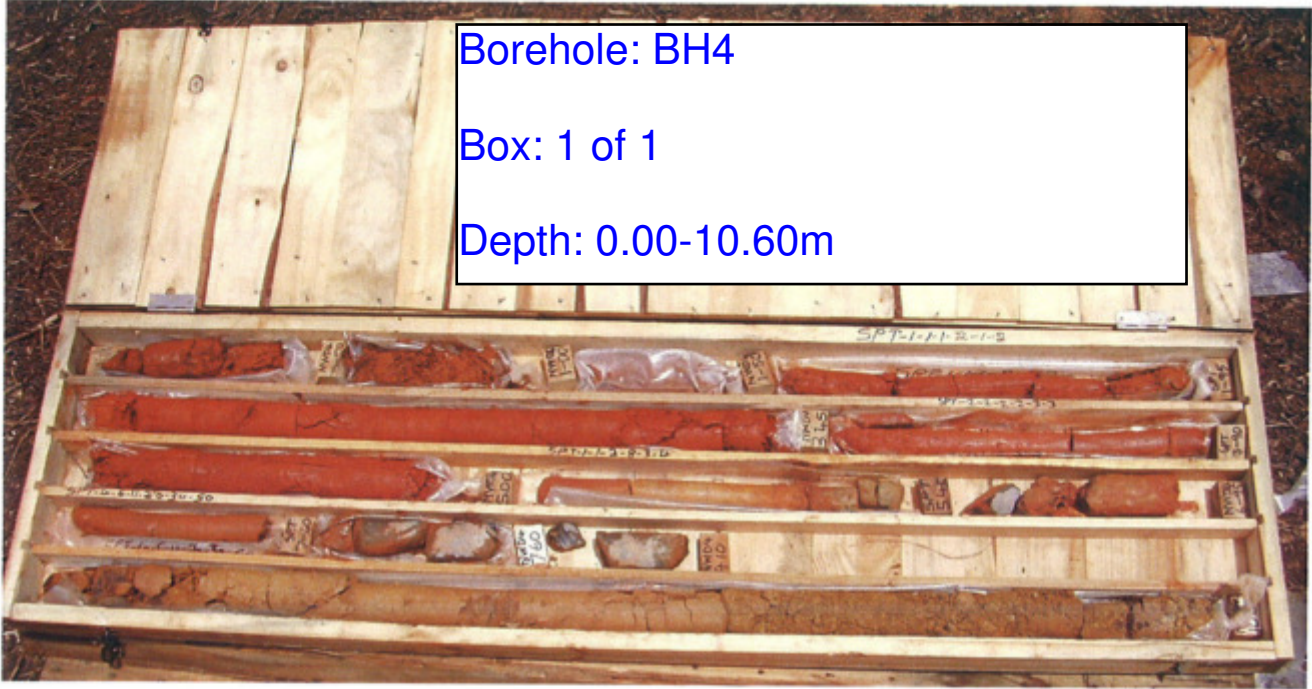


Borehole: BH3

Box: 1 of 1

Depth: 0.00-09.70m





Borehole: BH4

Box: 1 of 1

Depth: 0.00-10.60m



Borehole: BH5

Box: 1 of 1

Depth: 0.00-10.60m



Borehole: BH6

Box: 1 of 2

Depth: 0.00-09.25m



Borehole: BH6

Box: 2 of 2

Depth: 09.25-12.25m

APPENDIX B1.3

CASCADES DEVELOPMENT

HOLE No: BHV3/1

Sheet 1 of 2

JOB NUMBER: 000

ROCK FABRIC
 MF -massive
 BF -bedded
 FF -foliated
 CF -cleaved
 SF -schistose
 GF -gneissose
 LF -laminated

GRAIN SIZE
 FG -fine grained
 MG -medium grain
 CG -coarse grain

JOINT SPACING
 VCJ -very close spacg
 CJ -close spacing
 MJ -medium spacing
 WJ -wide spacing
 VWJ -very wide spacng

JOINT ROUGHNESS
 SLJ -slickensided
 SJ -smooth
 RJ -rough

JOINT SHAPE
 CUR -curvilinear
 PLA -planar
 UND -undulating
 STE -stepped
 IRR -irregular

ROCK HARDNESS
 EHR -extremely hard rock
 VHR -very hard rock
 HR -hard rock
 MHR -medium hard rock
 SR -soft rock
 VSR -very soft rock

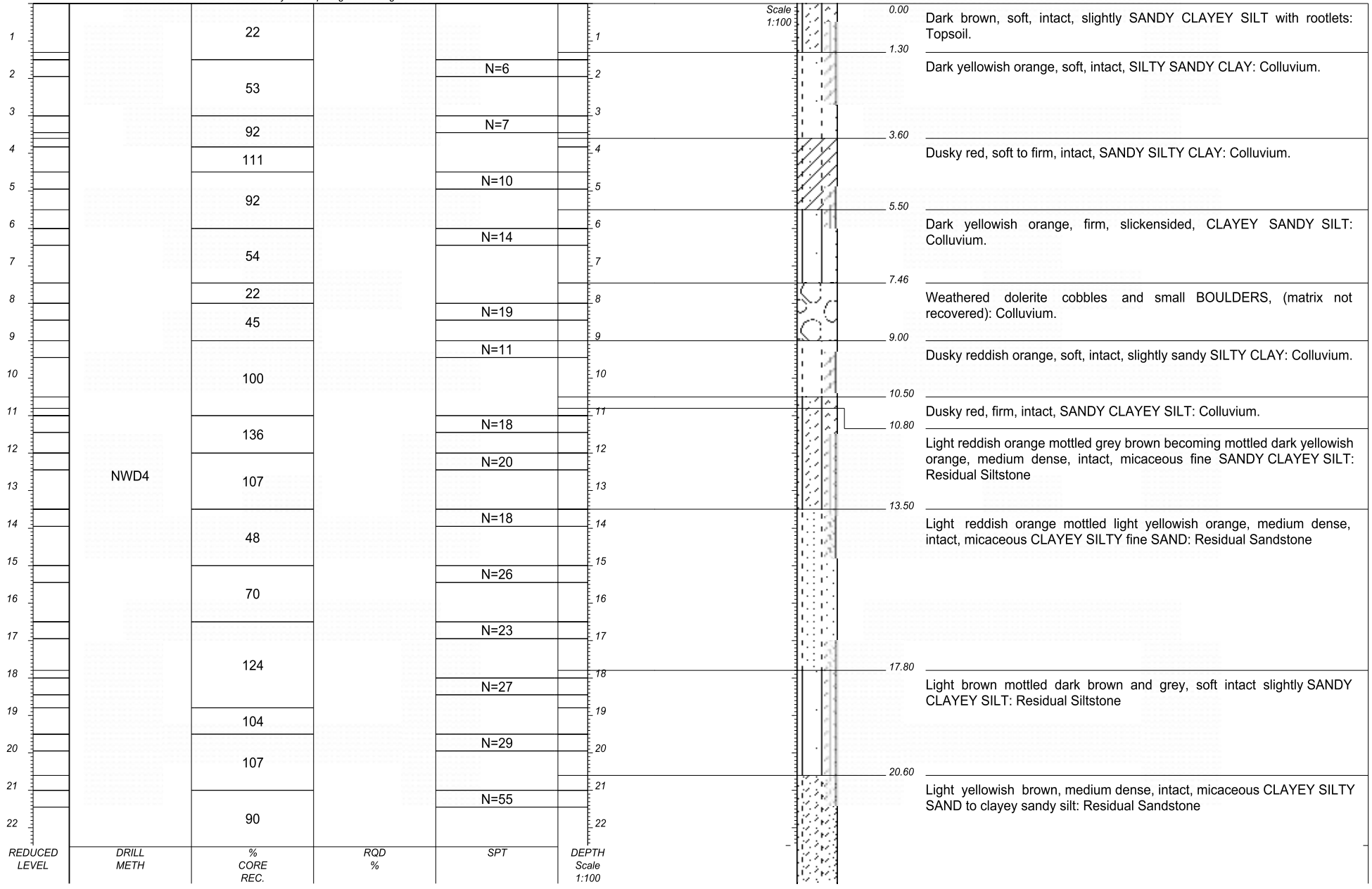


Cascades Development

HOLE No: BHV3/1

Sheet 1 of 2

JOB NUMBER: 000



NWD4

HOLE No: BHV3/1

Sheet 2 of 2

JOB NUMBER: 000

ROCK FABRIC
MF -massive
BF -bedded
FF -foliated
CF -cleaved
SF -schistose
GF -gneissose
LF -laminated

GRAIN SIZE
FG -fine grained
MG -medium grain
CG -coarse grain
JOINT SPACING
VCJ-very close spacg
CJ -close spacing
MJ -medium spacing
WJ -wide spacing
VWJ-very wide spacng

JOINT ROUGHNESS
SLJ-slickensided
SJ -smooth
RJ -rough
JOINT SHAPE
CUR-curved/linear
PLA-planar
UND-undulating
STE-stepped
IRR-irregular

ROCK HARDNESS
EHR-extremely hard rock
VHR-very hard rock
HR -hard rock
MHR-medium hard rock
SR -soft rock
VSR-very soft rock

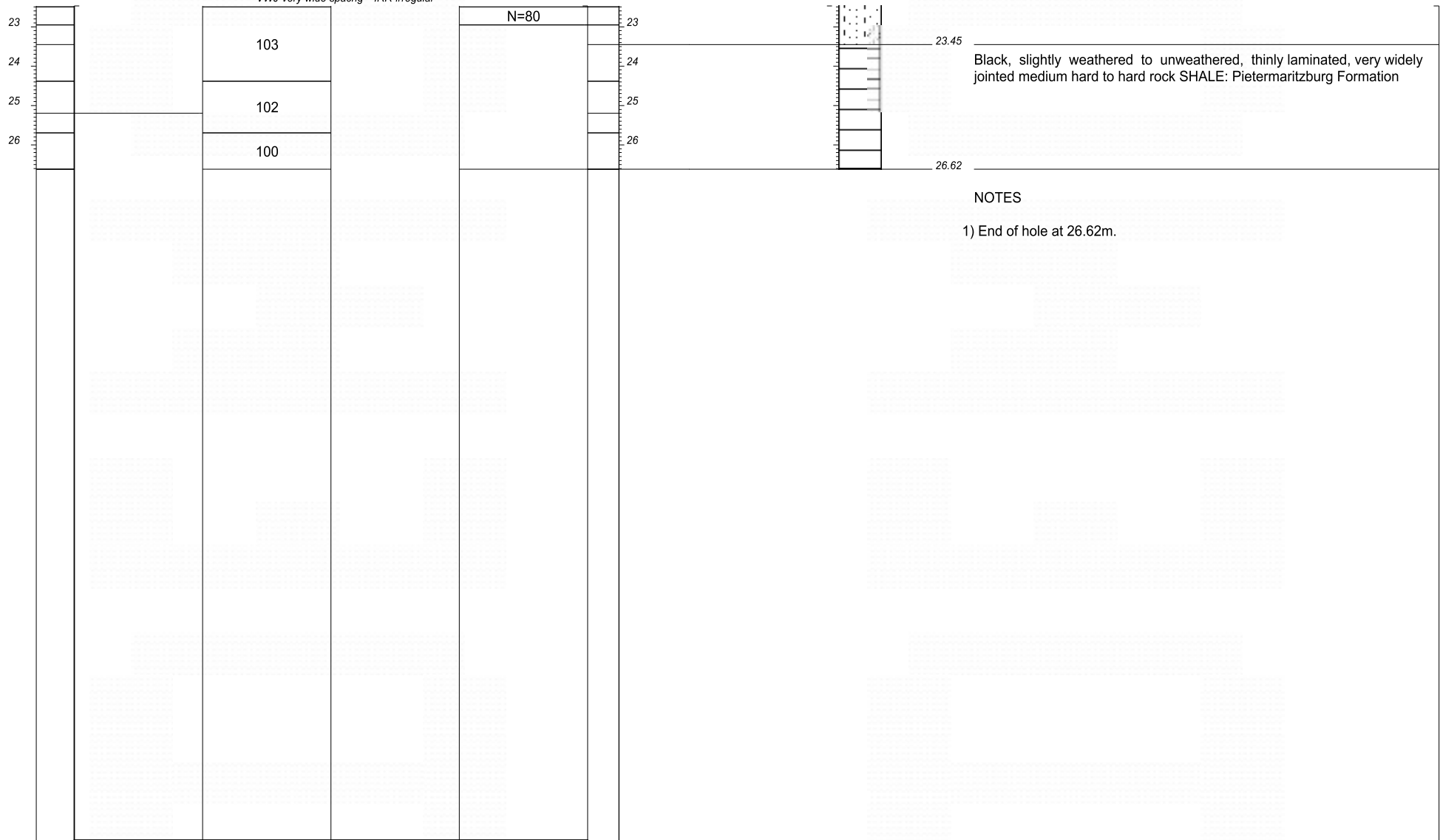


Cascades Development

HOLE No: BHV3/1

Sheet 2 of 2

JOB NUMBER: 000



Black, slightly weathered to unweathered, thinly laminated, very widely jointed medium hard to hard rock SHALE: Pietermaritzburg Formation

NOTES
1) End of hole at 26.62m.

REDUCED LEVEL	DRILL METH	% CORE REC.	RQD %	SPT	DEPTH Scale 1:100	CONTRACTOR : Continuous Core	INCLINATION : VERTICAL	ELEVATION :
						MACHINE : DRILLED BY : Louis Burger PROFILED BY : S. BOK	DIAM : NWD4 DATE : August 2005 DATE : Sept 2005	X-COORD : Y-COORD :
						TYPE SET BY : HDS SETUP FILE : A3.SET	DATE : 24/04/2017 11:54 TEXT : ..D\161055Village3BH's.txt	HOLE No: BHV3/1

HOLE No: BHV3/2
Sheet 1 of 2

JOB NUMBER: 000

ROCK FABRIC
MF -massive
BF -bedded
FF -foliated
CF -cleaved
SF -schistose
GF -gneissose
LF -laminated

GRAIN SIZE
FG -fine grained
MG -medium grain
CG -coarse grain

JOINT SPACING
VCJ -very close spacg
CJ -close spacing
MJ -medium spacing
WJ -wide spacing
VWJ -very wide spacng

JOINT ROUGHNESS
SLJ -slickensided
SJ -smooth
RJ -rough

JOINT SHAPE
CUR -curvilinear
PLA -planar
UND -undulating
STE -stepped
IRR -irregular

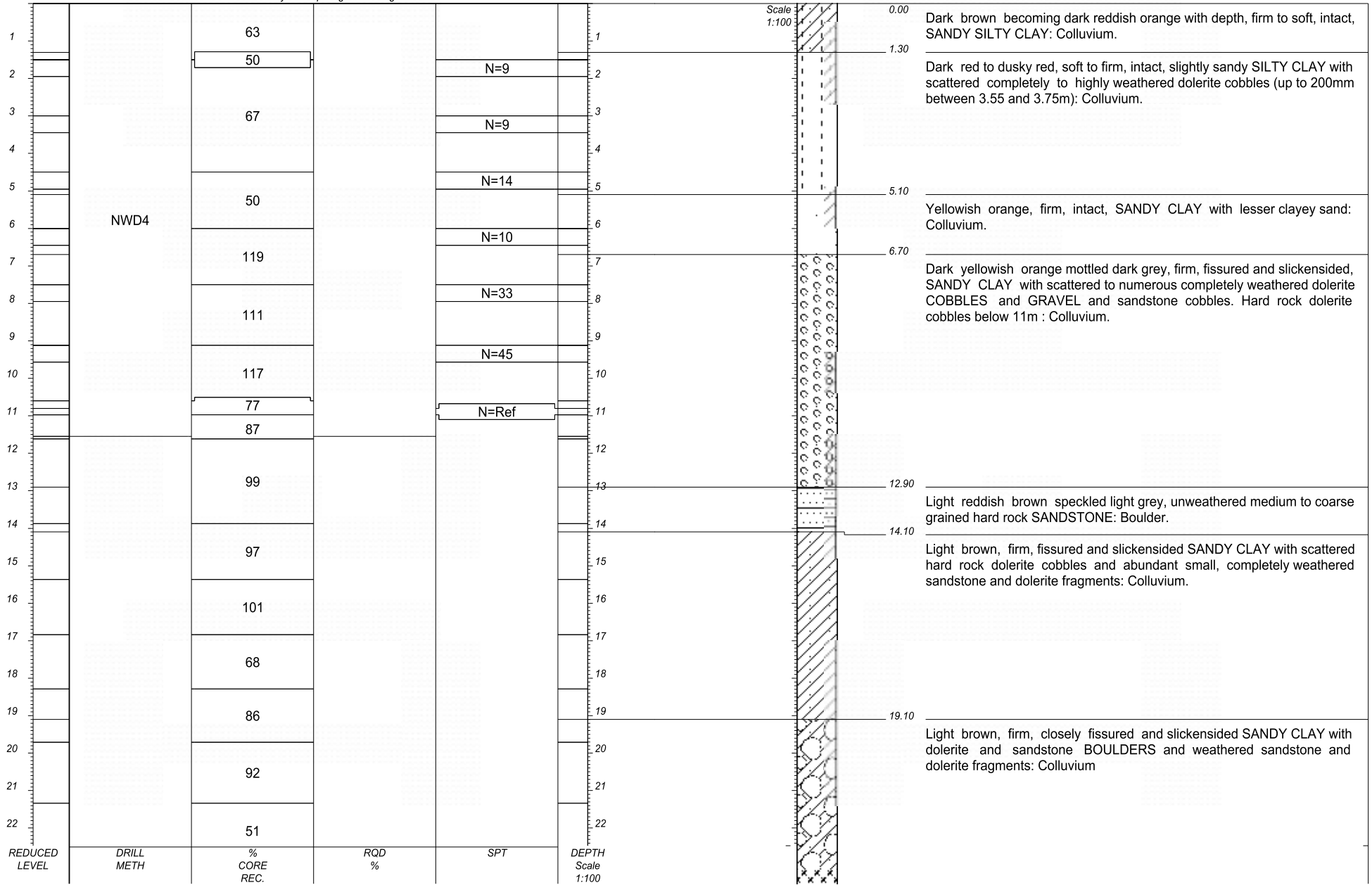
ROCK HARDNESS
EHR -extremely hard rock
VHR -very hard rock
HR -hard rock
MHR -medium hard rock
SR -soft rock
VSR -very soft rock



Cascades Development

HOLE No: BHV3/2
Sheet 1 of 2

JOB NUMBER: 000



HOLE No: BHV3/2

Sheet 2 of 2

JOB NUMBER: 000

ROCK FABRIC
MF -massive
BF -bedded
FF -foliated
CF -cleaved
SF -schistose
GF -gneissose
LF -laminated

GRAIN SIZE
FG -fine grained
MG -medium grain
CG -coarse grain

JOINT SPACING
VCJ-very close spacg
CJ -close spacing
MJ -medium spacing
WJ -wide spacing
VWJ-very wide spacng

JOINT ROUGHNESS
SLJ-slickensided
SJ -smooth
RJ -rough

JOINT SHAPE
CUR-curvilinear
PLA-planar
UND-undulating
STE-stepped
IRR-irregular

ROCK HARDNESS
EHR-extremely hard rock
VHR-very hard rock
HR -hard rock
MHR-medium hard rock
SR -soft rock
VSR-very soft rock

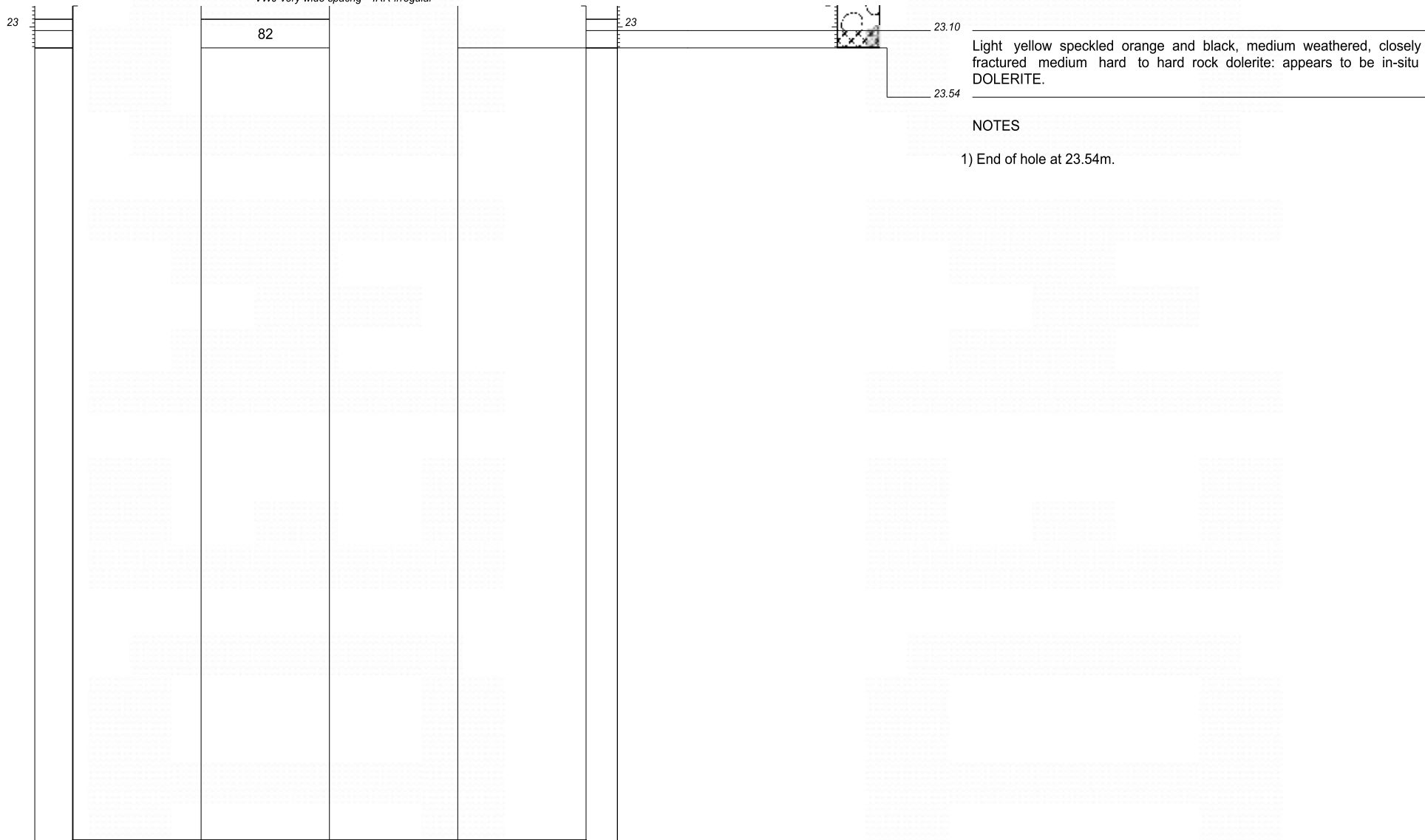


Cascades Development

HOLE No: BHV3/2

Sheet 2 of 2

JOB NUMBER: 000



REDUCED LEVEL	DRILL METH	% CORE REC.	RQD %	SPT	DEPTH Scale 1:100	CONTRACTOR : Continuous Core	INCLINATION :	ELEVATION :
						MACHINE : DRILLED BY : Louis Burger PROFILED BY : S. BOK	DIAM : NWD4 DATE : August 2005 DATE : Sept 2005	X-COORD : Y-COORD :
						TYPE SET BY : HDS SETUP FILE : A3.SET	DATE : 24/04/2017 11:54 TEXT : ..D\161055Village3BH's.txt	

HOLE No: BHV3/2

HOLE No: BHV3/3
Sheet 1 of 2

JOB NUMBER: 000

ROCK FABRIC
MF -massive
BF -bedded
FF -foliated
CF -cleaved
SF -schistose
GF -gneissose
LF -laminated

GRAIN SIZE
FG -fine grained
MG -medium grain
CG -coarse grain

JOINT SPACING
VCJ -very close spacg
CJ -close spacing
MJ -medium spacing
WJ -wide spacing
VWJ -very wide spacng

JOINT ROUGHNESS
SLJ -slickensided
SJ -smooth
RJ -rough

JOINT SHAPE
CUR -curvilinear
PLA -planar
UND -undulating
STE -stepped
IRR -irregular

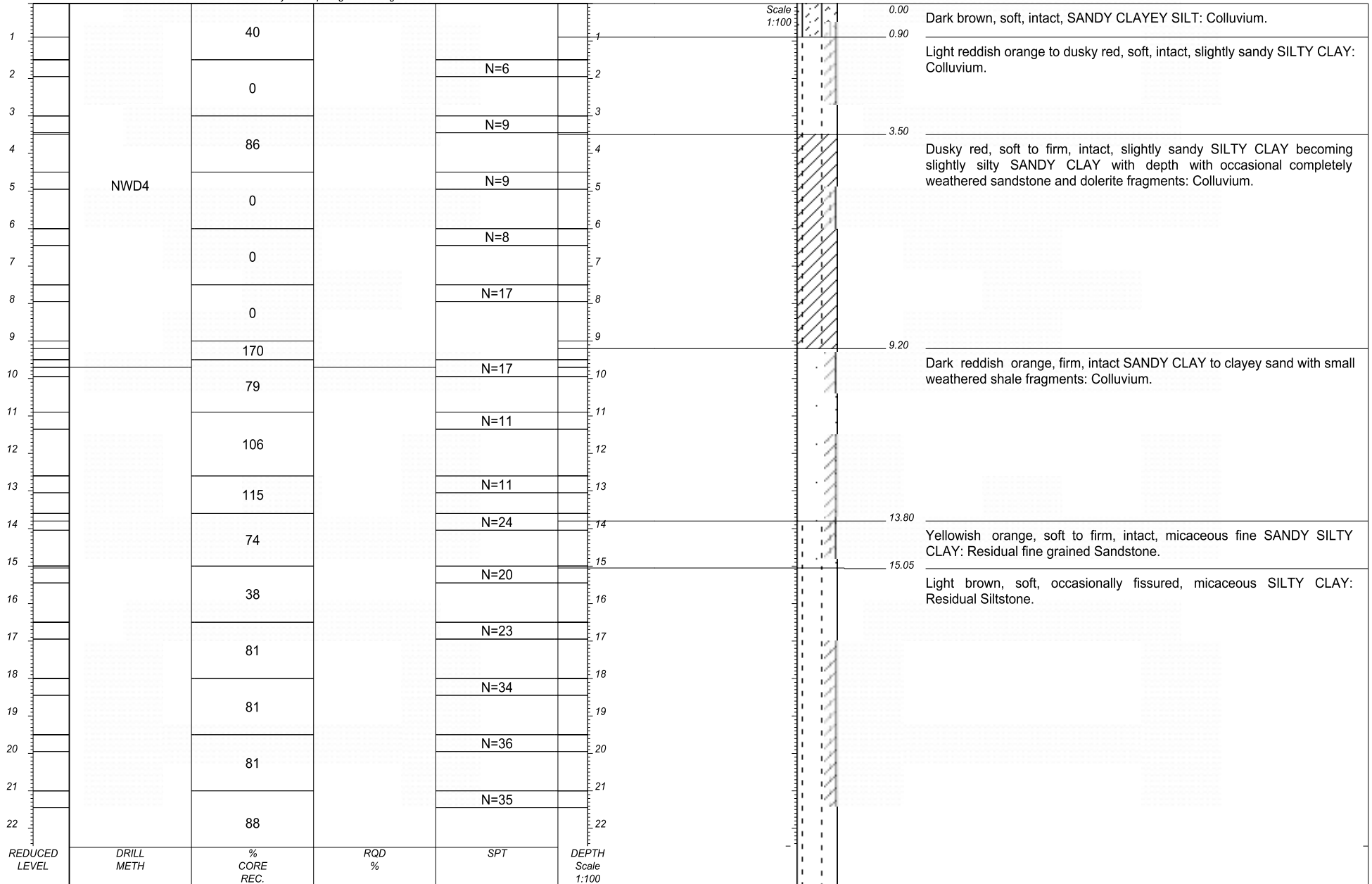
ROCK HARDNESS
EHR -extremely hard rock
VHR -very hard rock
HR -hard rock
MHR -medium hard rock
SR -soft rock
VSR -very soft rock



Cascades Development

HOLE No: BHV3/3
Sheet 1 of 2

JOB NUMBER: 000



HOLE No: BHV3/3

Sheet 2 of 2

JOB NUMBER: 000

ROCK FABRIC
MF -massive
BF -bedded
FF -foliated
CF -cleaved
SF -schistose
GF -gneissose
LF -laminated

GRAIN SIZE
FG -fine grained
MG -medium grain
CG -coarse grain
JOINT SPACING
VCJ-very close spacg
CJ -close spacing
MJ -medium spacing
WJ -wide spacing
VWJ-very wide spacng

JOINT ROUGHNESS
SLJ-slickensided
SJ -smooth
RJ -rough
JOINT SHAPE
CUR-curved/linear
PLA-planar
UND-undulating
STE-stepped
IRR-irregular

ROCK HARDNESS
EHR-extremely hard rock
VHR-very hard rock
HR -hard rock
MHR-medium hard rock
SR -soft rock
VSR-very soft rock

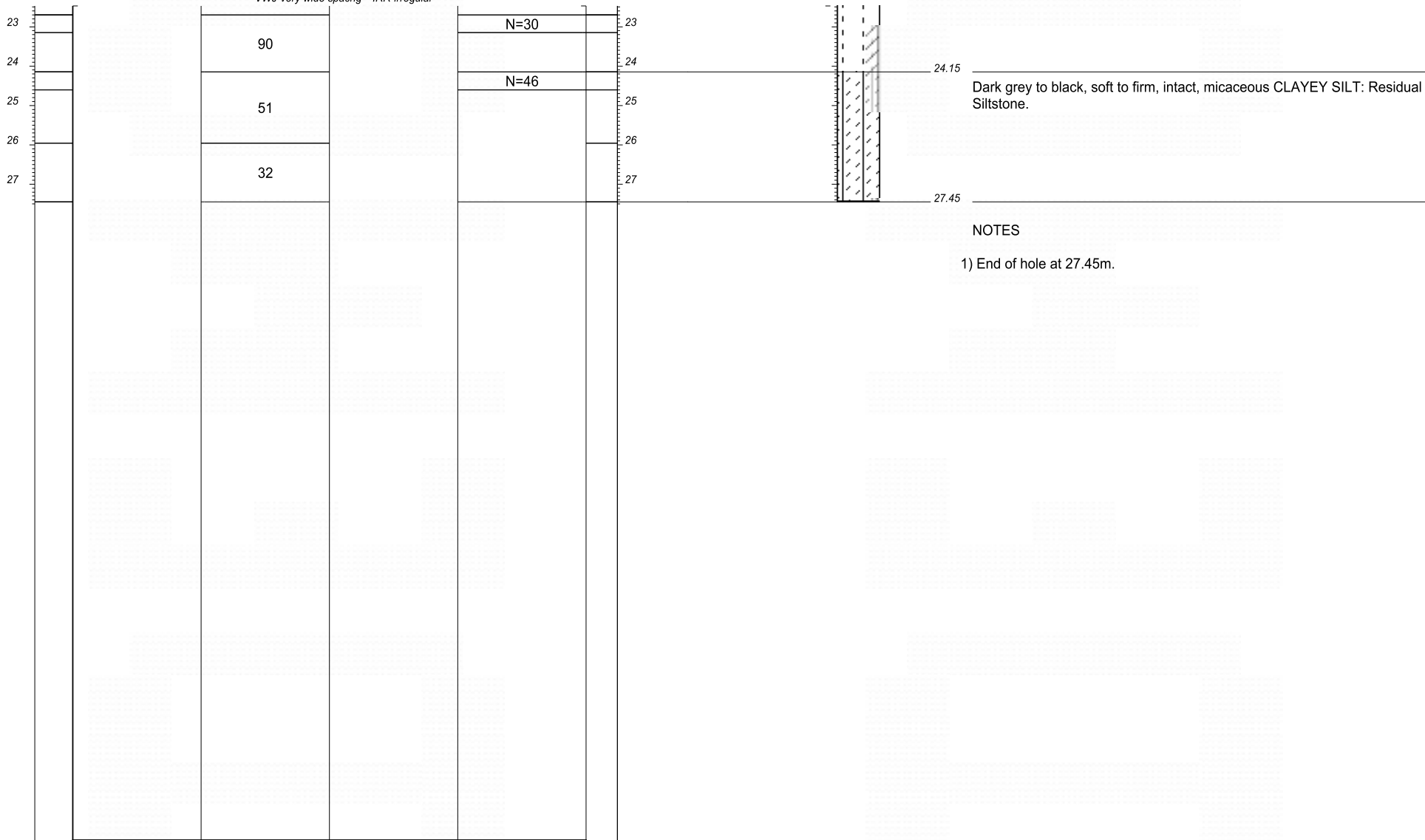


Cascades Development

HOLE No: BHV3/3

Sheet 2 of 2

JOB NUMBER: 000



NOTES
1) End of hole at 27.45m.

CONTRACTOR : Continuous Core
 MACHINE :
 DRILLED BY : Louis Burger
 PROFILED BY : S. BOK
 TYPE SET BY : HDS
 SETUP FILE : A3.SET

INCLINATION :
 DIAM : NWD4
 DATE : August 2005
 DATE : Sept 2005
 DATE : 24/04/2017 11:54
 TEXT : ..D\161055Village3BH's.txt

ELEVATION :
 X-COORD :
 Y-COORD :

HOLE No: BHV3/3

HOLE No: BHV3/4

Sheet 1 of 1

JOB NUMBER: 000

ROCK FABRIC
MF -massive
BF -bedded
FF -foliated
CF -cleaved
SF -schistose
GF -gneissose
LF -laminated

GRAIN SIZE
FG -fine grained
MG -medium grain
CG -coarse grain
JOINT SPACING
VCJ -very close spacg
CJ -close spacing
MJ -medium spacing
WJ -wide spacing
VWJ -very wide spacng

JOINT ROUGHNESS
SLJ -slickensided
SJ -smooth
RJ -rough
JOINT SHAPE
CUR -curvilinear
PLA -planar
UND -undulating
STE -stepped
IRR -irregular

ROCK HARDNESS
EHR -extremely hard rock
VHR -very hard rock
HR -hard rock
MHR -medium hard rock
SR -soft rock
VSR -very soft rock

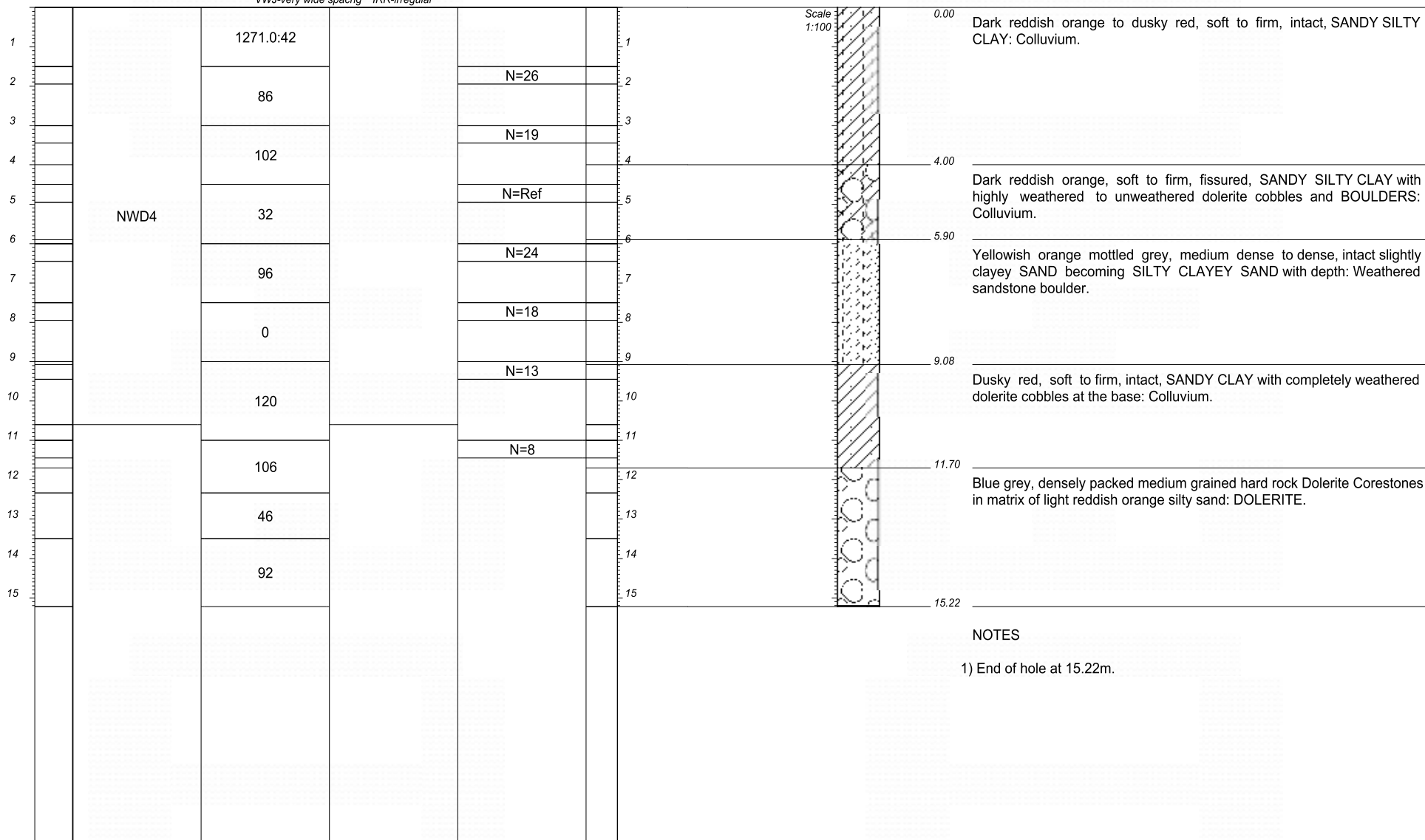


Cascades Development

HOLE No: BHV3/4

Sheet 1 of 1

JOB NUMBER: 000



NOTES
1) End of hole at 15.22m.

CONTRACTOR : Continuous Core	INCLINATION :	ELEVATION :
MACHINE :	DIAM : NWD4	X-COORD :
DRILLED BY : Louis Burger	DATE : August 2005	Y-COORD :
PROFILED BY : S. BOK	DATE : Sept 2005	
TYPE SET BY : HDS	DATE : 24/04/2017 11:54	
SETUP FILE : A3.SET	TEXT : ..D\161055Village3BH's.txt	

HOLE No: BHV3/4

HOLE No: BHV3/5
Sheet 1 of 2

JOB NUMBER: 000

ROCK FABRIC
MF -massive
BF -bedded
FF -foliated
CF -cleaved
SF -schistose
GF -gneissose
LF -laminated

GRAIN SIZE
FG -fine grained
MG -medium grain
CG -coarse grain

JOINT SPACING
VCJ -very close spacg
CJ -close spacing
MJ -medium spacing
WJ -wide spacing
VWJ -very wide spacng

JOINT ROUGHNESS
SLJ -slickensided
SJ -smooth
RJ -rough

JOINT SHAPE
CUR -curvilinear
PLA -planar
UND -undulating
STE -stepped
IRR -irregular

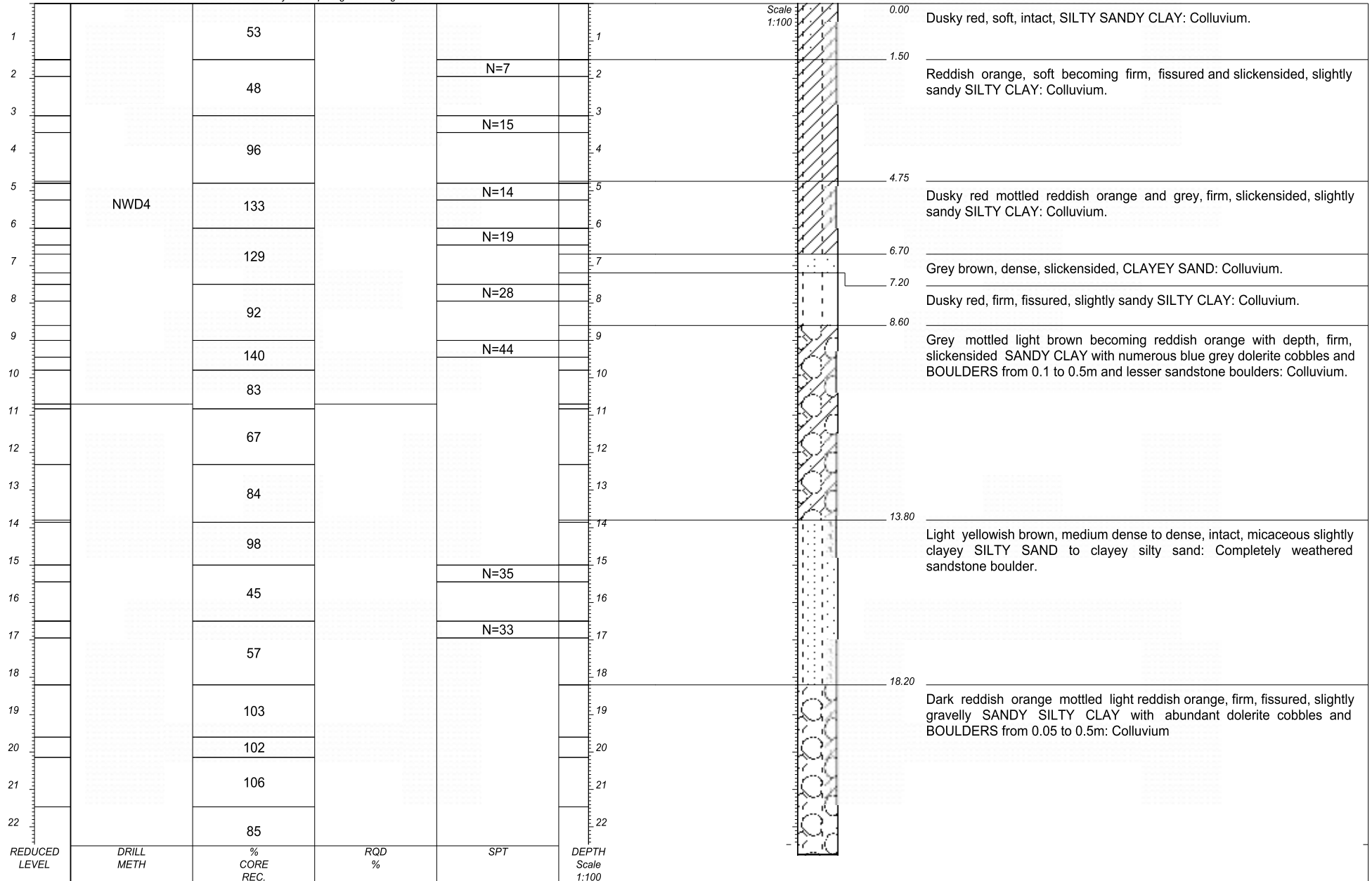
ROCK HARDNESS
EHR -extremely hard rock
VHR -very hard rock
HR -hard rock
MHR -medium hard rock
SR -soft rock
VSR -very soft rock



Cascades Development

HOLE No: BHV3/5
Sheet 1 of 2

JOB NUMBER: 000



HOLE No: BHV3/5

Sheet 2 of 2

JOB NUMBER: 000

ROCK FABRIC
 MF -massive
 BF -bedded
 FF -foliated
 CF -cleaved
 SF -schistose
 GF -gneissose
 LF -laminated

GRAIN SIZE
 FG -fine grained
 MG -medium grain
 CG -coarse grain

JOINT SPACING
 VCJ-very close spacg
 CJ -close spacing
 MJ -medium spacing
 WJ -wide spacing
 VWJ-very wide spacng

JOINT ROUGHNESS
 SLJ-slickensided
 SJ -smooth
 RJ -rough

JOINT SHAPE
 CUR-curved/linear
 PLA-planar
 UND-undulating
 STE-stepped
 IRR-irregular

ROCK HARDNESS
 EHR-extremely hard rock
 VHR-very hard rock
 HR -hard rock
 MHR-medium hard rock
 SR -soft rock
 VSR-very soft rock



Cascades Development

HOLE No: BHV3/5

Sheet 2 of 2

JOB NUMBER: 000

22.75

NOTES

1) End of hole at 22.75m.

REDUCED LEVEL

DRILL METH

% CORE REC.

RQD %

SPT

DEPTH Scale 1:100

CONTRACTOR : Continuous Core

MACHINE :
DRILLED BY : Louis Burger
PROFILED BY : S. BOK

TYPE SET BY : HDS
SETUP FILE : A3.SET

INCLINATION :

DIAM : NWD4
DATE : August 2005
DATE : Sept 2005

DATE : 24/04/2017 11:54
TEXT : ..D\161055Village3BH's.txt

ELEVATION :

X-COORD :
Y-COORD :

HOLE No: BHV3/5

	BOULDERS	{SA01}
	GRAVEL	{SA02}
	SAND	{SA04}
	SANDY	{SA05}
	SILT	{SA06}
	SILTY	{SA07}
	CLAY	{SA08}
	CLAYEY	{SA09}
	SANDSTONE	{SA11}
	SHALE	{SA12}
	DOLERITE	{SA18}{SA42}

CONTRACTOR :
MACHINE :
DRILLED BY :
PROFILED BY :
TYPE SET BY : HDS
SETUP FILE : A3.SET

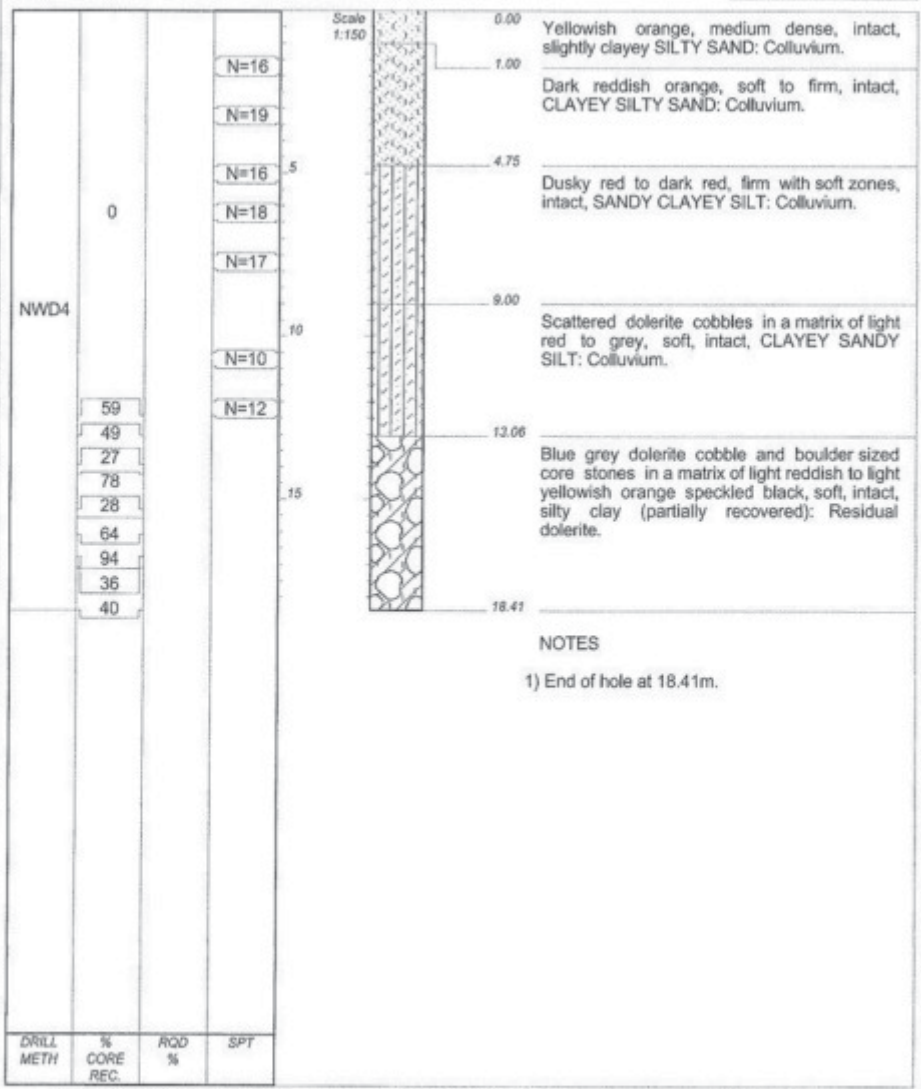
INCLINATION :
DIAM :
DATE :
DATE :
DATE : 24/04/2017 11:54
TEXT : ..D\161055Village3BH's.txt

ELEVATION :
X-COORD :
Y-COORD :
LEGEND
SUMMARY OF SYMBOLS

LOWER NATIONAL PARK DEVELOPMENT

BHV4/1

HOLE No: BHV4/1
Sheet 1 of 1
JOB NUMBER: 16-1055



NOTES
1) End of hole at 18.41m.

DRILL METH	% CORE REC.	RQD %	SPT

CONTRACTOR: Continuous Core
MACHINE:
DRILLED BY: Louis Burger
PROFIED BY: S. BOK
TYPE SET BY: S. Bok
SETUP FILE: BH-TERR4.SET

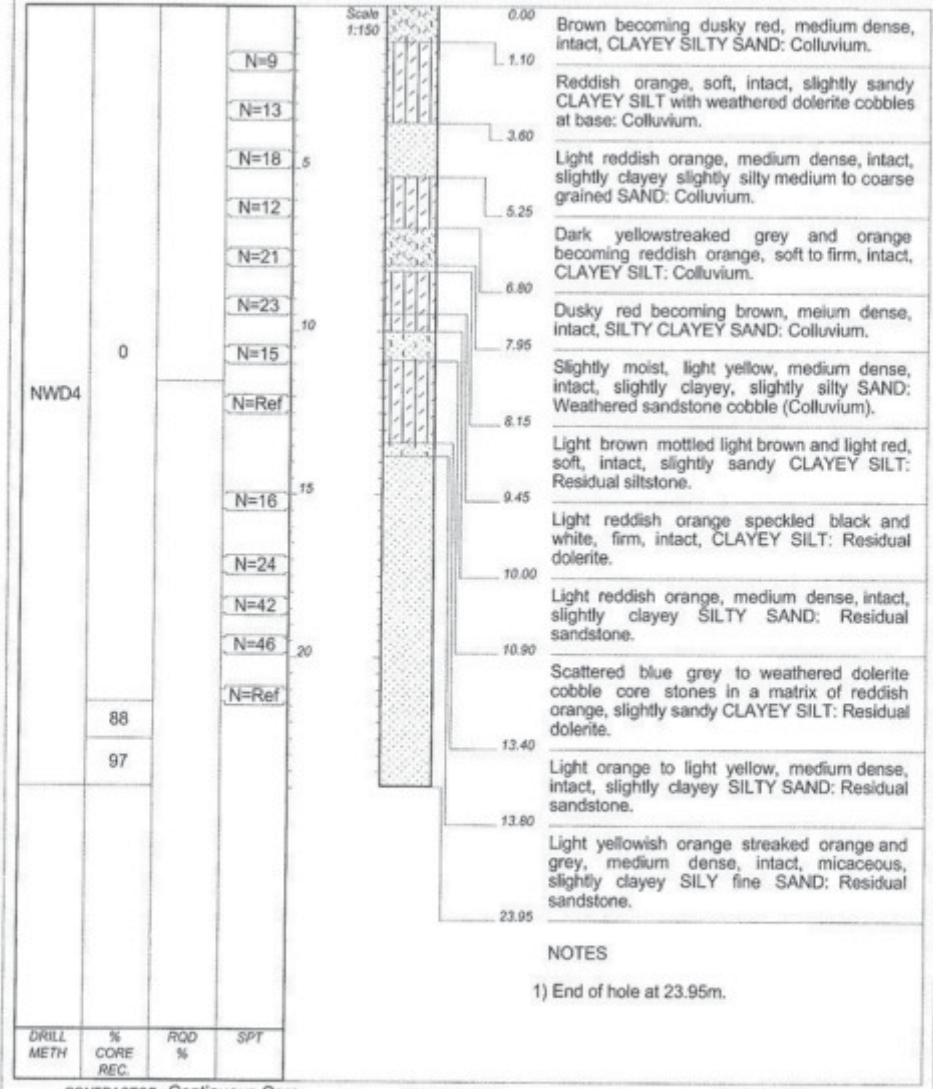
INCLINATION: VERTICAL
DIAM: NWD4
DATE: September 2005
DATE: Oct 2005
DATE: 14/11/05 08:25
TEXT: ..C:\DOTPLOT\16-105-7.TXT

ELEVATION:
X-COORD:
Y-COORD:

HOLE No: BHV4/1

BHV4/2

HOLE No: BHV4/2
Sheet 1 of 1
JOB NUMBER: 16-1055



NOTES
1) End of hole at 23.95m.

DRILL METH	% CORE REC.	RQD %	SPT

CONTRACTOR: Continuous Core
MACHINE:
DRILLED BY: Louis Burger
PROFIED BY: S. BOK
TYPE SET BY: S. Bok
SETUP FILE: BH-TERR4.SET

INCLINATION: VERTICAL
DIAM: NWD4
DATE: September 2005
DATE: Oct 2005
DATE: 14/11/05 08:25
TEXT: ..C:\DOTPLOT\16-105-7.TXT

ELEVATION:
X-COORD:
Y-COORD:

HOLE No: BHV4/2

HOLE No: BHV4/3

Sheet 1 of 1

JOB NUMBER: 000

ROCK FABRIC
MF -massive
BF -bedded
FF -foliated
CF -cleaved
SF -schistose
GF -gneissose
LF -laminated

GRAIN SIZE
FG -fine grained
MG -medium grain
CG -coarse grain

JOINT SPACING
VCJ-very close spacg
CJ -close spacing
MJ -medium spacing
WJ -wide spacing
VWJ-very wide spacng

JOINT ROUGHNESS
SLJ-slickensided
SJ -smooth
RJ -rough

JOINT SHAPE
CUR-curved/linear
PLA-planar
UND-undulating
STE-stepped
IRR-irregular

ROCK HARDNESS
EHR-extremely hard rock
VHR-very hard rock
HR -hard rock
MHR-medium hard rock
SR -soft rock
VSR-very soft rock

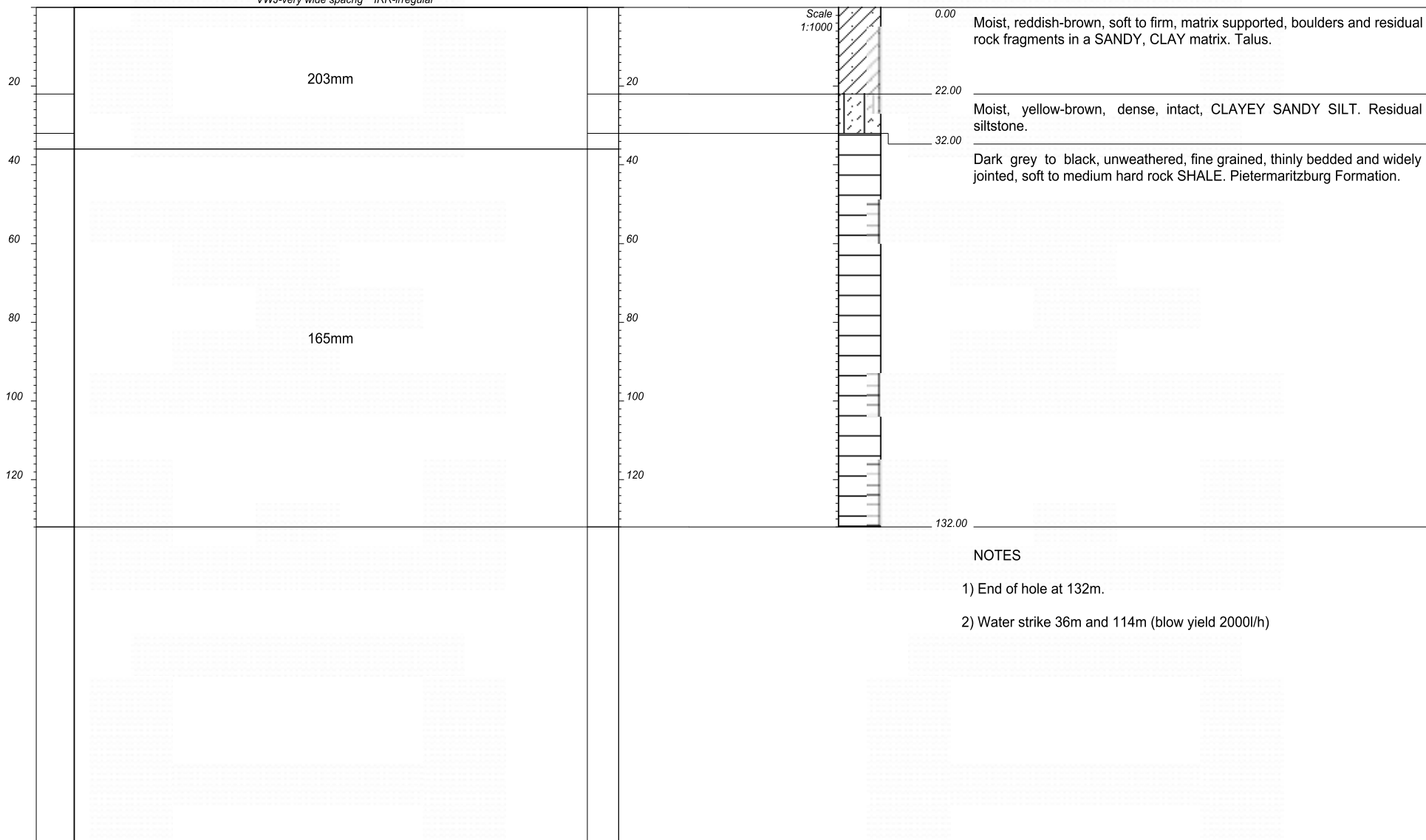


Lower National Park Development

HOLE No: BHV4/3

Sheet 1 of 1

JOB NUMBER: 000



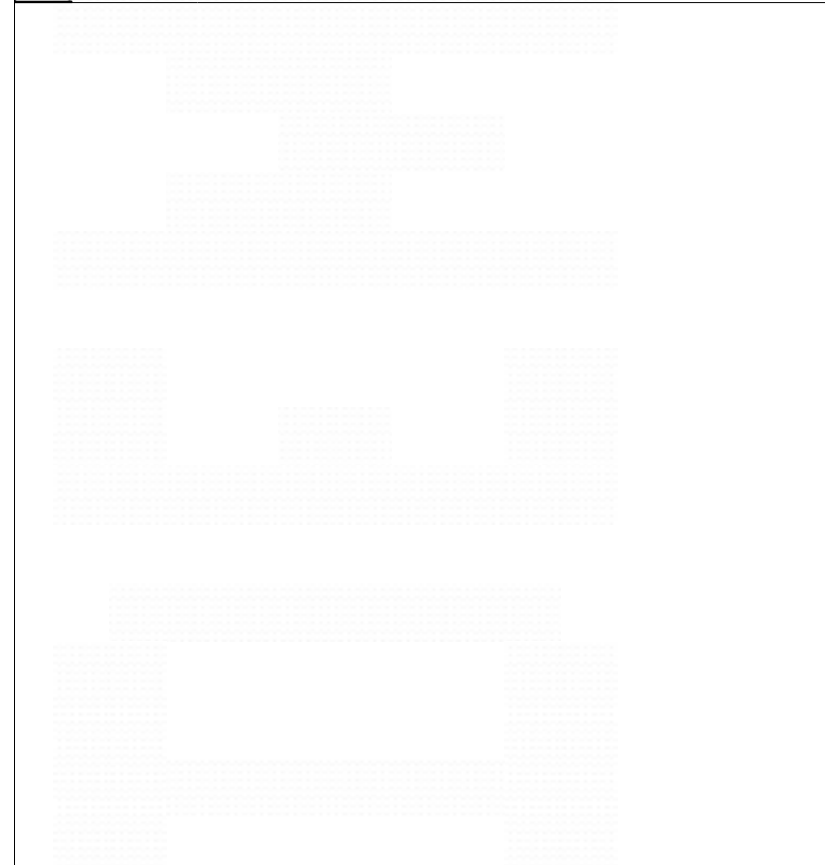
CONTRACTOR :
MACHINE :
DRILLED BY :
PROFIED BY : K. Singh
TYPE SET BY : K.Singh
SETUP FILE : A3.SET

INCLINATION : VERTICAL
DIAM : 203
DATE : 24 May 2016
DATE : June 2016
DATE : 24/04/2017 12:01
TEXT : ..res\ANNEX\BLNPD\BH43.txt

ELEVATION :
X-COORD :
Y-COORD :

HOLE No: BHV4/3

	SANDY	{SA05}
	SILT	{SA06}
	CLAY	{SA08}
	CLAYEY	{SA09}
	SHALE	{SA12}



CONTRACTOR :
MACHINE :
DRILLED BY :
PROFILED BY :

TYPE SET BY : K.Singh
SETUP FILE : A3.SET

INCLINATION :
DIAM :
DATE :
DATE :

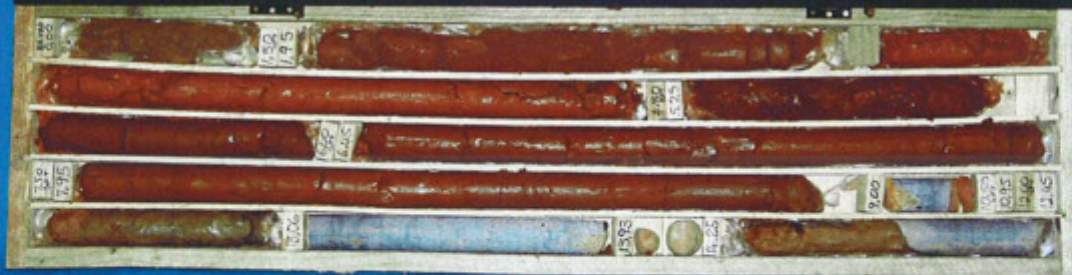
DATE : 24/04/2017 12:01
TEXT : ..res\ANNEXB\LNPD\BH43.txt

ELEVATION :
X-COORD :
Y-COORD :

Borehole: BHV4/1

Box: 1 of 2

Depth: 0.00-15.32m



Borehole: BHV4/1

Box: 2 of 2

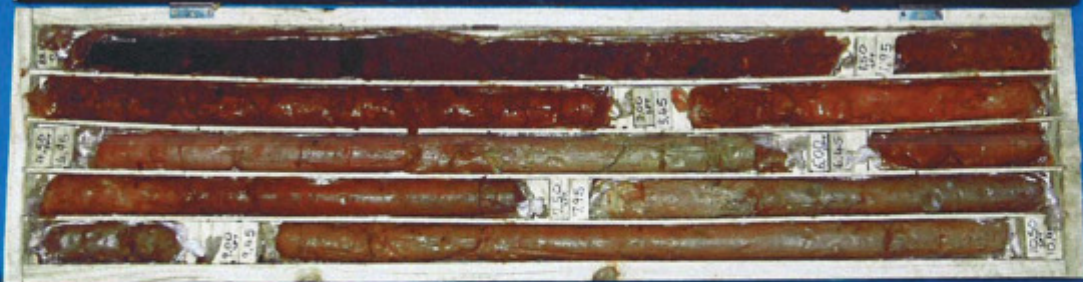
Depth: 15.32-18.41m



Borehole: BHV4/2

Box: 1 of 3

Depth: 0.00-10.95m



Borehole: BHV4/2

Box: 2 of 3

Depth: 10.95-22.51m



Borehole: BHV4/2

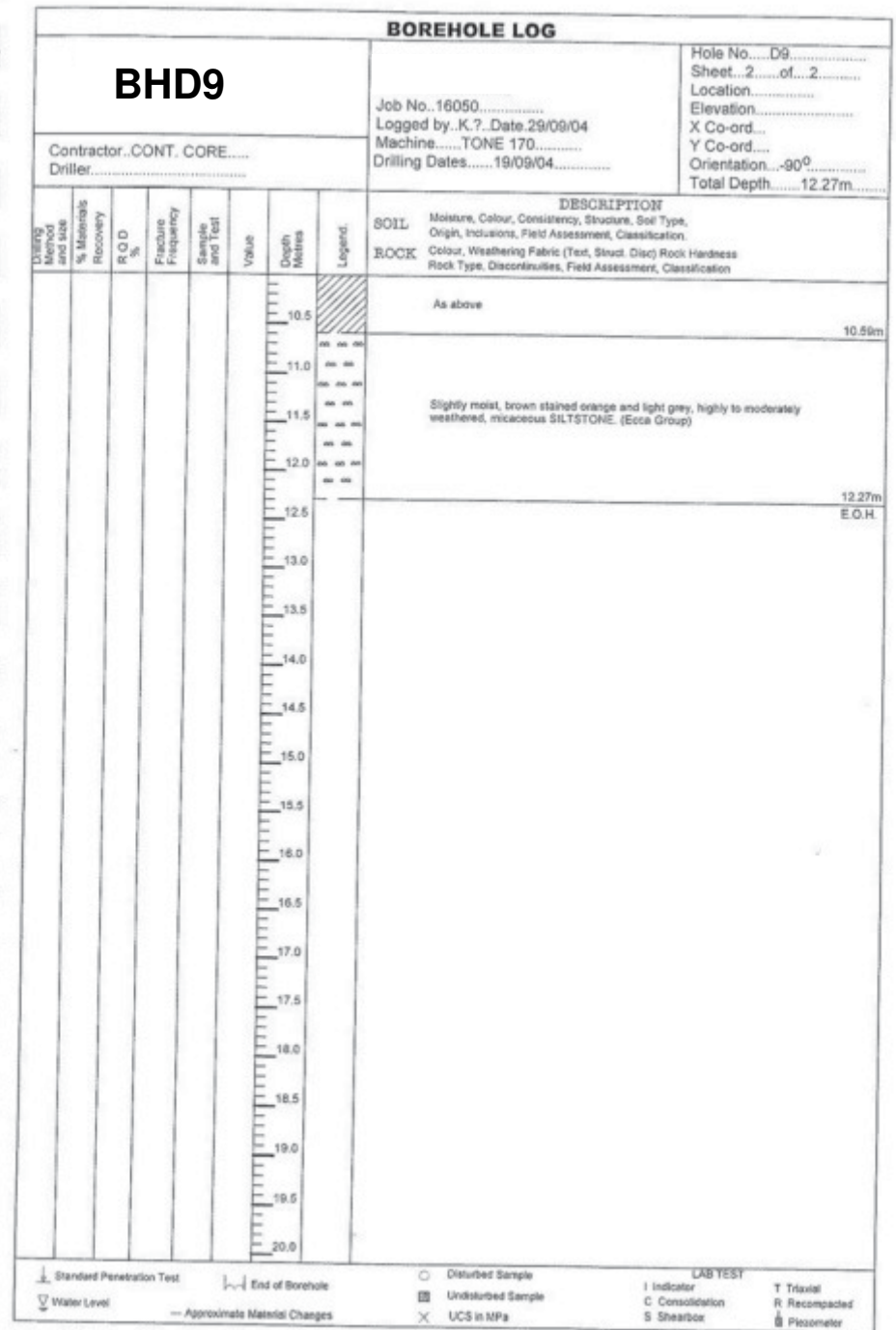
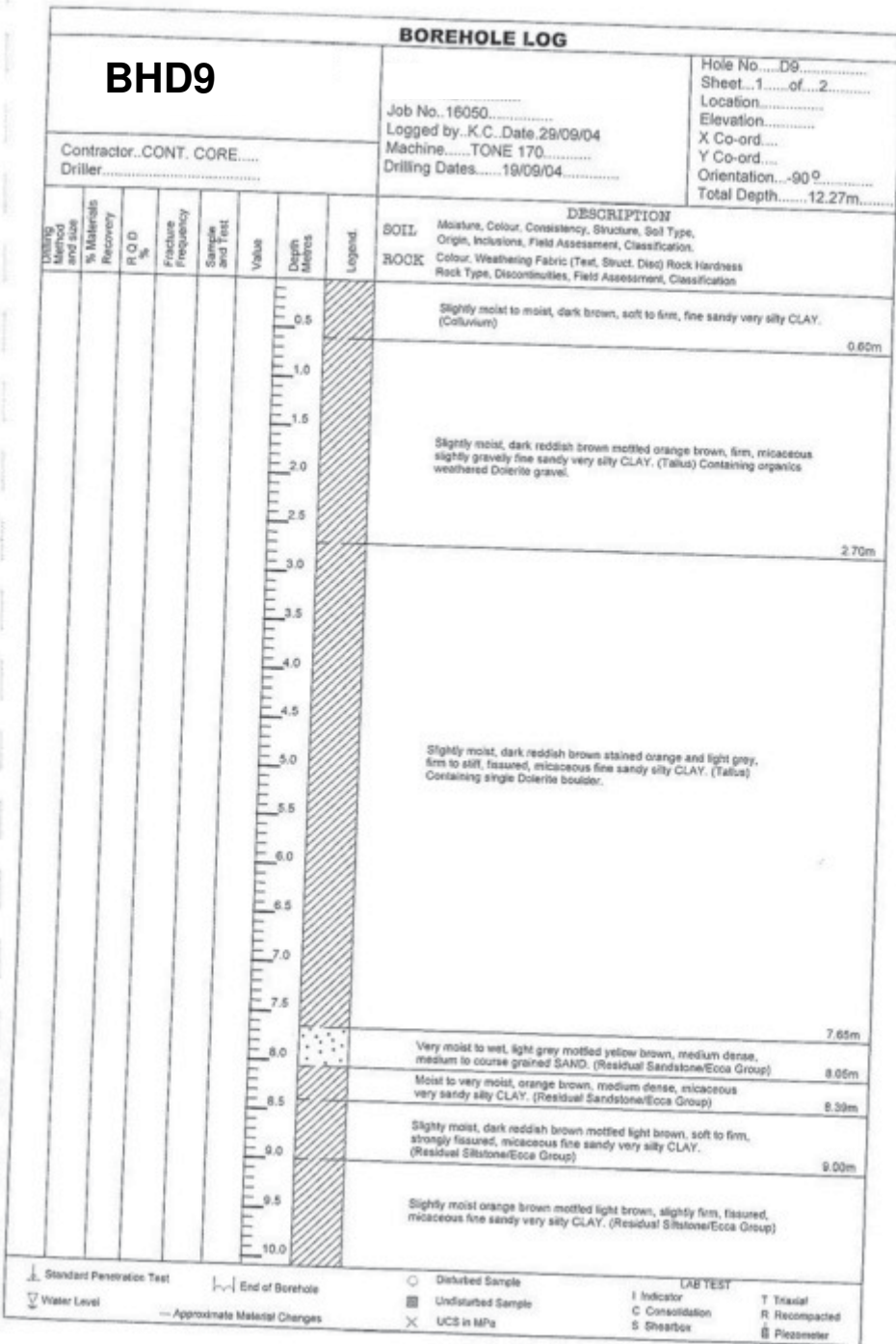
Box: 3 of 3

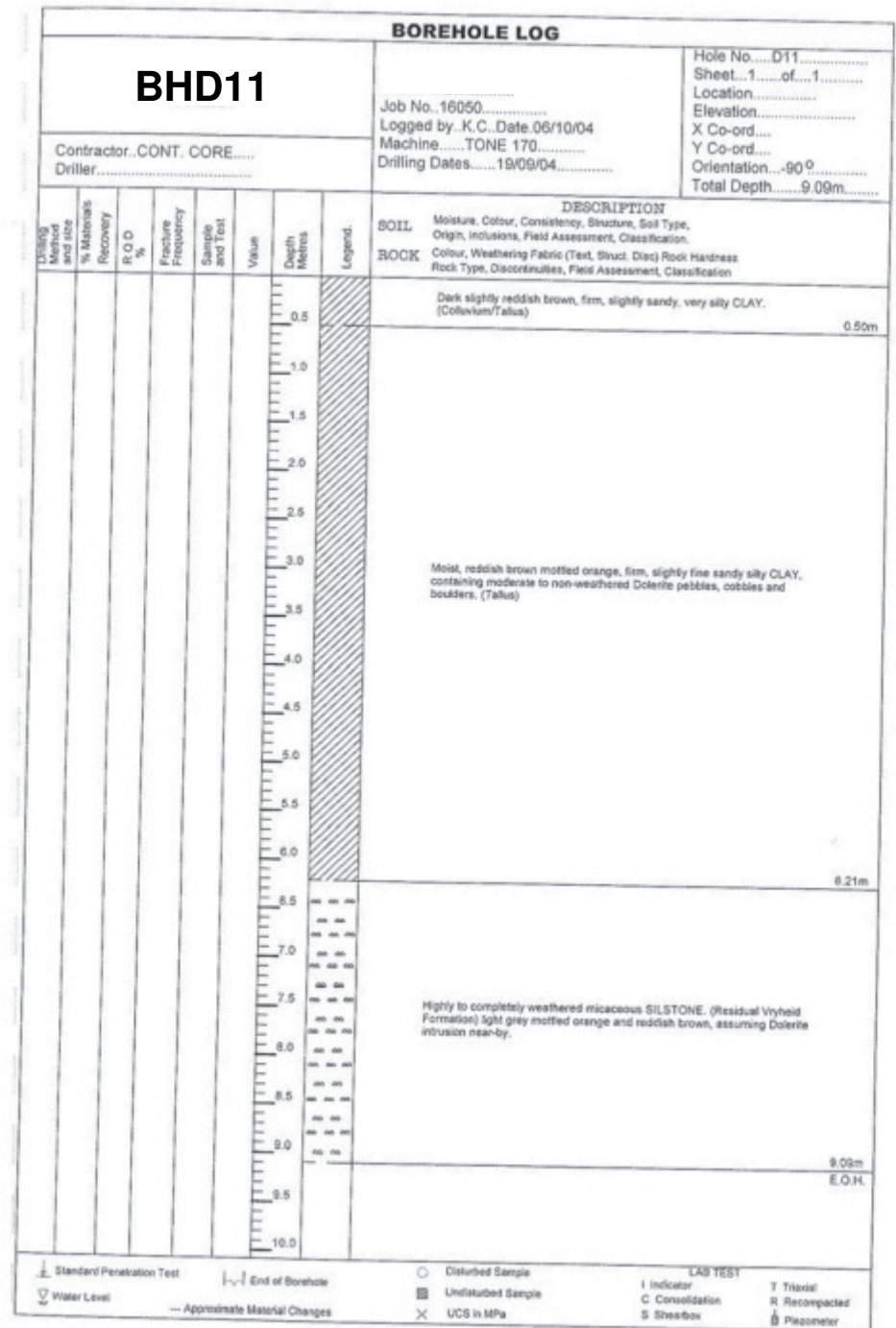
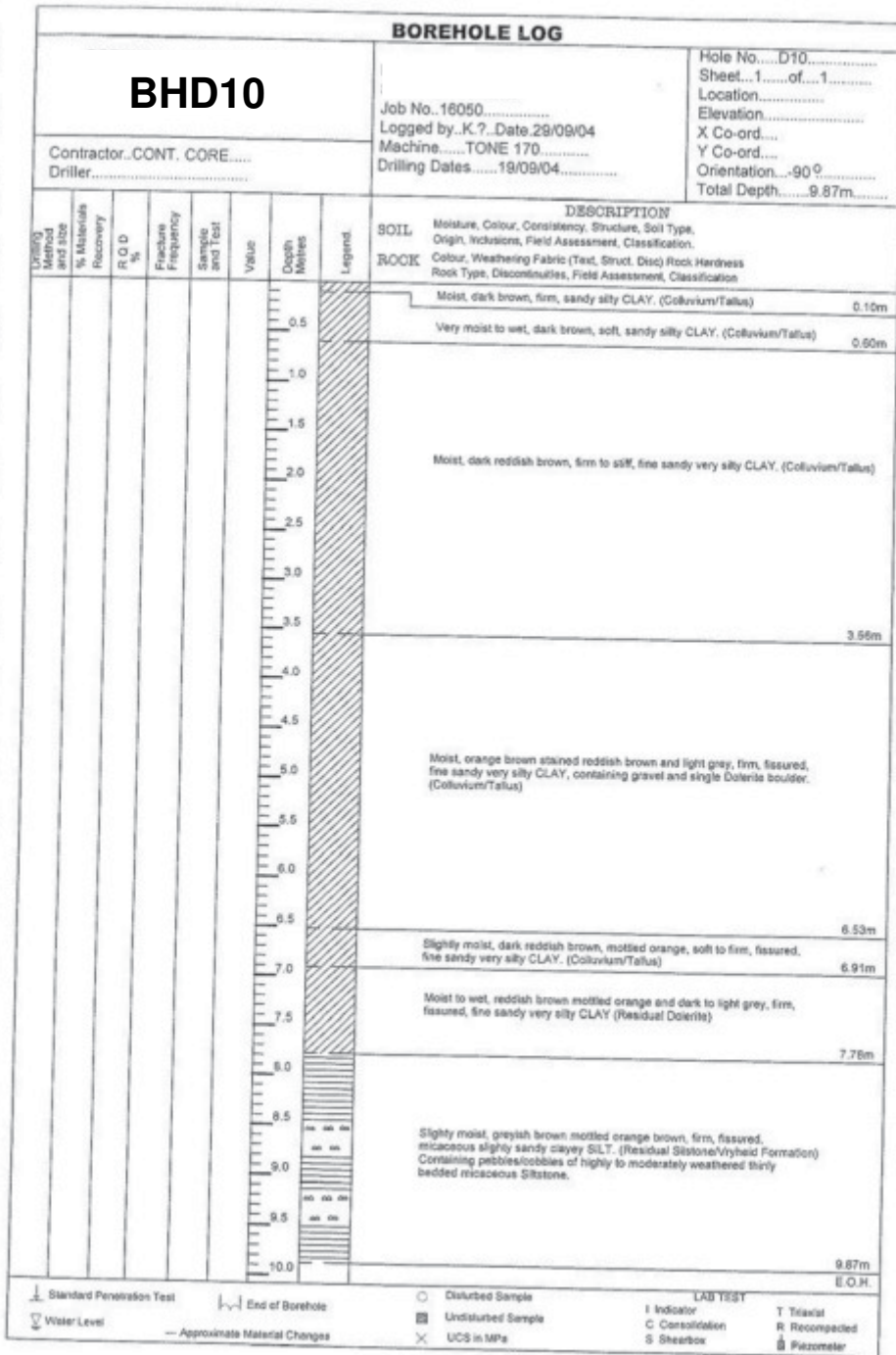
Depth: 22.51-23.95m

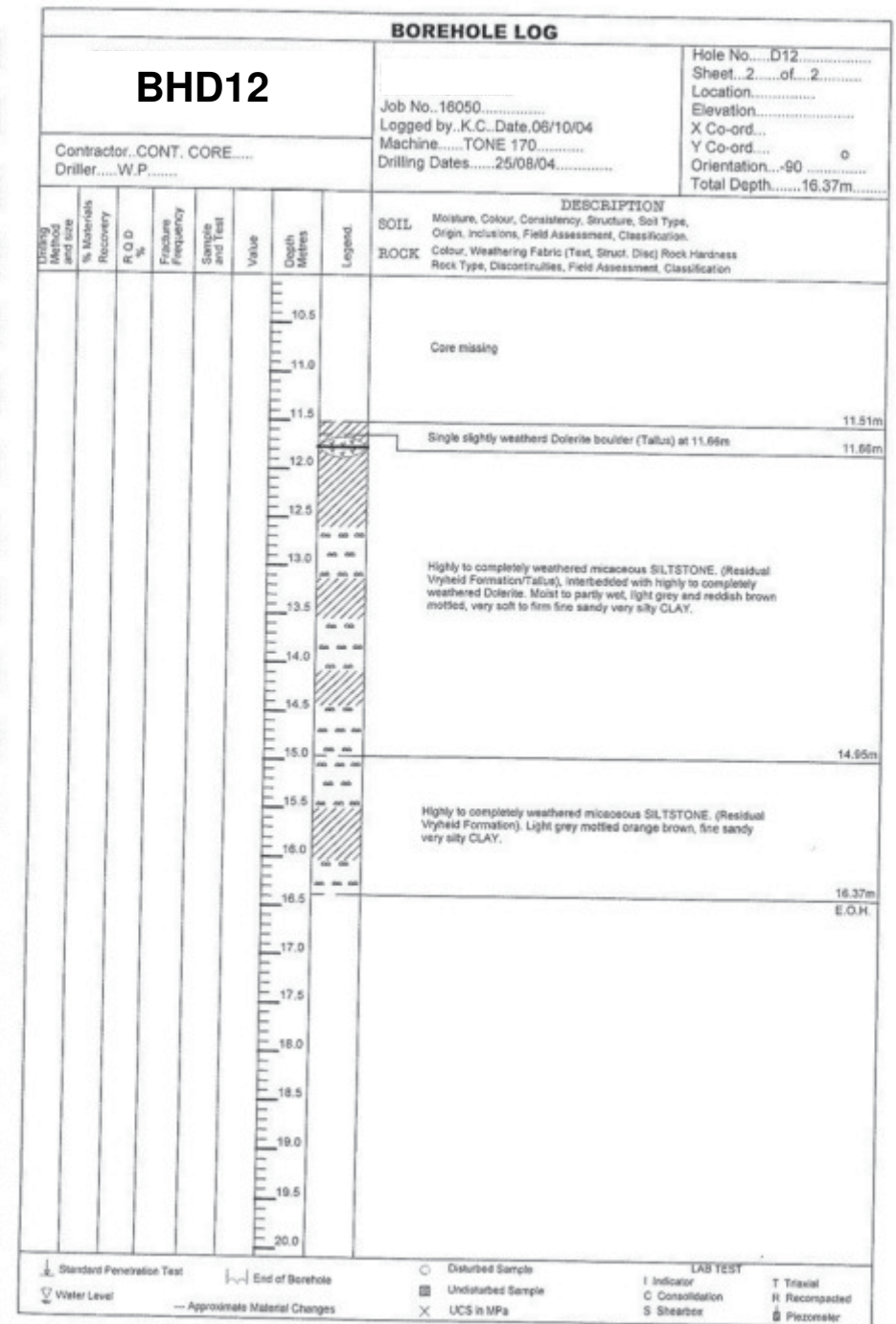


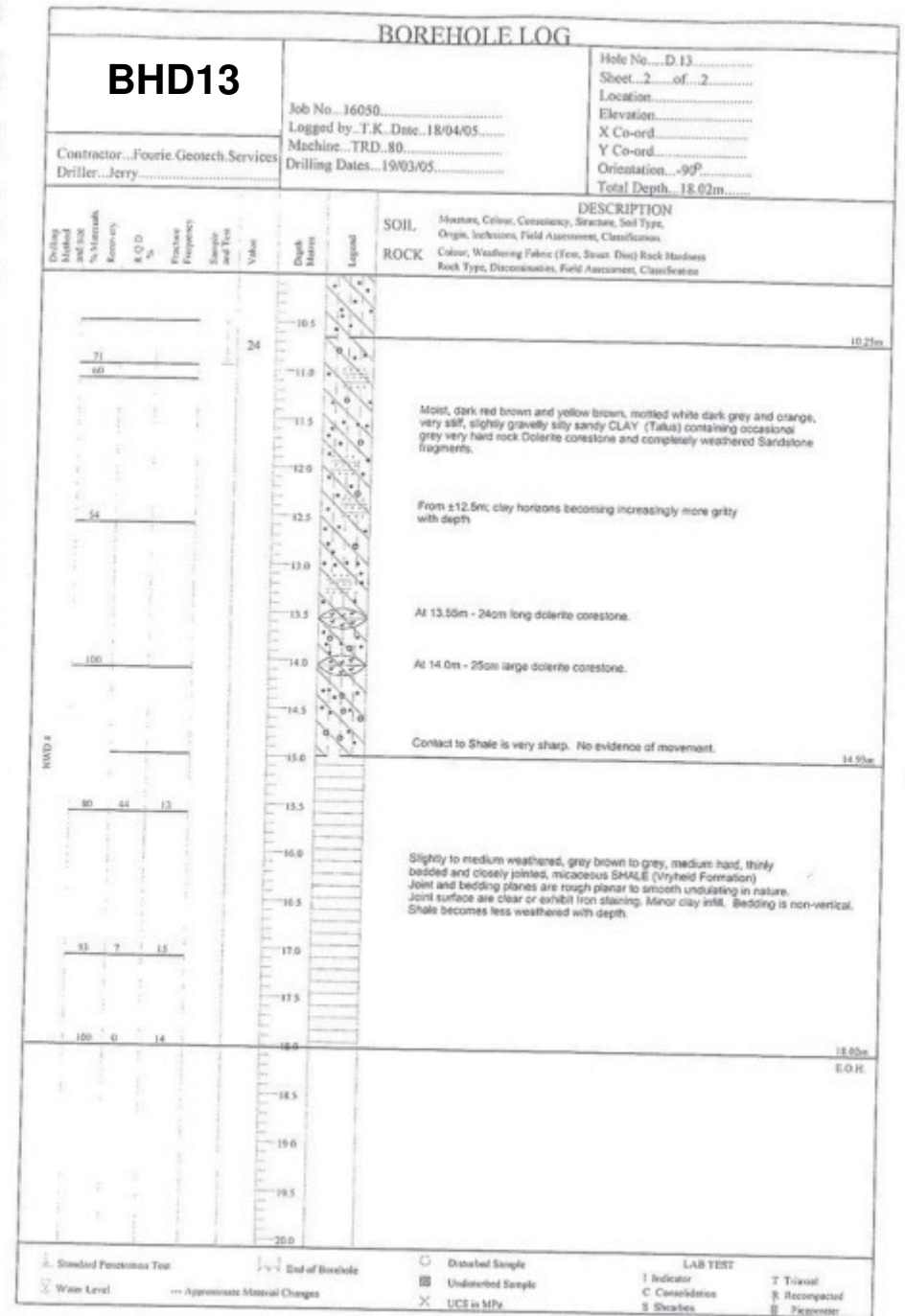
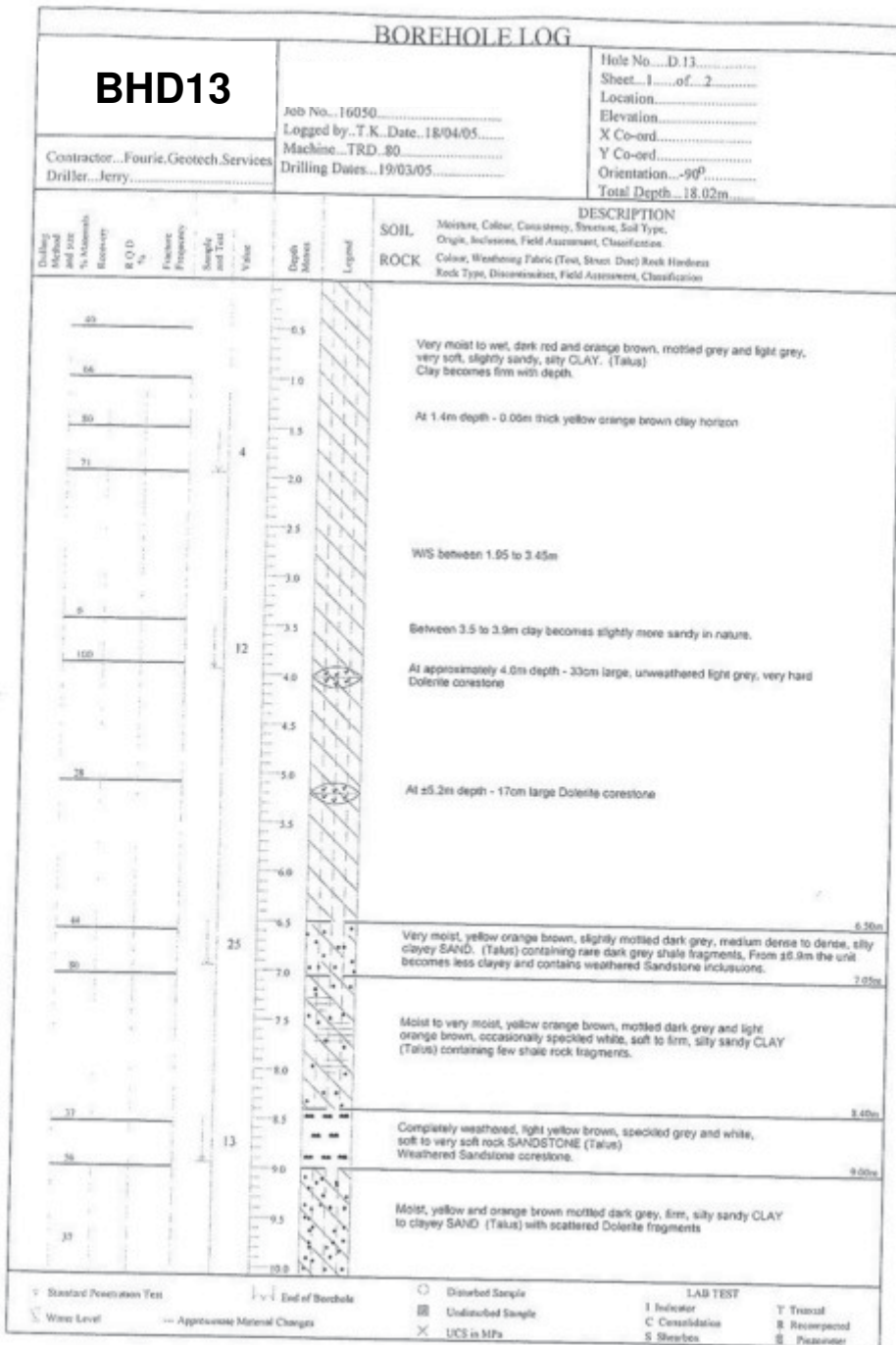
APPENDIX B1.5

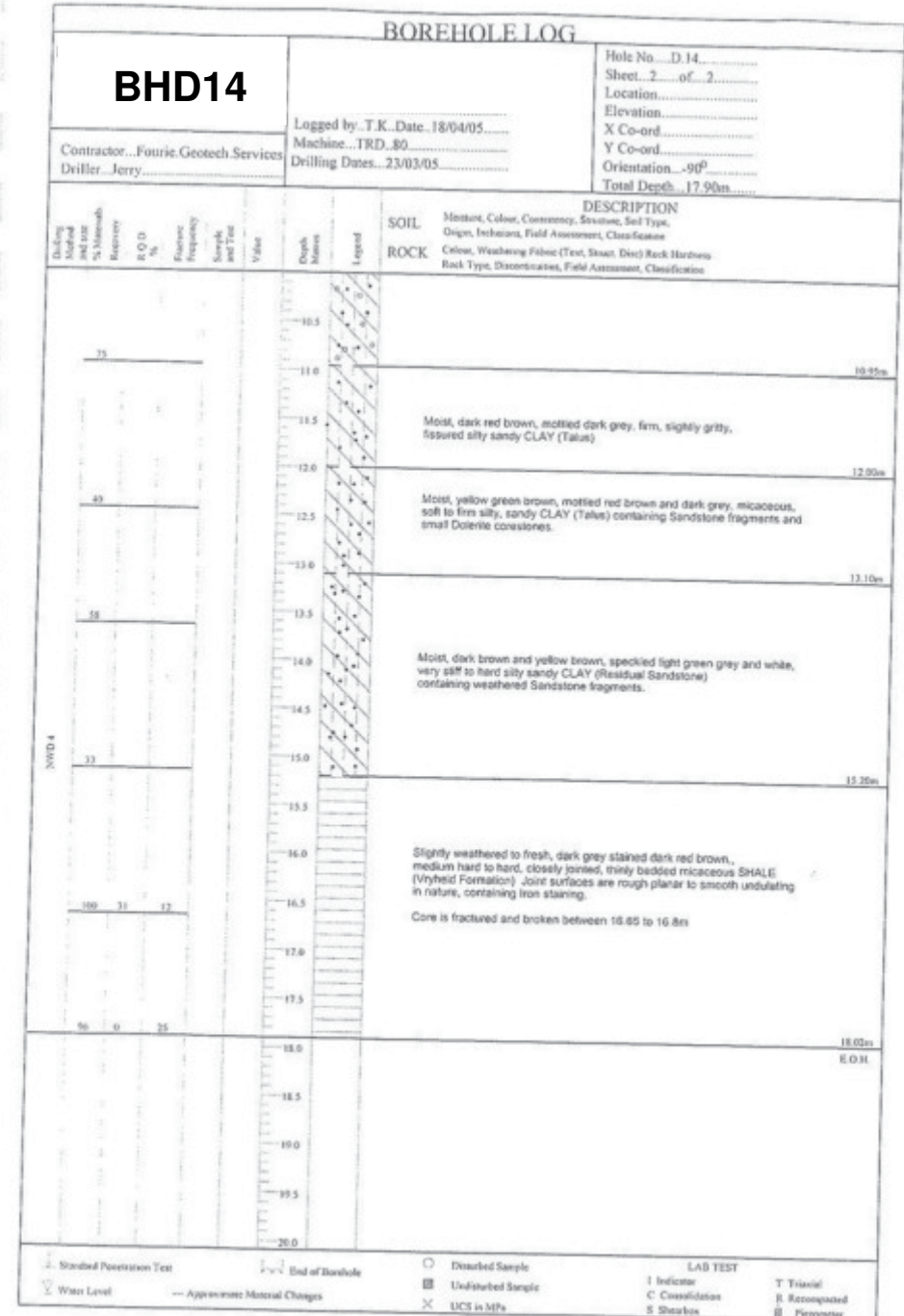
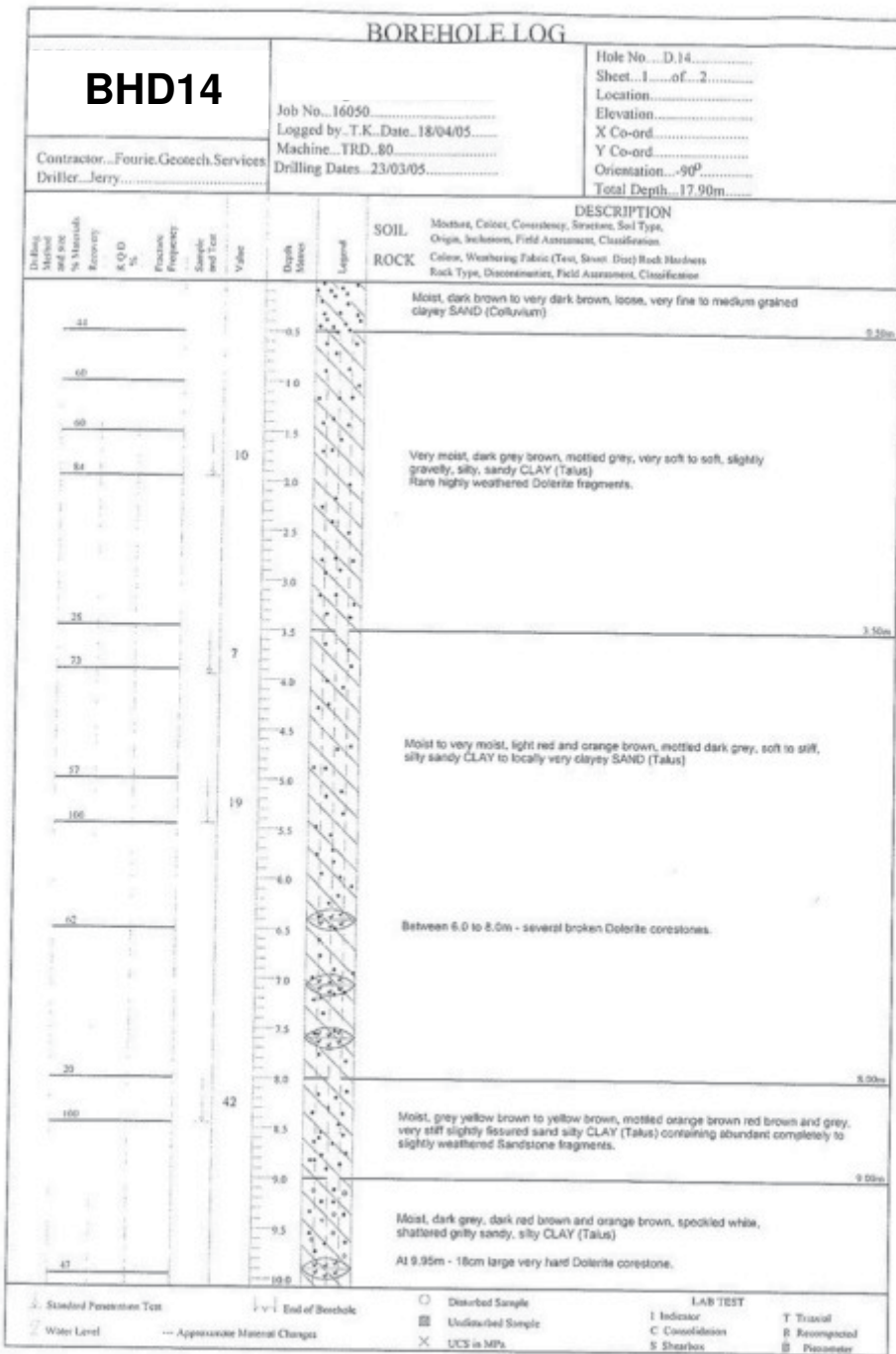
MONTROSE PARK DEVELOPMENT

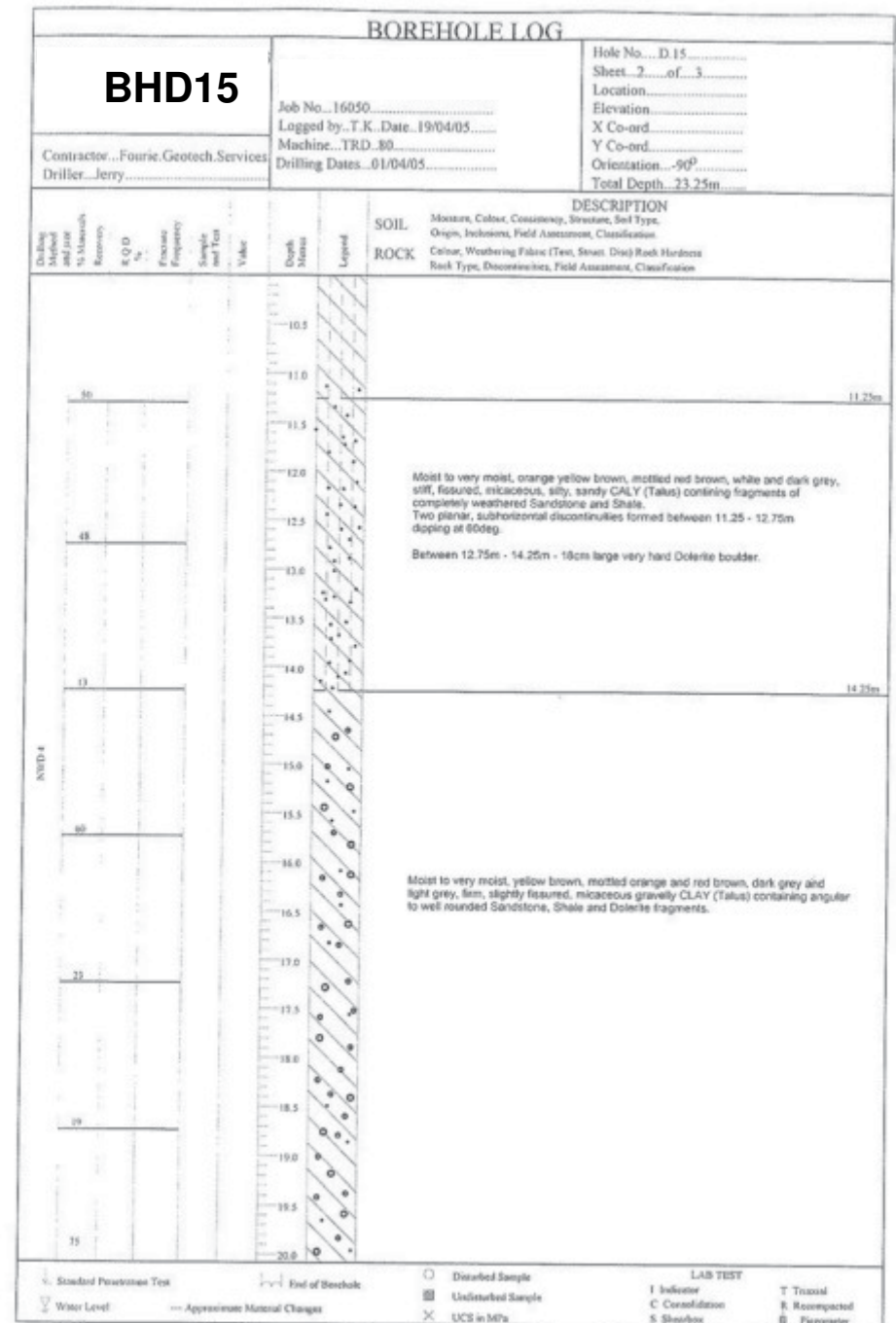
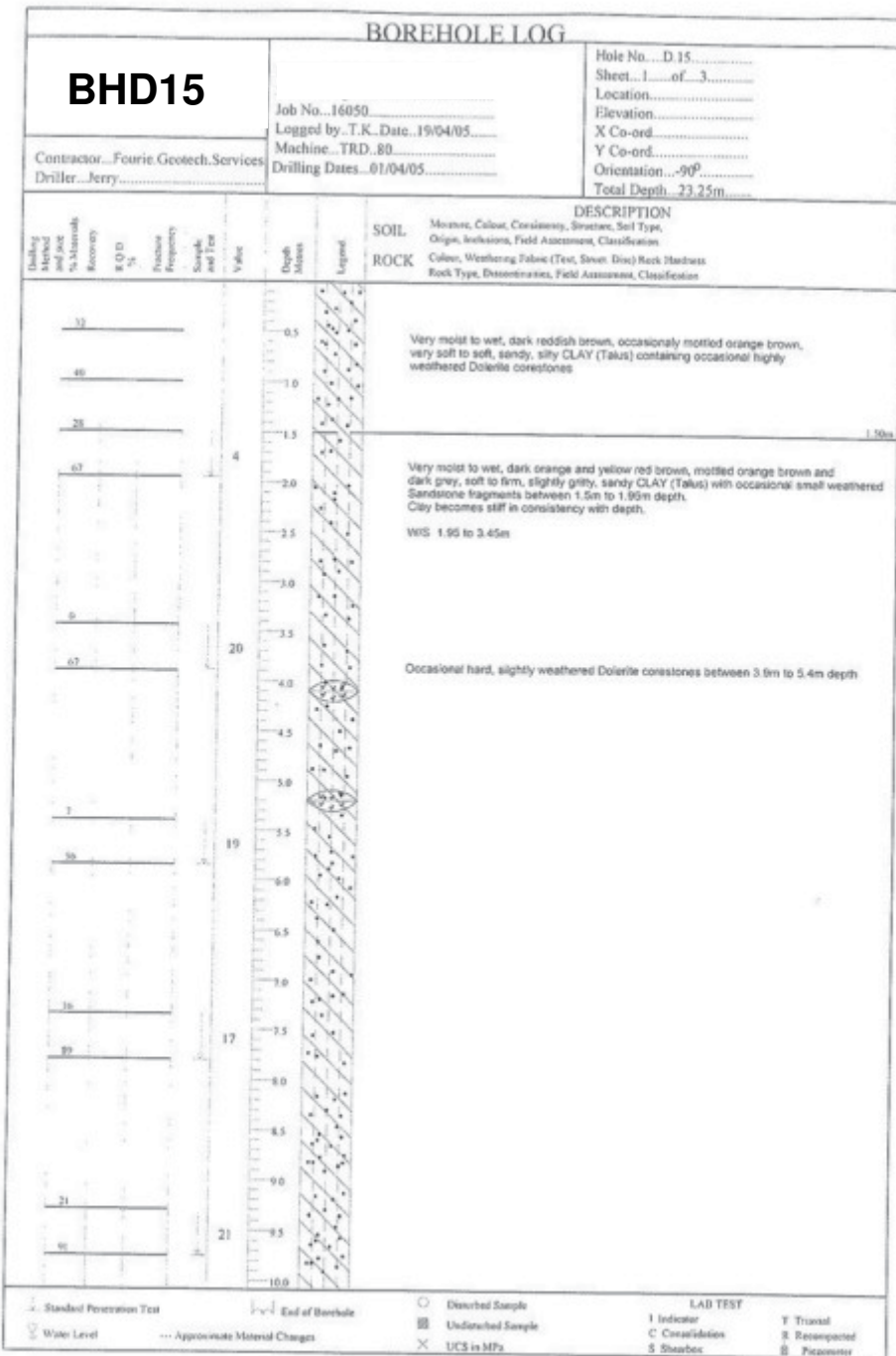


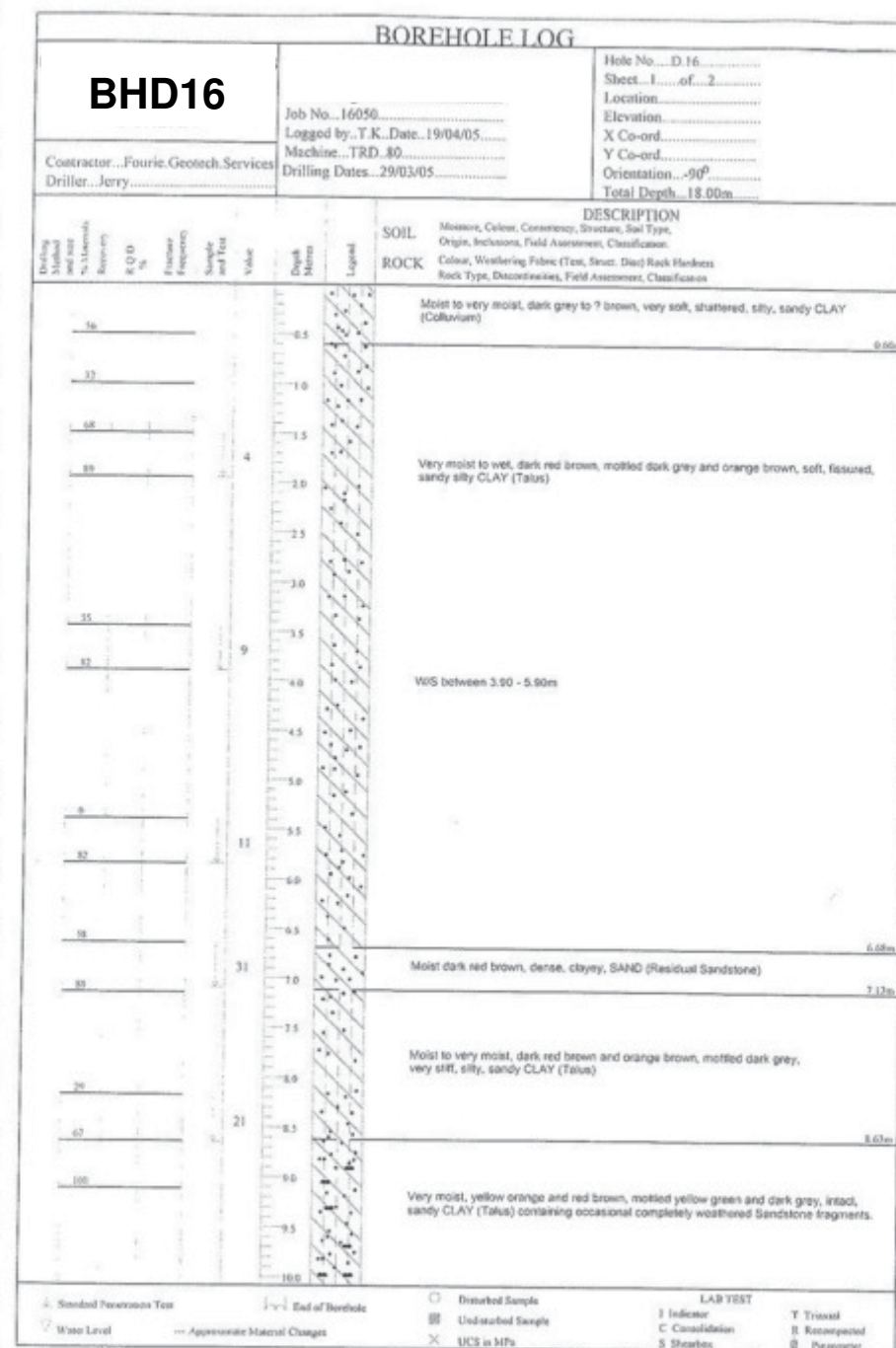
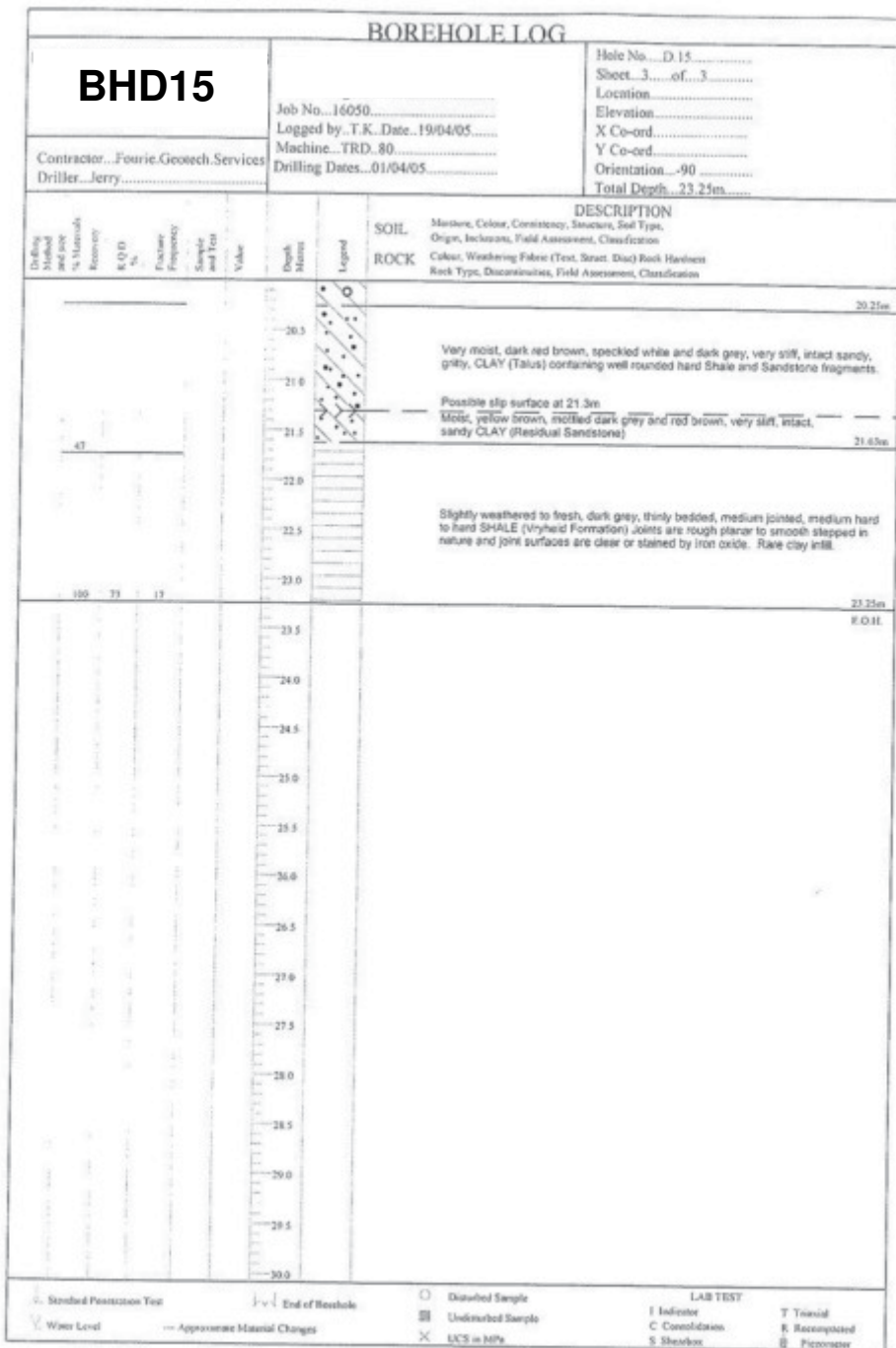


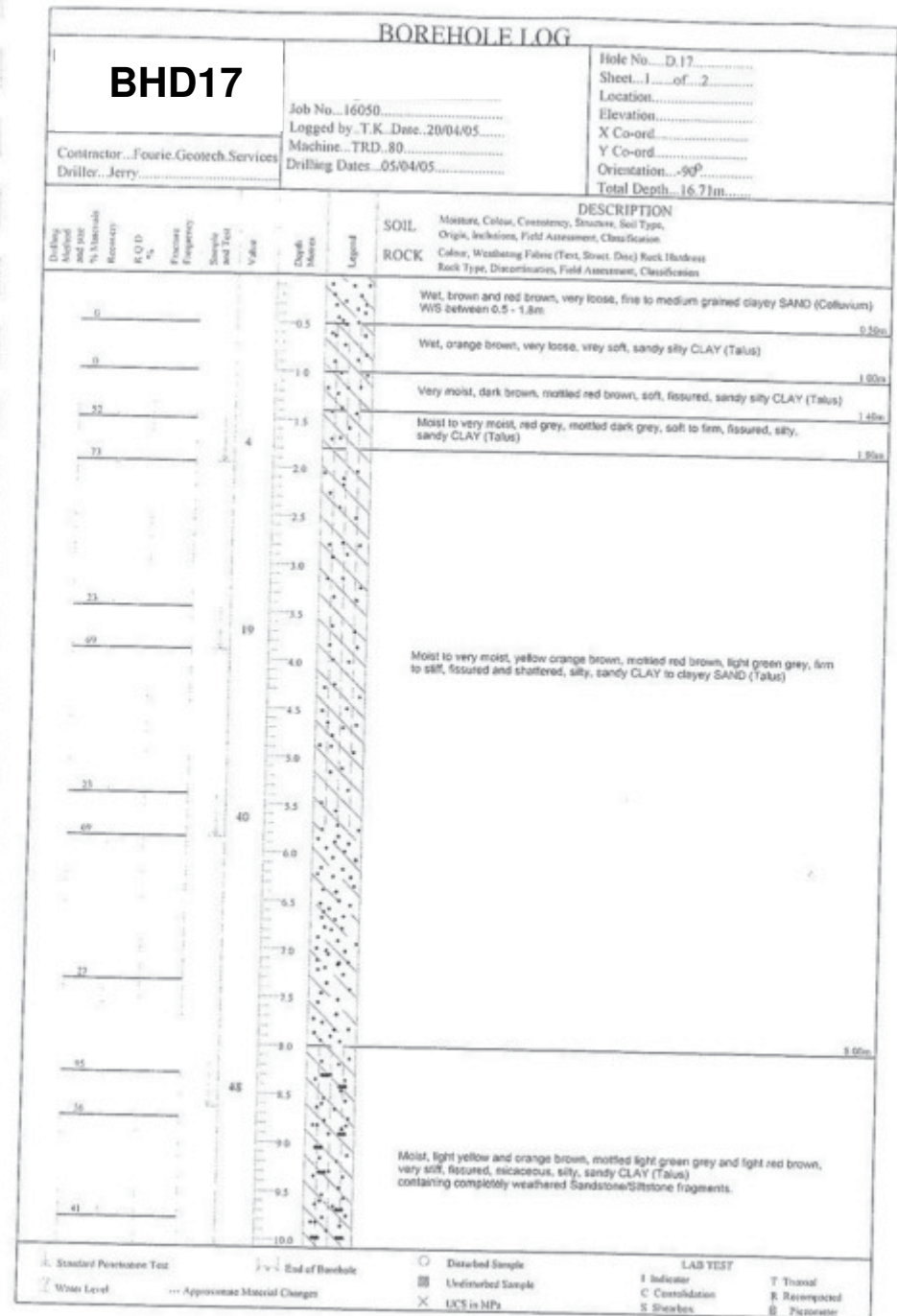
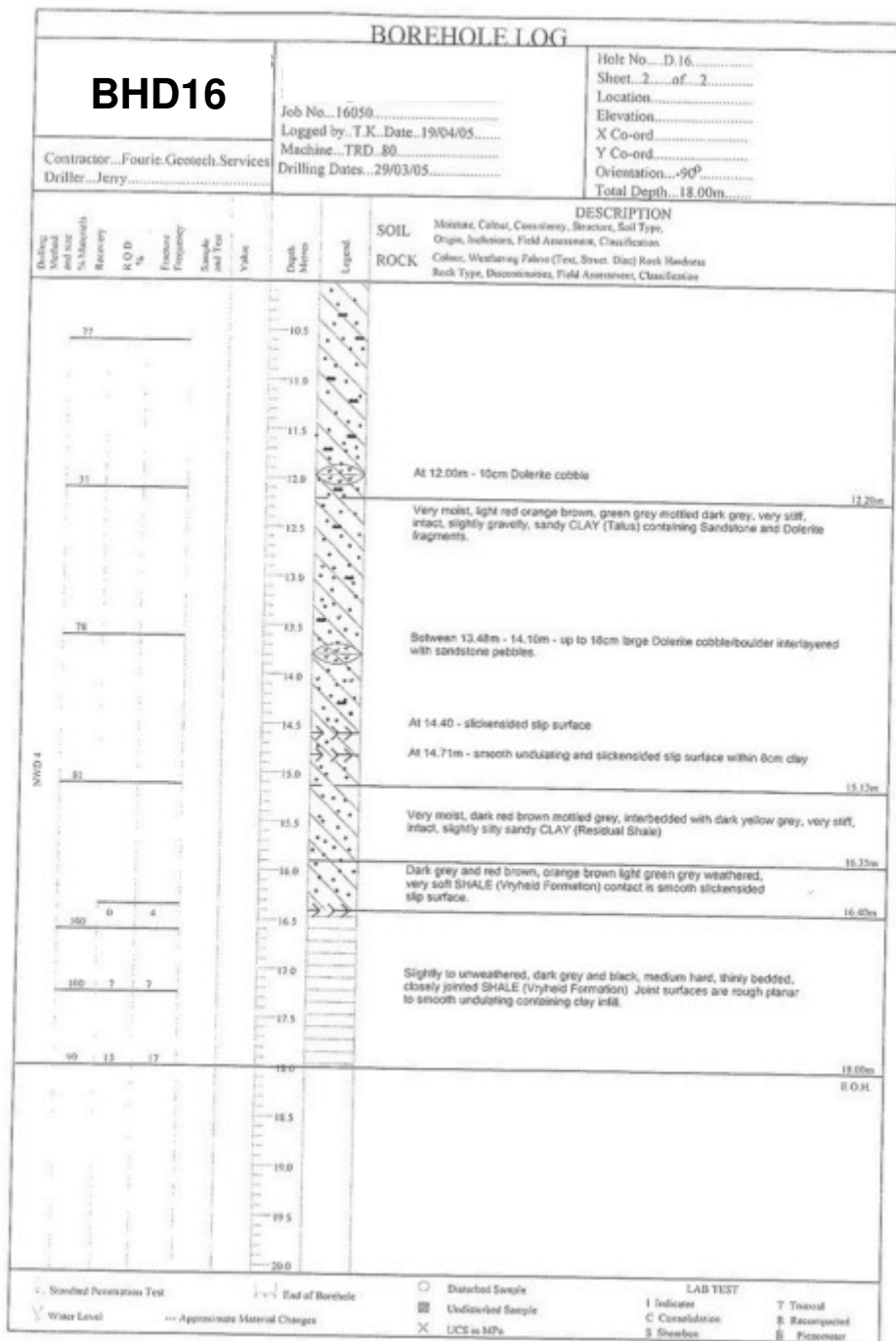


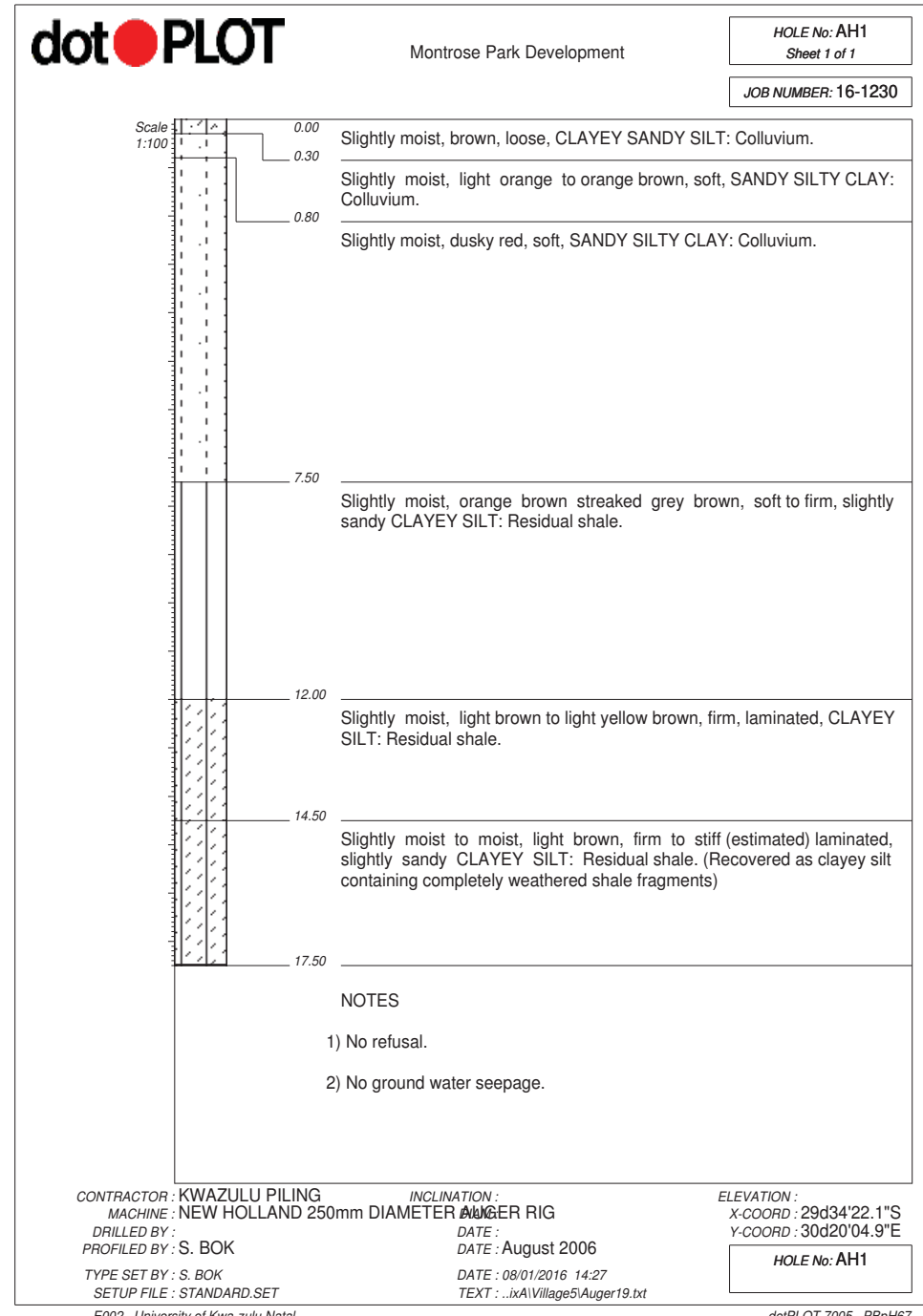
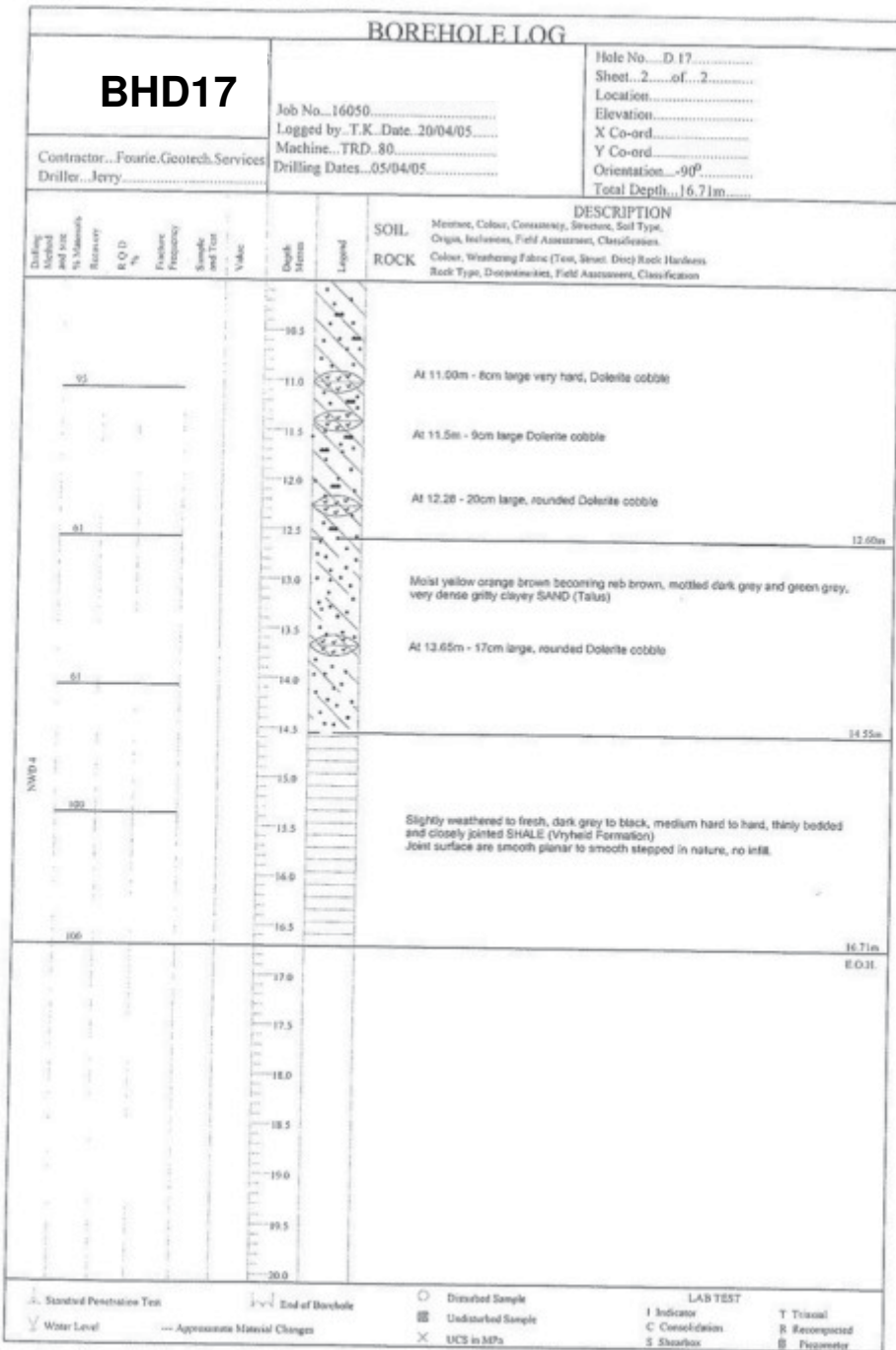


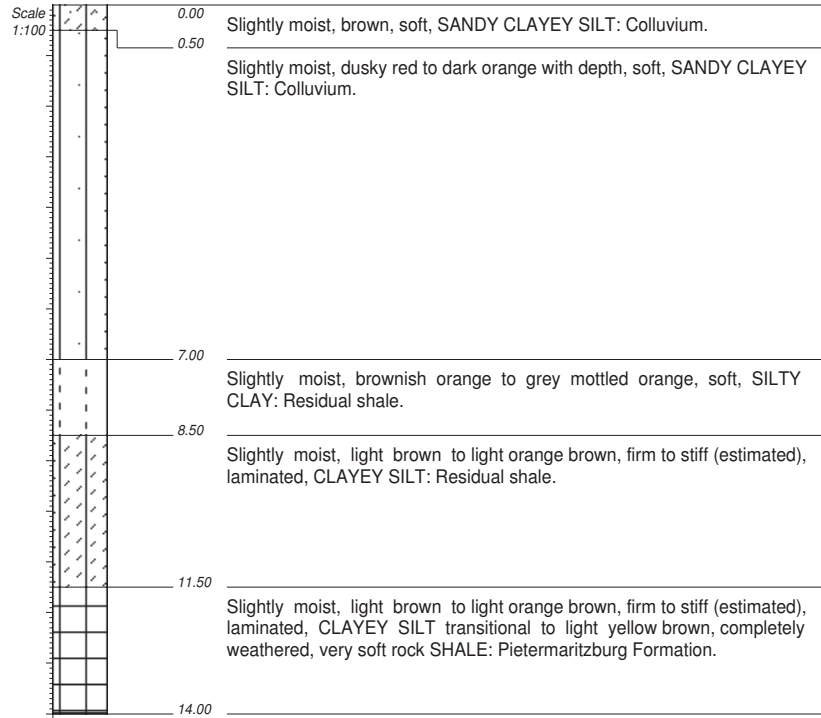












NOTES

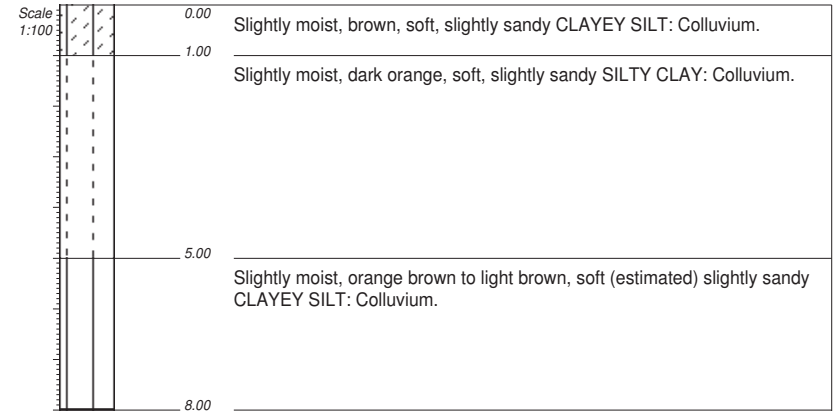
- 1) Refusal of auger at 14.0m in weathered shale rock.
- 2) Standing water level at 10.3m (measured after 4 days).

CONTRACTOR : KWAZULU PILING
 MACHINE : NEW HOLLAND 250mm DIAMETER AUGER RIG
 DRILLED BY :
 PROFILED BY : S. BOK
 TYPE SET BY : S. BOK
 SETUP FILE : STANDARD.SET

INCLINATION :
 DATE : August 2006
 DATE : 08/01/2016 14:27
 TEXT : ..\xA\illage5\Auger19.txt

ELEVATION :
 X-COORD : 29d34'21.4"S
 Y-COORD : 30d20'04.7"E

HOLE No: AH2



NOTES

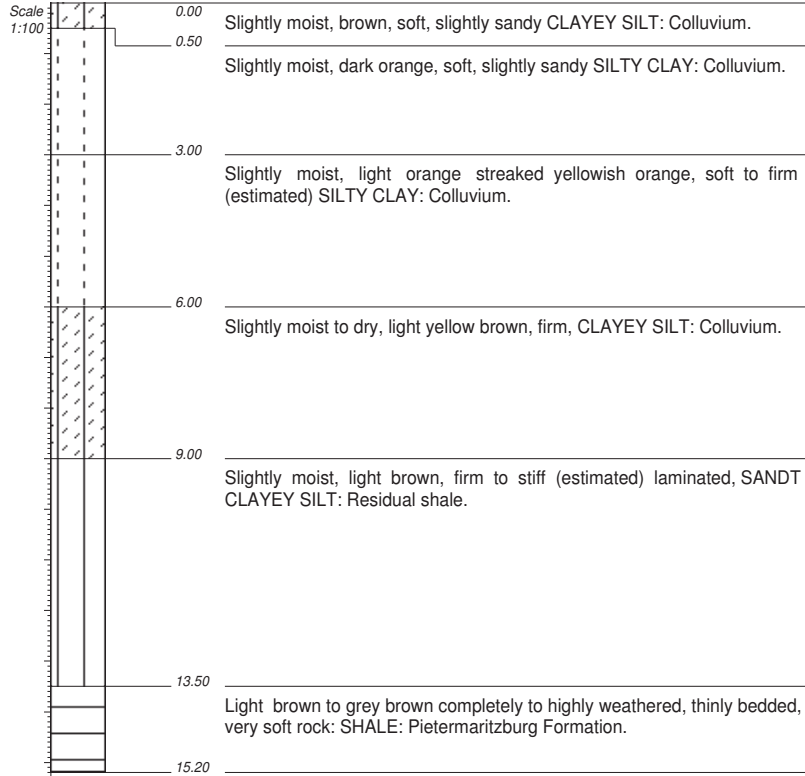
- 1) Refusal of auger at 8.0m on dolerite boulder/s.
- 2) No ground water seepage. Standing water level not recorded.

CONTRACTOR : KWAZULU PILING
 MACHINE : NEW HOLLAND 250mm DIAMETER AUGER RIG
 DRILLED BY :
 PROFILED BY : S. BOK
 TYPE SET BY : S. BOK
 SETUP FILE : STANDARD.SET

INCLINATION :
 DATE : August 2006
 DATE : 08/01/2016 14:27
 TEXT : ..\xA\illage5\Auger19.txt

ELEVATION :
 X-COORD : 29d34'23.0"S
 Y-COORD : 30d20'03.0"E

HOLE No: AH3



NOTES

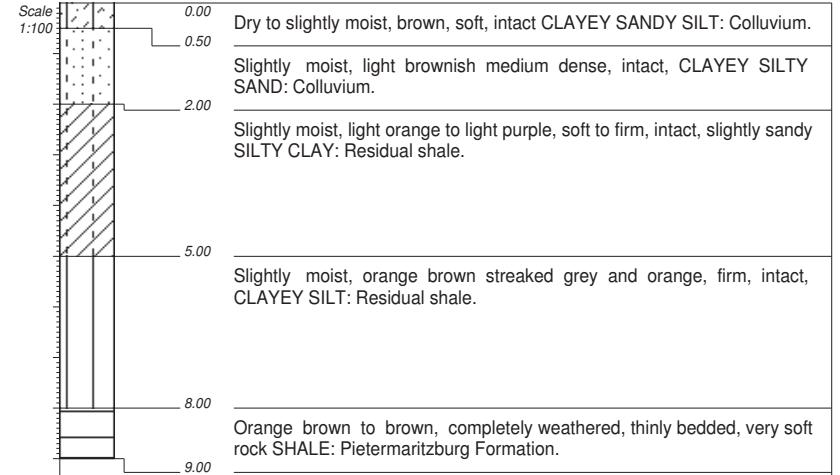
- 1) Refusal of auger at 15.2m in weathered shale rock.
- 2) Standing water level at 14.5m (measured after 4 days).

CONTRACTOR : KWAZULU PILING
 MACHINE : NEW HOLLAND 250mm DIAMETER AUGER RIG
 DRILLED BY :
 PROFILED BY : S. BOK
 TYPE SET BY : S. BOK
 SETUP FILE : STANDARD.SET

INCLINATION :
 DATE : August 2006
 DATE : 08/01/2016 14:27
 TEXT : ..\xA\illage5\Auger19.txt

ELEVATION :
 X-COORD : 29d34'23.0"S
 Y-COORD : 30d20'03.3"E

HOLE No: AH4



NOTES

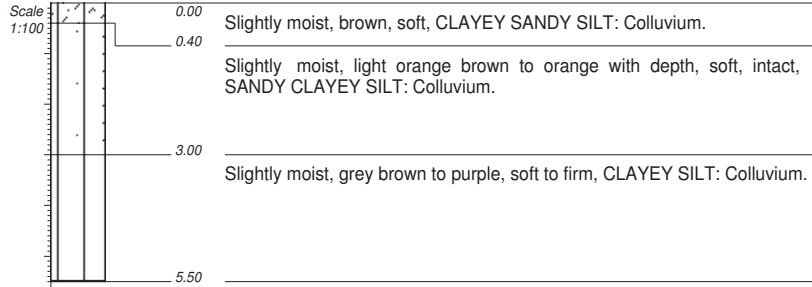
- 1) Refusal (very slow advance) of auger at 9.0m.
- 2) Slow advance below 8.0m.
- 3) No ground water seepage.
- 4) Boulder encountered at 0.5m.

CONTRACTOR : KWAZULU PILING
 MACHINE : NEW HOLLAND 250mm DIAMETER AUGER RIG
 DRILLED BY :
 PROFILED BY : S. BOK
 TYPE SET BY : S. BOK
 SETUP FILE : STANDARD.SET

INCLINATION :
 DATE : August 2006
 DATE : 08/01/2016 14:27
 TEXT : ..\xA\illage5\Auger19.txt

ELEVATION :
 X-COORD : 29d34'30.8"S
 Y-COORD : 30d20'10.1"E

HOLE No: AH5



NOTES

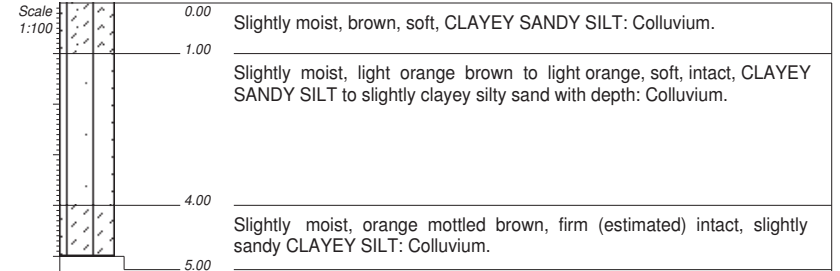
- 1) Refusal of auger at 5.5m on boulder.
- 2) No ground water seepage.

CONTRACTOR : KWAZULU PILING
 MACHINE : NEW HOLLAND 250mm DIAMETER AUGER RIG
 DRILLED BY :
 PROFILED BY : S. BOK
 TYPE SET BY : S. BOK
 SETUP FILE : STANDARD.SET

INCLINATION :
 DATE : August 2006
 DATE : 08/01/2016 14:27
 TEXT : ..\xA\ Village5\Auger19.txt

ELEVATION :
 X-COORD : 29d34'31.6"S
 Y-COORD : 30d20'11.1"E

HOLE No: AH6



NOTES

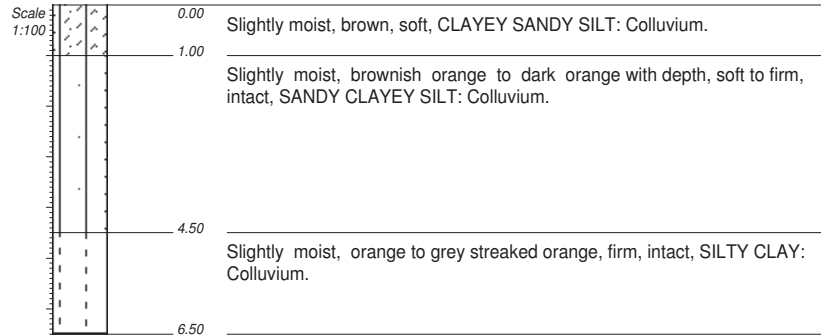
- 1) Refusal of auger at 5.5m on dolerite boulder/s.
- 2) Boulder encountered at 4.0m.
- 3) No ground water seepage.

CONTRACTOR : KWAZULU PILING
 MACHINE : NEW HOLLAND 250mm DIAMETER AUGER RIG
 DRILLED BY :
 PROFILED BY : S. BOK
 TYPE SET BY : S. BOK
 SETUP FILE : STANDARD.SET

INCLINATION :
 DATE : August 2006
 DATE : 08/01/2016 14:27
 TEXT : ..\xA\ Village5\Auger19.txt

ELEVATION :
 X-COORD : 29d34'32.1"S
 Y-COORD : 30d20'10.7"E

HOLE No: AH7



NOTES

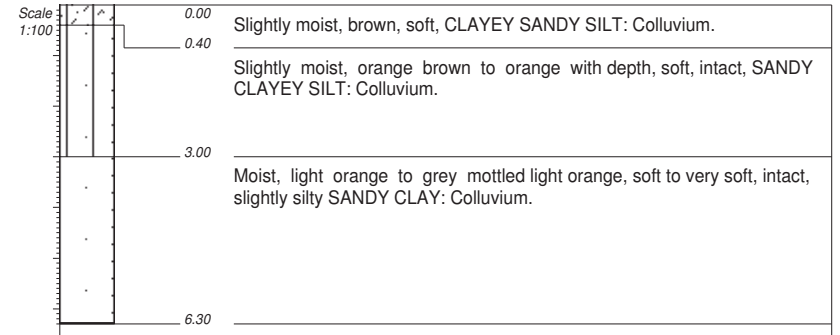
- 1) Refusal of auger at 6.5m on dolerite boulder.
- 2) No ground water seepage.

CONTRACTOR : KWAZULU PILING
 MACHINE : NEW HOLLAND 250mm DIAMETER AUGER RIG
 DRILLED BY :
 PROFILED BY : S. BOK
 TYPE SET BY : S. BOK
 SETUP FILE : STANDARD.SET

INCLINATION :
 DATE : August 2006
 DATE : 08/01/2016 14:27
 TEXT : ..\xA\ Village5\Auger19.txt

ELEVATION :
 X-COORD : 29d34'32.0"S
 Y-COORD : 30d20'09.7"E

HOLE No: AH8



NOTES

- 1) Refusal of auger at 6.3m on boulder.
- 2) Ground water seepage towards base of hole.
- 3) Standing water level at 2.7m overnight.

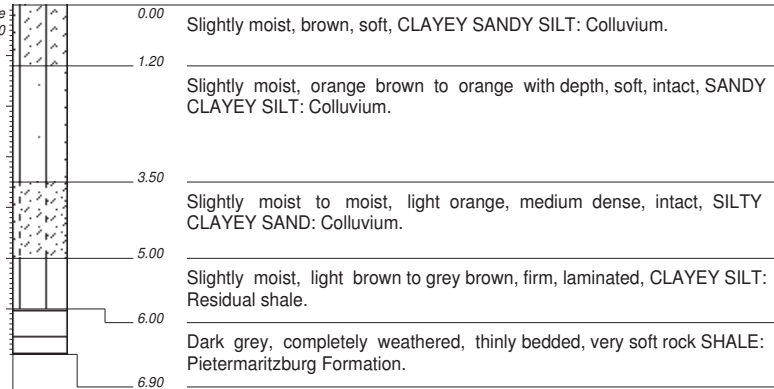
CONTRACTOR : KWAZULU PILING
 MACHINE : NEW HOLLAND 250mm DIAMETER AUGER RIG
 DRILLED BY :
 PROFILED BY : S. BOK
 TYPE SET BY : S. BOK
 SETUP FILE : STANDARD.SET

INCLINATION :
 DATE : August 2006
 DATE : 08/01/2016 14:27
 TEXT : ..\xA\ Village5\Auger19.txt

ELEVATION :
 X-COORD : 29d34'33.3"S
 Y-COORD : 30d20'11.7"E

HOLE No: AH9

Scale
1:100



NOTES

- 1) Refusal (very slow advance) of auger at 6.9m in completely weathered shale.
- 2) Standing water level at 5.0m overnight.

CONTRACTOR : KWAZULU PILING
MACHINE : NEW HOLLAND 250mm DIAMETER AUGER RIG
DRILLED BY :
PROFILED BY : S. BOK
TYPE SET BY : S. BOK
SETUP FILE : STANDARD.SET

INCLINATION :
DATE : August 2006
DATE : 08/01/2016 14:27
TEXT : ..\xA\Village5\Auger19.txt

ELEVATION :
X-COORD : 29d34'34.0"S
Y-COORD : 30d20'11.4"E

HOLE No: AH10

	SAND	{SA04}
	SANDY	{SA05}
	SILT	{SA06}
	SILTY	{SA07}
	CLAY	{SA08}
	CLAYEY	{SA09}
	SHALE	{SA12}

CONTRACTOR :
MACHINE :
DRILLED BY :
PROFILED BY :

INCLINATION :
DIAM :
DATE :
DATE :

ELEVATION :
X-COORD :
Y-COORD :

TYPE SET BY : S. BOK
SETUP FILE : STANDARD.SET

DATE : 08/01/2016 14:27
TEXT : ..\xA\Village5\Auger19.txt

LEGEND
SUMMARY OF SYMBOLS